The Principles of Shaped Wheelchair Seat Cushioning Design

By
Shona Michael, MSc, MA

A Thesis Submitted for
the Degree of Doctor of Philosophy
in the Faculty of Medicine,
University of London.

October 1993

Biomedical Engineering Department
Institute of Orthopaedics
University College London
Royal National Orthopaedic Hospital
Brockley Hill, Stanmore
Middlesex, HA7 4LP

ABSTRACT

The aim of this work is to determine the principles by which the optimum design of shaped wheelchair seat for an individual can be established.

A system for producing individually contoured cushioning using computer-aided design and manufacturing techniques was developed and tested. Nonlinear finite element (FE) models of the seated buttock were developed from measurements of an able-bodied individual. Soft tissue force-deflection characteristics, tissue depth, body surface geometry and the weight supported through the buttock were measured during sitting. The combined soft tissues were modelled as an incompressible hyperelastic material. Interface pressure distributions calculated from the analyses were found to be similar to pressure distributions measured between corresponding shaped seat surfaces and the subject.

The effects of seat shape, contour depth, interface friction and misalignment of the body on the seat were examined. The results of the FE analyses suggested that the closer the contours of the seat to the contours of the buttock prior to loading, the lower the distortional stress concentrations and hydrostatic pressure gradients in the soft tissues around the pelvis during sitting. It appeared that the stresses in the soft tissue around the sacrum are sensitive to posture and changes in position of the body on the seat. When the dorsal surface of the sacrum has a postero-inferior orientation, a lot of load is transferred through the sacrum and there is a high distortional stress concentration in the soft tissues. When the body moves about on the seat and there is a high interface friction coefficient, the soft tissues are constrained by the interface forces and additional distortional stresses develop in the soft tissue.

The principles can be applied to the design of shaped seating for individuals and groups of people with similar seating needs.

ACKNOWLEDGEMENTS

To my supervisor, Professor P.S.Walker, for his direction throughout this study and for enabling me to obtain equipment and training as it was required.

For Financial Support

The Development Trust for the Young Disabled.

The Institute of Orthopaedics, University College London.

For Clinical Guidance and Facilities

Mrs P. Pope and Dr K. Andrews of the Royal Hospital and Home, Putney; Mrs P. Copley of John Grooms Hospital & Home for the Disabled, Edgware and Dr N. Mustapha of Garston Manor Rehabilitation Centre, Garston.

The residents of the Royal Hospital and Home, Putney and John Grooms Hospital & Home for the Disabled, Edgware for giving me their time.

The staff of the Occupational Therapy Department at the Royal National Orthopaedic Hospital, Stanmore.

For Technical Guidance

The staff of the Biomedical Engineering Department, Institute of Orthopaedics, University College London.

Mr M. Shears and Mr P. Dallard of Industrial Engineering, Ove Arup Partnership.

Dr R. Richards of Biomedical Engineering, University of Surrey.

For the Free Use of Equipment

Mr S. Hughes of Biomedical Engineering, University of Surrey.

Dr T. Sayegh of Medicare Products Ltd.

Dr A. Linney and Ms A. Combes of Department of Medical Physics and Bioengineering, University College and Middlesex School of Medicine.

The staff of the Radiotherapy Department, Northwick Park Hospital.

Also I especially wish to thank Tony Olanlokun, Joan Michael and Duncan Michael for their encouragement and for reading this manuscript.

TABLE OF CONTENTS

Page No.

LIST OF FIGURES

CHAPTER 1 INTRODUCTION

The general purpose of the work reported in this thesis is to reduce the frequency of pressure sores and discomfort experienced by chair-bound people, by extending the understanding of the factors which influence these phenomena. The direct aim of the work is to determine the principles by which the optimum design of shaped seat for an individual can be established and to investigate whether the principles can be used to design shaped supporting surfaces for groups of people with similar seating needs.

There is a prevalence of chair-bound people in the adult population of Great Britain of about 0.7 percent (Wood & Badley, 1988). Fenwick (1977) conducted a survey of wheelchair users in the United Kingdom. He found that 63 percent of wheelchair users divided almost equally into people with osteoarthritis, rheumatoid arthritis, multiple sclerosis and hemiplegia. Paraplegics and tetraplegics only formed about 6 percent of the total wheelchair-bound population. The distribution of the types of cushion amongst the chair-bound population has not been extensively documented. In a study where the wheelchair cushions of thirty-two people with spinal cord injuries were recorded,12 used an air-filled cushion,16 used a foam and 4 used a gel (Chung & Weimar,1989).

Bardsley conducted a survey of chair-bound people in the Tayside region of Scotland (1984). He found that about 0.5 percent of people in the region had seating which limited their functional capabilities through failing to provide support in a manner consistent with their medical, physical and psychological requirements. In Bardsley's survey, the elderly comprised 80 percent of the needy group whereas people with cerebral palsy comprised about 12 percent The rest of the group had disorders such as multiple sclerosis, muscular dystrophies, spinal cord lesions and rheumatoid arthritis.

The whole area of study is affected by the feasibility of working with subjects, by the vast range of factors within and outside the body which affect the system and by the non-invasive methods available for studying these phenomena which occur essentially within the body. Computer-aided measurements and analytical techniques, mathematical modelling, subjective clinical tests and other measurement methods were all used for investigating the system. In spite of these circumstances a self consistent and complete work has been achieved which the author hopes will prove to be of some benefit to people in the future.

1.1 Seating and Cushioning Needs of Chair Bound Peopie

Prolonged discomfort whilst sitting is common for people in wheelchairs. It can be due to muscle fatigue, to high interface humidity and temperature and to locally high loading of regions of the body-support interface. It is often related to a poor sitting posture. For these people the function of the wheelchair cushion is to provide a comfortable interface between the seated person and the mobility base.

Some chair bound people are at risk of developing pressure sores. Typical sites for pressure sore formation are under the skeletal bony prominences, such as the ischial tuberosities, trochanters and sacrum. For these people the cushion has an additional function of redistributing the body weight away from the areas of soft tissue where pressure sores are likely to develop. The aetiology of pressure sores is discussed in detail in Section 1·3. People who cannot move around in their chair are at risk of pressure sores because they cannot vary the load distribution on the buttocks. There is an extra risk of pressure sores when there is reduced sensation over a part of the body, because there is no sensory feedback from excessive tissue loading. There is also a high risk of pressure sores in people who have a sitting posture or orthopaedic deformities that lead to excessive localised loading of the tissues (Drummond et al,1985).

Another vital function of seating is the control of sitting position. At its simplest the cushion or seat can provide lateral forces to stabilize the position of the pelvis in the seat and provide forces to the distal thigh to abduct the hips. Commonly a person may have a non fixed lateral tilt to the pelvis and a spinal scoliosis whilst sitting in a wheelchair. Corrective loading can be applied through the cushion to reduce or remove the pelvic obliquity. For some people who have a partly fixed orthopaedic deformity, a seating intervention to 'correct' posture could produce even higher localised loading of a part of the body and an unacceptably increased risk of pressure sores. A balance between corrective forces and an even load distribution has to be reached when considering cushioning for such cases.

1.2 Structure and Function of the Buttocks and Thighs During Sitting

The position, structure and function of the tissues of the buttock and thighs have to be well understood, for seat cushioning to be produced that meets the needs of chair bound people. The available information is summarised in this section.

The body is supported on a seat through the posterior aspects of the pelvis and femurs. Compared to during standing, the lumbar curve is flattened during sitting and the pelvis has less of a supero-anterior tilt. This is because as a person sits down, the hips are flexed and tension develops in the posterior thigh and the gluteal muscles. The muscles pull on the pelvic girdle at the points of insertion and this causes the infero-anterior pelvic rotation. Then in order to maintain the upright position for the trunk, the lumbar curve flattens (Keegan,1953). A fuller description of the anatomy which is relevant to seating is now given.

The ischial tuberosities are the major bony structures through which load is transferred to the seat during sitting. For US adults, the average distance between the tips of the two tuberosities is 132 mm (Diffrient et al, 1974). The ischial tuberosity provides the point of attachment on the pelvis for the hamstring muscles (long head of biceps, semitendinosus, semimembranosus) and for adductor magnus. Adductor brevis and gracilis attach along the ischiopubic ramus. The medial area of the ischial tuberosity is covered by fibro-adipose tissue, which is divided by intersecting fibrous septa. There is sometimes a bursa between the tuberosity and the margins of gluteus maximus. This is a flat sac of synovial membrane which allows the more superficial tissue to move over the ischium. As with all bony surfaces, the pelvis is covered with a fibrous periosteal layer.

The sacrum is located between the posterior medial aspects of the ilium and the fifth lumbar vertebra. There are strong ligamentous attachments across the sacro-iliac joints which restrict movement. On the dorsal surface of the sacrum there are longitudinal rows of small bony protruberances. There are foramina lateral to the intermediate row of protruberances, through which pass the posterior branches of the sacral nerves. There is a thin layer of tissue covering and well attached to the dorsal surface of the sacrum. Clark et al (1989) measured the depth of soft tissue over the sacrum of elderly patients. For the subjects with pressure sores the mean depth was 8 mm whilst it was 13.7 mm for the other subjects. The sacrum can be heavily involved in load bearing during sitting if the pelvis is rotated supero-posteriorly. The coccxy is the bony structure at the tip of and separate from the sacrum. The ischium is connected to the sacrum by sacrotuberous and sacrospinous ligaments.

The hip joint links the proximal femur to the lateral aspects of the pelvis. The head of the femur and acetabulum are surrounded by a strong, dense fibrous capsule. The iliofemoral, ischiofemoral, and pubofemoral ligaments have positions outside of the capsule. Externally the capsule is separated from adjacent muscles by bursae. The greater trochanter projects laterally at the junction of the femoral neck and shaft. In normal sitting the femoral heads are separated by the pelvis and the shafts converge distally so that the knees almost touch.

The gluteal muscles together with the superficial fascia form the bulk of the soft tissue in the buttock region. During sitting the muscles are positioned lateral to the ischial tuberosity. Gluteus maximus is the largest and most superficial muscle mass in the region. The muscle is attached to the external surface of the pelvis around the posterior superior iliac spine, the dorsal lower sacrum, coccyx, sacrotuberous ligaments and the fascia covering gluteus medius. The muscle attaches into a line along the proximal third of the posterior shaft of the femur. Gluteus medius attaches to a larger area of the external ilium anterior to the attachment of gluteus maximus. The posterior third is deep to gluteus maximus and the rest is covered only by deep fascia. Gluteus mimimus attaches to the external ilium anterior to the attachment of gluteus medius. Both gluteus medius and minimus attach distally to the greater trochanter.

There is a well developed layer of adipose superficial fascia covering the gluteal muscles. This is loose connective tissue, deep to and continuous with the dermis, in which there is an abundance of adipose cells. Nerves, blood vessels and lymphatics are located mainly in the deeper parts and there are also skin muscles. The subcutaneous tissue is not as well vascularized as the dermis. The adipose tissue is generally more abundant and widely distributed in females. The gluteal fold forms the distal border of the buttock; the superficial fascia condenses and is pinned to the underlying deep fascia. For adults in the United States the maximum width of the body at the hips during sitting is on average, 330 mm for males and 409 mm for females (Diffrient et al, 1974).

The soft tissue of the dorsal thigh consists of the deep subcutaneous tissue, the hamstring and adductor muscles, and the skin. Compared to in the buttock, the deep fascia is well developed and the subcutaneous tissue less so. The deep fascia is composed chiefly of compact, regularly arranged collagen fibres. The fibres of the deep fascia may condense into a sheet which connects with the adjacent muscles. Wherever deep fascia contacts the periosteal covering of bone, it fuses with it thus allowing the pull of the attached muscles to be transmitted to the bone.

The hamstring muscles run along the posterior femur and cross both the hip and knee joints. Biceps femoris is the most lateral of the hamstrings. The muscle mass runs along the length of the femur and attaches distally to the fibula and tibia. Semitendinosus lies slightly medial to biceps and attaches into the medial tibia. Semimembranosus runs along the femur medial to semitendinosus. Adductor magnus, brevis and gracilis are positioned along the posterior femur medial to the hamstrings. Fibres of adductor magnus attach to a ridge which runs along the length of the proximal femur to the medial femoral condyle. Adductor brevis attaches to the proximal and central portion of the posterior femur. The bony structures, associated ligaments and muscle attachment points are illustrated in Figure 1.

The skin consists of two layers, the epidermis and the dermis. The epidermis is the outer layer of the skin. It consists of densely packed cells with no vascular supply. The cells are dead and the outer ones are continually lost from the body to the environment. The dermis consists of collagen and elastin fibres, a network of blood and lymphatic vessels, nerves, hair follicles, sebaceous and sweat glands. In the dermis collagen constitutes 75 percent of skin dry weight, elastin about 4 percent. The collagen and elastin fibres in the dermis run mainly parallel to the skin surface, with the collagen fibres randomly arranged in the directional elastin network. A hydrophilic gel, called ground substance occupies the space between the fibres and the vascular and lymphatic networks. The ground substance can vary from being water-like to gel-like in viscosity.

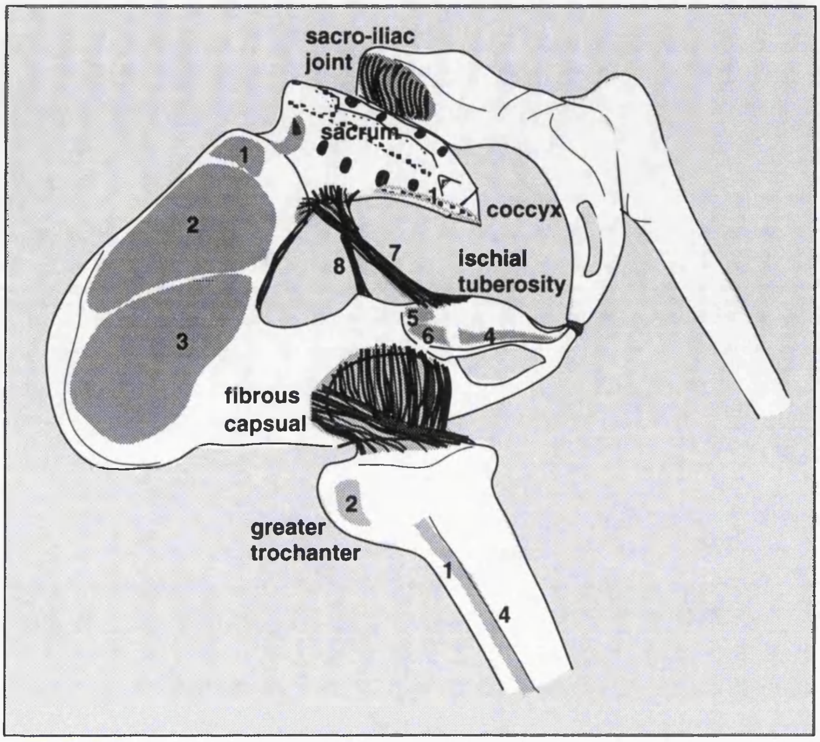

FIGURE 1
Pelvis and proximal thighs showing main ligaments and areas of muscle attachment

1. Gluteus maximus	5. Semitendinosus & long head of biceps
2. Gluteus medius	6. Semi membranosus
3. Gluteus minimus	7. Sacrotuberous ligament
4. Adductor magnus	8. Sacrospinous ligament

1.3 Aetiology of Pressure Sores

A knowledge of the aetiology of pressure sores is important for the design of seating and cushioning for chair bound people. The factors which contribute to the formation of pressure sores have been extensively studied by correlational studies on patients, measurements of blood flow, tissue oxygenation, skin temperature and hyperemia on human subjects when the tissues are under load, and also by the induction of pressure sores in animals. Some of these studies are described below, and discussed in terms of possible mechanisms for pressure sore formation.

The term 'pressure sore' can describe both abrasion damage to the epidermis and also an open ulcer caused by external loading, which extends through the soft tissue to the bone and nearby joints. Damage to the epidermis and dermis and localised hyperaemia after a period of loading are all classified as superficial pressure sores. Ulcers where bone and muscle are involved are deep pressure sores. Deep sores often appear in an area of previously normal tissue, several hours after a period of loading (Barton & Barton, 1981). A region of necrotic tissue is initially observed.

Over the next few weeks the dead cells liquefy and break down. The contents of the sore are discharged, leaving behind an empty cavity. A deep sore is usually more extensive in the subcutaneous tissues than at the surface of the epidermis.

There have been studies on animals where the skin is subject to an externally applied constant pressure for a time period (Daniel et al, 1985; Dinsdale, 1974; Kosiak, 1959). After loading the sites were examined for tissue damage. The readings were repeated over a range of applied pressures. Inverse relationships between the time taken for a pressure sore to form and the magnitude of the applied pressure were reported. Reswick and Rogers (1976) published a curve of similar form showing tolerable applied pressure versus time on the bony prominences of humans. The curve was based on pressure measurements on volunteers, pressure measurements in clinical situations where the skin had shown signs of potential breakdown after a period of loading and retrospective reports of clinical situations that had lead to tissue breakdown. Although the curve was based on unstandardised and indirect measurements, the form of the pressure-time relationship has been central to the development of a hypothesis for pressure sore formation and of clinical practice for the prevention of pressure sores.

There were considerable differences between the above studies in the duration of loading that produced a pressure sore at a given level of pressure. Differences in methodology (for example, animal models, anatomical loading sites and indenter geometries) could have resulted in differences in load transfer to the tissues and in the physiological response of the tissues to the load. Daniel et al loaded the tissue over the greater trochanter of paraplegic swine. The measurements were made six weeks after the spinal cord had been transected when considerable muscle atrophy had occurred. He noted that pressure sores could be produced in paraplegic swine in a shorter time than with normal swine. Muscle atrophy may well have been an important factor contributing to this difference. In this study, as well as in others such as that of Nola and Vistnes (1980), damage to the deep subcutaneous tissues was noted when the skin surface was still intact. These lesions may have been the earliest stages of deep pressure sores.

Because restricted blood flow is likely to be an early stage in the formation of pressure sores, there have been studies to examine the effects of tissue loading on blood flow and tissue oxygenation. The aetiology of pressure sores is not fully understood, so the results of these studies cannot be extrapolated directly to the formation of pressure sores. Bennet et al (1979) and Dinsdale (1974) investigated the effects of surface shear forces on the formation of pressure sores and on blood flow. In Bennet's study the thenar eminence of healthy subjects was loaded against a device in which pressure, shear and photoplethysmographic blood flow transducers were embedded. The combined effects of normal applied pressure and interface shear stress were investigated. They found that in the presence of interface shear stress there was a decrease in the pressure required to prevent blood flow. It is difficult to extrapolate from this study to the bony prominences at the pelvis where pressure sores often occur, because of the profoundly different anatomy of the two regions. Dinsdale loaded the posterior superior iliac spines of pigs. He found that ulcers occurred at pressures as low as 200 mmHg (26.7 kPa) in the presence of friction, where as pressures of at least 480 mmHg (64.0 kPa) were necessary to produce an ulcer when there was no friction. He was not however able to detect a significant difference in blood flow in the tissues which received only pressure and those which received pressure and shear, with isotopic blood perfusion measurement techniques. This result is surprising and appears to contradict that of Bennet's study. However dissimilar blood flow measurement techniques and loading sites were chosen. It may be that Dinsdale and his coworkers did not measure the blood perfusion at the exact location of tissue damage. Another limitation of this study is that the magnitude of the shear stresses which were applied was not reported.

The effect of loading on tissue oxygenation has also been investigated by monitoring the localised partial pressure of oxygen transcutaneously. An electrochemical electrode is mounted on the skin surface, which is heated to maintain vasodilation. Typically a loader is indented into the skin and the transcutaneous oxygen level (Tc-pO_2) under the loader is monitored after each load step. There is a decrease in Tc-pO_2 levels under prolonged applied pressure. Bader and Gant (1988) reported that the Tc-pO_2 reduced slightly at low applied pressure and then at a greater constant rate as the pressure increased. Wide variations between people were reported in the pressure to reduce the Tc-pO_2 to a fraction of its original unloaded value. For example to achieve a 50 percent reduction from the unloaded value, pressures in the range from 22 mmHg to 92 mmHg (2.9 to 12.3 kPa) were required. Seiler and Stahelin reported that the decrease in Tc-pO_2 with applied pressure was linear (1979). They noted the decrease was much greater over the trochanter than over the quadriceps. This difference in behaviour at the two loading sites is likely to have been due to larger internal stresses developing in the soft tissues at the trochanter compared to in the quadriceps. It is difficult to extrapolate with certainty from Tc-pO_2 results at elevated temperatures to the conditions where the body tissues are normally loaded because an elevated skin temperature gives rise to an increase in capillary blood pressure in the skin (Landis, 1930).

Ek et al (1987) and Seiler et al (1986 and 1983) measured the effects of lying on a mattress on the transcutaneous partial pressure of oxygen and blood flow over the trochanter and sacrum. In some cases the partial oxygen pressure and blood flow over the bony prominences were reduced to zero. However this may not have been the case if the rigid transducer had not been situated at the interface between two soft objects. Bennett et al (1981) embedded a blood flow transducer in a rigid, planar wheelchair seat, so the transducer surface was flush with the surface of the seat. The sensor was the same combination of pressure, shear and blood flow transducers which were described by Bennet et al (1979). They measured the pressure at which blood flow occlusion occurred during static sitting on the seat. Occlusion was observed at pressures above 120 mmHg (16.0 kPa) in young male subjects, whereas some geriatric subjects occluded at pressures of less than 20 mmHg (2.6 kPa). The difference between the two groups may have been due to differences in the extent and properties of the tissues, the physiological response to loading, or a combination of the above factors.

The effects of intermittent loading on transcutaneous partial pressure of oxygen and blood flow have also been investigated. The sacrum was loaded with an interface pressure for a period of about 12 minutes and then the load was removed for about 3 minutes (Bader, 1990). The loading cycle was subsequently repeated. During each loading period there were fluctuations in Tc-pO_2. For most subjects there was partial recovery during the initial loading period. Also the effects of the applied load decreased with successive loading cycles. However for certain people from the group of subjects who were elderly, immobile or insensitive to pressure, a different response to repeated loading was observed. There was no recovery during the initial loading period and the Tc-pO_2 returned to its initial value very slowly after the load had been removed. Also successive loading periods further reduced the Tc-pO_2 readings.

It is thought that bacteria can contribute to tissue breakdown or delayed healing of pressure sores. Daniel et al (1985) compared the formation of pressure sores in paraplegic pigs which had, and had not been injected with staphylococcus bacteria. They found that greater tissue damage occurred in the pigs which had been infected, and the bacteria accumulated in the damaged area. A correlation between fecal incontinence and the presence of pressure sores has also been shown in hospitalized patients (Allman, 1986). Other studies have been reported which show significant correlations between the patient's age, the presence of fractures, tobacco smoking, length of paralysis, protein malnutrition, anticoagulation therapy and the presence or worsening of pressure sores (Jordan & Barbenel, 1983; Pinchofsky-Devin & Kaminski, 1986; Allman et al, 1986; Frisbie, 1986; Thiyagarajan & Silver, 1984; Lamid & El Ghatit, 1983). However these studies do not show causative relationships, because of the difficulties in finding a control group in which the other pressure sore related factors are equivalent.

Pressure sores occur when cell death results from the application of external loads to the soft tissues of the body. The intermediate stages to presssure sore formation are not well understood. Some hypotheses for the formation of pressure sores are discussed below. Krouskop et al (1978) suggested that a major factor contributing to tissue necrosis in pressure sores is anaerobic metabolic waste products accumulating in the tissues where lymphatic drainage is restricted. Lymphatic drainage is brought about by the contraction of smooth muscle in the lymphatic vessel walls. Surface loading of the soft tissues could create the hypoxic conditions which can damage smooth muscle, thus impairing lymph drainage. During hypoxia substances such as histamine, which further inhibit smooth muscle activity are released into the body fluids. In 1981 Reddy et al suggested that interstitial fluid may also have a crucial role in the formation of pressure sores. Interstitial fluid may flow out of the tissues which are under load and this could result in direct contact between the fibroblast cells. The contact could inhibit collagen synthesis or even cause cell wall rupture. On removal of the load a negative intercellular pressure could result in capillary bursting.

In 1983 Krouskop integrated and expanded on these proposed mechanisms of pressure sore formation. He suggested that in anoxic conditions and when certain trace elements are not available, collagen is synthesized which is unstable at room temperature and is water soluble. As the collagen is washed out of the soft tissues, any load applied to the tissues is transferred to the other soft tissue components such as fibroblast cells, blood and lymph vessels, interstitial fluid and elastin fibres. This could then lead to interstitial fluid flow and restricted lymphatic drainage. So factors such as diet, spinal cord injury and emotional stress which affect the collagen metabolism are important factors in pressure sore formation. Also as a person ages the collagen in the body becomes stiffer and less strong. Also the amount of elastin in the tissues is reduced. These changes could reduce lymphatic drainage and increase interstitial fluid transport when the tissues are subject to surface loading. A schematic diagram of the mechanism suggested by Krouskop is shown in Figure 2.

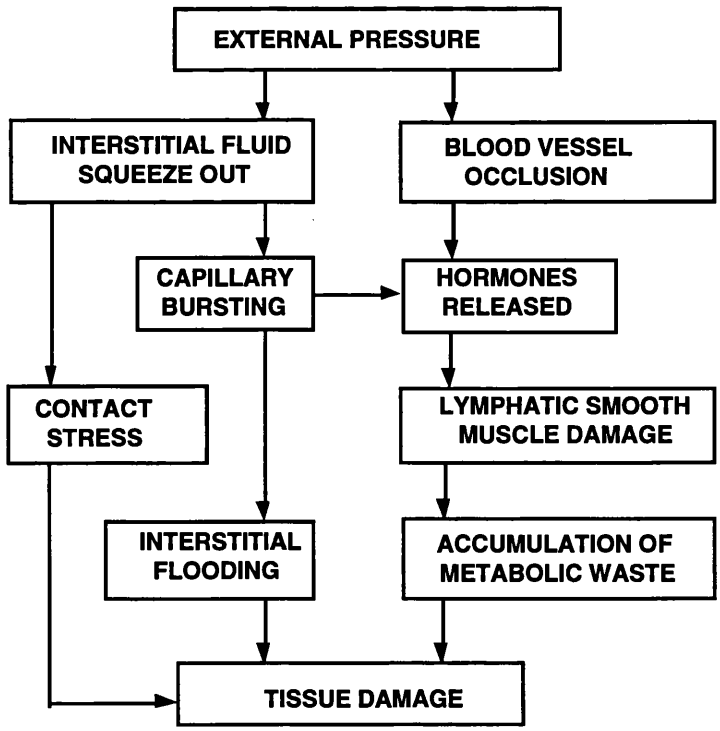

FIGURE 2

Possible stages in the formation of a pressure sore (Krouskop, 1983)

It has been suggested that loading the skin surface could cause dermal fibrinolytic inhibition and this would lead on to fibrin deposits in the intercellular space and capillaries; this could cause capillary occlusion and reduced nutrient transport to the cells, leading to cell necrosis when the tissues are under load, and prolonged healing of pressure sores (Seiler and Stahelin,1986). The authors measured low fibrinolytic activity in the dermal tissue around a pressure sore compared to in other regions. However this hypothesis does not explain the subcutaneous origin of many deep pressure sores. Also the reduced fibrinolytic activity may have been an effect rather than a cause of the pressure sore.

From the above review it is apparent that empirical studies to examine the formation of pressure sores have been limited by the inaccessible location of many sores and the unacceptability of causing a sore on a human subject. Nevertheless external applied pressure and pressure duration have been shown to be crucial factors in pressure sore formation. The hypotheses put forward by Krouskop and Reddy are consistent with the effects of load magnitude and duration. Unfortunately the experimental methods that are available do not give sufficient information on the intermediate biochemical and biomechanical events to test out these hypotheses.

It would be useful to have more information on the critical intermediate mechanical and biological stages in the formation of a pressure sore. It has been shown that when a load is applied to the body surface the localised response of the tissues depends on the anatomical location of loading, the direction of loading and the pathology of the person. Also early damage to deep subcutaneous tissues has been observed. It might be found that factors such as paralysis, age and metabolic condition affect the nature and extent of the soft tissues around the bony prominences and therefore the stresses and strains that develop in the tissues in response to an applied load. The application of surface shear stress is also likely to affect the internal stresses and strains. The few studies that have examined load transfer through the tissues under the influence of a compressive load are discussed in Section 1·4.

1.4 Material Properties of the Soft Tissue of the Buttocks

General Description of Properties

In this section the properties of the dermis, adipose tissue, muscle and the combined soft tissues are briefly discussed in terms of their composition. Soft tissues are anisotropic and highly inelastic. They show stress relaxation when held at a constant strain. When held at a constant stress they show creep behaviour. They show hysteresis when subject to cyclic loading and unloading. When repeated cyclic loads are applied to a specimen, the load-elongation curve alters over the initial cycles but eventually reaches a steady state. This process is called preconditioning. For many tissues the cyclic loading and unloading curve is largely insensitive to strain rate. Also under most test conditions the stresses in the soft tissues are highly nonlinear with respect to strains; the gradient of the stress-strain curve increases with increasing strain.

With subcutaneous adipose and dermal tissue, properties are largely determined by the state of the network of collagen and elastin fibres. Elastin fibres are virtually elastic up to large strains. The stress-strain curve for a uniaxial extension is close to linear. Collagen fibres have higher stiffness and strength compared to elastin fibres. At small tensile strains, the elastin fibres elongate and the collagen fibres begin to align along the direction of tension. The tissues are in a relatively low stiffness region. As the strain increases the collagen fibres straighten out and support a greater amount of the load. Once the collagen fibres are aligned, the tissue stiffness along the direction of alignment is much greater (for example, Markenscoff & Yannas, 1979; Manscot & Brakkee, 1986). The ultimate tensile strain in dermal tissue can be from less than 60 to over 100 percent, depending on the age of the person, whereas the U.T. strain in adipose tissue is about 25 percent (Yamada, 1973; Duck, 1990). During the preconditioning process the structure of the tissue organises with the cycling. Eventually a steady state is reached at which no further changes will occur.

Muscle tissue is composed of fibres grouped into bundles. Each muscle fibre is made up of interleaved bundles of the proteins actin and myosin. Connective tissue fills the spaces between fibres within a bundle. Each bundle is surrounded by a stronger connective tissue sheath and the whole bundle is surrounded by an even stronger sheath, at which significant movement can occur. Young's modulus is found to be very much larger in tense muscle compared to relaxed muscle. Values of 0.0062 MPa and 0.11 MPa were reported at 10 percent strain in relaxed and in tense muscle respectively (Krouskop et al, 1987). The measurement method used to obtain these values is described later in this section. The ultimate tensile strain in muscle is between 50 and 100 percent (Yamada, 1973; Duck, 1990).

The flow of extra-cellular fluid in a compressed region of soft tissue contributes to the viscous component of tissue deformation (Tregear, 1966). Ziegert and Lewis (1978) compared the indentation response of the combined soft tissues covering the anterior tibia and of a physical model where rubber was used to simulate the soft tissue layer. In some tests the stiffness of the soft tissues was larger when it was measured with indenters of small contact area, compared to when it was measured with large indenters. However with the rubber model, the smaller indenters gave smaller stiffnesses. The authors attributed the difference between the model and the soft tissue system to the flow of extra-cellular fluid from under the small indenter. With the tissue system the smaller indenters could displace more fluid and the remaining soft tissues would become stiffer, whereas fluid flow could not have occurred in the rubber.

The combined soft tissues at specific anatomical sites have a stiffness which increases with compressive strain, when subject to indentation tests (Todd, 1989; Bader & Bowker, 1983; Zeigert & Lewis, 1978). The slope of the stress-strain curve is approximately linear in the high strain region. Also it has been shown that the soft tissues become stiffer and more viscous with age (Kirk & Kvorning, 1949; Kirk & Chieffi, 1962; Alexander & Cook, 1976). This is thought to be due to an increase in the cross links between collagen fibres and an increase in the porosity and permeability of the soft tissues (Bader & Bowker, 1983).

Previous Studies to Determine Material Properties

Studies to determine the material properties of soft tissues are reviewed. Testing methods, experimental data and mathematical representations are included. The material properties of the soft tissues are usually measured by applying a known load and by measuring the associated changes in dimensions. Testing may be on living tissue or on excised soft tissue specimens. In vitro, specimens of known composition and dimensions can be tested under well defined loading conditions. However once the specimen is taken out of the body, the tissue properties may be altered by fluid-loss and the trauma of dissection. With in-vivo testing, the interaction between the different tissues and tissue components contributes to the measured deformations.

Constitutive equations may allow one to predict the deformations which would result from the application of specified forces, since they express in an intrinsic manner the response of a material to a force. The coefficients in the equation can be calculated by measuring the response of a material to a known load. The formulations that are normally used to characterize the behaviour of engineering materials are of limited use in describing the behaviour of the soft tissues under generalized loading conditions because of the complex structure of the tissue. Mechanical testing methods range from direct load application to acoustic interrogation. Indentation tests are mainly reviewed in the following paragraphs. The loading of the soft tissues in the indentation tests is similar to the loading of the soft tissues when a person is seated, in that the skeletal bony prominences can be considered to make an indentation into the soft tissues as the body is loaded against a seat.

A **linearly elastic** model can be used to characterize the soft tissues. Often small cyclic peturbations about an equilibrium state are measured and the modulus calculated from the gradient of the stress-strain curve. The calculated modulus is specific to the strain state in the tissues. It may be applicable to deformations at different strain rates for tissues whose behaviour is insensitive to strain rate.

A mathematic analysis of the indentation of articular cartilage by a rigid punch was developed by Hayes et al (1972). The articular cartilage was modelled as a linearly elastic infinite layer, rigidly restrained on its underside. Expressions were obtained for indentation by a plane-ended cylinder and by a sphere. The shear modulus of the articular cartilage was found to be a function of load, indenter displacement, cartilage thickness, indenter geometry and Poisson's ratio. It was assumed that only small strains developed in the cartilage, that negligible friction developed between the indenter and the cartilage, and that there was negligible deformation of subchondral bone. Cartilage is viscoelastic, so the deformation has to be measured either immediately after a step load has been applied or after the creep phase when an asymptotic level of indentation has been reached, for consistent results to be obtained. The modulus however is only valid under these conditions. Armstrong et al used the expression derived by Hayes to estimate Young's modulus for articular cartilage in compression (1980). They tested specimens from the femoral heads of human subjects.

Young's modulus of the combined skin and subcutaneous soft tissues of the thigh and forearm have been estimated using Hayes' expression (Bader and Bowker, 1983). Both young, healthy subjects and elderly subjects were tested. A 20 mm diameter plane ended indenter was used on the forearm and a 40 mm diameter indenter on the thigh. Poisson's ratio was assumed to be 0·3 and the thickness of the tissues was estimated with skin fold callipers. Loads of 3·7 and 8·8 N were applied through the forearm and thigh respectively. The stiffness modulus was calculated to be between 1 and 3 kPa and to vary with age, sex and anatomical site. It is likely that linearly elastic, small strain conditions did not strictly apply during all stages of the tests. Also the values for the stiffness modulus are highly dependent on the value of Poisson's ratio. Poisson's ratio was assumed rather than measured.

The wide variations in the elastic moduli of the soft tissues have been reported between different subjects, anatomical sites and authors. These variations can be partly accounted for by differences in tissue composition between specimens. Also the derivative of the stress - strain curve under finite loading conditions is not identical to the derivative of the stress-strain curve under a small displacement about an equilibrium condition. In addition the strain level may not be consistent between the tests.

The time dependent material properties of the tissues have been characterized with **viscoelastic** models. Relaxation and creep curves can be established for a material together with its response to a periodic forcing function. For cyclic oscillations the amplitude and phase angle of the complex modulus can be plotted with respect to the frequency of oscillation. If a model can be found whose relaxation, creep, hysteresis and complex modulus agree with the experimental data, then the material can be described by this model. The constants are determined by curve fitting against the experimental data. The determination of the constants is not unique, so many functions may fit the data.

Wave propagation techniques have been used in a study where the tissue properties in the residual limb of amputees were measured *in vivo* under a compressive load (Krouskop et al, 1987; Malinauskas et al, 1989). It was assumed that the tissues can be represented as a linear viscoelastic 'Kelvin' medium that is isotropic and orthogonal. A pulsed Doppler ultrasound device was used to apply a sinusoidal acoustic peturbation, that was a combination of pure shear and pure compression at a frequency of about 10 Hz, to the skin surface. The phase shift in the returning wave from various tissue depths was measured from three locations in the device, so the components of displacement could be calculated. The Doppler methodology can be used for *in vivo* subcutaneous measurements of tissue properties because contact with the tissue being measured is not necessary. The depth resolution was better than 0·1 mm.

The creep and stress relaxation behaviour of soft tissues have been characterized with continuous relaxation and retardation spectra (for example Barbenel, 1972). It is assumed that the spring and dashpot elements are numerous and form a continuous distribution over retardation time (τ). In one study a generalized Kelvin model was utilized to describe articular cartilage under a constant compressive load (Parsons and Black, 1977). Assuming numerous and closely spaced retardation times the creep function for the model is :-

$$J_d(t) = \int J(\tau)\,[1 - \exp(-t/\tau)]\;d\tau \qquad J(\tau) = \text{retardation spectrum}$$

From the substitution $\tau J(\tau) = L(\tau)$ it can be shown that the part of the integrand in brackets can be approximated to a step function and the first derivative of the viscous component of compliance with respect to the logarithm of time gives an approximate value for $L(\tau)$ at that time. For articular cartilage, the curve of compliance against the logarithm of time was approximately linear between 0·42 and 1184 seconds after the load had been applied and was flat in the other regions. Thus the retardation spectrum was constant between these times and was zero at other times.

Bader and Bowker (1983) used the generalized Kelvin model described above to characterize the time dependent deformation of the combined soft tissues of the forearm and thigh under constant indentation loading. The curve of compliance against the logarithm of time for the soft tissue was found to be a continuous curve which generally increased with time. The authors attributed this variation in retardation spectrum to the relative movement between soft tissue components.

The linearly viscoelastic models do not take account of structural changes in the material, such as interstitial fluid flow leading to an internal redistribution of the phases within the material. Also the nonlinear stress-strain characteristics of the tissues are not taken into account, so models are normally only valid under infinitisimal strain conditions. In addition models may not be valid under test conditions other than the ones used to establish the material constants. Fung (1972,1981) developed nonlinear constitutive equations by considering relaxation functions that were functions of strain, and creep functions that were functions of stress. These were more applicable to finite deformation conditions than the linear models discussed above. He also proposed a model involving a continuous spectrum of time constants, that had hysteresis behaviour which was insensitive to the frequency of cyclic loading.

Hyperelastic models have also been used to characterize the behaviour of the soft tissues. When the tissues are deformed, it is assumed that the stored strain energy is a function of the deformation state. The form of the strain energy density function in the model is proposed, and the stress-strain relationship obtained from the strain energy function by differentiation. The behaviour of the model is compared with the deformation behaviour of the tissues under the same experimental conditions. Strain energy functions with polynomial and exponential terms have been examined for tissues such as mesentery, skin, arteries and lung tissues. Fung has been an important investigator in this area (for example Tong & Fung,1976; Fung, 1981).

The functions utilize finite deformation theory and thus the models are applicable to large strain conditions. The models are most useful when there is a unique relationship between stress and strain in the soft tissues under a specific loading state. For cyclic loading and unloading the functions describe the behaviour after preconditioning, and it is assumed that the behaviour is insensitive to strain rate. The inelastic aspects of the behaviour of the soft tissues cannot be described with these models. Some of the studies to test out proposed functions for soft tissues under various loading conditions are described in the paragraphs below.

Veronda and Westmann have used a hyperelastic model to described the behaviour of cat skin *in vitro* (1970). The skin was subjected to incremental uniaxial loads, so the axial extension increased from 1 to about 2. At each load increment the skin was left to reach its equilibrium state before the extension was measured. The skin was found to be compressible and anisotropic under the experimental conditions. However the cross-sectional area was assumed to be isotropic in the formulation of the strain energy function from the experimental data. The strain energy function that was found to give a reasonable approximation to the behaviour of the skin was as follows:

$$W = c_1 (\exp\beta(I_1-3)-1) + c_2 (I_2-3) + g(I_3)$$

c_1, c_2, β are material constants; W is the strain energy density; I_i are the strain invariants; $g(1) = 0$. The values of the material constants were obtained by curve fitting against the experimental data. The applicability of the function to multiaxial data was not tested.

In a similar study Allaire et al modelled the uniaxial tensile behaviour of skin *in vivo* (1977). The strain energy function was assumed to be :

$$W = A (I_1-3) + B (I_2-3) + C (I_3-1)^2 - (A+2B) (I_3-1)$$

A, B and C are material constants. Once again in this study it was assumed that orthogonal strains normal to the applied stress were equal. Furthermore the strain normal to the skin surface was estimated rather than directly measured. The model was found to be valid only over a limited extension range (extension ratios from 1 to 1·25). The value of the constant B was found to be negative and of similar magnitude to the constant A (about 5×10^5 N/mm^2).

Sahay et al used a similar approach to characterize the material properties of brain tissue (1992). A simple spherical shell model of the brain was assumed. The internal space contained ventricular fluid and the space surrounding the brain was filled with epidural fluid. The inflation in the brain under finite strain conditions was found to depend on the magnitude of the pressure difference across the tissue, the radial thickness of the shell and the properties of the shell material. The Hart-Smith function was proposed as the strain energy function to describe the brain tissue. The derivatives of this function are shown below:

$$\frac{\partial W}{\partial I_1} = G\exp\left(k_1(I_1-3)^2\right) \qquad \frac{\partial W}{\partial I_2} = G\frac{k_2}{I_2}$$

G, k_1 and k_2 are material constants. The experimental data was obtained from brains of 10 dogs. Fluid was infused into the ventricular space in the brain at a controlled rate and the changes in ventricular and epidural pressure were measured. The correlation between the theoretical and experimental results was good at high pressures, but was less good at lower pressures.

Biaxial loading gives a fuller picture of the relationship between stress and strain components, than the uniaxial loading described above. Tong and Fung (1976) proposed a strain energy function for rabbit skin under biaxial tensile loading in plane stress conditions. In this stress state the strain energy is a function of the in-plane strain components (e_{11}, e_{22}, e_{12} where e_{ij} are the components of the Lagrangian finite strain tensor). It was found that the stress-strain relationship for the skin under cyclic loading and unloading was unique after pre-conditioning, and the behaviour was insensitive to strain rate. The proposed function was as follows:

$$\rho_o W = \frac{1}{2}(\alpha_1 e_{11}^2 + \alpha_2 e_{22}^2 + \alpha_3 e_{21}^2 + \alpha_3 e_{12}^2 + 2\alpha_4 e_{11} e_{22})$$

$$+\frac{1}{2}(c\exp[a_1 e_{11}^2 + a_2 e_{22}^2 + a_3 e_{12}^2 + a_3 e_{21}^2 + 2a_4 e_{11} e_{22} + \gamma_1 e_{11}^3 + \gamma_2 e_{22}^3 + \gamma_4 e_{11}^2 e_{22} + \gamma_5 e_{11} e_{22}^2])$$

where α_i, a_i, γ_i and c are constants and ρ_o is the density of the material. The constants were determined from the experimental stress-strain relationships with the strain e_{11} fixed and then with the strain e_{22} fixed. After the constants had been calculated for a particular specimen in a specific experiment the function fitted the data from that test well, but had only limited success at predicting behaviour from another experiment (same specimen, different transverse stretch, different preconditioning).

Hyperelastic models for the soft tissue are valid under the finite strain conditions that are often encountered in the soft tissues when the body interfaces externally with load carrying devices. However it is difficult to take account of the inelastic, anisotropic nature of the soft tissues with models such as those described above. The experimental conditions in the above studies are unlike those in the present study, so immediate conclusions cannot be drawn on the validity of this approach for modelling the soft tissues of the seated buttock. The approach is examined in more depth in subsequent chapters of this thesis.

Structurally based theories have been developed to describe tissues as diverse as skin and articular cartilage. Lanir has developed structural models for the stress-strain relations in specimens of fibrous connective tissues with various geometries and loading conditions. Lanir's conceptual model for deformations in flat membranous tissues consists of a linearly elastic network of elastin fibres and an undulating network of linearly visco-elastic collagen fibres. The collagen fibres are relatively stiff when straightened out. The initial analysis for biaxial deformations was based on structure and equilibrium considerations (1979). The behaviour of the material was found to depend on the material properties of the fibrous components and also the initial distribution of fibres through the material. Thermodynamic considerations were introduced later to simplify and extend the analysis (1983). Shoemaker showed that a similar structural model could fit bi-axial experimental data from human skin and canine pericardium (1986). However the calculated material parameters did vary between different tests on the same specimen and so were not generally applicable to all deformation states.

Multiphase theories have also been developed to describe the dynamic behaviour of hydrated connective tissues. The theoretical equations to describe the system are derived from the continuity equation for the mixture, momentum balance equations for the two phases within the mixture and the constitutive equations for the solid and liquid phases. One of the first multiphasic theories developed was linear biphasic theory (Mow and Lai, 1980). The solid phase in the tissue was assumed to be isotropic, incompressible, porous, permeable and linearly elastic. The fluid phase was assumed to be inviscid and incompressible. In an extension to this model, the nonlinear permeability of the solid is taken into account. The extent of fluid motion depends on the permeability of the solid phase, which depends of the level of dilatation in the solid matrix. The behaviour of the model was found to resemble the compressive creep and stress relaxation behaviour of articular cartilage under low load levels and low strain rates.

The biphasic theories discussed above are limited to application in systems with infinitesimal strain conditions, however more recently a finite deformation biphasic theory has been developed by Kwan et al (1990). The constitutive equations for the solid and liquid phases are derived from strain energy density functions that are scalar functions of Green's deformation tensor. The particular form of the function was selected that gave a physically realistic response. Analytical results compared well with experimental results on articular cartilage under one-dimensional confined compression.

Lanir has characterized the instantaneous response of the skin on the human forehead to indentations of small magnitude with a finite deformation biphasic theory (1990). The skin was assumed to be an incompressible solid-fluid mixture. The solid phase was linearly elastic in the plane of the skin. Normal to the plane of the skin the fibres were assumed to lose their stiffness under compression. Normal and in plane deformations were assumed to be independent. The loads supported hydrostatically in the fluid were also taken into account. With a suitable choice of material constants, the theoretical model was found to resemble the experimental results. This model only has application to modelling the instantaneous response to small deformations in thin soft tissue layers, because of the assumptions in the development of the model. It could not be expected to describe the seated buttock which has a greater depth of soft tissue and undergoes greater deformations. Also the state of the tissue after the flow of extracellular fluid had ceased is of interest for this system.

The structural models described above help our understanding of the behaviour of the soft tissue. Unfortunately they are not at present well enough developed to be used directly to model the seated buttock which has a complex geometry, contains multiple materials and interfaces, and undergoes large deformations.

Measurements of Load Transfer Through the Soft Tissues

There have been a few studies to examine how a load, applied to the surface of the skin, is transferred to the underlying soft tissue structures. The coupling between skin surface loading, load transfer to the tissues and deformation within the tissues has been studied using animal models. The experimental data relating to load transfer is very limited.

Le et al measured the pressure within the tissues and interface pressures around the trochanter of paraplegic pigs as they lay supported against a flat surface (1984). The tissue pressure was measured through a hypodermic needle. The needle was initially inserted into the tissues within a larger diameter needle, the purpose of which was to guide the sensing needle. The larger diameter needle was withdrawn from the tissue after insertion. The pressure was transmitted to a miniature solid state pressure sensor. A fluid injection system gave a constant flow of fluid through the needle to the tissues. The measured pressures were found to increase with depth below the skin surface and were greatest directly under the bony prominence. Maximum in-tissue pressures over five times those at the body-support interface were measured in vivo.

Dodd and Gross measured the pressure in the soft tissues over the iliac wings and over the last dorsal spinous process of pigs when 4 and 8 Kg loads were applied to the skin through a foam pad (1991). Interface pressures were also measured. A modified wick-in-needle catheter was used to measure the pressure in the tissues. A window was ground in the side of a hypodermic injection needle. The needle was then filled with a Teflon-impregnated, polyester fibre. The system was conected to a solid state pressure transducer. The purpose of the fibre was to allow the tissue pressure to be transferred up the needle to the measurement system. The authors found that over the spinous process the tissue pressures were about 42 percent of the interface pressure where as only about 28 percent of the load was transferred to the interstitial fluid over the iliac wings. Pressures in the tissues of up to 81 mmHg (10.8 kPa) were measured. The difference between the load transfer characteristics reported by Le et al (1984) and Dodd & Gross (1991) cannot fully be accounted for by variations in anatomy and methodology at the test sites. It may be that in the earlier study, the hypodermic needle caused altered hydration states, leading to high pressure readings in the tissues. The above studies help us to understand how a load is shared between the hydrostatic and distortional components when it is applied to the skin surface.

Dodd & Gross also measured the internal deformations in the tissues over the iliac spine of a pig using stereoradiography. Radio-opaque markers were implanted in the tissues around the iliac spine (1991). The position of the markers was recorded radiographically from two positions when loads were applied to the skin surface through a foam pad. The displacement of the markers was then calculated from the position data. Displacements as large a 14 mm were measured after prolonged loading. The authors reported that three-dimensional shearing occurred in the tissues. There did not appear to be twisting in the soft tissues about the vertical axis. The position of the origin relative to the bony prominence is not well documented in this study, and thus the precise tissue deformation that occurred at the bony prominences cannot be identified.

In spite of the incomplete knowledge of the material properties of the tissues and the limitations of the mathematical representations, the loading of the tissues has been studies with analytical models. Some of the models are discussed in the next section.

1.5 Previous Stress Analyses Involving Soft Tissues

Stress analyses of the soft tissue which aim to improve our understanding of its behaviour and to predict its response to a load are discussed in this section. The meniscus of the knee has been analysed, as have the soft tissues at the buttock and in the residual limbs of amputees. It is difficult to construct a realistic model of combined soft tissue systems such as the buttock, if the model is based solely on measurements of isolated components such as muscle and skin. There undoubtedly are deformation mechanisms involving interaction between soft tissue components. For example, the gluteal muscles may slip laterally with respect to the ischial tuberosities during sitting and the extent to which they are able to move depends on whether gluteal bursae are present.

Most authors have assumed a linearly elastic stress-strain relationships for the soft tissues. Chow and Odell (1978) used the finite element method to investigate the stresses and deformations in the buttock during sitting. A 33 element axisymmetric mesh was used to model the soft tissues surrounding a rigid bony core. The soft tissue was modelled as a linearly elastic, homogeneous isotropic layer with Young's modulus of 15 kPa and Poisson's ratio of 0·49. Various load and displacement conditions were applied to the nodes on the external surface of the soft tissues. These were to simulate the buttock supported by fluids, by a rigid friction-less flat surface, by foam cushions and by a modified cosine pressure distribution. An iterative procedure was used to take account of the changes in element orientation that occur during the solution, whilst still retaining infinitesimal strain theory in the model. The authors proposed that von Mises stresses are important indicators of a risk of pressure sores in the tissues, since they show the degree of deformation in an incompressible material. Both the von Mises and hydrostatic stresses within the model were examined. It was found that the more uniform the pressure loading at the interface, the greater the fraction of the load supported hydrostatically and the lower the von Mises stresses in the elastic layer. Young's modulus was selected from measurements on a synthetic gel, and the results of the analyses were compared with results from a physical replica where a gel was used to simulate the soft tissues. These factors limit the extent to which the model resembles the human buttock.

Todd (1990) has also used finite element modelling to examine the deformations and the stresses in the tissues during sitting. She has reported a 2-dimensional plane strain model of the buttock with a combined muscle and fat layer (Young's modulus 14 kPa ; Poisson's ration 0·49) and a skin layer (Young's modulus 50 kPa ; Poisson's ration 0·3). Reynolds (1988) produced FE models of lower limb amputation stumps. This work was intended to be an aid to the computer-based design and manufacturing system for lower limb sockets (Dewar & Reynolds, 1986). Youngs modulus values for the soft tissues in the finite element model were calculated from indentation tests on the leg. Values ranged from 50 kPa in the popliteal region and medial to the tibia on the anterior surface of the leg, to 145 kPa in the region of the patellar tendon. Poisson's ratio was assumed to be 0·45. The analyses suggested that interface friction and distal end bearing have the most significant effect on the load distribution within the soft tissues. In common with Chow's work these analyses assumed linear elasticity and infinitesimal strain theory. Iterative loading was used to take into account changes in element orientation during loading. Unfortunately with this method the solution does not take into account changes in element area as it procedes. The error in the large deflection solution increases with the incompressibility of the material and the size of the applied strain. This limitation is discussed in depth in Chapter 4.

A biphasic description of the tissue was employed in an axisymmetric finite element model of the meniscus in the knee (Spilker et al, 1992). An incompressible linearly elastic solid phase and an incompressible, inviscid liquid phase were considered. The solid phase had a much greater modulus in the circumferential direction, compared to in the transverse sections which was considered to be isotropic. This particular formulation was selected because of the circumferental fibre distribution in the meniscus. Infinitesimal strain theory was used so there was a limit to the magnitude of the deformations that could be studied. The initial dynamic response of the model to a step load at the femoral surface was examined. During the initial period after the onset of loading, the fluid phase carried a large part of the applied load. The maximum internal pressure in the fluid was larger in magnitude than the maximum transverse stresses, and of similar magnitude to the circumferental stress in the solid phase. The pressure in the fluid phase decreased as it flowed out of the loaded area.

Some studies have used nonlinear elastic material properties and finite strain theory to model the soft tissues. A two-dimensional plane stress physical model of the buttock was developed by Reddy et al (1982). The model was made of a semicircular slab of P.V.C. gel cast around a wooden core. The gel simulated the soft tissue around the ischial tuberosity. A grid of shallow holes filled with white paint was etched into the gel. This allowed the deformations in the gel to be photographed when the model was loaded vertically against various cushion surfaces. The finite strains and extension ratios were then calculated from the displacement measurements at each grid point. The form of the strain energy function relating strain energy density (W) to the principal strain invariants (I_1, I_2, I_3) was assumed to be $W= A(I_1-3)/2$ for the P.V.C. gel. It was assumed that the gel was incompressible and the value of the constant A was 6 kPa. The principal stresses in the gel were calculated from the principal extension ratios. Regions of high compresive and shear stress were identified. The authors compared the performance of various cushioning materials (1982 and 1987). The effects of the shape of the bony tuberosity were also investigated with two similar models (Cadadai & Reddy, 1992). The study showed that in general shear stresses obtained with a cylindrical columnar bony core were greater than those obtained from the model with a bony core with a rounded end. These studies are limited by the extent to which the gel can resemble the soft tissues of the buttock. The model cannot take into account the anisotropic and viscoelastic nature of fluid-filled tissues. But the theory upon which the studies are based, is valid under the finite strain conditions that are encountered in the soft tissues, unlike with the analyses discussed previously. There is a nonlinear relationship between stress and strain with a gel. For the material defined by the above strain energy function, the material would stiffen with increasing uniaxial compression, similarly to the soft tissues, but would soften under increasing uniaxial extension. Another limitation of the studies is that more comprehensive testing of the gel would probably have shown that it could not be accurately described by the above strain energy function (Treloar, 1975). Also the tissues in the section through the buttock are unlikely to be in a state of plane stress, as was the gel in the two dimensional model.

1.6 Current Designs of Wheelchair Cushion and Seat

Current designs of wheelchair cushioning and seating are reviewed in this section. The basic seat in most wheelchairs comprises a seat and backrest that are made of material. A cushion may be required on a wheelchair seat to improve comfort, reduce the risk of pressure sores and provide some postural support to the seated person. There are more comprehensive seating systems available for people who require a greater level of postural support or comfort when they are sitting in their wheelchair.

Some cushions are filled with a fluid such as a thixotropic gel, air or water. The body is intended to sink into fluid-filled cushions, so that there is a large area of the body available for load bearing. The fluid should flow until it provides a uniform support over the body/seat interface. A thixotropic gel has a temporary reduction in viscosity when disturbed, but then becomes more viscous. Thus the gel flows away from the higher load bearing areas of the body when it is initially sat upon and the cushion then stabilizes. A tensioned, curved membrane produces a radial pressure. When someone sits on a cushion, significant tension may occur within the covering material in the area of maximum curvature (Shaw & Snowdon,1979). If this is under the bony prominence, loading of the body will become concentrated at these locations. In many current designs of fluid-filled cushion, cover tension has been minimised by the presence of excess material in the bag containing the fluid, and by dividing the bag into separate sections.

The body-cushion interface temperature does not usually become elevated after a period of sitting on gel and water-based cushions (Seymour & Warren,1985). This effect is probably due to the relatively high heat capacity of gel and water in these cushions. This feature is beneficial for the comfort of people in a warm environment and for controlling the metabolic rate in the tissues at that location. Some gel and water-filled cushions are heavy, weighing up to six kilograms. Such cushions can be inconveniently difficult to lift in and out of chairs. The displacement of the fluid within the cushion as a person's centre of gravity shifts about can lead to sensations of unsteadiness. This problem is reduced in cushions where the flow of the gel is limited by separate compartments with restricted orifices between them or by the presence of foam inside the cushion. Gels get used in combination with other materials in many cushion designs. These designs exploit the weight distributing properties of gels while reducing the stability and cover tension problems discussed above.

Most foam cushions are made from polyurethane and are light in weight, less expensive than other specialist cushions and available in a wide range of shapes, sizes and hardnesses. Foams used in a cushion to support the weight of the body usually have an indentation hardness (BS 4443 Part 2, Method 7) between 125 and 250 newtons. The values correspond to the force required to produce an indentation of 40 percent of the thickness of the test specimen under specified loading conditions. Foam cushions can degrade fairly rapidly during service; there is a decrease in hardness, thickness and load-distributing properties. Bottoming out may occur and may result in an increased discomfort and a risk of pressure sores. An elevated temperature, a moist environment, prolonged loading and exposure to ultraviolet light are all thought to contribute to the phenomenon (Noble et al, 1984). Polyurethane foam in the untreated state is flammable. Foam for cushioning has to be combustion modified, so that it is less flammable. Cushion covers also have to be made of a flame resistant material (Statutory Instrument, Furniture & Furnishings (Fire) (Safety) Regulations, 1988). Foam cushions such as the Vasio-Para™ have been shaped with cut-outs under the areas where the body weight should be relieved. The Vasio-Para has a large cut-out area over the ischial tuberosities, sacrococcygeum and perineum. In order to reduce the tension in the upper layers of the foam (which localises loading under the bony prominences) the upper region of the foam can be cut into a series of contiguous blocks. These blocks can be compressed without building up tensile forces along the surface.

Some severely disabled people may require a support over multiple areas of their body due to poor postural stability and established or potential skeletal deformities. A moulded seat (Nelham, 1975), a shapable matrix seat (Cousins,1982), or a bead seat insert (Silverman,1986) may offer an effective support. Moulded seats are made of vacuum formed sheets of thermoplastic and plastazote. The matrix body supports are made from plastic and metal components linked into a matrix by ball and socket joints. They can be adjusted at the joints, so that many shapes can be produced. Bead seat inserts are made of polystyrene beads in a polyurethane matrix. All these seating systems are lined with compliant foams to improve on comfort and can be fitted into a mobility base.

Body-contoured seat cushions can be used to control pelvic position, accommodate deformities of the pelvis, hip and femur, redistribute the body weight away from pressure sensitive areas and improve comfort (Michael & Walker,1990; Sprigle et al.,1990- B; Sprigle & Chung, 1989; Sprigle et al.,1988). They do not provide any support directly to the trunk. 'Off the shelf' seats and cushions with shallow contours are useful for some people who have difficulty maintaining their pelvic position and who suffer from discomfort over the buttock during sitting. The improved control of the pelvic position may have a beneficial effect on trunk position. A much more intimate support is possible with individually contoured seats and cushions. Individualised contoured cushions have been used for pressure sore prevention by some chair bound people. It is possible to tailor the support to the person's individual requirements. It is necessary to measure the shape of the buttocks for an individually contoured cushion to be produced.

1.7 Methods of Measuring Body Surface Shape

Body surface shape measurement methods that have potential application to the production of shaped seating are reviewed in this section. The shape of the buttocks is highly dependent on the position of the skeleton, muscle tone, externally applied loads and the direction of gravity. Thus the body has to be in a sitting position during shape measurement for seat production. Another consideration is that with some measuring devices that make contact with the body surface, the surface may become distorted by the measuring procedure.

There are two categories of body surface shape measurement techniques. There are techniques where an impression of the body is made in a deformable material and the deformation is measured. There are also techniques where no physical contact is made between the body and the measuring device. One approach to seat design is for the body shape to be measured when the weight of the upper body is supported through the buttocks and optimally distributed through the tissues to avoid pressure sores, maintain comfort and maintain the required posture. This approach lends itself to the former category of measurement techniques.

There is a facility at the University of Virginia for measuring the shape of the interface between the body and various foam support surfaces (Brienza, 1988; Sprigle & Chung, 1989). The facility was developed as part of a CAD/CAM wheelchair cushion production system. They have built a chair, which has a flat polyurethane foam block as the seat. A matrix of 64 linear potentiometers is embedded in predrilled holes in the foam block. During measurement, the subject sits on the foam and the interface depth is calculated from the potentiometers' output voltages. A linear interpolation between these depth measurements is made on a computer. A pin-matrix shape measurement system has been developed and works on similar principles (Gargano et al, 1986). The seat of the measurement chair is an array of metal rods with spheres at their ends. The rods are supported on an air-filled bladder. The subject sits on the chair and the rods are locked into position. A customised cushion is subsequently produced from the shape formed by the pattern of rod ends.

Vacuum consolidation is by far the best established method of replicating the shape of the body for seating (Cochrane,1990; Nelham, 1975; Bardsley; 1984). An impression of the body is made in a flexible bag, filled with expanded polystyrene beads of about 5 mm diameter. The bag cover is thin, loosely-fitting and the beads filling the bag are free to flow. The subject sits on the bag in the required position and air is sucked out of the bag until it solidifies around the shape of the body.

Buttock shape has also been measured by sitting subjects on a gel pad (Kadaba et al., 1984). The seat of a wheelchair was made from a polymethyl methacrylate (PMMA) plate with a 3 cm thick layer of PVC gel on top. A B-Scan ultrasound transducer, controlled by a stepper motor, was positioned under the plate and measured the position of the gel-buttock interface. The measurement methods described above involve the body supported on a deformable material and measurement of the interface shape. Whilst the loads applied to the body are likely to be fairly uniformly distributed over the interface, it is difficult to control the load distribution during measurement.

Another approach to seat design is for the shape of the surface of the buttocks to be measured when no surface loads have been applied. Shape modifications could be included at a later stage of production. The shape of the 'undeformed' seated buttock is difficult to measure because of the difficulty in supporting the body in the seated posture without loading the buttock. This approach lends itself to non-contact body shape measurement techniques.

Non contact body shape measurement techniques based on photo-reflectometric principles have been used for measuring head, back, amputation stump, and foot shape (Moss et al, 1987;

Houston, 1989; Turner-Smith et al, 1988; Bao, 1989). A point, line or plane of light is projected onto the body and the reflected light is then viewed from an angle by a camera. Multiple marking observations from the surface of interest enable the topology to be calculated. Scanning times of 1 to 2 seconds for the whole of the back have been reported with the ISIS system (Turner-Smith, 1988). The application of these optical techniques has not been pursued for the production of shaped seating. Whilst the techniques do not deform the shape which they are measuring and are comparatively quick to execute, it could be difficult to find a body position which was suitable for scanning and which is similar to the sitting position. If the body is in a position that is not the sitting position, there will be a difference in muscle tone that will lead to a difference in the shape of the buttocks.

1.8 Manufacturing Methods for Shaped Seating

In this section, methods of manufacturing shaped seating are reviewed. A moulded seat is produced by vacuum forming a sheet of thermoplastic over a casting of the seated body (Nelham, 1975; Bardsley, 1984). The casting itself is made with a vacuum consolidation technique and the casting modified appropriately prior to vacuum forming of the seat. A sheet of cross-linked closed cell polyethylene (Plastazote, BXL Plastics Ltd., Croydon) is first vacuum formed over the casting. Then a sheet of acrylonitrile-butadiene-styrene (ABS) is formed over the inner layer of Plastozote. Localised shape adjustments are achieved after vacuum forming with a hot air gun. The final moulded support is fitted into the mobility base, or static seat, by means of a simple tubular framework. Once a moulded seat has been vacuum formed the shape is difficult to modify, but once the seat is in service it is usually maintenance free.

In another technique bead seats are made directly with the vacuum consolidation procedure (Silverman, 1986). A polyurethane matrix is added into the bag of polystyrene beads. This sets over a three hour period after vacuuming. During this time the bag can be locally manipulated into the chosen shape.

In a third method Shapable Matrix body supports are made from plastic and metal components linked by multiple ball and socket joints (Cousins et al,1982). The shape is determined during the fitting procedure, in which the client is suspended in a frame and the matrix is adjusted at its joints. The matrix is then overlaid with compliant foams and can be subsequently fitted into any appropriate mobility base. An advantage of the Matrix system is that the shape can be modified in response to a change in a person's needs.

Two methods of manufacturing custom contoured foam seating from the pin matrix shape measurement system have been reported (Gargano et al. ,1986; Welter & Zysman, 1987). One method involves injecting a self generating foam into a bag which swells to occupy the cavity under the pin array. At the time of its publication, problems were reported with finding a foam which was suitable for both injection moulding and cushioning. The other method involves cutting a block of solid foam with a cutting tool. The tool paths are determined by a mechanical linkage between the tool and the contours of the surface formed by the pin array.

The group at the University of Virginia have designed and built a computer aided manufacturing system for wheelchair cushioning (Brienza et al., 1988). It consists of a three-axis milling machine, computer numerical controller (CNC) and a microcomputer. There is a position and velocity feedback control system. A spherical wire brush tool spinning at 4200 r.p.m is used to cut the foam. They found that cutting with a 25 mm radius tool and 12.5 mm position increments gave a suitable balance between a short cutting time and quality of the finished surface. A time of 20 minutes is reported for cutting each cushion. Computer aided manufacture has the advantage of speed and versatility. Changes in material and shape can be employed without significant rework.

1.9 Scope and Methodology in the Present Study

The present study investigates the effects of shaped supporting surfaces on the soft tissues of the buttock. The aim of the study is to determine the principles by which the optimum design of shaped seat for any individual can be established. A reduction in the loading of the soft tissues at the pelvic bony prominences was the primary criterion by which the shape of the seats were optimised. This was chosen of the basis that the reduced loading may reduce the discomfort and pressure sore risk associated with seating for some chair-bound people. Another consideration was the provision of lateral supporting forces through the seat to improve sitting posture. Furthering our understanding of the mechanisms by which pressure sores form and developing new analytical techniques to model soft tissue deformation are outside the immediate focus of this thesis.

A computerised system for producing individually shaped seating was developed and tested (see Appendix 1). The experience of creating and operating this facility also provided the initiative and direction for the study which is reported in the rest of this thesis, and also for the provision of a small-scale service to patients from the Royal National Orthopaedic Hospital. Partly qualitative criteria were used in the design of seat cushions. The cushion shape was based on the shape formed by the subject when sitting on a bead-filled deformable bag. Modifications to the shape of the bag were made if it was thought that the interface pressure distribution or sitting posture of the subject could be improved. The foam that was used for the seat cushioning was selected in the belief that it could provide lateral supporting forces to the buttock in the contoured cushions, and could also spread out of the heavily loaded areas under the bony prominences in the flat cushions. Other providers of shaped seating or cushioning have reported similar design criteria. To improve the design and assessment of shaped seating and cushioning, more qualitative and systematic design criteria are required. The behaviour of the seated buttock is investigated in the following chapters in an attempt to develop these criteria.

A combined modelling and empirical approach is chosen to investigate the buttock-seat interaction. Experimental measurements are used to set up a theoretical model of the buttock-seat system and the measurements are compared with the results of the analyses. The information that can be gained from a purely empirical study is limited because the system is not fully accessible. For example, invasive measurements are not generally possible. There are also large variations between the bodies of subjects, so numerous measurements are required to examine the system fully. By developing a theoretical model it is possible to study a fully quantified system, to vary parameters in a controlled manner, and to get information on otherwise unknown aspects of the behaviour of the system. However there can be problems with obtaining the information on stucture and behaviour that is required to develop the model. Also complex interactions may occur with the real system which are difficult to model.

In the experimental studies the buttock is examined in a simplified form that is accurate and consistently measurable. Some of the body-related variables in the system are held constant by making measurements on a single able-bodied individual, in a predetermined sitting position. Variations in body weight, body geometry and tissue properties have an effect on the body-support interaction and so the variations would eventually have to be considered to comprehensively examine the effects of shaped supporting surfaces.

A finite element modelling technique is selected as being the most appropriate for this study. The technique is chosen from consideration of the geometric and material complexity of the body-support system. It is possible to take into account the large strains that occur when the system is loaded. The choice of specific modelling method for this study is discussed in depth in Chapter 4. In the analyses the tissues are studied in the equilibrium state when the fluid flow from the tissue under load has already ceased. This is probably the typical state of the soft tissue in the buttock of a person who cannot adjust his position on the seat. For such people localised discomfort and pressure sores from prolonged periods of sitting are common problems. The experimental measurements are made at least four minutes after loading in order to correspond as closely as possible to the equilibrium state.

The combined soft tissues under the pelvis are modelled as a homogeneous, isotropic elastic material. This is a simplification of the true system described in Sections 1·2 and 1·4 where the dermis, subcutaneous adipose tissue and muscle each have composite structures. Thus there is a limit to the extent to which the model can resemble reality. Nevertheless the model incorporated certain essential features such as the large deflections in the soft tissues, the nonlinear stress-strain behaviour of the tissues and the geometric complexity of the bone and soft tissue layers.

The states in the FE models that correspond to situations where there is a danger of pressure sores forming in the tissues have to be identified. Because of our incomplete knowledge of the cause of pressure sores, there is no established criterion that can be used to identify these situations. Krouskop hypothesised that blood vessel occlusion and interstitial fluid squeeze out are important stages in the mechanism (1983).

A general state of stress in a material can be considered in terms of pure hydrostatic and distortional components. The distortional stress state in the material can lead to a change of shape. This stress state is equivalent to the superposition of simple shear stress states on 5 sets of shear planes. A hydrostatic stress state in a material can lead to a change of volume in a compressible material, but for an incompressible material does not result in a deformation.

When the tissues of the body are subject to surface loading, the interstitial fluids may flow and the blood vessels may become occluded, as distortional stresses result in a change in shape of the tissues. Therefore in the analyses the magnitude of the localised distortional stress in the soft tissue-like material is used as the main criterion for comparing the performance of shaped seat surfaces. Hydrostatic stresses are also considered because hydrostatic stress gradients may result in interstitial fluid flow. In addition the calculated interface pressures and deformations are examined to enable a comparison with interface measurements to be made. When interpreting and extrapolating from the analytical results, the biological factors affecting pressure sore formation, such as the types of tissue in the region, their physiological state and the state of the body systems associated with them, are also taken into account.

A mathematical expression was required to describe the magnitude of the distortional stress state at a point, which was independent of the coordinate system used to describe the stress state. Non zero symmetric functions of the principal stresses were considered (such as the second and third stress invariants). It is often assumed that yielding in materials occurs when the second stress invariant reaches a specified value (von Mises yield criterion). The von Mises stress is a uniaxial stress which is equivalent to the distortional stress state, in that the second stress invariant has the same value. It can be shown that

$$\text{Von Mises stress.} = \left(\frac{1}{2}\left((\sigma_1-\sigma_2)^2+(\sigma_2-\sigma_3)^2+(\sigma_3-\sigma_1)^2\right)\right)^{0.5}$$

where $\sigma_1, \sigma_2, \sigma_3$ = principal stresses

In the subsequent chapters, the von Mises stress is used to compare the 3 dimensional distortional stress state at locations in the analytical models.

The multiple methods of investigation that are used in this work are selected as being the most relevant and feasible for examining the problem that has been described in this chapter.

CHAPTER 2 METHODOLOGY FOR EXPERIMENTAL STUDIES TO DETERMINE INTERFACE PRESSURE AND ANATOMICAL SHAPE

2.1 Background and Scope

In this chapter experimental methodologies and equipment are described. These are the basis of studies to obtain the information required to develop and verify the analytical model of the system. A 3 dimensional position measuring device is described. Also methods of measuring interface pressure, body surface shape and pelvic shape are discussed. Additional experimental studies are reported in Chapter 3. The results of these studies are required for the initial analytical model.

An able-bodied adult female person is subjected to all the procedures and measurements described in Chapters 2 and 3. She is twenty-six years old, has no known pathologies and is neither emaciated nor obese. A single subject is chosen so that extensive baseline measurements can be obtained.

Whenever it is possible the measurements that are reported in Chapters 2 and 3 are taken after more than four minutes sitting, when most of the time dependent soft tissue deformations have occurred (Zeigert and Lewis, 1978; Kirk & Chieffi, 1962). In some studies the experimental errors caused by postural variations increase with time. When it is thought that these errors outweigh the effects of fluid flow in the soft tissues, the measurements are recorded.

To reduce the effects of postural variations on the system, most of the measurements reported in Chapters 2 and 3 are taken with the body in a reference sitting position. This is upright with the muscles in a relaxed state. The back is against a vertical support, located 35 mm behind the buttock. The seat surface is horizontal and extends along the thigh to a position 230 mm behind the patellar. The feet are placed on a horizontal surface, that is 320 mm in front of and 432 mm below the seat. A tightly-fitting, customised, rigid orthosis is worn over the front of the body to help to maintain this posture. The orthosis extends along the thighs to a position below the knees and up the trunk to the sternum. It covers the lateral parts of the thighs and the lower trunk. The sitting position is shown schematically in Figure 3. Measurements are much more consistent when the orthosis is worn.

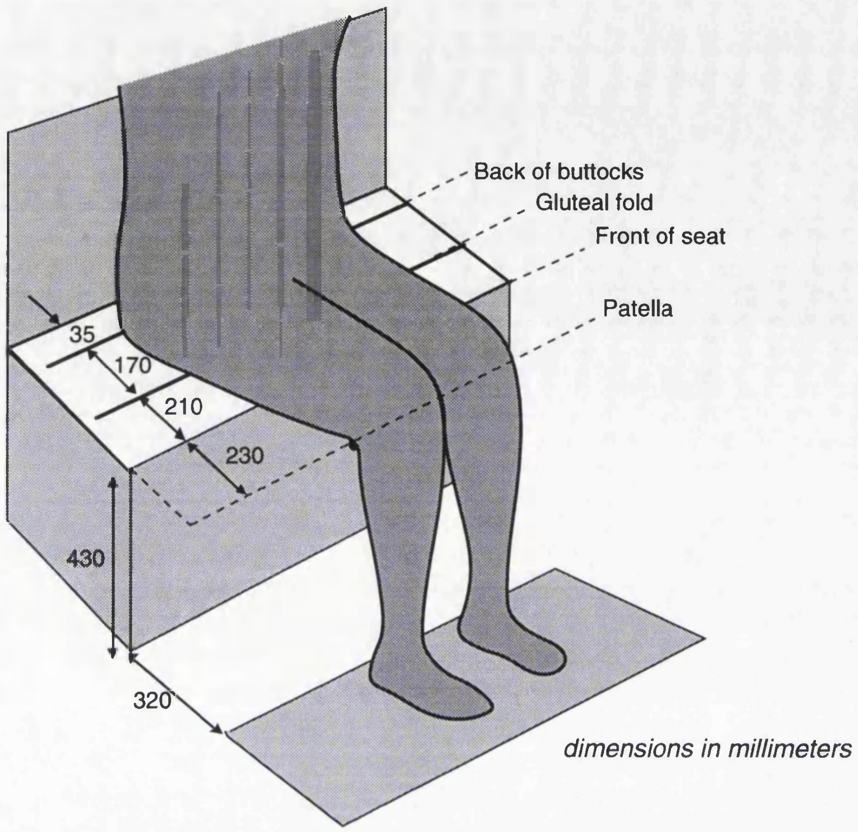

FIGURE 3 Reference sitting position for experimental studies

2.2 Measurement of Position with 3Space ISOtrak

Three dimensional position information was obtained with the 3 Space ISOtrak® (Polhemus Navigation Systems) in many of the experimental studies reported in this thesis. The device has been used in biomechanics studies to measure the motion of body parts such as the knee and spine (Hindle and Pearcy, 1989; Hefzy et al, 1992). In this study position measurements were made on replicas of the body surface and the pelvis, a contoured seat and on impressions of the body in a flexible bead-filled bag.

The device consists of an electronics unit to which an electro-magnetic source and a stylus sensor are attached. The electronics unit contains the hardware to drive the system and the primary software for the control of data aquisition. The source emits low frequency electromagnetic pulses from three coils positioned orthogonally to each other. The receiving unit within the stylus also has three orthogonal antenna coils. The position and orientation of the stylus relative to the sensor can be calculated at the electronics unit from the signal in the antenna coils in the receiving unit.

The device was interfaced with an Apple Macintosh portable computer to enable data aquisition and storage to be controlled through especially written software. Position and orientation readings could be made at frequencies upto 60 Hz, or when prompted from the computer keyboard. The system is sensitive to the proximity of magnetic objects, so measurements were performed in an environment which was free of these.

To calibrate the 3 Space ISOtrak over a period of time, the sensor and source were fixed to a rigid surface. The position of the sensor relative to the source was measured with the device in continuous mode over a period of minutes. Variations of up to 0·3 mm in the readings were found. The Space ISOtrak was also spacially calibrated in a high-density polyethylene rig. The electromagnetic source was rigidly fixed to part of a prismatic joint which was made to undergo incremental displacements by rotations of a lead screw. 180 degree rotations of the M10 lead screw produced displacements of 0·75 mm. The readings were found to be accurate to 0·3 mm when the sensor was within a 80 cm radius of the electromagnetic source (see Appendix 2).

The experimental procedures involving this device are described elsewhere in this thesis.

2.3 Measurement of Body Shape with Casting Technique

A technique for measuring the shape of the buttocks from plaster castings was developed. The buttock shape was measured both during sitting on a flat surface and when the body was in the sitting position but when there was no contact between the buttock and the seat. With this method it was possible for the subject to maintain a well-controlled sitting posture during the measurements of the suspended buttock shape, but it did not exclude the possibility of soft tissue deformations due to contact with the measurement medium. The information was used to improve the theoretical model of the buttock-seat interaction and to produce a seat with the same shape as the suspended buttock.

<u>Measurement of Suspended Buttock Shape</u>

The shape of the buttock was measured from plaster castings of the freely suspended buttock. A casting seat was built which allowed the body to be held in the sitting position with the left buttock fully unsupported (see Figure 4). When the subject sat on the seat, the weight of the upper body was supported through the thighs, the right buttock and the left arm. Templates were used to enable the subject to maintain a repeatable symmetrical position similar to the reference sitting posture. The templates were shaped to the profile of the body and were attached to the seat such that they were in contact with the sacrum and the left thigh. Markings were made on the skin which were aligned with the templates before each casting was made. There was not enough space around the casting chair for the subject to wear the closely fitting orthosis during the casting process.

Six castings of the left buttock were made. To prevent adhesion between the skin and the plaster, a pair of thin nylon tights was worn. As the plaster hardened, more of it was poured into the gap between the body and the plaster. It took about 7 minutes for each casting to set.

Randomly spaced points at about 10 mm intervals on the inner surface of the castings were measured with the 3Space ISOTrak. The data sets from the castings were transformed so the surfaces were coincident. The surfaces were aligned at the lowest points, in the sacral region and along the central sections. The data sets were then transformed into a spherical coordinate system. The origin of this coordinate system was 50 mm from the central plane, 130 mm above the lowest point on the surface and 130 mm in front of the tangent to back surface.

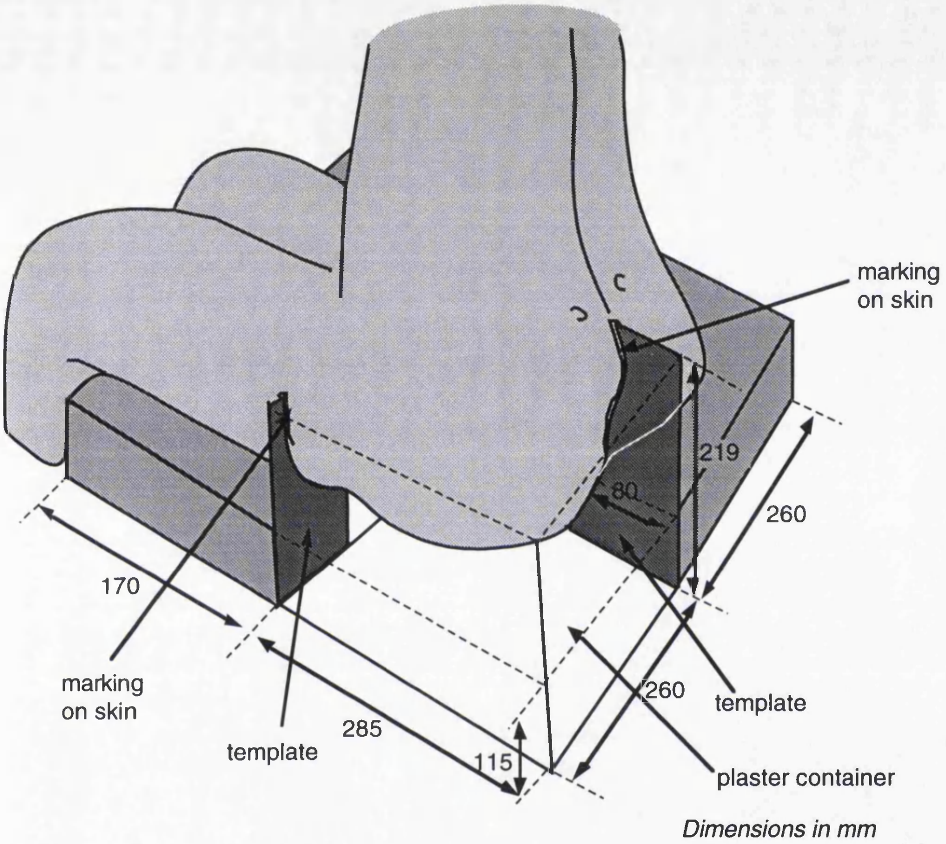

FIGURE 4
Casting seat for measurements of shape of suspended buttock

For each casting a regular grid of points at five degree intervals over the buttock surface was calculated with a Fortran program which was based on the fifth-order polynomial smoothing routine, from a commercially available software library (Surf, IMSL Math/Library, Fortran Subroutines for Mathematical Applications, 1989). The surfaces were then averaged at each grid point. Initially the variation in the radial coordinates was over 10 mm over more than 30 percent of the data points. These points were removed from the surface if there were no more accurate points nearer the edges of the surface. The greatest variations were at the front medial and lateral areas and along the central section. The shape differences were probably due in part to localised displacement of the soft tissue when the casting seat was nearby. Also the smoothing routine would have become more inaccurate near the edges of the measured surfaces.

Commercially available solid modelling software, which was part of a finite element modelling software package (ANSYS, Swanson Analysis Systems Inc., USA), was used to display the shape of the buttock. The average surface data was first imported onto a VAX computer, where a Fortran program was written to create a text file of ANSYS commands. The program ANSYS read the command file, plotted the data points and connected adjacent points into quadrilateral areas. Because there was a large range in each coodinate data point at positions along the central section, the shape of the body surface at this section was digitised from a sagittal MRI scan and was imported into ANSYS and aligned with the rest of the average buttock surface.

The resulting buttock shape is displayed and discussed in Chapter 6.

Measurement of Seated Buttock Shape

The shape taken up by the buttock, when the subject was sitting on a flat surface, was measured with a similar casting technique to the one described above. The casting seat was a horizontal planar rigid surface within an enclosure 160 mm deep, 450 mm wide and 250 mm long. Templates were attached to the front of the enclosure which were shaped to a vertical profile of the thighs. Another template was temporarily positioned over the sacrum before plaster of Paris was poured into the box. These helped the subject to sit in a repeatable symmetric sitting position and prevented the plaster from escaping out of the front of the container .

Six castings were made. Both buttocks were cast simultaneously and to prevent adhesion between the skin and the plaster, a pair of thin nylon tights was worn. Random points were measured with the Space Tracker over the inner surfaces of all the castings. The data sets were divided into the left and right buttock and then transformed so the plane of the seat, the central vertical plane of the castings and the area around the sacrum were coincident. Then the data files were transformed to a spherical axis system. Average radial coordinates were calculated at 2 degree intervals using a Fortran program which called the 5th order polynomial smoothing subroutine (Surf, IMSL Library). The calculated data set for the average surface was read and displayed by the solid modelling part of the ANSYS finite element software.

At the outline of the right buttock, points were calculated by the smoothing algorithm which were below the plane of the seat surface. These points were removed from the data file.

The resulting buttock shape is displayed and discussed in Chapter 6.

2.4 Measurement of Body Shape with Laser Scanner

The shape of the buttock was also measured with a technique where there was no contact between the measuring device and the body region to be measured. The buttock surface shape was compared with that measured by the casting technique.

The measurements were taken with a laser scanner at University College London (Moss et al, 1987; Linney et al, 1989). The laser scanner operates in the following manner. A laser projects a vertical line of light onto the body. The line is in the field of view of a video camera. The device on which the body is supported is rotated about a vertical axis until the line has passed over the whole of the chosen area of the body. It was difficult to configure the body in a posture which was both similar to the sitting position and suitable for scanning. It was not practical to make major adjustments to the scanning apparatus. The tightly-fitting orthosis was positioned on the measuring chair so that the subject could kneel in a stable position in the orthosis, with the thighs near vertical, the hips flexed and buttocks in the field of view of the camera.

The data was transformed by the author into spatial coordinates with algorithms which were given by the developers of the system. The shapes measured by the scanner and from the castings were compared graphically. The central planes of the two shapes were transformed so that they lay in the plane where y=0 in a Cartesian coordinate system. It was difficult to proceed further with the alignment because there were no other equivalent references on the two shapes. The data points on the central sections of the casting and laser scanned shape were sparse and so could not be used. Finally an arbitrarily-chosen section on the left buttock, 2 cm to 2·5 cm lateral to the central section, was taken as the reference. The shapes were transformed so that these sections were superimposed (between x=-10 cm and x=3 cm).

The resulting buttock shape is displayed and discussed in Chapter 6.

2.5 Measurement of Pelvic Shape from Magnetic Resonance Images

A non-invasive method of measuring the shape of the pelvis was required. A technique based on magnetic resonance imaging (MRI) was selected because MRI gives good depiction of soft tissue contrast, involves low energy radio frequency radiation doses and has multi-planar imaging facilities. The information on the shape of the pelvis was used to improve the theoretical model of the buttock-seat interaction.

Magnetic resonance images are formed when the body is subject to a static magnetic field and a perpendicular radio frequency field. Precession of the proton spins within the tissues under the influence of the changing field, produces a changing magnetic field. This induces a voltage in receiver coils around the body, which is proportional to the proton density. By monitoring the time taken for the spins to return to their rest state when the radio frequency voltage is removed (relaxation times), information can be obtained on the structure within which the proton is held. Protons which are tightly bound in a crystalline structure have long relaxation times, whilst those in water have short relaxation times. Tissues with low water or high collagen content thus appear dark in magnetic resonance images. Fatty tissues produce a high intensity signal, muscles and hyaline cartilage produce an intermediate signal and the signal from cancellous bone depends on its composition (Hutchison,1976).

The body tissues in the region of the pelvis were imaged with a nuclear magnetic resonance scanning device. Photographs were taken of sections through the pelvis at 10 mm intervals in the sagittal, coronal and transverse planes. During imaging the subject lay prone and relaxed on a couch within the scanner. It was not possible for the subject to flex the hips during scanning, due to the limited space within the scanning column. The photographic plates were enlarged to life size. A photograph of a transverse section through the femoral heads is shown in Figure 5.

A physical model of the pelvis was then produced from the photographic plates. The model provided a convenient method of aligning the replicas of the bony sections obtained from the photographic plates and obtaining interpolated shape information from between the sections. The bony areas in the photographs of the transverse sections were replicated in 5 mm-thick balsa wood. The relative alignment of the pieces was determined from the location on the photographs of the central plane on the body and the outside of the scanning tube. The sections were then stuck together with 5 mm-thick balsa wood spacers between them. The shape information between the measured sections was interpolated from the adjacent sections and the spacers were filed down by hand.

The shape of the pelvis was measured from the model. Lines were drawn over the surface of the physical model which intersected each of the sections about 40 times (see Appendix 2). The points of intersection of the lines and the sections were digitised with the 3Space ISOtrak. This provided position information from the whole of the surface of the model.

Once again the pelvic shape was plotted within ANSYS by means of a command file written to include the measured data. Adjacent keypoints were connected into quadrilateral areas. The connectivity commands were initially written into the command file, then corrections were made interactively in ANSYS, in regions where they were required by the irregular geometry of the pelvis. The pelvic shape is displayed and discussed in Chapter 6.

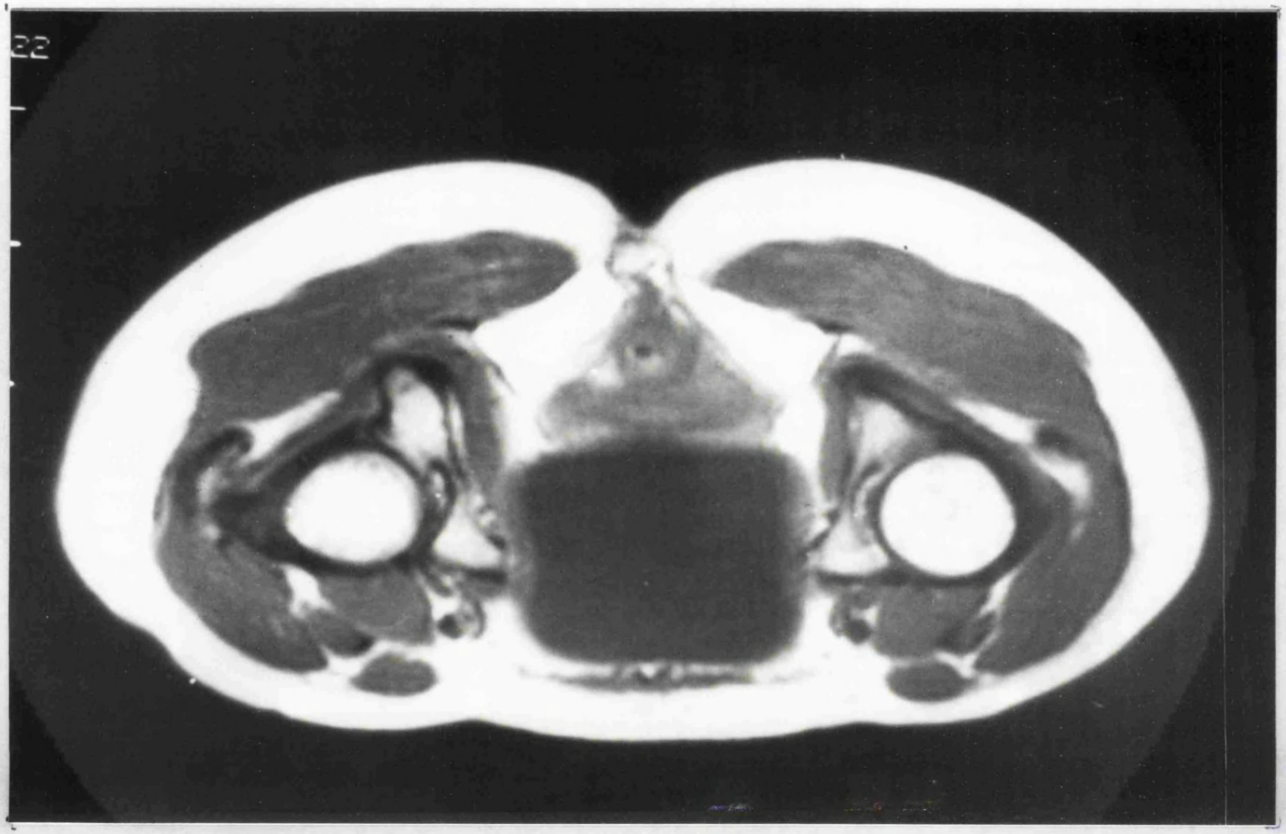

FIGURE 5

Coronal section through buttocks showing pelvis, femoral heads, gluteal muscles and subcutaneous adipose tissue, imaged with nuclear magnetic resonance

2.6 Measurement of Interface Pressure with Electro-pneumatic Measuring Device

The pressure distribution was measured with an electro-pneumatic pressure monitor (Interface Pressure Measurement System, MediTechnics, Putney). It consisted of 12 transducers and a control and display unit. The electro-pneumatric transducers were made of a flat polyethylene sac, 80 microns thick and 10 mm in diameter. Each transducer contained an electrical contact 5 mm in diameter deposited on the inner surface of the opposite walls of the sac. Air was automatically pumped into the transducers until the pressure in the sac was equal to the pressure at the interface. The circuit opened and the sac deflated until the switch was again closed. This process was repeated such that the pressure in the transducer fluctuated about a constant value. A photograph of the pressure monitor is shown in Figure 6.

The system was calibrated under static load conditions between a rubber bag and a flat rigid surface. The pressure within the rubber bag was compared to that registered on the monitor display unit. The pressure monitor calibration is discussed in Appendix 2. Over their operating range, which was from 0 to 300 mmHg (0 to 40·0 kPa) all the transducers were found to be reproducible, linear to within 4 mmHg (0·53 kPa) and accurate to within 7 mmHg (0·93 kPa).

Measurements on a planar seat

A 20 mm grid of points was drawn over a 12 mm thick perspex plate. The outline of contact between the body and the surface was marked on the under-side of the plate. Transducers were positioned at 12 of the grid points and the subject sat on top of the plate in the reference sitting position. After pressure readings had been recorded, the subject stood up and repositioned on the surface. The experimenter ensured that the outline of contact was coincident with the previously measured outline, by observation through the perspex plate. The pressure at each grid point was measured 4 times in total. If the range of the readings was greater than 10 mmHg, a further set of readings were taken at that point. The process was repeated at other sets of grid points, until the whole of the contact area had been measured.

The pressure readings directly under the ischial tuberosity were found to be very dependent on the orientation of the pelvis. Small changes in posture and position on the seat which were not detectable or controllable with the orthosis or contact area observations, were thought to be the cause of the pressure variations. In some of the areas where the pressure readings were greater than 150 mmHg (20·0 kPa), it was not possible to take four consecutive readings which had a range of less than 10 mmHg. In these cases 12 readings were taken and averaged.

The resulting interface pressure distribution is displayed and discussed in Chapter 5.

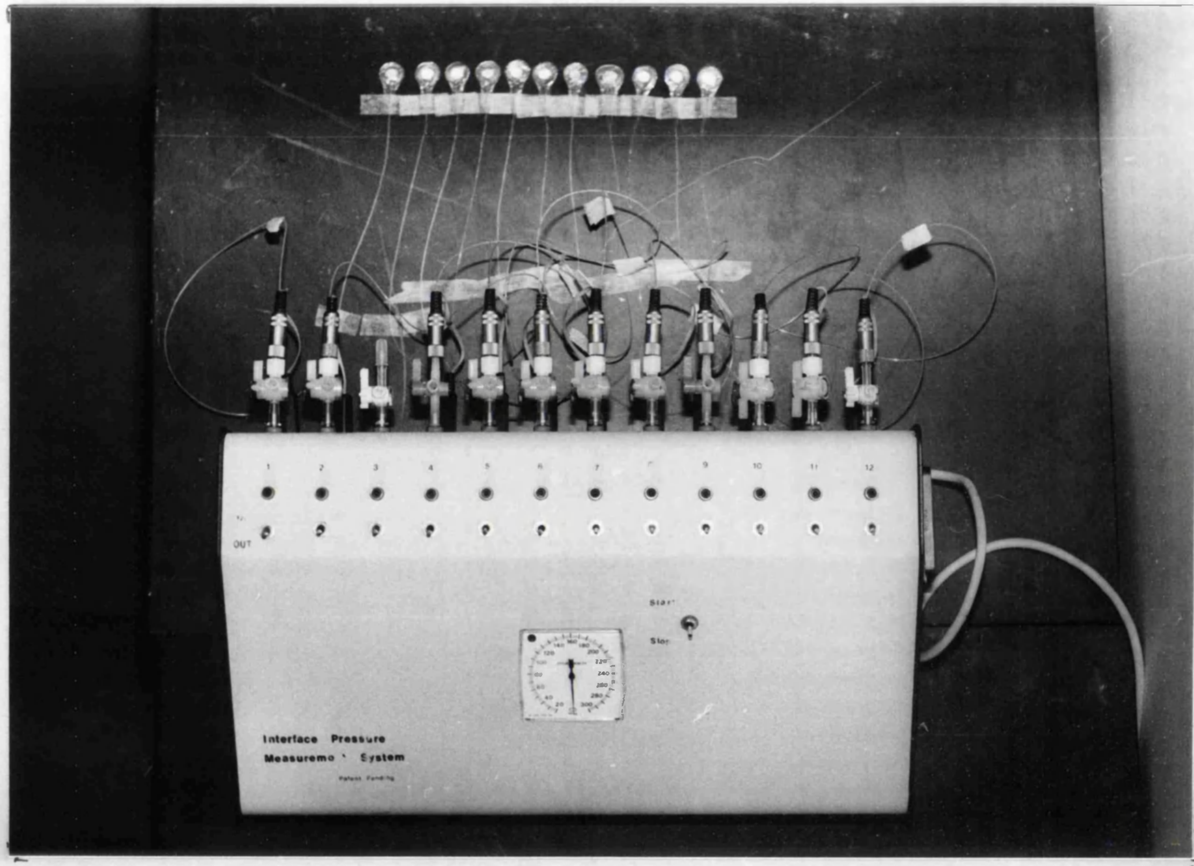

FIGURE 6

12-channel interface pressure monitor with electronic / pneumatic feedback control loop

Measurements on a body contoured seat

The interface pressure distribution was measured when the subject was sitting on a seat which had the same shape as the suspended buttock. The interface pressure distribution was compared to those calculated in the analytical models of the buttock supported on contoured seats.

A rigid seat was made which had the same shape as the suspended buttock, measured by averaging the shape of castings. Since only the left buttock had been measured from the castings and shape information for the right side of the seat was required, the position data were reflected across the central plane of the body. Because of the highly curved nature of the seat shape it was not possible to make the seat on a 3-axis milling machine with the simple production process described in Appendix 1. The data file which contained the left and right sides of the seat was divided into four parts, such that each could be manufactured with the 3-axis milling machine. These were the right and left sides, central, and back sections. Each part was made separately on the 3-axis CNC milling machine in rigid polyurethane foam (Pedilen®, Otto Bock, Duderstadt, Germany). A 5-mm ball-nosed cutting tool was used to mill out the surfaces. After they had been milled, the blocks were stuck together using Pedilen foam as the adhesive. The surfaces were finished by hand.

The shape of the suspended thighs had not been measured with the castings of the suspended buttock for practical reasons. The shape of the thigh section of the seat was based on a casting of the thighs, taken with the subject sitting in the rest of the seat (described above), and with the femurs horizontal. Similarly to with the buttock section, this section was also manufactured on the CNC machine, stuck to the rest of the seat with Pedilen® foam using reference markings to align this section, and finished by hand.

The accuracy for the finished surface was measured with the 3Space ISOTrak position measuring device. A grid of points at about 20 mm intervals was drawn by hand over the seat surface. The position of each of the grid intersection points was measured with the 3Space ISOtrak. A photograph of the seat is shown in Figure 7. The average shape of the castings of the suspended buttock and the manufactured seat were graphically superimposed in Appendix 2 in order to compare the shapes. The radius of curvature of the manufactured seat was slightly larger in the longitudinal plane. The difference between the two shapes was probably due to the back section not being squarely aligned to the rest of the seat when it was attached. The maximum difference in the position of the surfaces was about 0·5 cm and was at the junction of the back, central and lateral blocks.

The pressure distribution normal to the surface was measured with the electro-pneumatic pressure monitor, using a method of measurement which was similar to the one described in the

FIGURE 7

Rigid seat with similar shape to the suspended buttocks of the able bodied subject

above chapter. Transducers were positioned at 12 of the grid points and the subject was seated in the seat. After pressure readings had been taken, the subject stood up and repositioned on the seat. The pressure at each grid point was measured four times in total. If the range of the readings was greater than 10 mmHg (1·3 kPa), a further set of readings was taken at that point. The process was repeated at other sets of grid points, until the whole of the contact area had been measured. It was not possible for the subject to wear the orthosis whilst sitting on the seat, because of the deep and closely-fitting nature of the seat. However the subject reported being firmly help in position by the seat when she was seated.

The pressure readings under the sacrum were very variable. Small changes in posture and position on the seat which were not detectable or controllable were thought to be the cause of the pressure variations. In the areas where the pressure readings were greater than 150 mmHg (20·0 kPa), four consecutive readings had a range of greater than 10 mmHg. In these cases 12 readings were taken and averaged. The pressure distribution is displayed and discussed in Chapter 6.

CHAPTER 3 FURTHER EXPERIMENTAL STUDIES TO DETERMINE BODY PROPERTIES FOR INITIAL FINITE ELEMENT MODEL

The measurements that are reported in this chapter are used to set up the initial finite element model of the buttock loaded against a rigid planar seat. The vertical force-deflection characteristics of the buttock, the weight supported through the buttocks, the outline of contact between the body and the seat and the depth of tissue remaining under the ischial tuberosity are all measured during sitting on a flat surface. In Chapter 5 the initial model of the buttock-seat interaction is developed.

3.1 Measurement of Boundary of Contact

This study was to measure the boundary of contact between the buttocks and a flat rigid seat surface and to locate the position of the ischial tuberosities relative to the outline. The information was needed for the design of the buttock Tissue Stiffness Testing Device which is reported in Section 3 of this chapter and also to compare with the results of the finite element study which is reported in Chapter 5. A pilot test was performed to establish the method for the main trial and the repeatability of the outline measurements. This is reported in Appendix 2.

The horizontal platform was used as the seat in the study. It was covered in a thin paste of water and french chalk to outline the contact area and to reduce the friction at the interface. The subject sat in the reference position on the glass plate for 15 minutes. After this period the subject stood up and the paste was left to dry. The ischial tuberosities made elliptical marks on the plate with diameters of about 40 mm and 30 mm. It was assumed that the apex of the ischial tuberosities was at the centre of the marks. The outlines and centres of the ischial markings were digitised with the 3Space Isotrak. The identical procedure was repeated eleven times.

The average outline was calculated by aligning the digitised shapes and then fitting a polynomial curve through them. The outline coordinates were transformed, so that two orthogonal reference axes were coincident. The tangent to the back of the buttocks and the line perpendicular to the tangent and passing through the centre of the sacrum were the reference axes. The data was divided into four sections (right buttock, left buttock, right thigh, left thigh). Fifth-order polynomial equations were fitted to each of these sections.

The measured and the average outlines of contact are plotted in Figure 8. The equations describing the outlines are as follows. The square of the correlation coefficient describes the fit of the curves through the data.

<u>Equation 1 (right buttock)</u> from z = -10 to 150 mm ; from x = 0 to 200 mm.

$$\mathbf{Z} = 32{\cdot}53 - 0.896\,\mathbf{X} - 8.311.10^{-2}{\cdot}\mathbf{X}^{2} + 3.833.10^{-2}{\cdot}\mathbf{X}^{3} - 3.091.10^{-3}{\cdot}\,\mathbf{X}^{4} + 8.097.10^{-5}{\cdot}\mathbf{X}^{5}$$

Square of correlation coefficient =0.994 .... **3.1**

Equation 2 (left buttock) from Z -10 to 150 mm ; from X = 0 to -200 mm

$$Z=38{\cdot}76 +0.694.\mathbf{X} -0.1359 \cdot\mathbf{X}^2 -3.851.10^{-3}\cdot\mathbf{X}^3 -2.806.10^{-3}\cdot\mathbf{X}^4 -7.033.10^{-5}\cdot\mathbf{X}^5$$

Square of correlation coefficient =0.996 .... **3.2**

Equation 3 (right thigh) from Z =150 to 350 mm ; from X =150 to 200 mm

$$\mathbf{X}=14{\cdot}78 +2.823 \cdot \mathbf{Z} -0.155\cdot\mathbf{Z}^2 +2.300.10^{-3}\cdot\mathbf{Z}^3.+4.383.10^{-5}\cdot\mathbf{Z}^4 -1.138.10^{-6}\cdot\mathbf{Z}^5$$

Square of correlation coefficient =0.993 .... **3.3**

Equation 4 (left thigh) from Z=150 to 350 mm ; from X = -150 to -200 mm

$$\mathbf{X}=-634{\cdot}31+10.360 \cdot\mathbf{Z} -0.943 \cdot\mathbf{Z}^2 +4.127.10^{-2}\cdot\mathbf{Z}^3 -8.621.10^{-4}\cdot\mathbf{Z}^4 +6.974.10^{-6}\cdot\mathbf{Z}^5$$

Square of correlation coefficient =0.998 .... **3.4**

The variation in the outlines was also calculated. The coordinates in the buttock sections were transformed to a spherical axis system, centred at the position of the ischial tuberosity. The variation in the radial dimensions was calculated for each 10^{o} sector.

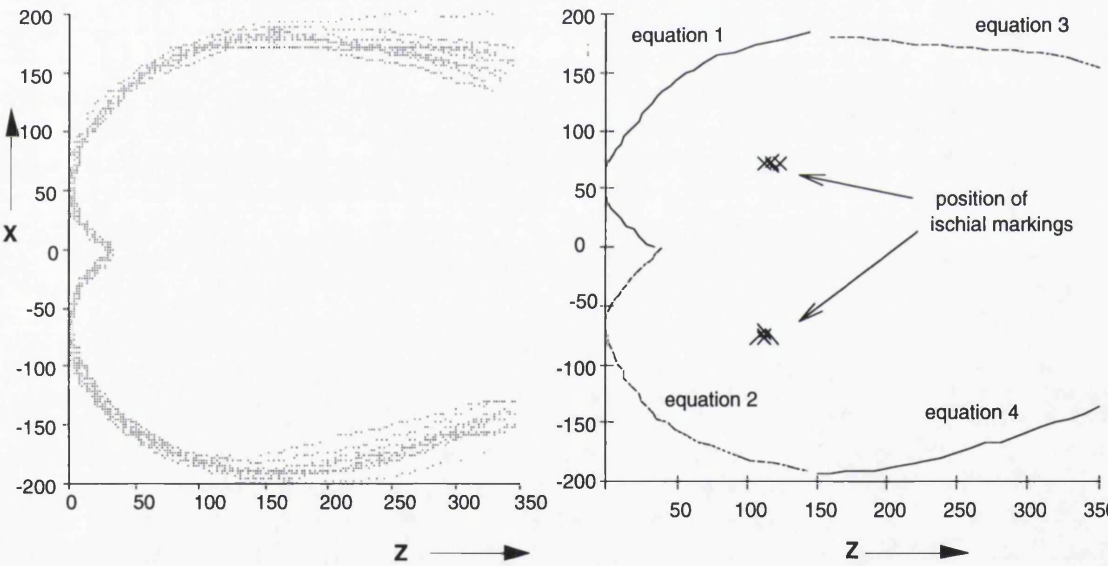

FIGURE 8

Measurement of boundary of contact between body and planar seat surface. (distances in mm).

By integrating the equations 1 and 2, the area of contact between the buttocks and the seat was estimated over the right and left buttocks for Z=0 to Z=170 mm. They were found be 32300 mm^2 and 33600 mm^2 respectively. The standard deviation in the position of the outline was up to 5 mm over the buttock region and gradually increased from this value along the length of the thigh. The mean standard deviation in the outline over the buttock region in the radial direction was 3.5 mm.

The variations in the radial dimensions during the main trial and the pilot trial (Appendix 2) were compared using the Independent T Test. The variation was significantly greater in the main study ($p<1\%$). The difference could be accounted for by body movements during measurement and the outline of the buttocks not being exactly spherical and therefore the radial displacement not always being perpendicular to the outline.

3.2 Measurements of Body Weight Through Buttocks

This study was to measure the total vertical load transferred through the buttocks as the subject sat on a flat surface in the reference sitting position. A lever-mechanism weighing machine was calibrated with known weights and a temporary platform was built around it. When the subject sat on the machine in the reference sitting position, the buttocks were supported on the weighing area and the thighs were supported through the rest of the platform. No attempt was made to achieve low interface friction conditions. The weighing was performed once at the start of the period when the subject was being measured and again when all the other measurements on the subject had been completed. Fifteen readings of the weight through the pelvis were taken at each session. The mean weight at the two sessions were compared with the Independent T Test.

	Test 1	Test 2
Average reading	40.7	40.9
Standard Deviation	0.4	0.3

The difference between the mean readings was not significant at the 10 percent level. Using the calibration curve, the overall mean load through the buttocks was calculated as 38.1 Kg.

3.3 Measurement of Soft Tissue Stiffness

The vertical load-deflection characteristics of one buttock were measured whilst the subject was sitting in the reference position. This information was required so that an analytical model of the seated buttock could be developed in which the soft tissues had similar force-deflection behaviour. The total depth of tissue under the ischial tuberosity was also required for the model. This was determined from the indentation results in this study and ultrasound tissue depth measurements on the seated buttock in Section 3·4.

A buttock Tissue Stiffness Testing Device (TSTD) was designed and built. This enabled known vertical loads to be applied to the left buttock with the subject seated and the resulting vertical indentation into the soft tissues of the buttock to be measured at each load level. During measurement the subject sat on a flat rigid seat, with the left buttock supported on a rectangular plate. By moving the plate vertically, it was possible to apply specific vertical loads to the left buttock. The vertical position of the plate at each load level was measured with the 3Space ISOtrak. The stiffness characteristics were measured during unloading of the tissues because it was easier for the subject to maintain her position when the loading plate was initially at maximum height. The maximum applied load was that supported through the left buttock with the subject sitting in the reference sitting position (the measurement of this quantity is described in Section 3.2). At this load level the top of the plate was flush with the rest of the seat.

The movement of the pelvis was assumed to be negligible during each set of measurements. As an aid to monitoring the position of the body during each set of readings, a vertical line was marked on the skin along the spine to the sacrum. A horizontal line was also marked between the cavities on the proximal sacrum. Three reference points were marked along these lines at positions where soft tissue displacements would not occur during sitting. The position of the body surface marking were recorded with the 3Space ISOtrak.

The TSTD is represented in Figure 9.

The design of the device is described below (where the numbers in brackets indicate parts labelled in Figure 9). The parts below the loading plate (1) were to ensure specific loads could be applied to the buttock by the loading plate. The plate was moved by means of a plunger (3), which was prevented from tilting under load by a closely-fitting slider (4). The load was applied to the system as a weight on a weighing pan (5). The load was transformed to a upward load through a low-friction pulley mechanism (2). The TSTD was made out of non-magnetic materials to enable the 3Space ISOtrak to measure accurately. The plunger was located under the approximate position of the ischial tuberosity.

To calibrate the system known weights were placed on the loading plate and weights were put on the weighing pan until the loading plate moved. The device was calibrated for upward and downward movement of the loading plate. It was found to be linear over the required range (0-200 N) and the readings were repeatable to within ±0.1 kg. The calibration results are shown in the Appendix 2.

The experimental procedure for each set of readings is described below. The loading plate and buttocks were covered with a film of detergent and water before measurement to reduce the effects of friction. The subject sat on the seat in the reference sitting position with the left buttock over the loading plate. An initial load of 19 Kg was applied through the loading plate and the body position was adjusted so the loading plate was flush with the rest of the seat and the pelvis was level. The weights were taken off the weighing pan in small increments. The subject supported the left side of the body with the left hand. After the removal of each load, the platform was gently rotated in the horizontal plane, to check there was no sticking due to friction effects. The vertical position of the loading plate was measured with the 3Space Isotrak a few minutes after each weight had been removed. The point at which loss of contact occurred

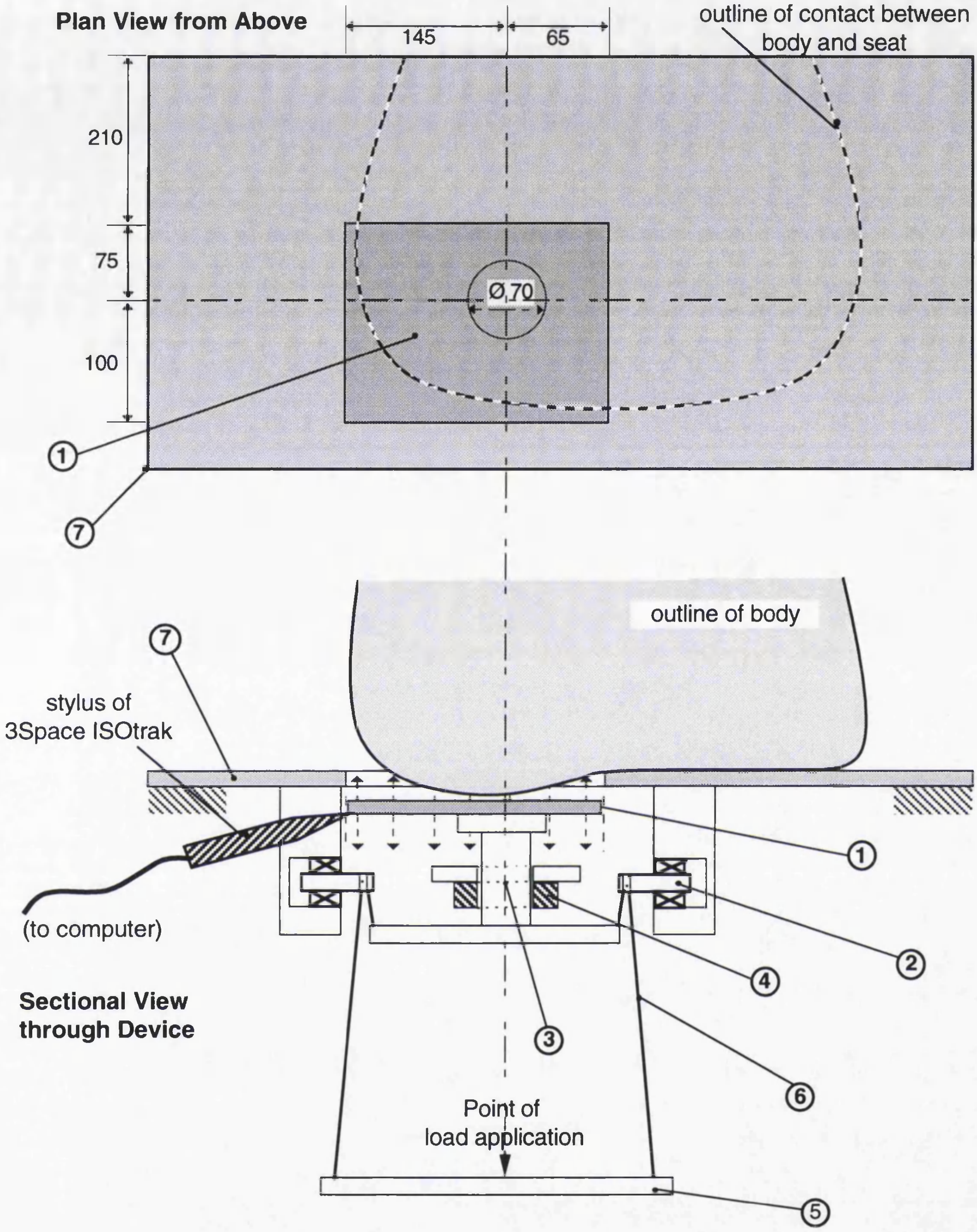

Parts

1 Movable loading plate (perspex) Range of motion 60mm	**4 Slider for plunger (high density polyethylene). Depth=24mm**
2 Roller bearing pulleys with grooved high density polyethylene shafts. 192mm between grooves	**5 Weighing pan (wood)**
3 Plunger (high density polyethylene) Spherical cross section, Ø=43mm	**6 Attachment strings for weighing plate (metal)**
	7 Fixed seat (plywood)

FIGURE 9
Tissue stiffness testing device for buttock in sitting position (dimensions in millimeters)

between the buttock and the seat was established by both the experimenter and subject independently. Changes in body position were monitored during each run by observation and measurement. Before and after each measurement set, the position of the body surface markings were measured with the 3Space Isotrak.

The readings were repeated 13 times in total. The TSTD calibration was repeated after the measurements. Data sets that involved an anterior-posterior or medial-lateral pelvic rotation of more than 2^{o}, or pelvic translations of more than 10 mm were disregarded in the analysis.

As expected the vertical stiffness of the soft tissues increased with increasing vertical displacement. The average vertical displacement of the surface of the buttock under the ischial tuberosity was 48.5 mm $\pm$ 1 mm. The indentation results were combined with the tissue depth measurements in Section 3·4, so that the engineering strains in the soft tissues could be calculated. The vertical stiffness of the soft tissues are represented in Figure 10 by an average applied load-strain curve.

The reference points moved to the right by a few millimetres during all of the sets of readings. One set of data was not included in the analysis due to a horizontal translation of more than 10 mm. The translation of the body to the right during the tests was probably as a result of a lateral force applied to the body, by the left supporting hand. This caused an overall translation because the seat-buttock interface friction was very low.

The random errors in this study are likely to be due to variation in the estimate of the point of 'no contact' at the end of each test. Also the initial sitting position may not have been consistent between readings and posture of the subject could have varied during each set of reading. There was no chronological order to the variations in the mechanical response of the tissues between measurement sets, so this was not likely to have a significant effect on the stiffness. Variation in the load applied by the TSTD are likely to be small because the calibration was consistent over repeated readings. The rigid seat supporting the right buttock and thighs may have have produced some constraint on the unsupported buttock.

3.4 Measurement of Tissue Depth

This study was to measure the depth of tissue under the ischial tuberosities when the subject was sitting in the reference position. This information was required to establish the total vertical depth of tissue under the ischial tuberosity for the seated subject, and hence the vertical engineering strains in the soft tissues of the buttock at a specific level of indentation.

A 9 MHz A-scan ultrasound transducer (Cutech, Stiefel Laboratories, DM70) was used. The transducer was embedded into a planar transparent perspex seat, so the head of the transducer was flush with the seat surface. Water was used as the acoustic coupling medium. The seat was made of transparent material, so the erythema under the ischial tuberosities could be located.

The subject sat on the seat with the transducer located under the buttock at the approximate position of the ischial tuberosities. After 4 minutes, the buttock was observed from under the seat. Positions adjustments were made if required so that the transducer was directly under one ischial tuberosity. The reflections from the interfaces were recorded. The procedure was repeated 10 times under each buttock. The depth measurements were as follows:

Right buttock depth (mm)	Left buttock depth (mm)
7.8	7.0
10.2	8.1
7.2	7.4
8.4	9.6
7.9	9.0
7.8	7.0
7.5	6.1
6.0	8.8
7.2	6.7
7.8	7.7
Mean 7.8 (range 6.0 to 10.2)	Mean 7.7 (range 6.1 to 9.6)

The depth calculations were based on an ultrasound velocity of 1580 m/s. In fact it could have varied from 1440 to 1620 m/s (Payne, 1985). However the errors from this assumption were much smaller than the measured variations in tissue depth and so were not considered further. Additional reflections from shallower depths were sometimes visible, but they were insufficiently repeatable to be able to calculate the depth of the interface from which they occurred.

By combining the indentation results with the depth measurements discussed above, it was possible to estimate the total depth of tissue under the ischial tuberosity prior to the application of surface loads to the buttock. This was calculated to be about 56 mm (7.7+ 48.5 mm).

The vertical strains in the soft tissues were then calculated from the indentation data in Section 3·3. The vertical strain in the tissues under the ischial tuberosity when the subject was sitting in the reference sitting position was about 86 percent. The vertical stiffness of the soft tissues was examined in vertical applied load- strain curves. The average applied load- strain curve for the left buttock is shown in Figure 10.

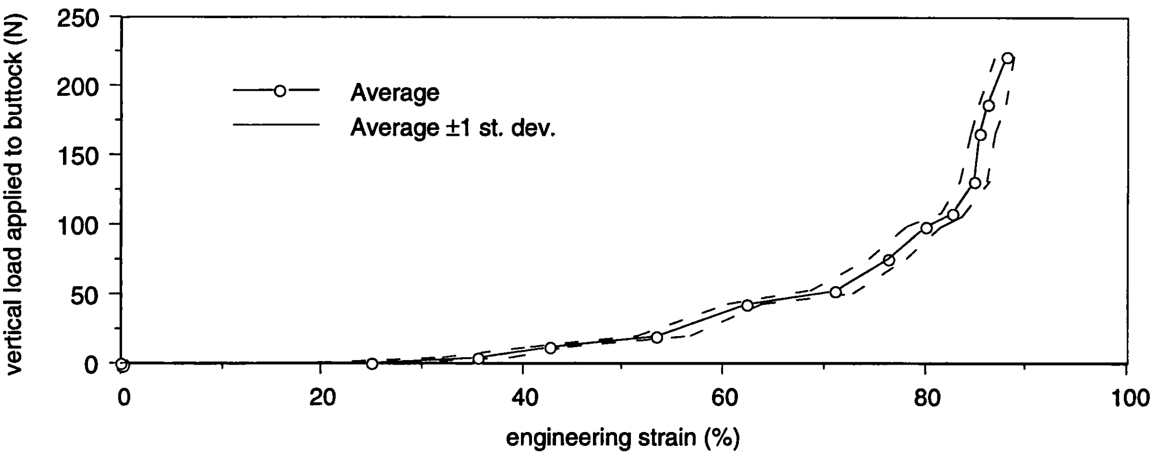

FIGURE 10

Vertical stiffness for soft tissue of left buttock

The geometry, loading and force-deflection behaviour which were measured in this chapter were put into the finite element model which is described in Chapter 5. The material constants of the tissue in the analytical model were obtained by comparing the experimental load- strain data with the behaviour of the analytical model.

CHAPTER 4 SELECTION OF METHODOLOGY FOR ANALYTICAL STUDIES

4.1 Selection of Modelling Method for Stress Analysis

It was necessary to decide on the modelling technique that would be used to study the system. A range of modelling techniques was reviewed so as to determine the one that was most suitable. A physical replica of the buttocks was considered. Also several methods using approximate solutions to the differential equations that describe the stress distribution in a structure (finite difference methods, Ritz method, finite element method) were considered.

It was possible to make a physical replica of the buttocks and seat. The structure and properties of the replica would be based on the structure and properties of the buttocks. The loading of the model would be more easily controlled than in the true system. Also when the model was loaded it would be easier to obtain measurements of the resulting internal and interface deformations and forces than with the true system. If the constitutive equations for the materials in the system were known and if the deformations that occurred within it could be measured, it would be possible to estimate the stresses in the system. One limitation of such an approach is that to change the structure or properties of the buttocks would require the fabrication of a new physical replica. Also it would be difficult to develop a physical replica of the buttock in non biological materials, that simulated the behaviour of the soft tissues.

The finite difference method could be used to obtain approximate solutions for the stress distribution in the buttocks. The method is based on the replacement of the partial differential equation and associated boundary conditions describing the stress distribution, by the corresponding finite difference equation with known stresses at certain nodes. The finite difference equations are solved to estimate the stress values at the nodes. The stress at nearby locations is estimated by interpolating to that position. The finer the mesh, the more accurate the estimate. There are difficulties in representing irregular geometries and boundary conditions with this method of approximation. A computer is required to obtain the numerical solution with analyses that involve relatively complex boundary geometries and loading conditions, due to the number of finite difference equations that are involved.

With the classical variational methods of approximation (such as Ritz method), variational calculus is used to estimate the stress function. The stress function is expressed in the form of a series $\phi = \Sigma a_i \phi_i$ (i=1 to N) ; where ϕ_i are functions which satisfy the boundary conditions and can minimise the integral expression and a_i are undetermined constants. The series is substituted into the integral expression associated with the particular problem, such that there is a function of the second degree in a_i. The magnitudes of the constants a_i are determined from minimising the function with respect to the constants a_i. With a suitable choice of ϕ_i it is usually possible to obtain a satisfactory approximate solution with only a few terms in the series. However it is difficult to construct approximate functions for irregular shapes. Even when the approximating function is available, the computation of associated coefficient matrices cannot be automated because the approximating functions are problem dependent.

The finite element method can also be used to obtain approximate solutions to stress analysis problems. It is more suitable than classical variational methods for problems that are geometrically complex, have discontinuous loads, or have discontinuous material or geometric properties. A model of the structure is divided into a finite number of parts (elements) which are interconnected at nodes. Functions are chosen that define the displacement within an element in terms of the nodal displacements. The stress state in an element is defined by the constitutive equations and the strain state of the material. The stiffness matrix, which relates applied nodal forces and nodal displacements, is calculated for each element and assembled into an overall stiffness matrix for the whole structure. The model is constrained at certain nodal positions and loaded at other positions. The finite element equations are then solved for the unknown nodal values. It is possible to obtain approximate values for the nodal displacements, strains and stresses within the structure. The finite element method of approximation lends itself to computerization. There are many commercially-available finite element software packages, where there is a wide choice as to the type of element formulations and loading conditions that can be built into a model.

The finite element method was selected to obtain solutions for the stresses and deformations in the buttocks and seat. This was because it is possible to model structures with nonlinear material properties, irregular interfaces and complex boundary conditions under large strains with commercially available software. It was intended to analyse the effects of the variations in seat and body-related parameters. The FE method with the Newton-Raphson solution procedure is discussed in detail in Appendix 4.

4.2 Geometric Non Linearities in Finite Element Analyses of Elastic Materials

In finite element analyses the geometric and material properties of the system are described within the finite element stiffness matrix. Solution procedures were reviewed in this section, so the ones that were most suitable for a finite element model of the soft tissues of the buttock during sitting could be established.

Geometric nonlinearities have to be considered in the FE analysis of soft tissue systems that undergo large deflections. The motion of an element can be made up of a strain, a rigid rotation and a rigid translation. The translational component does not affect the element's stiffness nor the loading and so does not have to be taken into account. However the rotation of the element with respect to the applied loads will lead to a change in the structural stiffness matrix. Also the strain can involve a change in an element's shape which, if it is large enough, may produce a significant change in the structural stiffness matrix. Thus to obtain an accurate solution with a large deflection problem, the change in orientation and shape of the elements should be taken into account.

Unfortunately the element areas are not updated during the large deflection FE solution and this leads to underestimates of the loads and stresses at a certain level of deformation. With an iterative FE solution, the stiffness matrix is updated as the solution proceeds. The initial stiffness matrix is based on the initial nodal positions. The nodal displacements are calculated from the first iteration. The nodal positions and stiffness matrix are then updated to take account of rigid body rotations. The solution continues with the nodal positions and stiffness matrix being recalculated at each iteration. The solution is held to have converged when the change in displacement from successive iterations is smaller than a preset criterion.

Reynolds showed the errors that can be caused by not taking into account changes in geometry for a simple large deflection problem in an incompressible elastic material (1988). The load versus height response to uniaxial, frictionless, compressive loading was calculated in a cylinder of homogeneous, isotropic material (see Figure 11). The material showed a linearly elastic relationship between true stress and natural strain. He calculated the load required to compress the cylinder to half of its initial height. He then repeated the analysis with a small deflection assumption and with a large deflection procedure. The estimated loads were compared to the exact one. The analyses are reproduced here because they highlight the limitations of using large deflection solution procedures in finite element analyses where the system undergoes large strains.

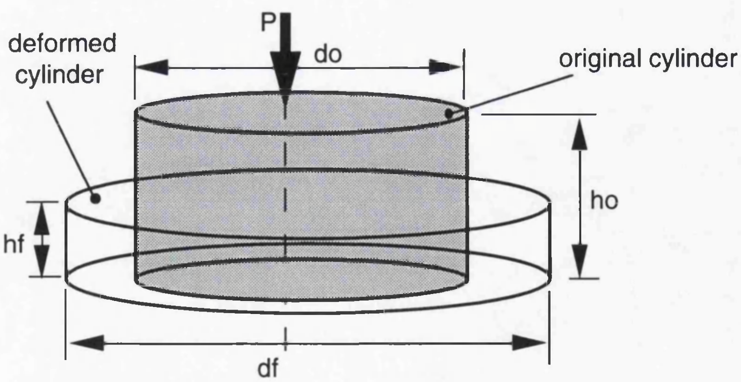

FIGURE 11

Compression of cylinder of linearly elastic material (Reynolds, 1988)

Exact Solution

The load required to compress the cylinder can be expressed as a function of the original dimensions of the cylinder and the instantaneous height. The derivation of the expression is described below.

The true stress (σ_T) is the ratio of the load to the instantaneous area.

$$\sigma_T = \frac{P}{A} = \frac{P}{\frac{\Pi}{4} d^2} \qquad \text{.................................} \qquad 4.1$$

where A, d are the instantaneous values of the cross sectional area and diameter. P is the applied load.

The natural lateral strain (ε_h) is the natural logarithm of the ratio of the instantaneous height to the original specimen height.

$$\varepsilon_h = \ln\left(\frac{h}{h_o}\right) \qquad \text{.................................} \qquad 4.2$$

where h is the instantaneous height, h_o is the original height.

At any stage of deformation there is a linear relationship between true stress and natural strain:

$$\sigma_T = E\varepsilon_h \qquad \text{.................................} \qquad 4.3$$

Where E=Young's modulus (relating true stress and natural strain)

An expression for the diameter at any instant can be formulated in terms of Poisson's ratio, the axial strain and the original specimen dimensions.

Poisson's ratio is the ratio of the lateral strain to the axial strain under uniaxial loading:-

$$\varepsilon_d = -\upsilon\,\varepsilon_h \qquad \text{.................................} \qquad 4.4$$

Where υ is Poisson's ratio, ε_d is the lateral strain.

The natural lateral strain can be expressed in terms of the instantaneous diameter and the original diameter.

$$\varepsilon_d = \ln\left(\frac{d}{d_o}\right) \qquad \text{.................................} \qquad 4.5$$

Where d_o is the original diameter.

Substituting 4.5 into 4.4 and rearranging gives the following expression for d

$$d = d_o \exp(-\upsilon\varepsilon_h) \qquad \text{.................................} \qquad 4.6$$

Substituting equations 4.2 into 4.6 and rearranging yields the following expression.

$$d=d_o\left[\frac{h}{h_o}\right]^{-\upsilon} \qquad \text{4.7}$$

Substituting equations 4.3 and 4.7 into 4.1 yields an expression for the load required to compress a specimen to a height h_f.

$$P=E\frac{\Pi}{4}d_o^2\left[\frac{h_f}{h_o}\right]^{-2\upsilon}\ln\left(\frac{h_f}{h_o}\right) \qquad \text{4.8}$$

Since the cylinder is made of incompressible material υ=0·5 and the load required to compress it to a height of 0·5 units is found to be -1·089 load units. The engineering stress required to cause the strain is -1·387 units.

<u>Solution assuming a linear nominal stress - engineering strain relationship (small deflection solution)</u>

If a linear relationship between nominal stress and engineering strain is assumed, the effects of geometric changes in the cylinder are neglected and the load required to produce a large strain is substantially underestimated. The magnitude of the error is examined below.

The nominal stress (σ_e) is the ratio of the applied load to the original cross section area

$$\sigma_e=\frac{P}{A_o} \qquad \text{4.9}$$

where A_o is the original cross-sectional area.

The engineering strain (e) is the ratio of the change in height to the original height

$$e=\frac{h_f-h_o}{h_o} \qquad \text{4.10}$$

A linear relationship between nominal stress and engineering strain is assumed.

$$\sigma_e=E'e \qquad \text{4.11}$$

Where E' is Young's modulus (relating nominal stress and engineering strain)

Substituting equations 4.9 and 4.10 into 4.11 and rearranging gives

$$P=E'\frac{\pi}{4}d_o^2\frac{h_f-h_o}{h_o} \qquad \text{4.12}$$

The force required for the compression is calculated to be -0·393 load units, some 36 percent of the exact value. This corresponds to an nominal stress of -0·5 units. Such a solution procedure is unsuitable for the modelling of the soft tissues of the buttock, because it grossly under estimates the stresses, required to produce a large deformation in an elastic material.

Solution using a large deflection incremental procedure

If the loads are applied in small steps and the length of the specimen is updated prior to each load increment, a better estimate of the load required to produce a large strain is obtained. However the loads that are required are still underestimated. The magnitude of the error is examined below.

An increment of load, ΔP, is considered which increases the applied stress on the specimen and deforms it to a shorter shape with a larger cross-sectional area. An expression for ΔP is as follows:

$$\Delta P = A\,\Delta\sigma + \sigma\,\Delta A \quad \text{.................................} \quad 4.13$$

Where A is area prior to load increment ; $\Delta\sigma$ is change in stress; σ is stress prior to load increment; ΔA is change in area.

The first term on the right hand side of 4.13 represents the part of the load increment that increases the stress over the instantaneous area. The second term represents the part of the load that produces an increase in the area of the specimen, at the current level of stress. Unfortunately in a incremental large deflection solution procedure, the load that produces a change in area of the element is neglected. The second term in 4.13 is assumed to have zero value through out the iterative process.

Since the stress at the start of a load increment is neglected, the stress increment is equivalent to the nominal stress. Substituting equation 4.11 into 4.13 gives:

$$\Delta P = A\,E'\frac{\Delta h}{h} \quad \text{...} \quad 4.14$$

where Δh is the change in height of the specimen.

The area, A, can be expressed in terms of specimen height using expression 4·7 for the instantaneous diameter.

$$A = \frac{\Pi d_o^2}{4}\left(\frac{h}{h_o}\right)^{-2\upsilon} \quad \text{.....................................} \quad 4.15$$

Substituting 4.15 into 4.14 gives the following expression for the load increment :-

$$\Delta P = E'\frac{\Pi}{4}\frac{d_o^2}{h}\left(\frac{h}{h_o}\right)^{-2\upsilon}\Delta h \quad \text{.......................} \quad 4.16$$

In the limiting case where Δh tends to zero, equation 4.16 becomes :

$$\frac{dP}{dh} = E' \frac{\Pi}{4} \frac{d_o^2}{h} \left(\frac{h}{h_o}\right)^{-2\upsilon} \qquad \ldots\ldots\ldots\ldots\ldots\ldots\ldots \qquad 4.17$$

Equation 4.17 may be integrated between the limits of an initial height h_o to a final height, h_f to give the expression below for the force required to compress the cylinder.

$$P = E' \frac{\Pi}{4} d_o^2 \, h_o^{2\upsilon} \left(\frac{1}{2\upsilon h_o^{2\upsilon}} - \frac{1}{2\upsilon h_f^{2\upsilon}} \right) \qquad \ldots\ldots\ldots\ldots\ldots\ldots\ldots \qquad 4.18$$

The force required to compress the cylinder P to half of its original height is calculated to be -0·785 loads units, some 72 percent of the exact answer. This corresponds to a nominal stress of -1·0 unit. In addition to the approximations discussed above, finite strain increments are applied in a solution and thus the errors are greater than those calculated above. The large deflection FE analysis is clearly better than the small deflection analysis at estimating the loads that are required to compress the linearly elastic incompressible material. However it still significantly underestimates the loads that are required.

By comparing equations 4·8 and 4·18 it is apparent that the error in the large deflection solution increases with the size of the applied strain and also with the compressibility of the material. The sensitivity of the large deflection solution to strain and Poisson's ratio is demonstrated in Figure 12.

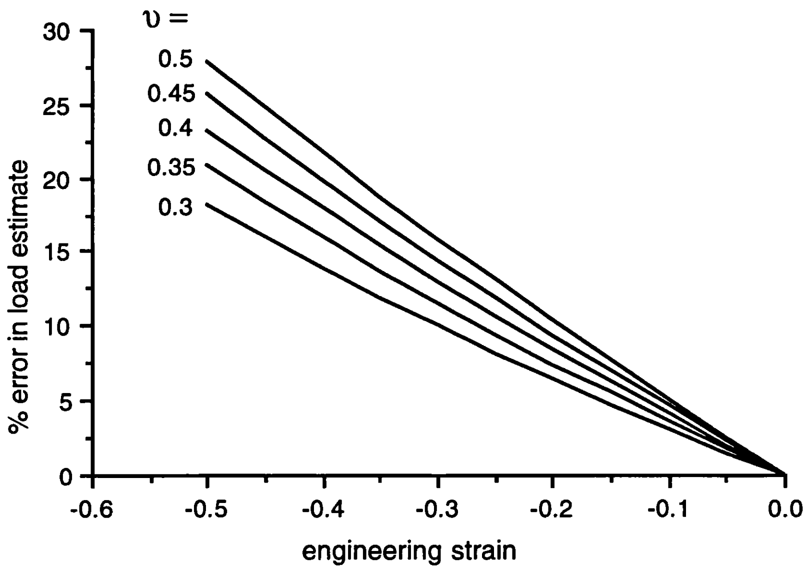

FIGURE 12

Sensitivity of error in large deflection solution to strain and Poisson's ratio

Greater accuracy can be achieved by FE analyses for problems that involve large strains. An example of such a FE analysis is the one that can be performed with hyperelastic materials. This formulation is described in more detail in Section 4·4.

4.3 Consideration of Material Properties in Finite Element Formulation

The material formulation is another area where errors may be introduced into an analysis if the tissues are modelled as a nearly incompressible elastic material. The equations of linear elasticity relating nominal stress and engineering strain, can be used with different elastic moduli at different strain ranges to model nonlinear behaviour in a piecewise manner. An iterative procedure is required to take account of the stiffness matrix that changes with displacement. However a small-strain assumption is also made in this type of formulation, and it is as such still unsuitable for modelling a system under larger strains, for the reasons discussed in Section 4·2.

When modelling nearly-incompressible elastic materials the solution is very sensitive to the assumed value of Poisson's ratio. For an isotropic material in many strain states, the denominator in the elasticity matrix includes a (1-2υ) term. For more detail see Appendix 4. For example, with a plane strain analysis, the elasticity matrix is

$$D=\frac{E(1-\upsilon)}{(1+\upsilon)(1-2\upsilon)}\begin{bmatrix} 1 & \frac{\upsilon}{1-\upsilon} & 0 \\ \frac{\upsilon}{1-\upsilon} & 1 & 0 \\ 0 & 0 & \frac{1-2\upsilon}{2(1-\upsilon)} \end{bmatrix}$$

Where E=Young's modulus; υ=Poisson's ratio.

if Poisson's ratio υ is assumed to have a value of 0·5 the solution method breaks down completely. At values of υ that are close to 0·5 the solution becomes very sensitive to the exact value of Poisson's ratio. For example, in a plane strain situation, when the strain components ε_x and ε_y are equal to 0·1, the stress components σ_x and σ_y would be equal to 3·36E when υ =0·49, but would only be equal to 0·69E when υ=0·45.

4.4 Finite Element Analysis of Hyperelastic Materials

The properties of hyperelastic materials are examined and in particular the hyperelastic material formulation in FE analyses involving large strains is discussed. Detailed information on nonlinear continuum mechanics and rubber-like elasticity can be found in Rivlin (1984) and Treloar (1975).

With the FE analysis of a hyperelastic material, no error is introduced into the calculations when large deformations and incompressible materials are considered, unlike with the analyses discussed in Sections 4·2 and 4·3. The stiffness matrix is a function of nodal displacements so an iterative procedure is necessary. The solution is also very sensitive to the rate of load application, so the load has to be applied in small steps. In the analyses, Green's deformation tensor and the Lagrangian finite strain tensor are calculated, both of which are suitable for describing finite strains. Also the true stresses in the system are calculated, thus the change in shape of the element during the solution is taken into account. A direct comparison with the linearly elastic analyses in the previous sections cannot be made because the stress-strain behaviour of a hyperelastic material is nonlinear. Appendix 4 includes a more detailed discussion of the finite element method for hyperelastic materials.

A material that is hyperelastic has a strain energy density function that is a scalar function of one of the strain or deformation tensors. For isotropic materials the strain energy function can be expressed in terms of the strain invariants. The strain invariants can be written in terms of the extension ratios λ_i which are the ratio of the deformed length to the original length. (see Appendix 3).

$$I_1 = \lambda_1^2 + \lambda_2^2 + \lambda_3^2 \quad I_2 = \lambda_1^2\lambda_2^2 + \lambda_2^2\lambda_3^2 + \lambda_3^2\lambda_1^2 \quad I_3 = \lambda_1^2\,\lambda_2^2\,\lambda_3^2 \quad \ldots\ldots\ldots\ldots\ldots \quad 4.18$$

As a material approaches incompressibility, the value of the third invariant I_3 approaches unity.

The derivative of the strain energy function with respect to a strain component determines the corresponding stress component. An expression for the engineering stress components can be formed in terms of the partial derivatives of the strain energy density function with respect to the strain invariants and the partial derivative of the strain invariants with respect to the extension ratios.

$$\sigma_i = \frac{2}{\lambda_i}\left(\lambda_i^2\frac{\partial W}{\partial I_1} + I_2\frac{\partial W}{\partial I_2} - \frac{I_3}{\lambda_i^2}\frac{\partial W}{\partial I_2} + I_3\frac{\partial W}{\partial I_3}\right) \quad (i=1,2,3) \quad \ldots\ldots\ldots\ldots\ldots \quad 4.19$$

Where σ_i =engineering stress; W =strain energy function.

This relationship can be simplified in simple deformation states if the form of the strain energy function is known. The Mooney equation is one simple formulation for incompressible hyperelastic materials. It is often used to describe the behaviour of natural rubbers and is as follows:-.

$$W = A\,(I_1-3) + B\,(I_2-3) \quad \ldots\ldots\ldots\ldots\ldots \quad 4{\cdot}20$$

Where A, B are constants. The sum of the constants A and B must be positive to ensure that the strain energy under a small shear deformation is positive. The stress-extension ratio relationships for a Mooney material in simple deformation states are discussed in Section 6.5.

The hyperelastic material formulation has been shown to have potential for use in an FE model of the seated buttock. Its application to such a model is reported in Chapter 5.

CHAPTER 5 INITIAL FE MODEL AND EXAMINATION OF THE SOFT TISSUE MATERIAL COEFFICIENTS

5.1 Background and Scope

A simple FE model is described in this chapter, based on the measurements on the human buttock that were reported in Chapter 3. The soft tissues are modelled as a Mooney-type material and the vertical force-deflection characteristics of the model are compared with those of the soft tissue of the buttock. Various material constants are examined and the Mooney material that behaves closest to the soft tissues is identified. Also the interface pressure distribution for the subject sitting on a planar surface is compared with that calculated from the model.

The Mooney equation has the following form in the finite element software ANSYS (Swanson Analysis Systems Inc, Houston, USA):-

$$W = A(I_1-3) + B(I_2-3) + C(^1/I_3^2 - 1) + D(I_3-1)^2 \quad \ldots\ldots \quad 5.1$$

Where A, B are constants; C & D are functions of A & B & Poisson's ratio υ; I_i are the strain invariants. This equation, which is in a form which is applicable to compressible materials, will henceforth be called the Mooney-Rivlin equation. As the material approaches incompressibility, the third and fourth terms in 5.1 become insignificant.

$$C=\frac{A}{2}+B \; ; \qquad D=\frac{1}{2}\left[\frac{(A(5\upsilon-2)+B(11\upsilon-5))}{1-2\upsilon}\right] \quad \ldots\ldots \quad 5.2\ a,\ b$$

The Newton-Raphson approximation technique is used to obtain a solution to the nonlinear finite element equation. The Newton-Raphson procedure involves multiple passes through the equation solver with an updated stiffness matrix at each pass. The results from each iteration are compared with those of the preceding iteration to see whether there are any significant changes in the displacement increments, status of the nonlinear elements and strain increments. When the changes between successive iterations are insignificant the load step converges. When the solution contains path dependent nonlinearities, the solution requires intermediate steps to be in equilibrium, in order to correctly follow the load path, so the total load is applied in multiple load steps. Finite element theory and its application to nonlinear problems are discussed in more detail in Appendix 4.

5.2 Finite Element Model

A model of the soft tissues of the buttock and a flat, rigid seat surface was constructed with the ANSYS finite element modelling package. The soft tissues of the buttock were assumed to be axi-symmetric with an elliptical external surface and an inner surface based on the shape of half of the pelvis, with the ischial tuberosity at the centre. It was considered unnecessary to model the pelvic structure because the deformations occurring in the bone were negligible compared to those occurring in the soft tissue. The model with dimensions and boundary constraints is shown in Figure 13.

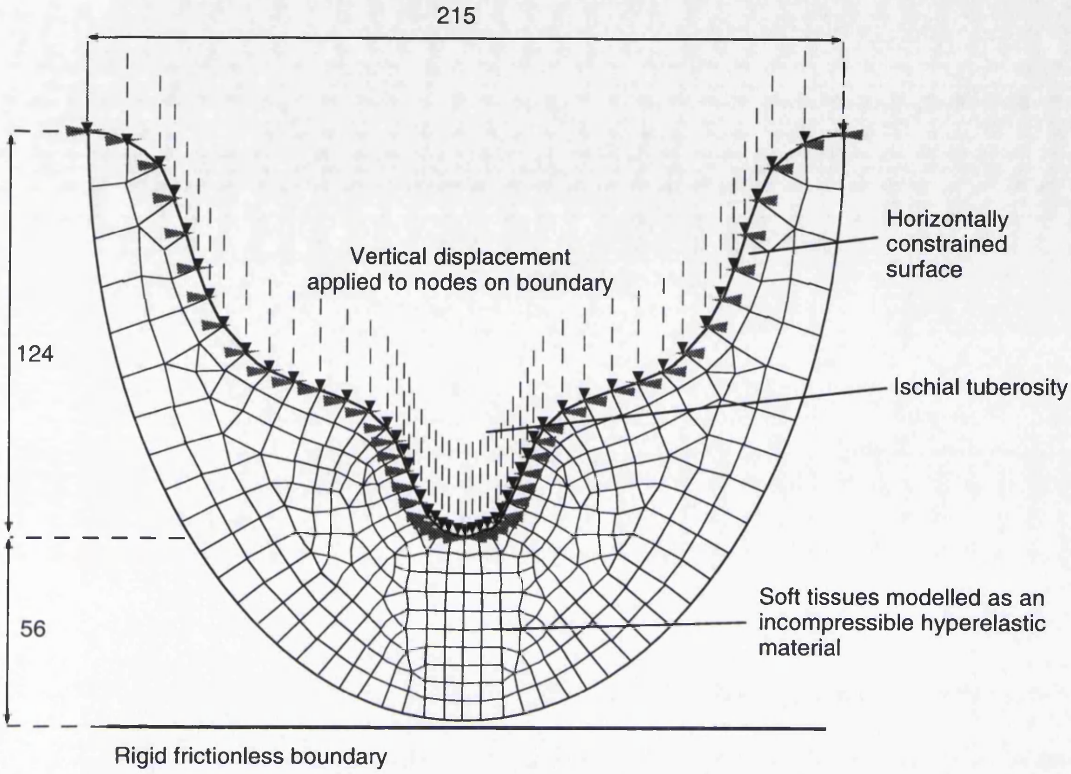

FIGURE 13

Axi-symmetric finite element model of buttock (dimensions in millimeters)

It was assumed that the soft tissues could be modelled by a homogeneous, isotropic, nearly incompressible Mooney-Rivlin material. The material was meshed with eight-noded quadrilateral STIF86 elements. The nodal degrees of freedom were UX and UY. The mesh was generated with the automatic facility within ANSYS. The degenerate triangular form of the element was only used when the irregular geometry of the shape to be meshed did not allow otherwise. The errors caused by the mesh density were checked by running an analysis with double the density and examining the difference in the stiffness and stress results. The mesh density under the ischial tuberosity was refined until it was about 4 times that in the rest of the structure. This produced a difference in the stress and stiffness results of less than 5 percent. 167 STIF86 elements were needed to model the soft tissue volume. The characteristics of these elements and the other elements in the FE analyses are described in Appendix 5.

The flat surface was modelled with fixed 1-noded STIF26 elements. When the nodes associated with the surface of the Mooney-Rivlin material came into contact with the boundary, they encountered a vertical stiffness. The boundary was given a stiffness of 50,000 force units/mm which limited the travel through the surface to less than 0·01 mm in all cases. No stiffness was applied along the length of the boundary, so the nodes were free to slide horizontally. 34 STIF26 elements were needed to model the surface.

Eight analyses were performed with different values for the material coefficients A , B and υ (see equation 5·1). The ratio of the coefficients covered the range of allowable values.

Set	1	2	3	4	5	6	7	8
A	8×10^{-5}	8×10^{-5}	8×10^{-5}	8×10^{-5}	8×10^{-5}	-0.5	-0.9	-0.95
B	2×10^{-7}	2×10^{-5}	8×10^{-5}	8×10^{-3}	8	1.0	1.0	1.0
υ	0. 49	0. 49	0. 49	0. 49	0. 49	0. 49	0. 49	0. 49
A/B	400	4	1	10^{-2}	10^{-5}	-0.5	-0.9	- 0.95

The nodes on the upper surface of the soft tissue were fixed in the horizontal plane. A vertical displacement was applied to the nodes at each load step. This was in the direction of the rigid surface. The displacement increment of 0·5 mm was applied at most load steps. The nodes on the outer surface of the buttock were unconstrained until they came into contact with the rigid surface. At this point they were fixed in the direction perpendicular to the surface, but still free to move along its length.

The analysis was solved on a DELL 325 computer with 4 MBytes of extended memory and an Intel 80387 maths co-processor. Each load step was solved in an iterative manner using the full Newton - Raphson solution method. The loads were applied until there was more than 87 percent deflection of the soft tissue under the ischium. At some points during the solution, it was necessary to apply displacement steps as small as 0·5 mm for convergence to occur. The displacement increment convergence criterion was set at 0·01 mm. The solution aborted if there was a convergence failure at any load step.

5.3 Results

The vertical load-deflection curves were normalised so the same vertical loads were supported when there was 86·1 percent vertical strain in the material under the bony prominence. This corresponded to the strain in the tissues under the ischial tuberosity that was measured with the subject sitting on a planar surface. The calculated stiffness curves were compared with the measured force-deflection data. The calculated and measured curves are shown in Figure 14 and the normalised load-deflection data in Appendix 6. For clarity, the results from sets 2, 4, 6 and 7 are omitted from the figure. The systems stiffened vertically as the applied displacement increased. As the A/B ratio (see equation 5·1) decreased the stiffness became more nonlinear.

When A was negative and its magnitude approached that of B, the solutions became unsolvable, due to bifurcations at the first load step. The calculated stiffness curve which was closest to the measured curve was that from set 8 with A = -0·95 and B = 1·0 .

The constants A and B were converted to Newton and millimetre units. The load units were selected such that the model supported 186·9 N vertical load at 86·1 percent deflection. This corresponded to the load supported through one buttock with the subject sitting on a planar surface. The values of A and B from each of the analyses are shown in the table below and in Figure 14 in N/mm^2 .

Set	1	2	3	4	5	6	7	8
A	2·6 E-3	1·8 E-3	9·9 E-4	1·6E-5	1·6 E-8	-1·3 E-3	-3·9 E-3	-5·0 E-3
B	6·4 E-6	4·6 E-4	9·9 E-4	1·6E-3	1·6 E-3	2·7 E-3	4·3 E-3	5·3 E-3

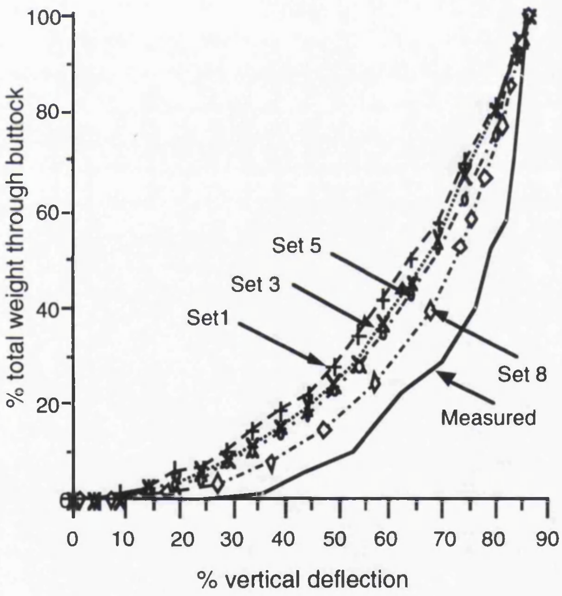

Normalised vertical force deflection curves calculated from FE analyses and measured on a subject

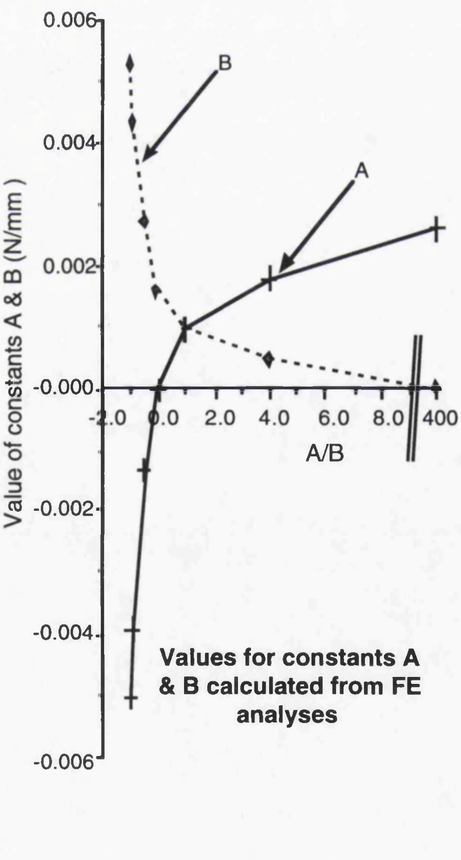

Values for constants A & B calculated from FE analyses

FIGURE 14

Stiffness results and material coefficients from FE analyses

The deformed model and the von Mises and hydrostatic stress distributions under the bony prominence are shown in Figure 15 for analysis no. 8 with the full body weight supported through the ischial tuberosities. The maximum von Mises stress and compressive hydrostatic stress were directly under the bony prominence. The hydrostatic stress gradients were also greatest in the area under the bony prominence. The material under the bony prominence moved in a radial direction once contact with the surface had been made. The maximum lateral nodal displacement at the surface of the soft tissue was 10·97 mm. The area of contact between the buttock and the surface was calculated to be 12100 mm^2. This was less than half the contact area measured under the buttock in Chapter 3.

5.4 Comparison of Experimental and Calculated Interface Pressures

The pressure distribution between the body of the subject and a flat rigid surface was examined and compared with the interface pressure distribution calculated from the theoretical model. The methodology and equipment used to make the measurements are described in Chapter 2.

The average pressure measured at each grid point is shown in Figure 16. For clarity approximate contours were drawn around the grid points above certain pressure levels. On both sides of the body there was a maximum pressure which was off the scale of the pressure monitor (over 300 mmHg) at the approximate position of the ischial tuberosity. Within 30 mm of these maxima the pressure was less than 100 mmHg (13·3 kPa). The interface pressure over the outer 50 mm of the area of contact was less than 40 mmHg (5·3 kPa).

An approximate pressure distribution between the soft tissue and the surface was calculated from the nodal positions and forces on the interface for the set 8 analysis. The vertical forces on nodes at the interface were assumed to be associated with half of the area of each of the two adjacent elements. Due to the axi-symmetric nature of the model, the forces on the central axis were calculated to be zero. A Stineman interpolation was made between the non-zero pressure results (Cricket Graph, Reference Manual). The data was not extrapolated to the central axis, due to the limited load information in this region.

In Figure 16 the calculated pressure distribution is shown and compared with four sections through the measured pressure distribution. The sections were all at 45 degrees to one another and all passed through the location of the peak pressure under the left buttock. The maximum pressure values calculated in the model were higher than the measured ones. However the calculated pressure distribution was similar in shape to the measured one. The maximum pressure was under the ischial prominence and the pressure then dropped off sharply to less than half the maximum value within 20 mm of the maximum.

Features of the model that might contribute to the differences between the measured and calculated distributions are discussed in Section 5·5.

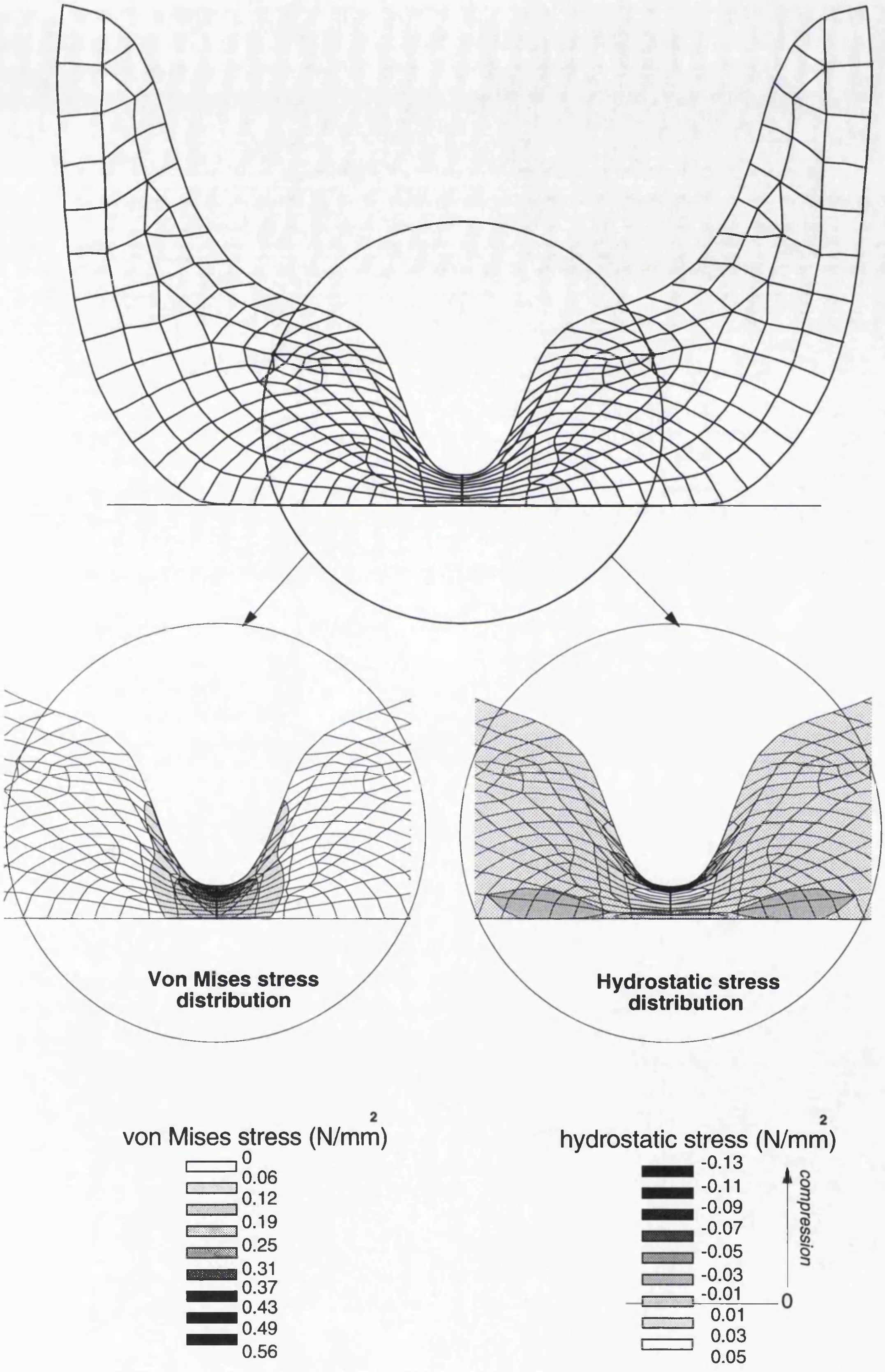

FIGURE 15
Deformed finite element mesh & stress distribution in soft tissue layer

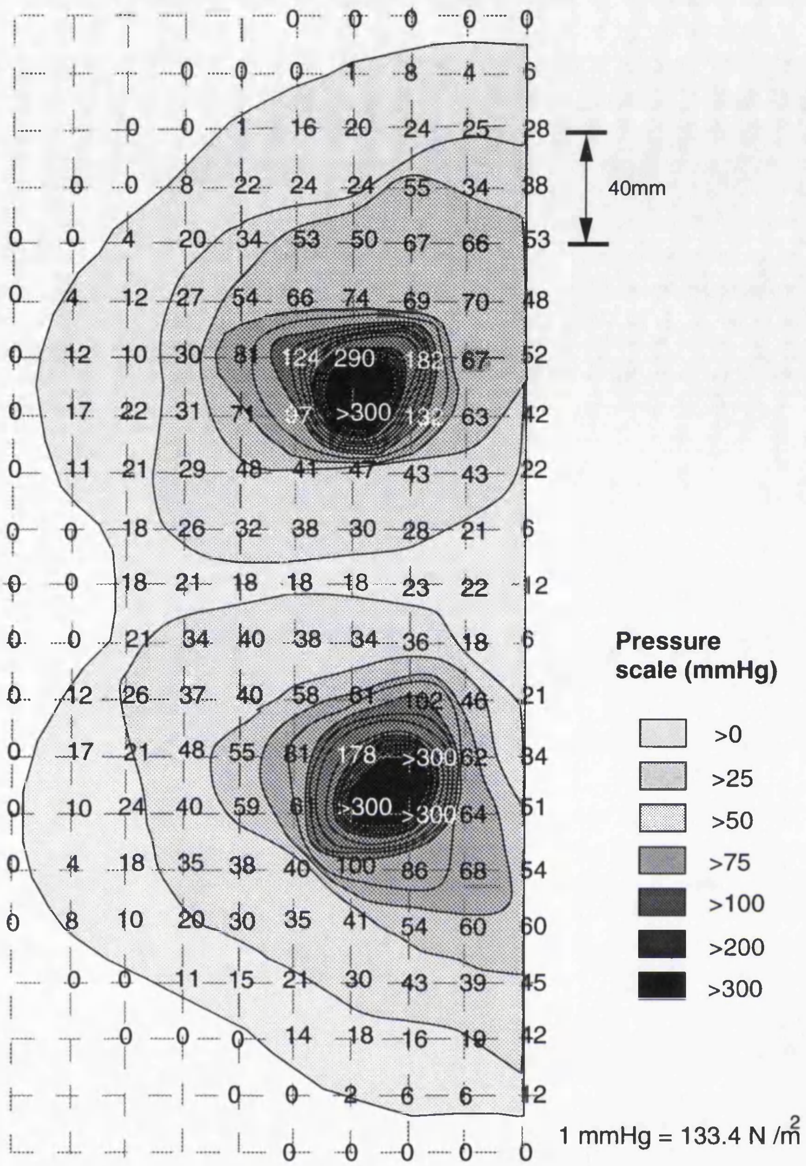

Measured pressure distribution

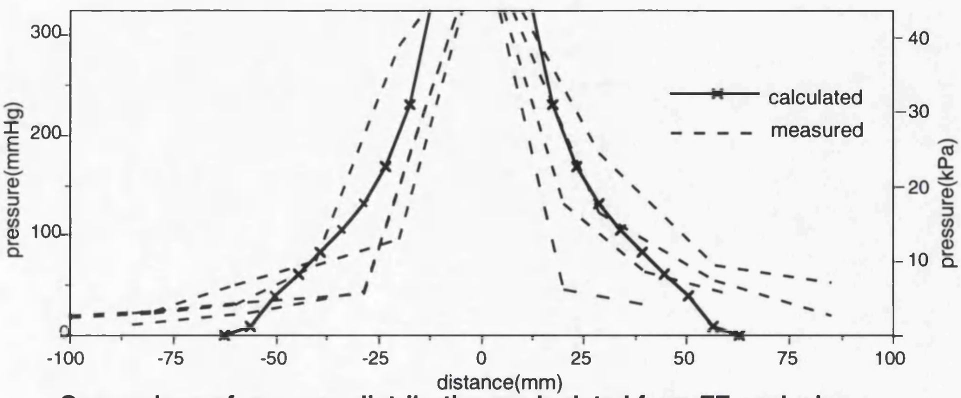

Comparison of pressure distributions calculated from FE analysis (set 8) and measured in 45 degree sections through left buttock

FIGURE 16
Interface pressure distribution between buttocks and planar surface

5.5 Discussion

Vertical force-deflection behaviour and an interface load distribution were calculated in the analyses which were similar but not identical to the measured behaviour of the buttock. In this section the limitations of the analyses are discussed.

The model of the buttock had a simple axi-symmetric geometry. The difference between the geometry of the model and that of the actual buttock is likely to have contributed to the relatively small calculated area of contact between the buttock and the seat, and hence the relatively large pressures calculated at the interface.

The interface shear forces were assumed to be zero in the theoretical model. Where as the interface friction was low during the tissue stiffness measurements, however it was unlikely to have been zero. In Chapter 7 of this thesis it is shown that the presence of interface shear forces leads to an increase in the nonlinearity of the vertical load-deflection behaviour. Thus a model with non-zero interface shear forces would have had vertical force-deflection behaviour that was closer to the measured behaviour.

The body forces on the buttock were not taken into account in the theoretical model. When the vertical stiffness curve for the soft tissue of the buttock was measured, the tissues were subject to a gravitational load. This would have tended to extend the tissues vertically. During the initial stages of the deformation, when the tissues began to be loaded by the seat, the deformations due to the effects of the gravity would have been overcome. Thus a model that took account of the effects of gravity would have had vertical force-deflection behaviour that was closer to the measured behaviour.

In the model the soft tissues in the buttock were assumed to be a single layer of homogeneous elastic isotropic material. As discussed in Chapter 1 the actual buttock tissues comprise skin, muscle and adipose tissue and each of these tissues is made up of multiple components. These composite structures give rise to inhomogeneous, anisotropic, viscoelastic material properties. As the tissues are loaded there will be a different response within each soft tissue component depending on its properties. The relative motion at the interface between the tissue components will contribute to the measured deformations. Also the extracellular fluid may flow out of a heavily loaded area during the initial stage of loading. These deformation mechanisms could contribute to the initial low vertical stiffness that was measured and could not be reproduced in the model with a single soft tissue layer.

A model with a multi-component, composite soft tissue structure could have produced vertical load deflection behaviour that was closer to the measured behaviour. However information on the material properties of each of the tissue components and the interface properties would be difficult to establish. Because of these difficulties, an anisotropic inhomogeneous description of the soft tissues was not attempted in subsequent analyses.

Also the load-deflection behaviour of the soft tissues in the analyses was compared with measurements only in the vertical direction. Information on the deflections occurring in the horizontal plane would have given a more complete picture of the in-vivo force-deflection behaviour of the soft tissues, and thus enabled a better comparison to be made with the analytical results.

It was thought that if the theoretical model had a more realistic geometry, there would be a closer correlation with the behaviour of the seated buttock. Chapter 6 describes studies to measure the surface geometry of the buttock and the internal bony geometry of the pelvis, in order to develop a more realistic FE model.

CHAPTER 6 EXAMINATION OF BODY GEOMETRY AND FURTHER DEVELOPMENT OF FE MODEL

In this chapter the geometry of the body is examined, in the belief that a comprehensive FE model of the body can be developed from these geometries. The buttock shape is measured both during sitting on a flat surface and when the body is in a sitting position but when there are no surface forces applied to the buttock. The shape information is used to improve the FE analyses of the buttock-seat interaction, to produce seats in the shape of the suspended buttock and to estimate the soft tissue deformations that occur during sitting on a planar seat.

6.1 Examination of the Suspended Buttock Shape

The shape of the freely suspended buttock was measured with the plaster casting technique described in Section 2.3. The resulting buttock shape is shown in Figure 17.

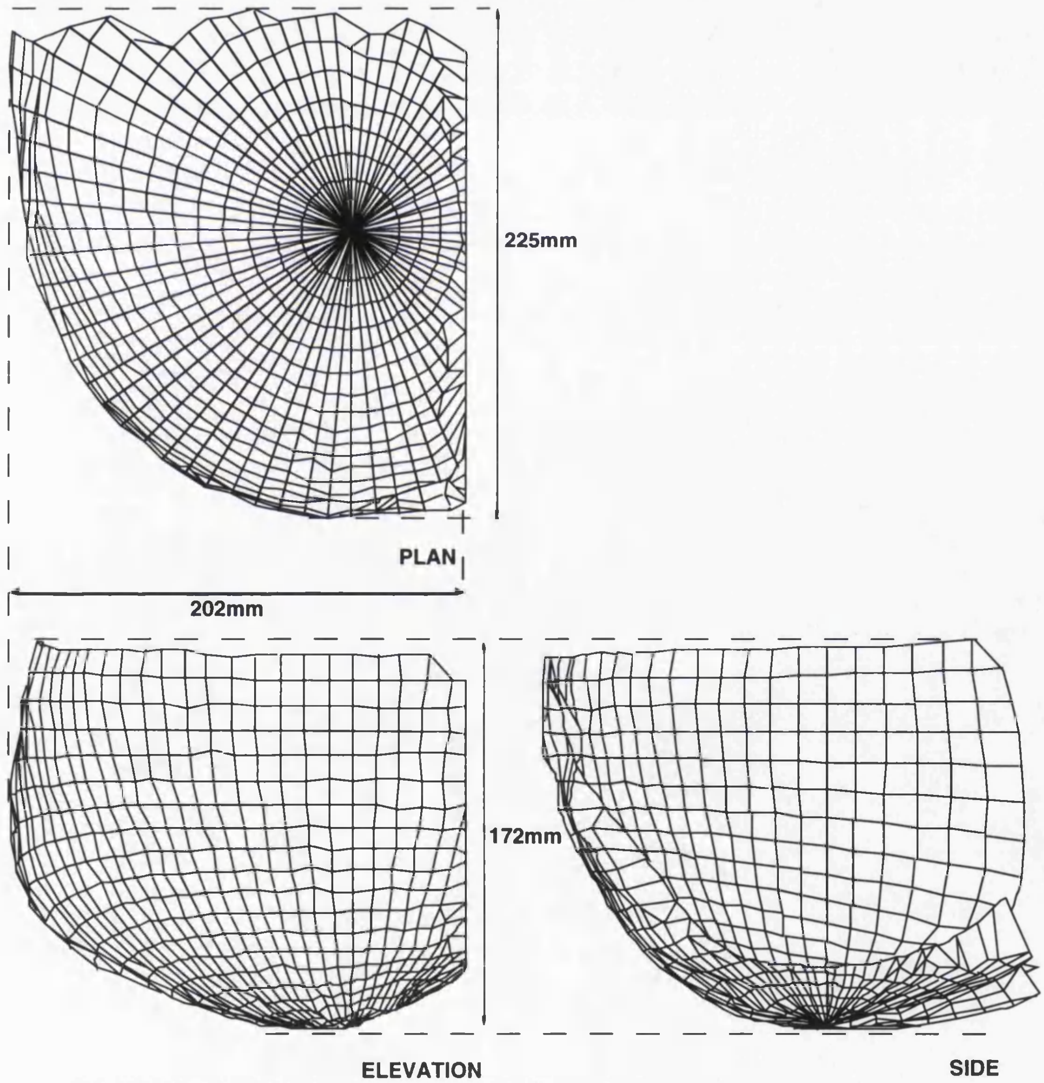

FIGURE 17
Average shape of castings of suspended buttock

The shape of the buttock was also measured with a laser scanner (see Section 2.4). Contour maps of the suspended buttock shape, measured with the scanner and from the castings, are compared in Figure 18. The superimposed sections used to align the shapes are also shown.

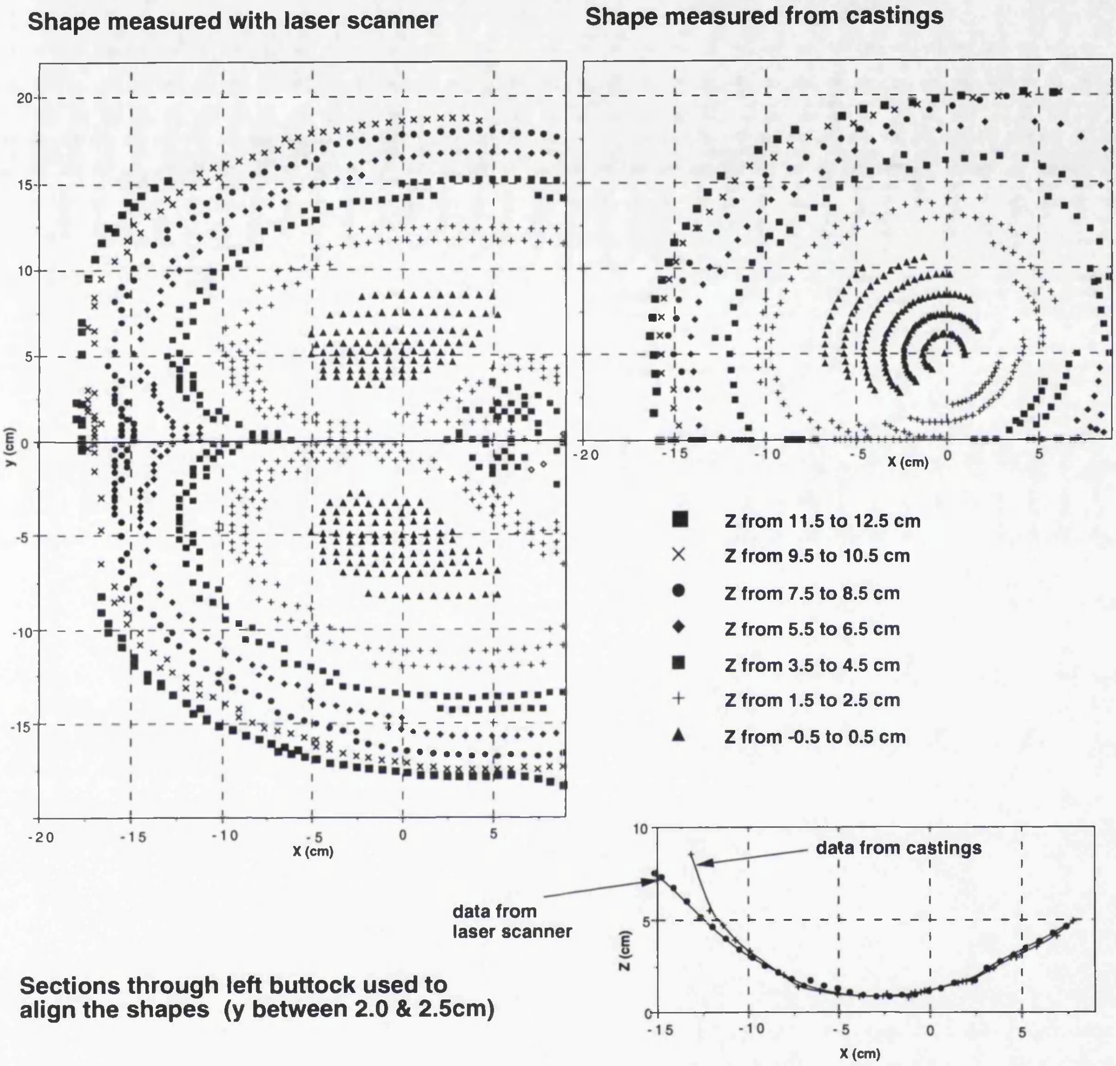

FIGURE 18
Comparison of shapes measured from castings and with laser scanner

By comparing the two shapes, it was apparent that the hips were more extended during the scanning process than during the casting process. Also the shape measured by casting was about 2 cm wider than the laser scanned shape in the region from x= -5 cm to 5 cm. This may have been due to the hips being more adducted when the laser scan was made.

For the subsequent tissue deformation estimate and the shaped seat production, the casting shape was used because of the difficulties in finding a position which was both similar to the sitting position and suitable for non-contact shape measurement.

6.2 Examination of Buttock Shape During Sitting on a Planar Surface

The shape of the seated buttock was measured with the casting technique described in Chapter 2 and an average shape was calculated. The average shape is shown in Figure 19.

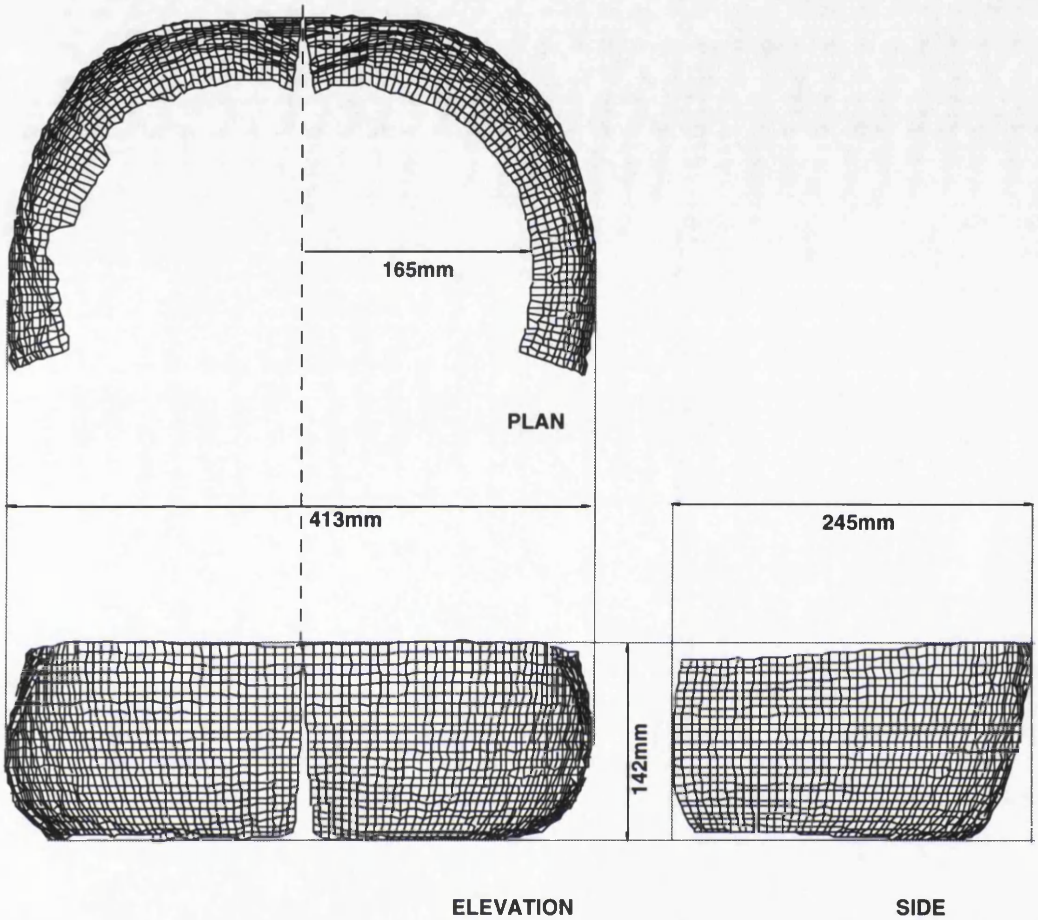

FIGURE 19
Average shape of buttock, measured during sitting on a planar surface

The outline of contact of the seat and body had a slight slope in the average casting shape. Since the original castings were horizontal when measured, this was thought to be due to the scarcity of measured data points in this region. The maximum width of the outline of contact between the seat and the buttock was smaller than that which was measured in Chapter 3 (16·5 cm compared to 18·5 cm). This difference may be due to the plaster of Paris laterally constraining the soft tissues or, more likely, to small amounts of liquid plaster flowing under the buttocks during the casting process.

The average shapes of the left buttock prior to and during sitting were graphically superimposed. This gave a crude estimate of the soft tissue deformations which might occur when the subject sat on a flat rigid surface. It was difficult to align the 'deformed' and ‘undeformed’ shapes since they had been calculated from castings of the buttock which were made at different times. The central plane of the shapes and the surface over the proximal posterior sacrum (13 cm to 15 cm above the seat) were superimposed. As an additional reference, the surfaces were transformed so that the suspended buttock surface was positioned within the seated buttock surface at the height of the seat. The surfaces were both transformed so the x axis was at the intersection of the seat and central planes, the y-axis was a tangent to the back of the seated buttock surface, and the z- axis was vertical. Sections through the superimposed surfaces are shown in Figure 20.

The aligned shapes suggest that the soft tissue of the buttock is displaced upward and outward during sitting on a flat surface. The maximum difference in the vertical position of the two surfaces was 3.0 cm and was located between x=10 cm and 10.5 cm ; y= 6 cm and 6.5 cm. The maximum difference in the position of the body surface in the horizontal plane was about 2.0 cm and was located between 2 cm and 6 cm above the seat surface. The horizontal displacement of the soft tissue between x=10 cm to 20 cm extended to 14 cm above the seat surface. This was in the region of the hip joint. The maximum vertical displacement was considerably less than that which was measured with the Tissue Stiffness Testing Device. This is likely to have been due to the soft tissues being displaced by plaster of Paris. The displacement could have been a result of increased hydrostatic pressure with depth of plaster or a result of movement of the body vertically downward during the time that the plaster was beginning to harden under the buttock.

6.3 Graphical Reconstruction of Pelvis From Magnetic Resonance Images

A graphical reconstruction of the pelvis was made using the methodology described in Chapter 2. A hidden line drawing of the pelvic reconstruction is shown in Figure 21. The right hip bone, sacrum and left posterior ilium were not reconstructed due to limited imaging in these regions. Approximate outlines of these regions of the pelvis are included in the figure to illustrate the measurements described below.

The soft tissue surrounding the pelvis consisted of muscle, adipose tissue and skin. The tips of the ischial tuberosities were about 150 mm apart. The distance between the tip of the ischial tuberosities and the acetabular centres was about 73 mm. The distances between the centre of the femoral heads was about 200 mm. The diameter of the femoral head was about 45 mm. The distance between the end of the sacrum and the centre of the pubic symphysis was about 115 mm. The minimum depth of soft tissue over the sacrum was about 9 mm. There was a minimum of 40 mm of tissue over the greater trochanters. The distance from the centres of the femoral heads to the skin surface was about 102 mm.

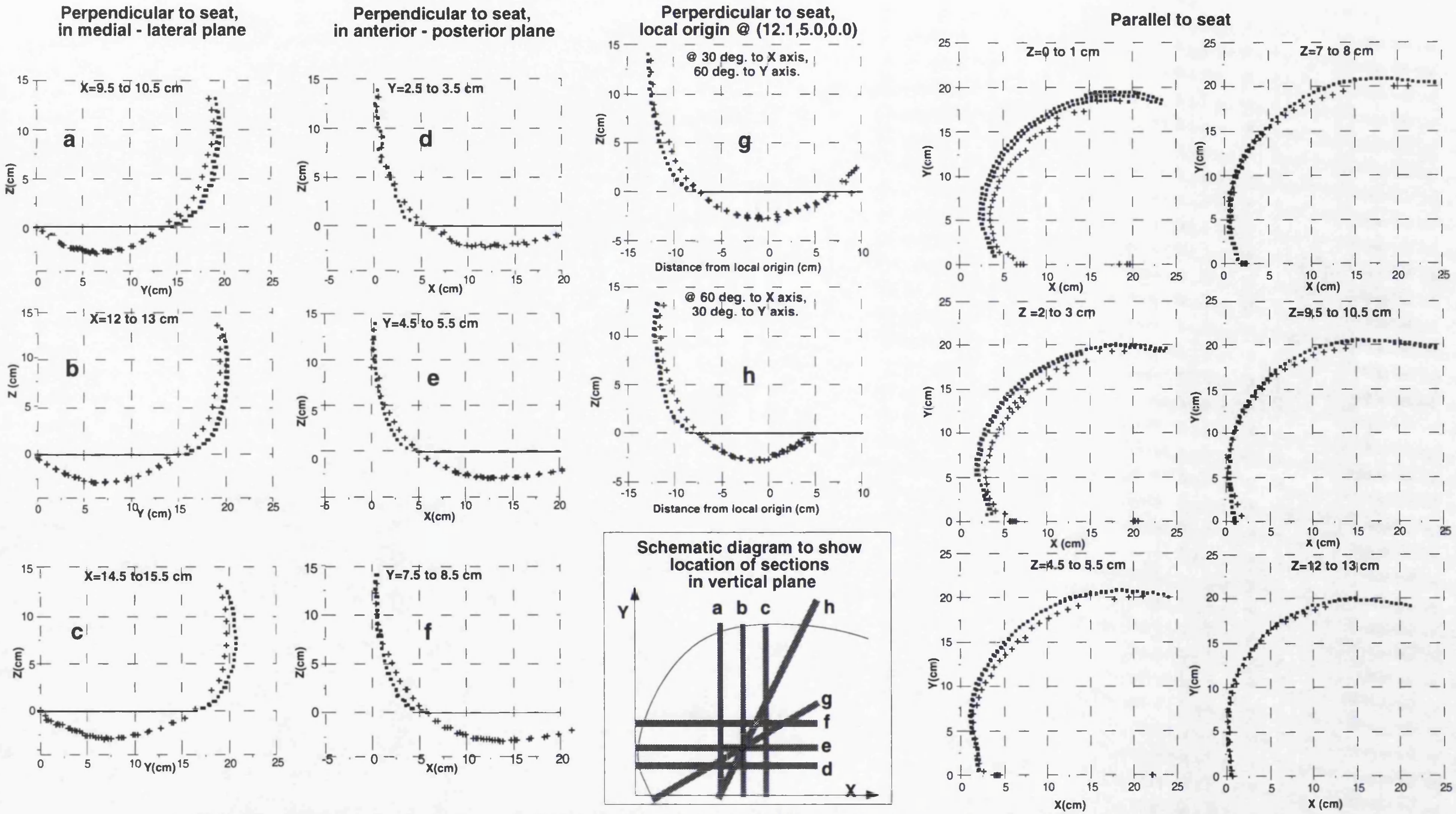

FIGURE 20 Sections through average buttock shapes measured by casting the suspended and seated buttock. The shapes were aligned to estimate the soft tissue deformations which occur during sitting on a flat rigid surface

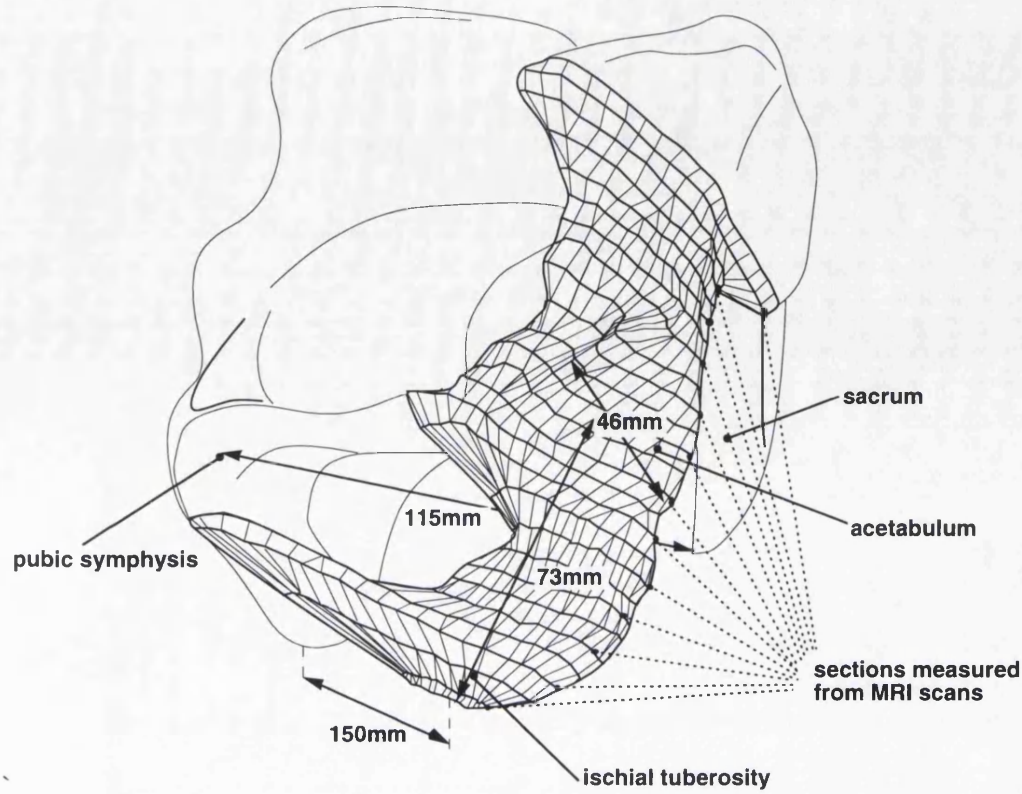

FIGURE 21
Graphical reconstruction of pelvis from MRI scans

The location of the pelvis within the suspended buttock shape was estimated to obtain more realistic geometric sections through the buttock for a finite element model. The alignment was partly based on the MRI scans. The perpendicular distances from the central plane to the ischial tuberosity, the posterior inferior and the anterior inferior iliac spine and the depth of tissue covering the posterior inferior iliac spine were measured from the scans. These measurements allowed the horizontal position of the pelvis to be located within the suspended buttock surface. The vertical position of the pelvis was based on the ultrasound measurements and the depth of tissue under the ischial tuberosity estimated from the alignment of the 'suspended' and 'seated' casting shapes. The resulting graphical reconstruction was sectioned in vertical planes through the ischial tuberosity at 45 degree intervals (see Appendix 7) .

A review of the results at this stage in the study made it apparent that the internal and external geometries measured in this chapter would have to be simplified in order to develop models with which it was possible to explore the numerous factors that affect seating. These simplifications were thought to outweigh the potential benefits of a geometrically comprehensive model. Nonetheless the geometric measurements reported in this chapter enabled the author to gain an understanding of the extent and location of the soft tissue deformations that occur during sitting on a planar rigid surface and to produce a seat based on the shape of the suspended buttock (see Chapter 2).

6.4 Further Development of FE Model

The finite element analyses reported in this section were to examine the sensitivity of the analytical results to the shape of the bony structure in the model and the precise values of the material coefficients (A, B and Poisson's ratio). The finite element analysis in Chapter 5 was repeated with a more realistic bony shape based on the shapes measured in this chapter, whilst still maintaining the simple axi-symmetric nature of the model. The Mooney-Rivlin material coefficients and the stress and deformation results from this analyses were compared with those calculated in Chapter 5.

<u>Effects of Model Geometry</u>

Once again the model was axi-symmetric with a elliptical external surface and a bony geometry based on the shape of half of the pelvis, with the ischial tuberosity along the axis of rotation of the model. The ischial tuberosity was modelled to be approximately 60 mm long, since this corresponded to the dimensions of the ischial tuberosity which was reconstructed from the magnetic resonance images. This was about 15 mm longer than the ischial tuberosity that was modelled in Chapter 5. 56 mm of soft material were modelled under the bony prominence. It was not considered necessary to model the bony pelvis because the deformations occurring in the bone were negligible compared to those occurring in the soft tissue.

The soft tissues were modelled as a homogeneous, isotropic, nearly incompressible Mooney-Rivlin material. The material was meshed with eight noded quadrilateral STIF86 elements. The nodal degrees of freedom were UX and UY. The mesh was generated with the automatic facility within ANSYS. The degenerate triangular form of the element was only used when the irregular geometry of the shape to be meshed did not allow otherwise. The mesh density under the ischial tuberosity was refined until it was 4 times that in some other parts of the structure. 167 STIF86 elements were needed to model the soft tissue volume. The model with dimensions and boundary constraints is shown in Figure 22 and compared with the FE model described in Chapter 5.

The finite element analysis was performed with the material coefficient ratio A/B equal to -0·94 and Poisson's ratio equal to 0·49. The material constants were selected so that, as in the previous analyses, when a load of 186·9 N was supported there was 86·1 percent deflection of the tissue under the ischial tuberosity. The vertical force-deflection curves and interface pressure distributions calculated from the two analyses were compared.

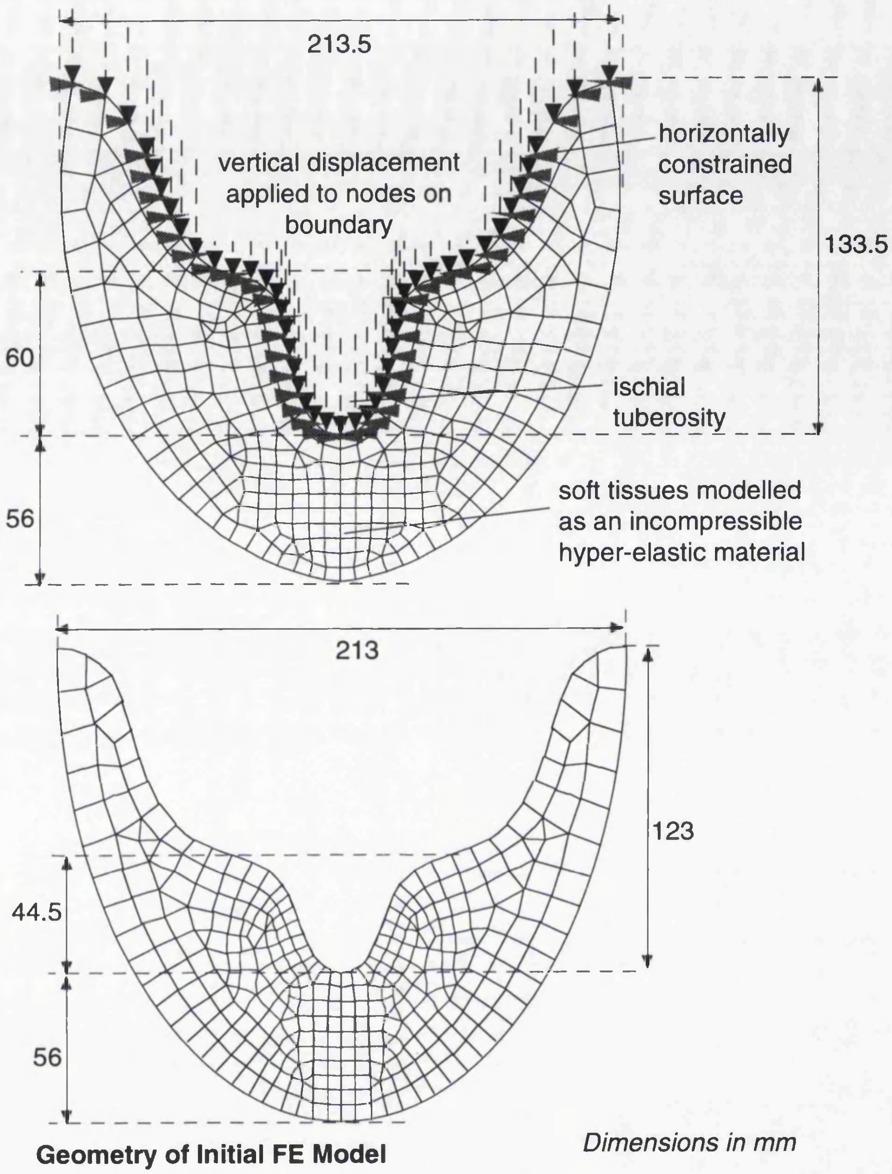

FIGURE 22

New FE model of soft tissues around ischial tuberosity and comparison with initial model

The stiffness curves were very similar in the two analyses. However there were considerable differences in the calculated interface pressure distributions. For the same weight of 186·9 N, much larger pressures were calculated under the model with the longer, more realistic ischial tuberosity. The stiffness curves and pressure distributions calculated from the two models are shown in Figure 23. The values of the material coefficients calculated from this analysis were A= -4.3 E-3 N/mm^2 and B= 4.7 E-3 N/mm^2. These were very similar to the values of A= -3.9 E-3 N/mm^2 and B= 4.3 E-3 N/mm^2 calculated in Chapter 5 as set 7 for the same material coefficient ratio and Poisson's ratio.

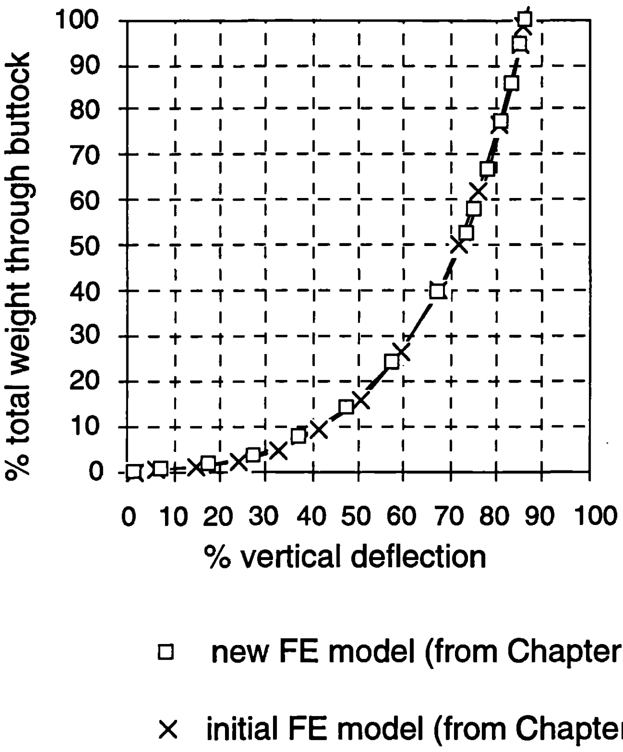

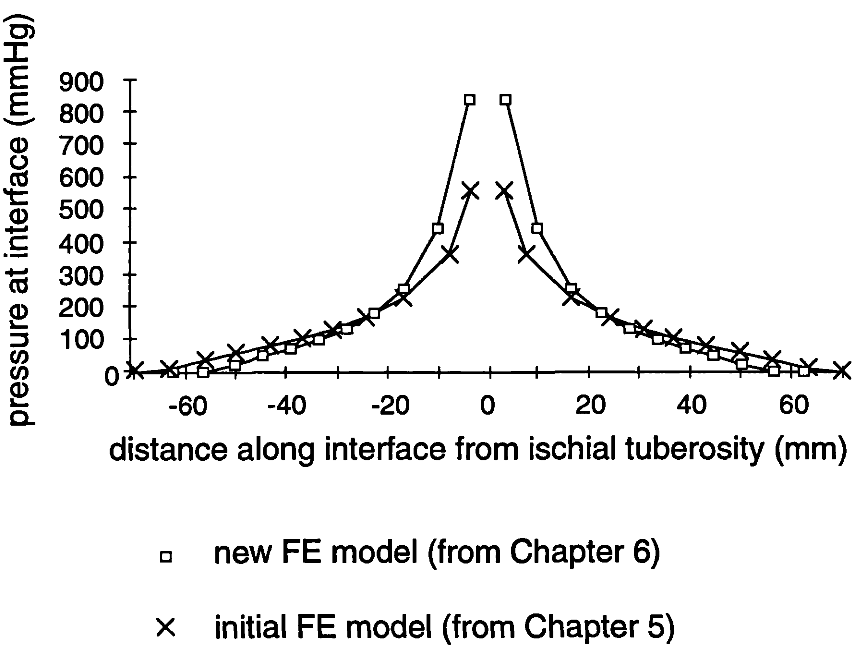

FIGURE 23

Stiffness curves and interface pressure distributions calculated from FE analyses in Chapters 5 & 6.

A/B=-0.94, 187 N supported through seats at 86 % vertical deflection

The Effects of Material Compressibility

The effects of the compressibility of the soft material on the stresses and deformation results from the FE analyses were investigated, since it had been identified that the solutions to large deflection, linearly elastic analyses of nearly incompressible materials are very sensitive to Poisson's ratio. Multiple analyses were performed and the stress and deformation results were compared, with a constant material coefficient ratio A/B of 10^{-5} and Poissions ratio's of 0·45, 0·475, 0·49 and 0·495. In each case 186·9 N were supported through the seat when there was 86·1 percent vertical deflection of the material under the ischial tuberosity. It was found that slightly smaller values for A and B were required when the soft materials became more incompressible. The maximum deflections were also slightly larger in the most incompressible material. However the distribution and peak values of the hydrostatic and von Mises stresses remained virtually unchanged over this range in Poisson's ratio. The results are summarised below :

A (N/mm^2)	B (N/mm^2)	υ	A/B	Max. von Mises stress (N/mm^2)	Max. compressive hydrostatic stress (N/mm^2)	Max. horizontal defln. (mm)
$0{\cdot}22 \times 10^{-7}$	$0{\cdot}22 \times 10^{-2}$	0·45	10^{-5}	0.26	0.07	11.1
$0{\cdot}22 \times 10^{-7}$	$0{\cdot}22 \times 10^{-2}$	0·47	10^{-5}	0.26	0.07	11.7
$0{\cdot}20 \times 10^{-7}$	$0{\cdot}20 \times 10^{-2}$	0·49	10^{-5}	0.26	0.07	12.9
$0{\cdot}19 \times 10^{-7}$	$0{\cdot}19 \times 10^{-2}$	0·495	10^{-5}	0.26	0.07	13.4

The Effects of Material Coefficients (A and B)

The effects of various ratios of material coefficients on the stresses and deformation results from the analyses were investigated. The value for Poisson's ratio was kept constant at 0·49 and A/B ratios of 10^{-5}, -0·2, -0·5 and -0·95 were examined. As previously described the values for the material coefficients were selected so that in each case 186·9 N were supported through the seat when there was 86.1 percent vertical deflection of the material under the ischial tuberosity. At large compressive strains the peak von Mises stresses increased when the value of B became more positive. However the form of the stress distribution did not alter. The increase in the peak von Mises stress was about 100 percent between the analyses with A/B ratios of 10^{-5} and -0·94 when 186.9 N was supported through the seat. The results are summarised below :

A (N/mm^2)	B (N/mm^2)	υ	A/B	Max. von Mises stress (N/mm^2)	Max. compressive hydrostatic stress (N/mm^2)	Max. horizontal defln (mm).
2.0 x10^{-8}	2.0 x10^{-3}	0.49	10^{-5}	0.26	0.07	12.9
- 4.6x10^{-4}	2.3 x10^{-3}	0.49	-0.2	0.28	0.07	12.7
-1.5 x10^{-3}	3.0 x10^{-3}	0.49	-0.5	0.32	0.08	12.3
- 4.6 x10^{-3}	5.1 x10^{-3}	0.49	-0.94	0.49	0.06	11.0

Bifurcations in the solution were found to be a problem with the more negative ratios of material coefficients (A/B). The singularities were found to occur less often when the loads were applied in smaller load steps and the stiffness of the 'rigid' interface was reduced (Oden, 1972; Supplement to Structural Nonlinearities Seminar Notes, User manual version 4.4, ANSYS,1990; theoretical reference manual, ANSYS, 1990). However using the computer hardware which was available, the most nonlinear FE solutions took more than 35 hours to solve with the stiffness of the interface at a satisfactorily high level and without the occurrence of singularities.

6.5 Theoretical Examination of Material Constants and Comparison with Soft Tissues of the Body

The stress - extension ratio relationships in simple deformation states were examined for a Mooney material. This was to finally decide upon the material constants to be used in the analyses to investigate seat design. The stress-strain relationships were established by simplifying equation 4·19 in Chapter 4 for the Mooney strain energy function described by equation 4.20.

For a uniaxial extension in an isotropic incompressible material, $\lambda_2^2 = \lambda_3^2 = \lambda_1^{-1}$ where λ_1 = extension ratio along the direction of tension. For a Mooney material it can be shown that the engineering stress - extension ratio relationship becomes :

$$\sigma=2\left(\lambda_1-\frac{1}{\lambda_1^2}\right)\left(A+\frac{1}{\lambda_1}B\right) \qquad \text{6.1}$$

Where σ=engineering stress and λ=extension ratio.

By examining the form of equation 6.1 and its derivatives $\frac{d\sigma}{d\lambda}$ and $\frac{d^2\sigma}{d\lambda^2}$, it is possible to determine the behaviour of materials under a uniaxial deformation for all values of the material constants A and B. The relationship 6·1 is plotted in Figure 24 for various values of the material constants. As an aid to comparing the stiffness curves under a compressive deformation, the

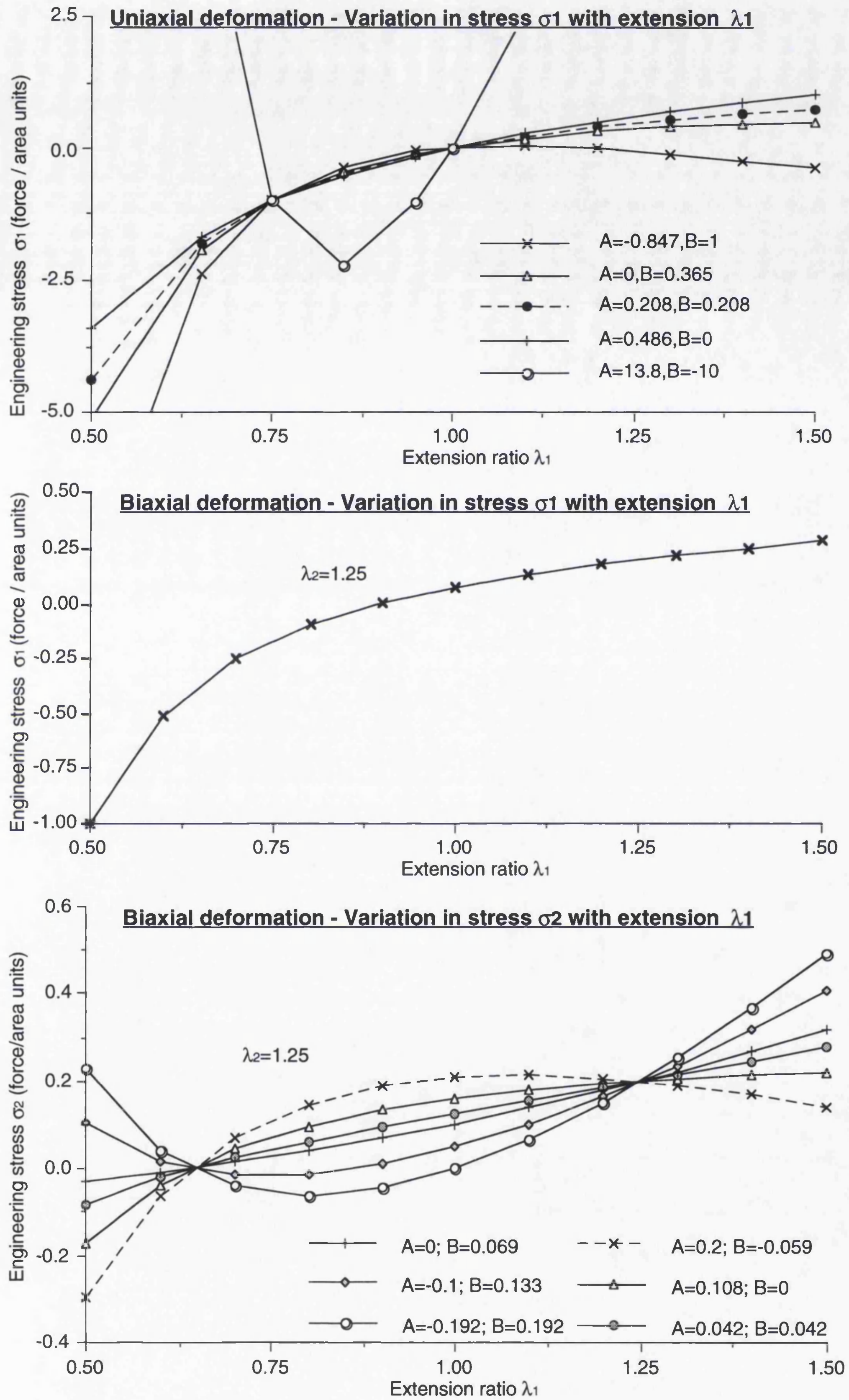

FIGURE 24
Variation in stress with extension ratio in Mooney materials

values of A and B are selected so that the magnitude of the engineering stress is unity when the extension ratio is 0·75. This means that A and B are linearly related by the equation

$$A=-\frac{4}{3}B+\frac{18}{37}. \qquad \text{6.2}$$

Under uniaxial compression the stiffness of the material increases with increasing compressive deformation as long as B is greater than $-{}^{1}/_{2}(A\lambda)$. The increase in stiffness with increasing compression is greatest when A is large and negative and B is postive. When B is less than $-{}^{1}/_{2}(A\lambda)$ the stiffness decreases with increasing compression. For large negative values of B and postive values of A, the applied compressive load may decrease with increasing compression and may become tensile.

The stiffness increases with extension when B is less than $-{}^{1}/_{2}(A\lambda)$. For other values of A and B the stiffness decreases with increasing extension. For large positive values of B and negative values of A, the tensile load may decrease and may become compressive. Thus it is not possible to define a single Mooney material that has a stiffness that increases under both increasing uniaxial extension and compression. The decrease in applied load with increasing compressive or tensile deformation is not physically realistic for the soft tissues of the body.

For a biaxial tensile deformation in an incompressible test-piece, one of the stretch ratios is dependent on the other two, so if λ_1 and λ_2 are independent, $\lambda_3 = \frac{1}{\lambda_1\lambda_2}$. It can be shown that the engineering stress - extension ratio relationships become:-

$$\sigma_1 = 2A\left(\lambda_1 - \frac{1}{\lambda_1^3\lambda_2^2}\right) + 2B\left(\lambda_1\lambda_2^2 - \frac{1}{\lambda_1^3}\right) \qquad \text{6.3a}$$

$$\sigma_2 = 2A\left(\lambda_2 - \frac{1}{\lambda_1^2\lambda_2^3}\right) + 2B\left(\lambda_2\lambda_1^2 - \frac{1}{\lambda_2^3}\right) \qquad \text{6.3b}$$

Where λ_1 = extension ratio in the direction of the stress σ_1 ; λ_2 = extension ratio in the direction of the stress σ_2

By examining the form of equations 6.3a and 6.3b and their derivatives, it is possible to determine the behaviour of materials under a biaxial deformation for all values of the material constants A and B. To simplify the deformation one of the extension ratios (λ_2) can be kept constant. The relationships in 6.3a and 6.3b are plotted in Figure 24 with $\lambda_2 = 1{\cdot}25$. As an aid to comparing the stiffness curves, the values of A and B are selected so that the magnitude of the engineering stress (σ_1) is unity when the extension ratio (λ_1) is 0·5. This means that A and B are linearly related by the equation

$$A=-\frac{25}{16}B+\frac{25}{231}. \qquad \text{6.4}$$

For a tensile stress σ_1 to produce an extension λ_1 when the extension λ_2 is unity, the sum of the constants A + B must be greater than zero. If the sum of the constants is less than zero, highly unrealistic behaviour is found (a compressive stress σ_1 is required to produce an extension λ_1). When the expression $\frac{A}{\lambda_2^2}+B$ is greater than zero, the stiffness in the λ_1 direction increases with increasing compression λ_1 and decreases with increasing extension.

As long as B is greater than $3A/(\lambda_1^4\ \lambda_2^4)$ the stiffness in the λ_2 direction increases with increasing extension λ_1 when the deformation in the λ_2 direction is constant. Unfortunately under the same conditions, the stiffness in the λ_2 direction decreases with increasing compression λ_1. When A is negative and B is positive, the compressive stress σ_2 may decrease with increasing compression λ_1 and may become tensile. When B is less than $3A/\lambda_1^4\ \lambda_2^4$ the stiffness in the λ_2 direction increases with increasing compression λ_1 and decreases with increasing extension. When A is positive and B is negative, the tensile stress σ_2 may decrease with increasing extension λ_1 and may become compressive.

For rubbers the value of A is found to be typically in the range from 0·1 Nmm^{-2} to 0·3 Nmm^{-2}. However B is found to be a function whose slope decreases as the strain invariant I_2 increases. Therefore the Mooney equation can only be used to model rubbers over limited strain conditions.

Unfortunately the determination of the form of the strain energy equation in a material is not a simple task: when measurements are made under simple deformation states the strain invariants are simply related and so the strain energy equation is only examined over a limited region of strain (Treloar, 1975; Kao & Razgunas, 1986). Ideally a material would be tested under homogeneous biaxial strain conditions over a wide range of strain. However in vivo tests on the buttocks would not allow homogeneous deformations to be applied and in vitro tests could only be conducted on the soft tissues in an animal model.

The properties of Mooney materials were compared to the previously reported stress-strain characteristics of the soft tissues (see Section 1·4). In vivo the soft tissues show a stiffness which increases with increasing uniaxial compression. Indentation measurements have been made at anatomical sites where the soft tissue is likely to have been mainly skin and also at sites where there will have been muscle, adipose tissue and skin in combination. A stress-strain curve that increases with increasing compressive strain is found in Mooney materials under uniaxial compression, when the constant B is greater than $-^1/_2(A\lambda)$. Under uniaxial extension muscle, adipose tissue and skin also show a stiffness that increases with strain. A stress-strain curve that tends to increase with increasing extension is found in Mooney materials when the constant B is less than $-^1/_2(A\lambda)$.

The deformation characteristics of membraneous specimens of human skin and canine pericardium have been reported under biaxial deformation conditions when one of the deformations is held constant (Shoemaker et al, 1986, Lee et al, 1985). The tissues stiffen with increasing extension λ_1 both in the direction of λ_1 and also in the direction of the constant extension λ_2. In the skin the stresses σ_1 and σ_2 and stiffnesses increased very rapidly at extension ratios λ_1 of above 1·58 when the strain λ_2 was constant at a value of 1·21. In the pericardium the stresses σ_1 and σ_2 and stiffnesses increased very rapidly at extension ratios λ_1 above 1·32 when the strain λ_2 was constant at a value of 1·34. As discussed in the preceeding paragraphs, for Mooney materials under the same deformation state, the stiffness tends to decrease with increasing extension in the $\lambda_1$direction when A+B is greater than zero (a material where A+ B is less than zero is unrealistic). The stiffness can either increase or decrease in the λ_2 direction depending on the values of A and B. As long as B is greater than $3A/\lambda_1{}^4\,\lambda_2{}^4$ the stiffness increases with increasing extension λ_1.

For finite element modelling of the soft tissues of the buttocks, the hyperelastic material formulation has advantages over large deflection, linearly elastic formulations. Calculated stresses are based on the deformed element shape rather than the original element shape. Also it is possible to model an incompressible material with a stiffness that increases with increasing compressive strain, with the Mooney strain energy equation. However it is not possible to define a Mooney material with a stiffness under uniaxial deformation that increases with increasing compression and also with increasing tension.

The analyses in the following chapters were performed with A=0·2x10^{-7} N/mm^2; B=0·2x10^{-2} N/mm^2 and Poisson's ratio =0·49. As defined the material would stiffen greatly under increasing uniaxial compression and soften to a lesser extent under increasing uniaxial tension. The applied load would approach a constant value at extension ratios above about 2. As seen in the previous chapter, if a material were to have been defined with a negative constant A, the compressive stiffness curve would have been closer to the measured behaviour. However in situations where the soft tissue is under tension, the calculated behavior would have been very unrealistic.

CHAPTER 7 UTILIZATION OF FE MODEL TO INVESTIGATE SEAT DESIGN

7.1 Background and Scope

The purpose of the work reported in this chapter is to investigate the effects of shaped seat surfaces on the stress state within the soft tissues with finite element modelling. It is hoped to establish how to optimally shape the seat surface supporting a chair-bound person. Up to this point in the study, a system for producing shaped supporting surfaces for the body has been developed and has undergone a small-scale clinical trial. Measurements of interface pressures, body shape and tissue deformations under load have also been made on an individual subject. In this chapter models of the system are developed, which allow the effects of various seat design parameters, such as seat shape, interface friction and body posture to be examined. The soft tissues around the ischial tuberosity are modelled because of their central location at the body-seat interface and the frequency of pressure sores in this area. The sacro-coccygeal area is modelled because of its susceptibility to pressure sores, particularly when the pelvis has a posterior orientation. This area is also of interest because of its sensitivity to the effects of interface shear forces.

The system under examination is complex and only partly accessible to direct measurements, thus the tool of mathematical modelling is useful for investigating this system. A model behaves according to established physical laws, such that the behaviour of the model resembles but is independent of the real system. A useful model should fit some known data from the system being studied, it should predict some data which can be checked against the real system and it should compute information which cannot be measured directly. The predictions of a model should be compared with the results from the real system, to determine the areas where it behaves similarly to the real world and to determine the areas where it can be improved. The discovery of discrepancies initiates crucial experiments and, eventually, to the development of further models which simulate the real system over a larger range of situations.

The structure and deformation mechanism of the soft tissue material examined in this work, are not fully known nor readily described by current continuum mechanics (see Chapter 1). The region of the model that simulates the composite soft tissues is a homogeneous isotropic Mooney-Rivlin material. The most appropriate material coefficients had been calculated in the previous chapters for the composite soft tissue layer.

A limit to the complexity of each model is vital so that the range of factors affecting the design of seating can be explored in a thorough way. Multiple analyses have to be performed where the parameter of interest is varied over its range and the other critical parameters are held constant. For each finite element solution, up to a hundred incremental deformations are applied to the model. Also multiple solution runs are necessary for each analysis, because of the sensitivity of the solution to the rate of load application and because of the difficulty in defining a geometrically complex interface within the finite element software.

A large amount of data is produced by the analyses and is used to compare the effects of the supporting surface. The stress distributions in the soft tissues of each of the models are compared. In particular the size and location of the maximum von Mises and hydrostatic stresses in the soft tissues are examined. It is not possible to display it all in the main text. In many cases the results are described briefly in the text and shown in the Appendices. The discussion and conclusions are based on the information in the Appendices as well as in the main text.

7.2 Investigation into Effects of Seat Shape on Tissues Surrounding the Ischial Tuberosity

The effects of ten shaped seat surfaces on the von Mises and hydrostatic stresses in the soft tissues were investigated. The shape of the seats ranged from flat to similar to the external shape of the soft tissue layer. It was hoped that from these studies the optimum shape for a seat or cushion surface could be determined and the sensitivity of the stresses in the soft tissue to the shape of the seat, could be established.

The rationale behind the choice of geometry for the FE model, the material formulation, boundary constraints and displacement loading is explained earlier in this thesis. The hyperelastic material coefficients were A=0·2 E-7 N/mm^2 ; B=0·2 E-2 N/mm^2 and Poisson's ratio (υ) =0·49.

The seat surfaces were modelled with 1-noded STIF26 elements. The points on the surfaces were displacement constrained so that they did not move as the soft tissue came into contact with them. The seats in models 1 to 5 were less 'steeply contoured' than the external surface of the soft tissue layer. The seat in model 6 was very similar to the shape of the external surface of the soft tissue layer. The seat in models 7 to 10 were more 'steeply contoured' than the external surface of the soft tissue layer. The effects of small shape variations on the calculated stresses, surface deformations and interface pressures were investigated with these last four models. The shapes are described in Appendix 8 and shown in Figure 25.

The software restricted the surface described by a STIF26 element to be either arc-shaped or a straight line. Thus the description of an interface with a complex shape required multiple elements. Multiple solution runs were need to analyse a model with such an interface. This was because the software ANSYS did not allow the nodes at the surface of the soft tissue to slide past the nodes on the seat surface. When the FE solution aborted due to this software restriction, the positions of the nodes on the boundary were slightly moved and the solution was repeated. When the nodes on the surface of the soft tissue came into contact with the seat surface, they encountered a stiffness normal to the surface. The boundary stiffness was 3 N/mm which limited the travel through the surface to less than 0·05 mm in all the analyses.

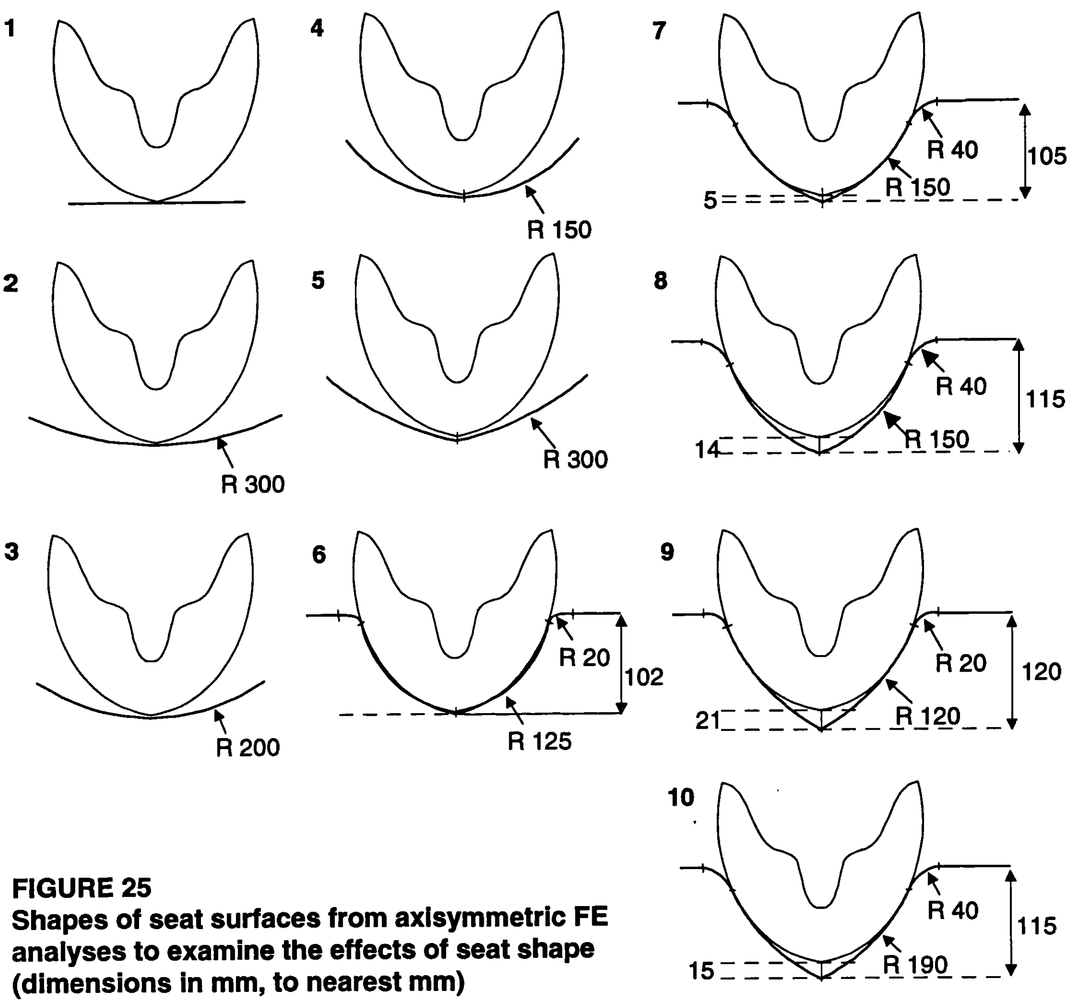

FIGURE 25
Shapes of seat surfaces from axisymmetric FE analyses to examine the effects of seat shape (dimensions in mm, to nearest mm)

Models with zero interface friction were analysed in this section. Thus there was no resistance to the nodes on the surface of the soft tissue sliding along the seat surface. The effects of friction are investigated in detail in Section 5 of this chapter. Analysis1 was repeated with double the mesh density in the soft tissue material. None of the results was altered by more than 5 percent in this model. Thus the original mesh density was considered sufficiently high. Since the localised stresses, deformations and interface pressures were greatest in this analysis, the mesh density was considered sufficient for all the other analyses. In each of the analyses, vertical displacements were applied to the upper surface of the soft tissue layer until a vertical load of over 186·9 N was supported through the seat. This load was measured in Chapter 3 as the weight applied through one buttock when the subject was sitting on a planar seat.

The location of the maximum von Mises stresses in the soft tissues was under the tip of the ischial tuberosity close to the bone-soft tissue interface in analyses 1 to 5. The von Mises stresses were generally smaller and much more evenly distributed in the analyses with more steeply contoured seat surfaces (analyses 2 to 6). For example, the maximum von Mises stress in the soft tissue layer was 26 times smaller in the analysis where the seat was shaped similarly to the undeformed buttock (analyses 6) compared to when the seat was planar (analysis 1).

The von Mises stress distributions were comparatively similar in analyses 6 to 10. The stresses were concentrated close to the bone-soft tissue interface, near the outline of contact between the soft tissue and the seat. The von Mises stress concentration under the tip of the ischial tuberosity in analyses 6 and 7 was not present in analyses 8, 9 and 10. This result suggested that to remove a stress concentration from the soft tissues under a bony prominence, the depth of the seat contouring should be locally increased in that region.

The hydrostatic stress components were usually smaller than the von Mises stresses in the same model. The peak compressive hydrostatic stresses were in the volume of soft tissue directly under the ischial tuberosity and the stresses were smallest in the upper lateral regions of the soft tissue material. The hydrostatic stresses were more evenly distributed and the maxima were lower with the more steeply contoured seat shapes (analyses 2 to 6). With the highly conforming seats (analyses 6 to 10) the hydrostatic stress distributions were similar. The peak compressive hydrostatic stress under the bony prominence decreased, as the seat was locally depressed by a few millimeters along the axis of revolution (see analyses 6 to 9). The decrease in peak hydrostatic stress under the bony prominence, and the transfer of hydrostatic stresses to the surrounding tissues with increasing seat conformity could be expected because of a redistribution of the vertical load from the area under the bony prominences to the surrounding tissues with increasing conformity.

Due to the displacement-controlled nature of the problem and the finite displacements applied at each load step, the stresses when the vertical load was 186·9 N were not calculated directly from the analyses. A linear interpolation between the results from the nearest displacement steps was made. The magnitude of the maximum von Mises and compressive hydrostatic stress for the different analyses is tabulated below (in stress units of N/mm^2).

Analysis	**1**	**2**	**3**	**4**	**5**	**6**	**7**	**8**	**9**	**10**
Max. von Mises stress	2.6e-1	1.7e-1	1.3 e-1	9.8e-2	3.3e-2	9.5e-3	9.2e-3	8.4e-3	8.3e-3	9.0e-3
Max. Hydro-static stress	6.6e-2	5.0e-2	4.3e-2	3.6e-2	2.1e-2	1.1e-2	9.8e-3	7.6e-3	6.7e-3	7.9e-3

The magnitude of the peak von Mises stresses in the soft tissues is plotted against increasing load in Figure 26. The von Mises stress distribution in the soft tissue of the buttock, is shown in Figure 27 for analysis 6 and 9.

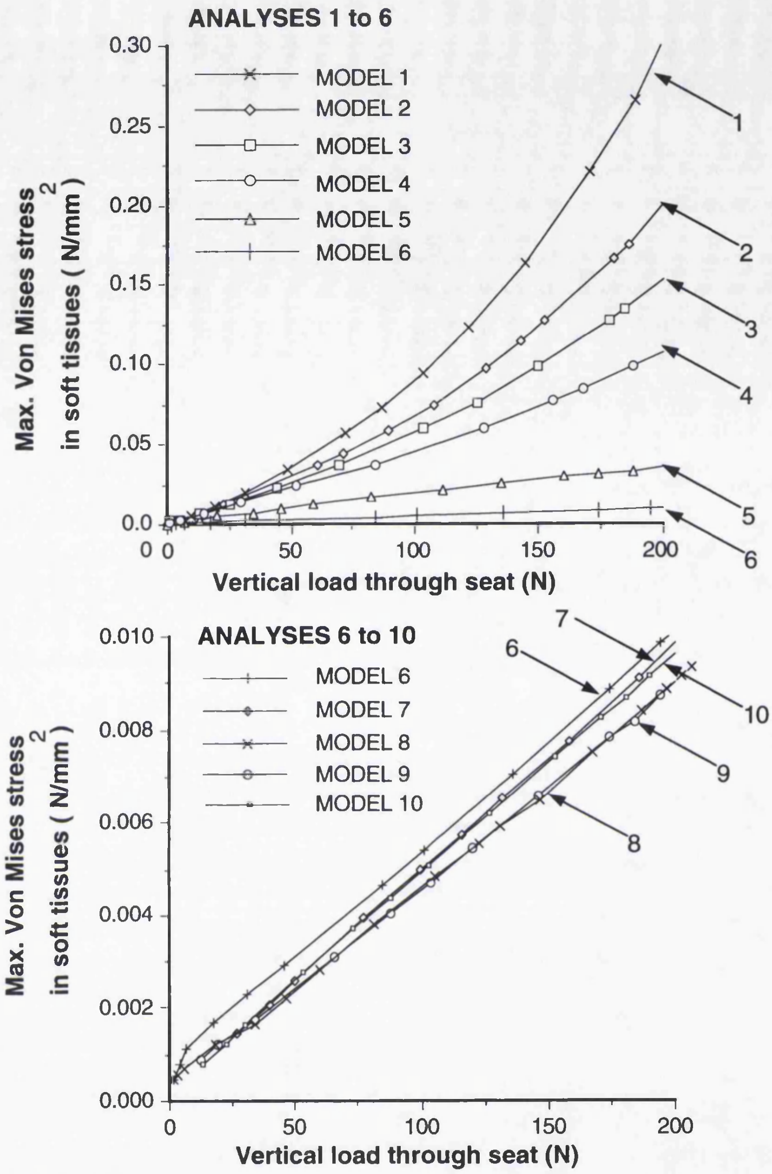

Figure 26
Maximum von Mises stress in soft tissues against vertical load supported throught seat. Results are from FE analyses of buttock to examine effects of seat shape

From this study it appears that small changes to the shape of the seat can further redistribute the stress maxima away from critical areas of soft tissue, such as those which are known to be at risk of pressure sores. The stresses under the ischial tuberosity could be reduced by increasing the depth of the seat in this region. The optimum design of shaped seating cannot be deduced from this study alone because of the multi-purpose nature of seating for chair-bound people and the simple nature of the model. Factors such as the desired sitting posture, the presence of deformities, the ability of the patient to move around on the seat have to be taken into account. Some of the other factors are investigated in the following sections.

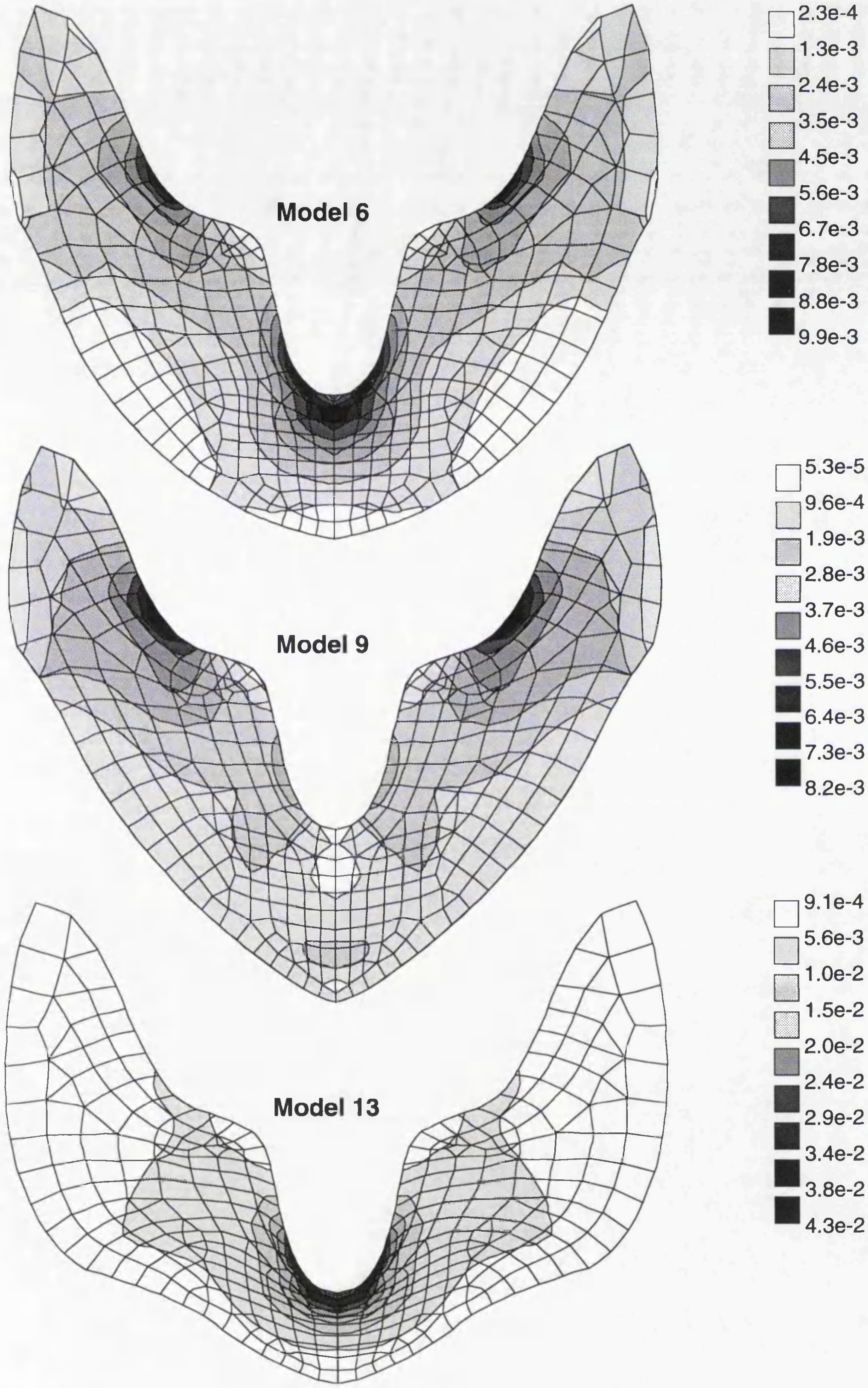

FIGURE 27
Von Mises stress distribution in soft tissues when load of 186.9 N is supported through seat

7.3 Investigation into Effects of Seat Contour Depth on Tissues Surrounding the Ischiai Tuberosity

The purpose of the FE study which is reported in this section was to investigate the effects of the depth of the seat contours on the stress state in the soft tissues. The analyses in the previous section had suggested that a seat, shaped similarly to the external body contours and at least 100 mm deep, could distribute and reduce the maximum stresses in the soft tissues, compared to a more planar seat surface. However a seat or cushion which is over 100 mm deep is not always a practical seat design because the sitter may need to change position in the chair.

Five FE models with different depths of seat (105, 80, 60, 40 and 0 mm) were analysed and the results were compared. The model of the buttock described earlier was used. The seat surfaces were defined, the solution run and the results compared using the methods described previously. As far as the software allowed, the remaining shape of the seat was kept constant between the analyses. The five seat shapes are shown in Figure 28 and are described in Appendix 8 (models 1,7,11,12 and 13).

The stress distributions in the soft tissues were compared, when a vertical weight of 186.9 N was supported through the seats. The maximum von Mises stress and compressive hydrostatic stress in the soft tissues are shown below for each analysis.

Analysis (mm)	1 (depth=0)	7 (depth=105)	11 (depth=80)	12 (depth=60)	13 (depth=40)
Max. von Mises stress (N/mm^2)	2.6e-1	9.2e-3	1.6e-2	2.5e-2	4.3e-2
Max. hydrostatic stress (N/mm^2)	6.6e-2	9.8e-3	1.4e-2	1.8e-2	2.5e-2

In all the analyses, there was a peak of von Mises stress in the soft tissue directly under the ischial tuberosity. The von Mises stresses were more distributed, and the maxima were lower when the seats were deeply contoured, compared to when the seat was planar. Even with a seat depth of only 40 mm (analysis 13), the peak von Mises stress in the soft tissue under the ischial tuberosity was less than a sixth of that in the analysis with a planar seat surface (analysis 1). The von Mises stress distribution in the soft tissue of model 13 is shown in Figure 27. The maximum stress is directly under the ischial tuberosity because there was not sufficient support further away from this area to move the maximum into another region. The magnitude of the peak von Mises stresses in the soft tissues is plotted against increasing load in Figure 29 for all the analyses.

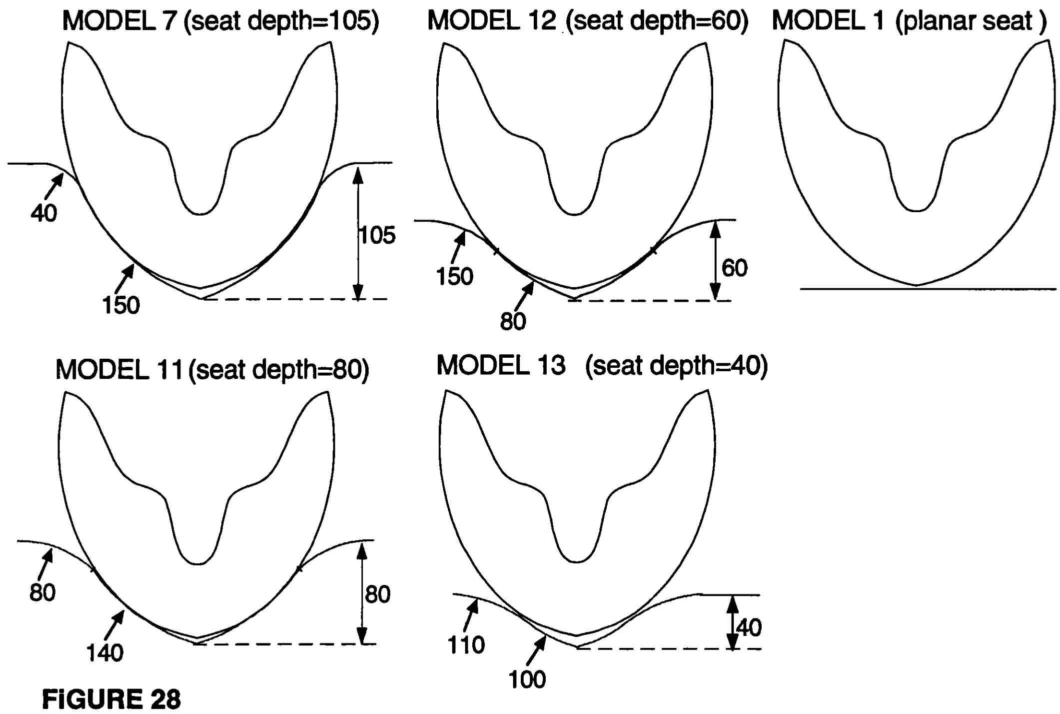

FIGURE 28
Shapes of seat surfaces from FE analyses of buttock to examine the effects of contour depth (dimensions in mm)

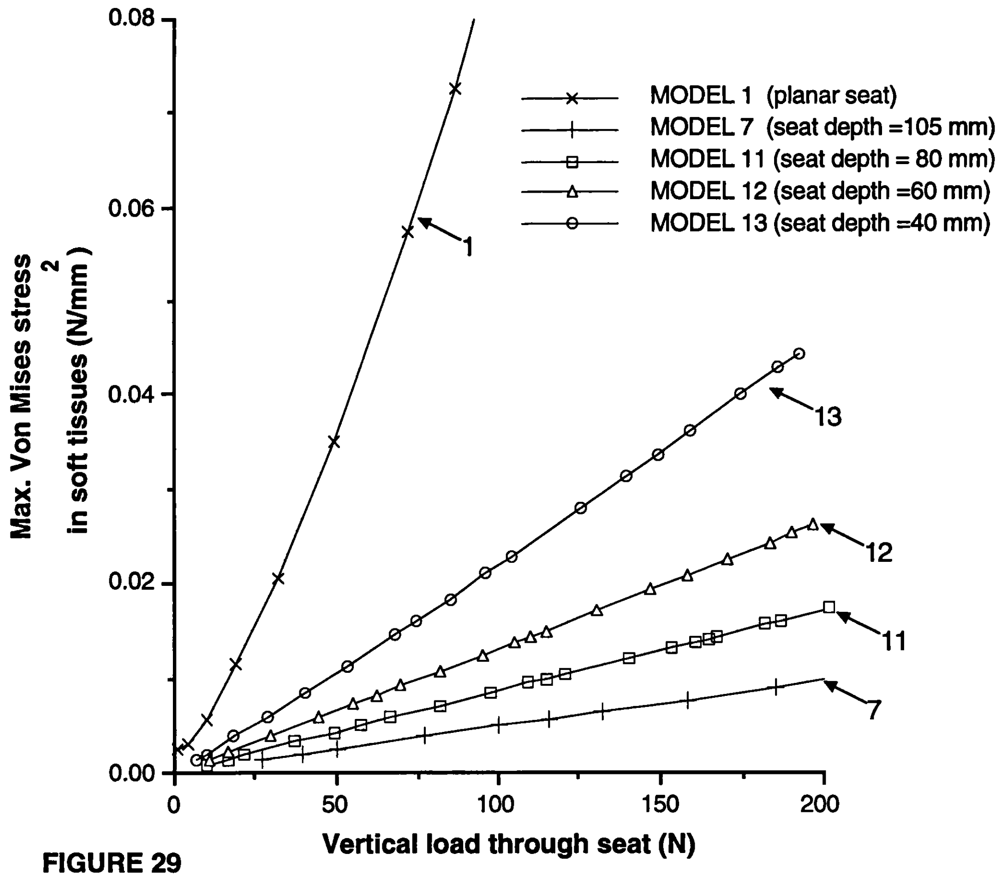

FIGURE 29
Maximum von Mises stress in soft tissues against vertical load supported through seat. Results are from FE analyses of buttock to examine the effects of contour depth

Similarly to in Section 7·2, the peak compressive hydrostatic stresses were in the volume of soft tissue directly under the ischial tuberosity and were smallest through the upper lateral regions of the soft tissue material. The stresses were more distributed and the magnitude of the peak stress was lower with the deeply contoured seats.

The results of the analyses suggest that substantial stress reductions can be achieved even when the seat surface is as little as 40 mm deep. In seat designs where the body is required to move about on the seat, substantial stress reductions may still be possible by the inclusion of shallow contours under the bony prominences. Shaped seats and cushions are likely to be of such a design, if they have to meet the needs of a larger group since one such need is likely to be movement on the seat. The shallow shaping of seating or cushioning could reduce the discomfort experienced by the chair-bound in the cases where this is caused by localised stresses or deformations in the soft tissues of the buttock.

7.4 Investigation into Effects of Seat Shape and Body Posture on Tissues Surrounding the Sacrum

The purpose of the work in this section was to examine the effects of seat shape and body posture on the stresses on the soft tissues around the sacrum, coccyx and perineum. The study was performed with a separate FE model to that which described the soft tissue around the ischial tuberosity. A simple model was developed so that multiple analyses could be performed.

For a plane strain problem, the normal and shear strains with components in the direction perpendicular to the plane under consideration are zero. It was assumed that the central section through the buttock was under this state of strain, because the material in this section was thought to be constrained in both lateral directions, by the adjacent tissue of each buttock when the buttocks were loaded symmetrically by the seat.

The geometry of the central section through the body was obtained from the magnetic resonance images (described in Chapter 6). The structures which were imaged as the subject lay prone, were assumed to be in the same relative position and to have the same shape when the hips were flexed and the body upright. The magnetic resonance image of the central sagittal plane was enlarged to life size and digitised with the electro-magnetic position measuring device (3Space ISOtrak). The outline of the body was digitised, together with the outline of the sacrum and the pubic symphysis. A file of ANSYS commands was written to display the digitised points. The command file was then read by the ANSYS software so that the points were plotted. Areas of soft tissue were formed from the imported points and then meshed using the automatic facility within the ANSYS software.

A mesh density was established, such that a model with double the mesh density did not produce changes in the internal stresses, surface deformations or interface pressures of more than 5 percent. The mesh density was checked with the model loaded against the seat described below as model A. The plane strain FE model with dimensions and boundary constraints is shown in Figure 30.

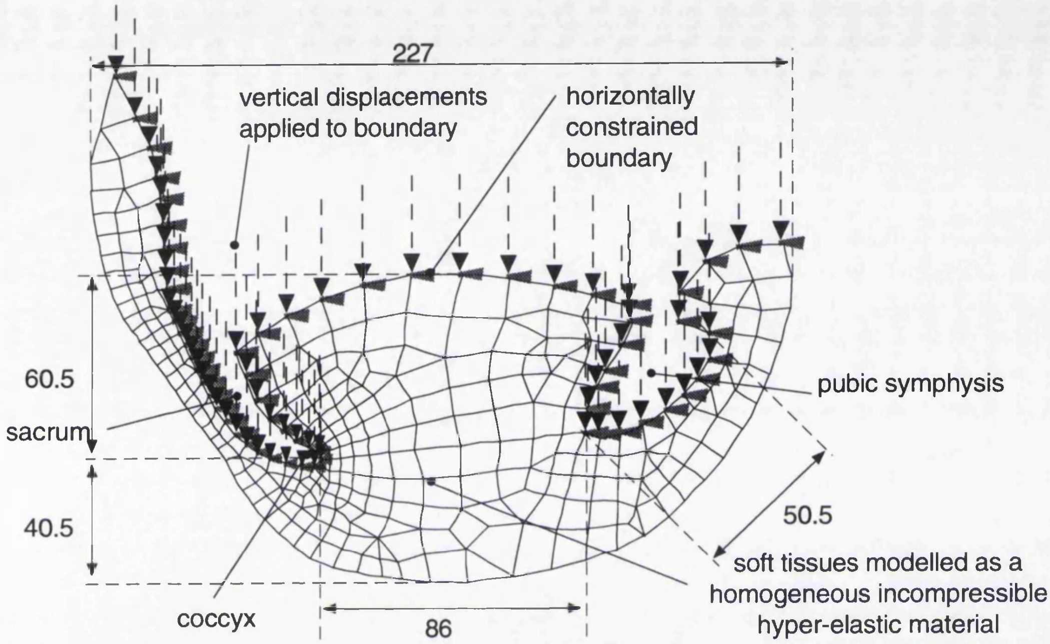

FIGURE 30

FE model of section through sacrum, with dimensions and boundary constraints (dimensions in mm, to nearest 0·5 mm)

As in the previous sections of this chapter, the material coefficients were as follows : A=0·2 E-7 N/mm^2 , B=0·2 E-2 N/mm^2 and Poisson's ratio (υ) =0·49. The material was meshed with eight-noded quadrilateral plane strain STIF84 elements. The nodal degrees of freedom were UX and UY. The degenerate triangular form of the element was only used when the irregular geometry of the shape to be meshed did not allow otherwise. 283 STIF84 elements were needed to model the soft tissue section.

The deformation of the soft tissues within the pelvis, more than 60 mm above the tip of the sacrum was assumed to be zero. The soft tissues at this level and at the interface with the sacrum and pubic symphysis, were displacement loaded vertically downward against the seat surfaces. The nodes on the loading surface were also constrained so that no lateral displacement of these nodes was possible. For planar surfaces this constraint was realistic because no lateral forces were generated when the body came into contact with the seat. For contoured seat surfaces this constraint was also thought to be realistic because the ischial tuberosities would 'engage' with the seat and be horizontally constrained, before the central section of the body had made contact with the seat.

Six combinations of seat design and body orientation were modelled. These models are described in Appendix 8 and are shown in Figure 31. In each model a friction free interface was assumed.

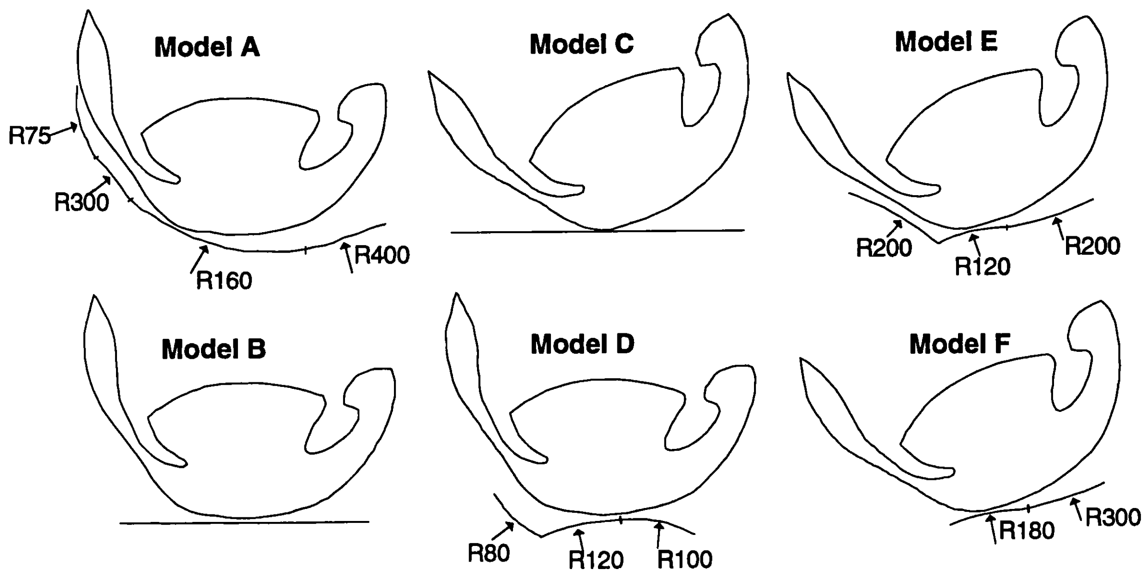

FIGURE 31
Shapes of seat surfaces from FE analyses of tissues around sacrum, to examine the effects of seat shape and body posture.

The magnitude of the vertical load through these models was estimated from interface pressure measurements on the able-bodied subject. The interface pressure distribution was reported in Chapter 5 for the subject sitting on a planar surface. Similar seats were described in models B and C. The interface pressure was also measured with the subject sitting on a seat, the central section of which was the same as that in model A . The seat and measured pressure distribution is described in Chapter 8. The calculations of the total vertical load from both the measured distributions are shown in Appendix 9. The vertical load through sections 1 mm thick was estimated to be 0·38 N through the planar seat and 1·85 N through the contoured seat.

The stress distributions in the soft tissues were compared in the analyses when 0·38 N was supported through the seats. The magnitude of the maximum von Mises stresses and compressive hydrostatic stresses is tabulated below :

Analysis	A	B	C	D	E	F
Max. von Mises stress (N/mm^2)	9·1e-3	4·5e-3	1·4e-2	6·2e-3	3·7e-3	5·0e-3
Max. hydrostatic stress (N/mm^2)	5·7e-3	4·7e-3	6·9e-3	5·2e-3	7·1e-3	5·6e-3

In all the analyses there was a concentration of von Mises stresses in the soft tissues surrounding the tip of the sacrum. Of the situations considered in the analyses, the stresses were most concentrated and the peak stresses were highest in the model where the pelvis was posteriorly rotated and the seat was planar (model C). There was also a high von Mises stress concentration under the sacrum in model A, where the seat profile was very high in the region of the sacrum. The von Mises stresses were most distributed and the maxima were lowest when the pelvis did not have a posterior tilt and the seat was flat (models B and D).

A seat profile which was low in the region of the sacrum was effective at redistributing stresses away from the sacrum when the pelvis was posteriorly rotated. Thus the peak von Mises stress in model E was just over a quarter of that in model C when the same body weight was supported. The von Mises stresses in model E were slightly lower than in model F in the soft tissues covering the sacrum. This was likely to be due to the larger area of contact between the body and the seat in model E. The magnitude of the maximum von Mises stresses in the soft tissues is plotted against increasing vertical load in Figure 32 and is shown for models C and E in Figure 33.

In each the analyses the hydrostatic stresses were most compressive in the region around or under the tip of the sacrum. The stresses were least compressive in the region around the proximal sacrum and anterior to the pubic symphysis. Model C produced the largest compressive stresses when a vertical load of 0·38 N was supported.

The vertical load through any section depends on the load supported through the rest of the interface which in turn depends on the shape design of the rest of the seat. It was therefore not possible to draw conclusions about the efficacy of these sections by just comparing the stresses when a constant vertical load was supported through the sections. When the pelvis was upright, the most even stress distribution was produced on seat profiles which were flat. However none of the profiles substantially removed the stresses around the tip of the sacrum. Thus, the most effective seat designs may enable the total load supported through the central section to be kept to a minimum by depressing the whole of this section relative to the rest of the seat. Areas of the buttock, other than the one which was modelled may be more suitable for supporting the body weight without causing excessive von Mises stresses in the soft tissue surrounding the pelvis.

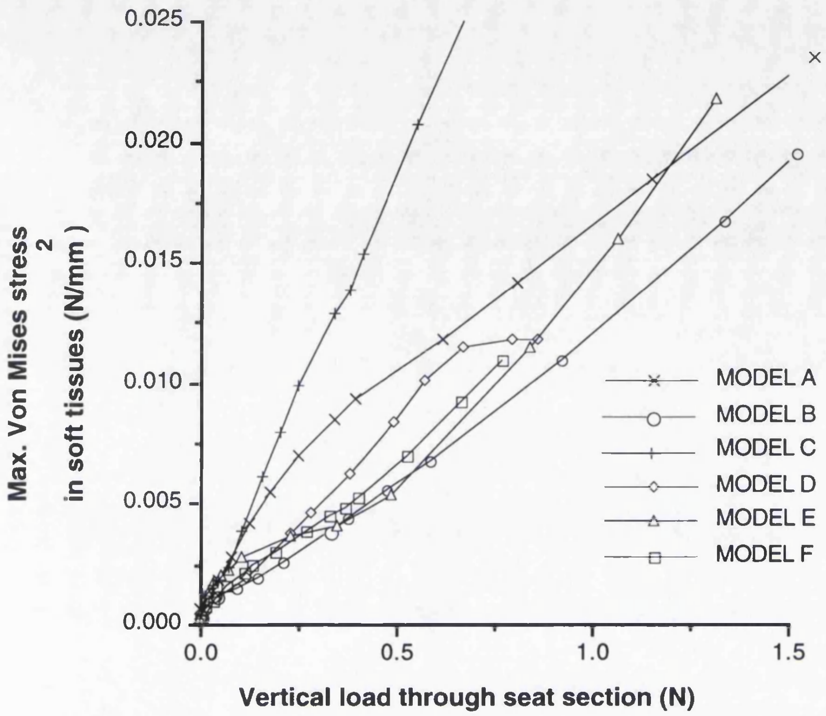

FIGURE 32

Maximum von Mises stress in soft tissues against vertical load supported through seat. Results are from FE analyses of tissues around sacrum to examine the effects of seat shape and body posture.

The high von Mises stresses when the posteriorly rotated buttock was loaded against a flat seat is further evidence of the high risk of pressure sores around the sacrum when the body is in this posture. When a seat is needed for a person whose pelvis is posteriorly tilted and where this cannot be altered by a seating intervention, the most effective seat design may lower the surface of the seat so that very little load is supported through the body in this region.

In most cases the maximum von Mises stresses in the sacral area were substantially lower than those that had been calculated under the ischial tuberosity. It may be that the sacral area is only at risk of pressure sores during sitting when the pelvis is substantially posteriorly rotated or when there are additional factors such as friction.

Up to this point the effects of seat shaping on two important regions of the buttock had been investigated. The effects of shape modifications on the stresses and deformations had been considered and the optimum shapes for redistributing stresses had been established. The next stage was to see how the results were affected by the presence of interface friction.

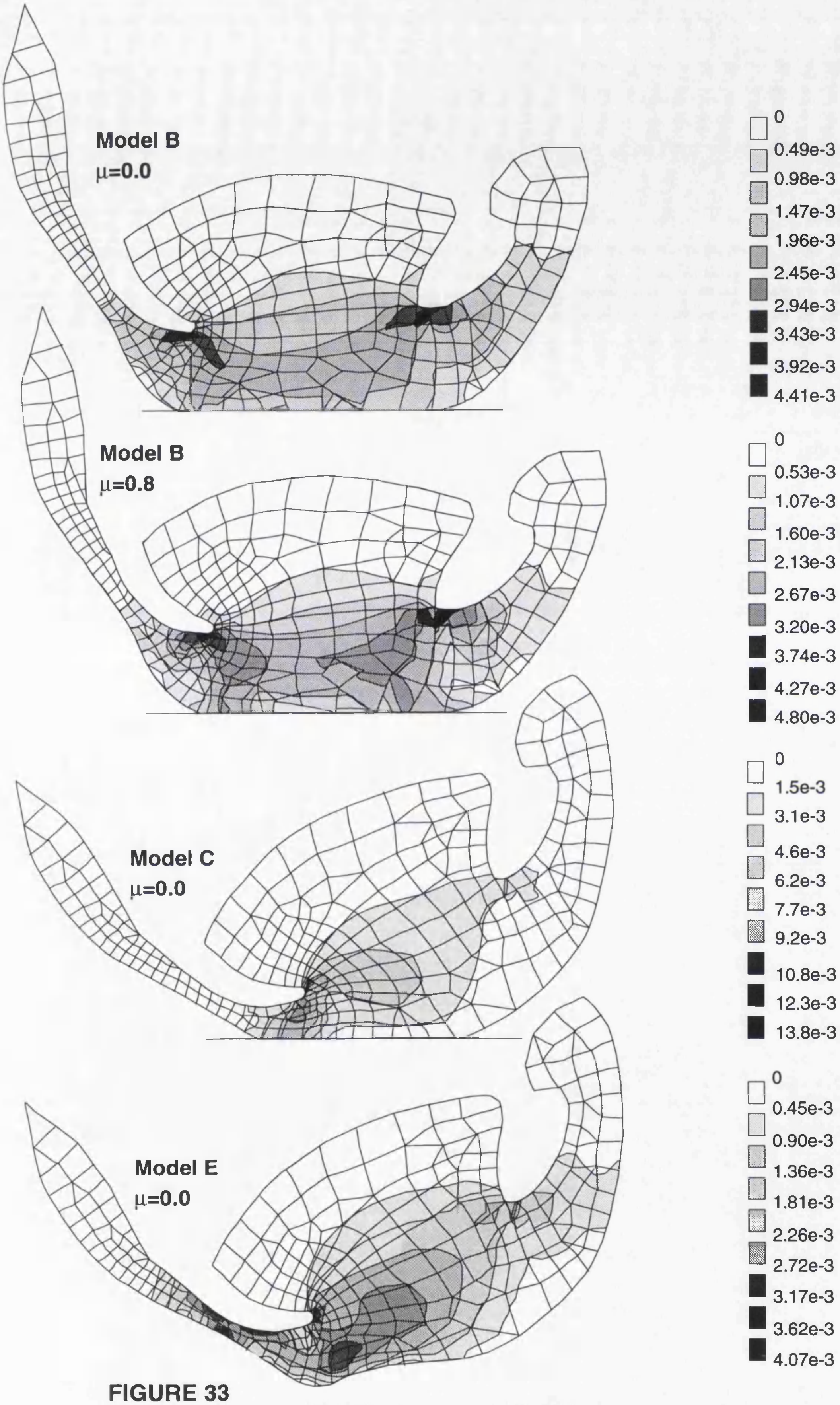

FIGURE 33
Von Mises stress distributions in soft material when 0.38 N is supported through seat sections

7.5 Investigation into Effects of Interface Friction on Tissues Surrounding the Sacrum

The effects of interface frictional forces on the stress state in the soft tissues when the buttock was supported on shaped seat surfaces was examined with FE modelling. Pressure sores, particularly those which develop around the sacrum of patients who tend to slide forward in their chair, are often said to be caused by interface shear forces. Lowthian measured the friction coefficient between bedding materials and skin at the wrist in wet and dry conditions (1983). He reported friction coefficients (μ) in the range from 0·4 to 0·8. In the following study the interface friction coefficient was varied from 0 to 0·8 on different seat surfaces and the effects on the stress distribution within the soft tissues were observed.

The two FE models of the body from the previous sections were remodelled with interface elements that provided a frictional resistance to motion along the interface. The analyses were repeated with different interface properties. The peak von Mises and hydrostatic stresses in the soft material were compared when the same vertical load was supported through the seats. The distributions of von Mises and hydrostatic stresses were also compared. The relative motion between the surface of the body and the shaped seat surfaces was monitored.

The interface between the body and the seat was defined with 2-dimensional STIF12 elements. These elements had two degrees of freedom at each node. The elements could be in three possible states during a solution (i. open, ii. closed and sticking, iii. closed and sliding). When the interface was closed, the elements possessed a stiffness both normal and tangential to the interface (K_n and K_s respectively). When the interface was open the elements had no stiffness in either direction. The characteristics of these and the other elements in the FE analyses are described in Appendix 5.

When the interface shear force was less than the frictional resisting force the nodes on the interface could move by a small amount which depended on the interface sticking stiffness, K_s. When the interface shear force (F_s) was greater than the frictional force ($F_n\,\mu$), the interface offered no resistance to sliding. The interface elements were considered to have converged if the status of the element did not change and the sliding forces did not vary by more than 10 percent between sequential iterations. It was difficult to define the model so the interface elements converged during the solution. The displacements had to be applied in very small steps and the interface stiffness was given values which were lower than might otherwise have been used.

In the following section the effects of interface friction with the rotationally symmetric model of the soft tissue around the ischial tuberosity and the plane strain model of the central section through the buttock were both examined.

FE Analyses to Show the Effects of Friction with Planar Seat Surfaces

Model B (see Figure 31) was analysed with interface friction coefficients of 0, 0·1, 0·4, 0·6 and 0·8. The material properties and upper boundary constraints were the same as those described in Section 7·4. The interface was defined with a normal stiffness of 0·2 N/mm and a shear stiffness of 0·025 N/mm. The shear stiffness value of the elements was selected to allow a nodal displacement along the interface in elements that were sticking of less than 0·2 mm, and to also enable the interface elements to converge. The normal stiffness value was selected that allowed nodal displacements into the surface of less than 0·2 mm. The upper surface of the model was displacement loaded vertically downwards against the seat section in 0·5 mm steps, until a load of over 0·38 N was supported through the seat section. This vertical load was determined from the pressure distribution when the able-bodied subject sat on a flat seat surface (see Appendix 9).

For the models with interface friction coefficients of 0 and 0·8 repeated extended analyses were made where, once 0·38 N was supported through the seat, the upper surface of the model was horizontally displaced. 0·3 mm displacement steps were applied until the upper surface had moved forwards on the seat by 12 mm. The stress states and deformations were then examined. A horizontal displacement of 12 mm was selected from real life observations, since forward displacements on a seat of this magnitude occur frequently. Due to the displacement controlled nature of the analysis, the stresses and displacements when a given load was supported, could not be calculated directly by the analyses. A linear interpolation between the results from the nearest displacement steps was made.

As the models were vertically loaded upto 0·38 N, shear forces built up at the nodes on the interface. When the shear forces were greater than the frictional resisting forces, the nodes moved along the interface until the shear forces had decreased to less than the critical value. When the friction coefficient was 0·6, all of the nodes which were in contact with the seat were sticking when the vertical load was 0·38 N. A larger friction coefficient did not produce significant changes in the resulting stresses and deflections. When the coefficient was 0·8 the total shear force at the interface was 0·1 N when 0·38 N vertical load was supported. As the interface friction increased the nodes were able to slip less far along the interface. The maximum nodal displacement along the interface when 0·38 N load was supported, was 5·9 mm when there was no interface friction and was 3·4 mm when the friction coefficient was 0·6.

The von Mises stress maxima were at the bone-soft tissue interface near the tip of the sacrum and under the pubic symphysis. There was a small increase in the maximum von Mises stress in the soft material as the nodes at the interface were constrained by frictional forces. When 0·38 N was supported, the peak von Mises stress was 7 percent larger when the friction coefficient was 0·4 compared to when there was no interface friction. Also the von Mises stresses in the soft material adjacent to the seat were lower when there was no interface friction. The von Mises stress distributions in the soft material with interface friction coefficients of 0·0 and 0·8 are shown in Figure 33 when about 0·38 N was supported through the seat sections. The magnitude of the maximum von Mises stresses in the soft material during the loading history is plotted in Figure 34. Some results when 0·38 N was supported are also tabulated below:

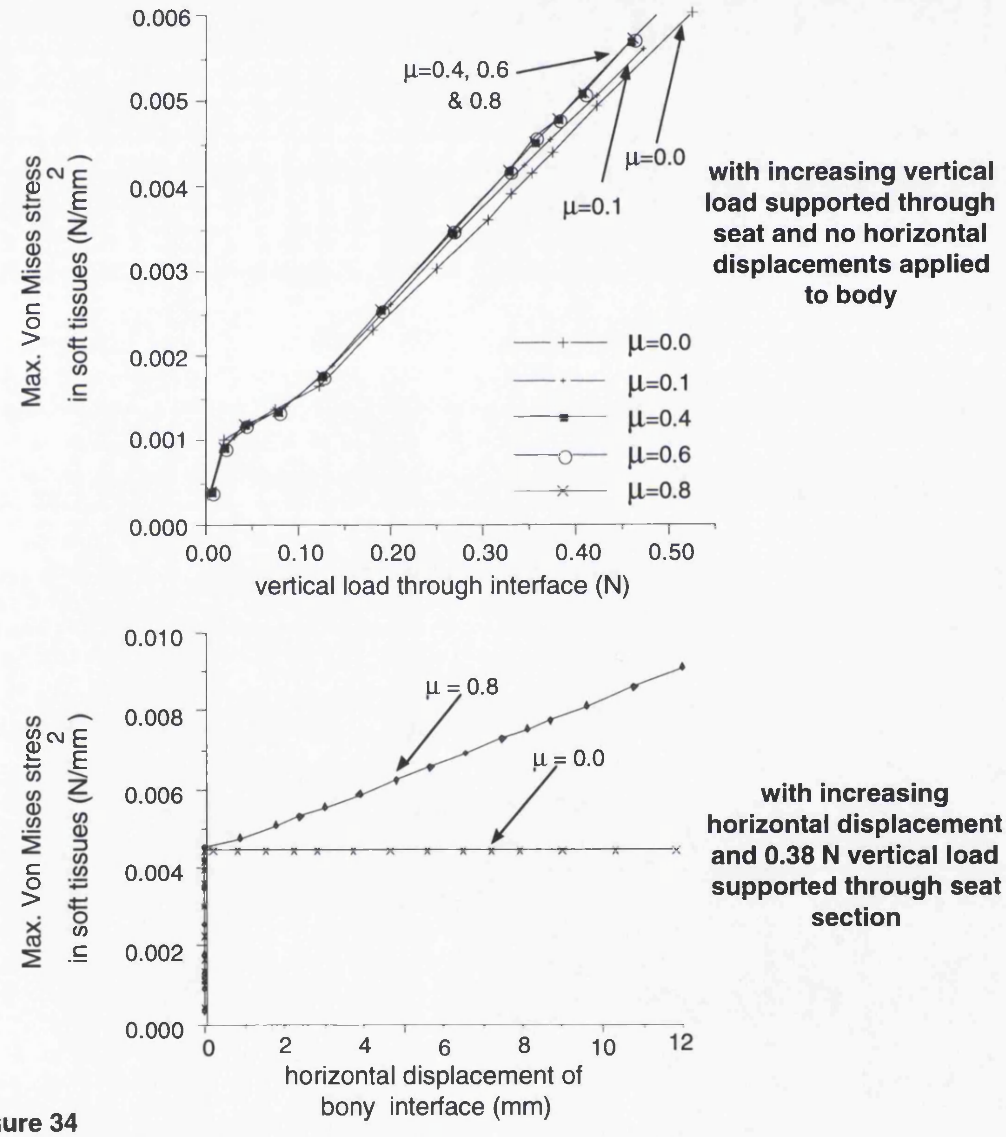

Figure 34
Results from FE analyses with model B to examine the effects of friction on the stresses in the soft material around the sacrum

Interface Friction Coefficient	0·0	0·1	0·4	0·6	0·8
Max. nodal displ. along interface (mm)	5·9	4·6	3·4	3·3	3·3
Sectional area of interface (mm^2)	95·7	93·8	92·0	91·9	91·9
Max. von Mises stress in soft material (Nmm^{-2})	4·4e-3	4·6e-3	4·8e-3	4·8e-3	4·8e-3
Max. hydrostatic stress in soft material (Nmm^{-2})	4·6e-3	4·7e-3	4·8e-3	4·8e-3	4·8e-3
Max. nodal displacement into seat (mm)	0·2	0·2	0·2	0·2	0·2
Max. nodal displ. during 'sticking' (mm)	-	0·1	0·2	0·2	0·2

When the interface friction coefficient was 0·8 and the body was moved horizontally along the seat surface, the peak von Mises stresses in the soft material around the sacrum increased at a steady rate. When body had moved horizontally by 12 mm the interface was still sticking and the peak von Mises stress in the soft material around the sacrum had doubled. The maximum compressive hydrostatic stresses were in the soft material near the mid-point of the interface with the seat. The peak compressive hydrostatic stresses were also slightly larger in the presence of interface friction. The magnitude of the maximum von Mises stress is plotted against horizontal displacement in Figure 34.

The effects of friction were also examined with the axi-symmetric model of the soft tissue around the ischial tuberosity. The loading surfaces was displaced vertically against a planar seat surface in 0·5 mm steps until 187 N was supported through the seat. The interface was defined with a normal stiffness of 2·5 N and a radial stiffness Of 0·7 N. The results from analyses with interface friction coefficients of 0·0 and 0·8 were compared. Due to the axi-symmetric nature of the model it was not possible to examine the effects of horizontal displacements of the body.

The effects of interface friction with this analysis were similar to those found with the analyses described above. When the interface friction coefficient was 0·8, the interface elements remained stuck when 187 N was supported through the seat and there was a slight increase in the peak von Mises stresses under the tip of the ischial tuberosity. The maximum hydrostatic stress was 80 percent larger. The vertical force-deflection curve became much more non-linear. The results are graphically presented in Appendix 10.

In the next section another FE model was analysed to see whether in certain situations, the effects of frictional forces were more severe than those reported above. In the next analysis some weight was support through the thin layer of soft material over the dorsal surface of the sacrum and a horizontal displacement was applied to the body.

Analyses to Show the Effects of Friction on the Soft Tissue Over the Dorsal Surface of the Sacrum

The effects of interface friction were examined with a model of a section through a person sitting on a seat where there was contact between the seat and the soft tissue over the dorsal sacral surface as a result of the postero-inferior orientation of the dorsal surface of the sacrum. The effects of sliding forward on the seat were also examined. The interface was defined with a normal stiffness of 0·2 N/mm and a tangential stiffness of 0·025 N/mm. The facilities within the ANSYS software for defining non-planar interfaces with friction properties in large deflection problems were very limited. STIF12 elements had to be used. Each element was defined with an interface orientation which remained fixed during the solution. The seat had to be defined so that no node on the surface of the body passed through the initial node of an adjacent interface element on the seat surface. For this reason it was necessary to have a gap between the two orientations of the seat section.

Analyses were solved with interface friction coefficients of 0 and 0·8. The upper loading surface was displaced downward in 0·2 mm displacement increments until 1·0 N was supported through the seat. The body was then displacement loaded in the direction of the seat under the sacrum (26.6^0 from horizontal) until a horizontal displacement of 7 mm had been applied. The displacements were applied to the upper loading surface in 0·25 mm steps. A horizontal displacement of 7 mm was selected from real life observations, since forward displacements on a seat of this magnitude occur frequently. The model was then unloaded in 1 mm displacement steps until 1·0 N was again supported through the seat. The same material properties were used as in the other analyses.

When 1·0 N was supported through the seat section, the peak von Mises stresses in the soft material over the dorsal surface of the sacrum were slightly lower than when there was no interface friction. However when the loading surface was displaced forward and downward, very large von Mises stresses developed in the model where the interface friction coefficient was 0·8. When the model had been displaced forward by 7 mm the maximum stresses were 3 times as large as when there was no interface friction.

When the loading surface had been unloaded until 1·0 N was supported through the seat section, the peak von Mises stresses were still very much larger in the model where there was interface friction. The peak von Mises stresses were located over the dorsal surface of the sacrum and at the point of contact with the back edge of the front part of the seat section. In Figure 35 the section through the seat, the loading history and the peak von Mises stresses over the loading history are all shown.

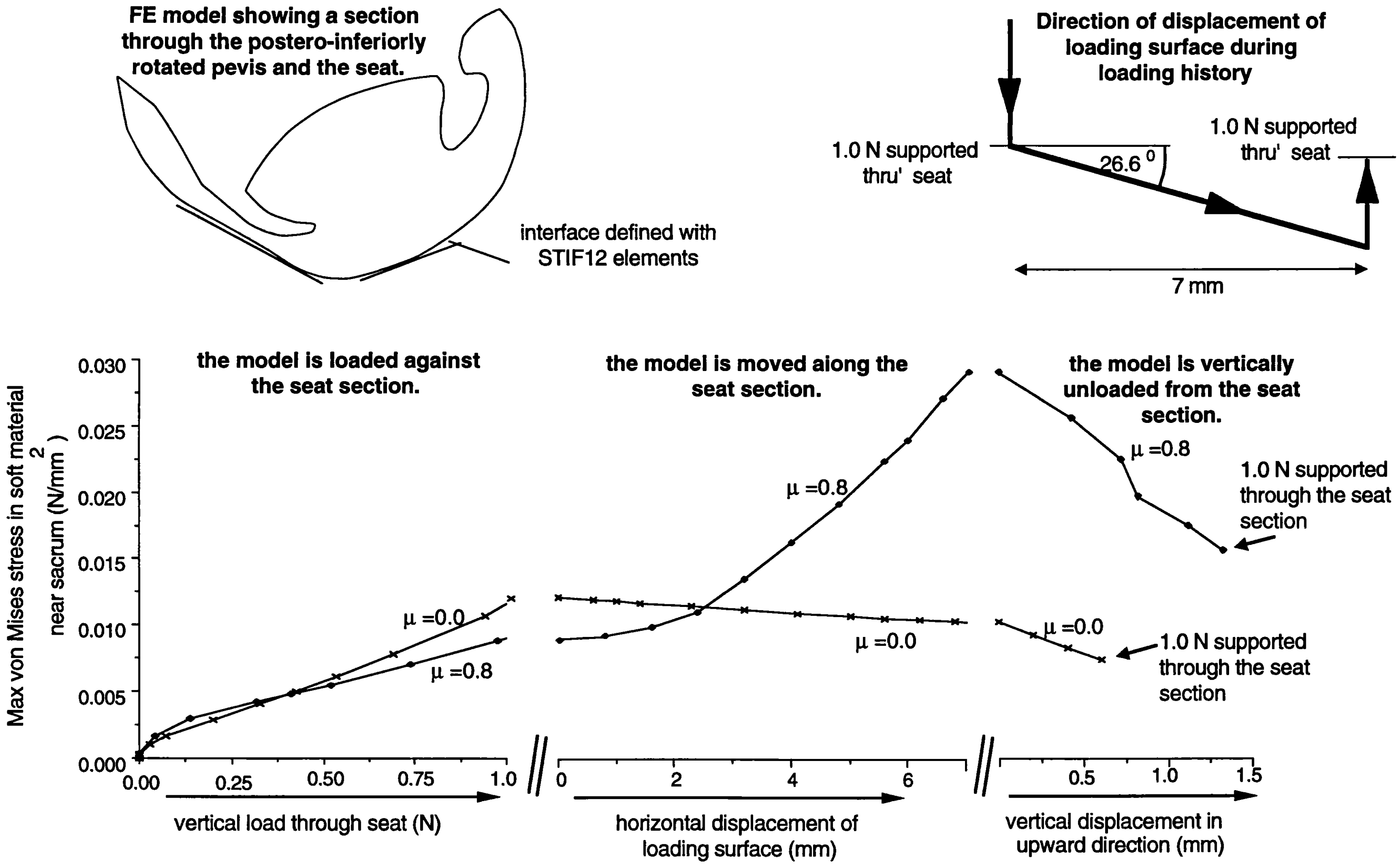

FIGURE 35
Analyses to show the effects of interface friction on the soft tissues over the dorsal surface of the sacrum

The effects of interface friction were highly dependent on the geometry and orientation of the seat and bony surfaces. They were also dependent on the magnitude and direction of loading. If the body remained stationary on the supporting surface and the surface was suitably curved, the soft tissues were prevented from flowing outwards from between the bony and seat interfaces by the presence of friction. This resulted in a reduction in the von Mises stresses in the soft material. However at low levels of soft tissue deflection and with planar seat surfaces this entrapment phemomenon did not have significant effects and the von Mises stresses slightly increased. When the body moved about in a horizontal direction on a seat surface and there was a high friction coefficient at the interface, the soft tissues were constrained by the interface shear forces and so additional von Mises stresses developed in the soft material.

The reduction in boundary stiffness which was required for the solutions to converge, was not thought to have affected the results significantly. This was because the displacements through the boundary and along the boundary when the interface was sticking were small compared to when the interface could slip.

7.6 Discussion

The theoretical studies reported in this chapter have suggested that shaped supporting surface can redistribute the loading in the tissues of the buttock away from areas that are at risk of pressure sores and can reduce the distortions in the tissues. The analytical results have to be interpreted with an awareness of the simple nature of the models that were used in the studies. For example, the soft tissue formulation in the models is a simplification of the soft tissue in the real system.

In the real system, with seating systems that do not conform to the shape of the body e.g. planar seats, it is likely that the uneven loading within the tissues would cause some extracellular fluid to be forced out of the region that was involved in load bearing and would cause increased loading on the structures remaining in the region. With seating systems that conform to the shape of the body e.g. contoured seats, the more even loading through the tissues could cause less flow of extracellular fluid. Thus, although the models are much less complex than the real system, the results are of relevance to understanding the behaviour of the seated buttock.

The model was based on measurements from one able-bodies individual. It is likely that if bodies with a less extensive soft tissue covering and with more viscous, less elastic tissues had been modelled, the potential for localised loading and distortions would have been greater and contoured seating would have had similar beneficial effects.

The location of the peak distortional stresses in the soft tissues was calculated to be at the interface with the bone. There were also high distortional stresses at the interface with the seat when the body moved around on the seat and there were high interface shear forces. In the real system muscle and fibrous tissue attachments to the pelvis and sacrum are likely to make the assumption of a constrained bone-soft tissue interface fairly realistic. The analytical results agree with intuitive reasoning, because of the constraint applied to the soft tissues at these interfaces. Maximum distortional and shear stresses have been calculated in similar locations in the analyses of Chow and Odell (1978), Cadadai and Reddy (1992) and Spilker et al (1992).

The homogeneity of the soft tissue in the model limits the level of information that can be gained from the analyses. Interactions between the soft tissue components cannot be modelled. Also our knowledge of the likely location or level of internal loading that can cause damage to different tissues is limited. It is likely that the muscles, nerves and arteries are more susceptible to damage due to loading than adipose tissues and the skin (Keane,1979; 1978-1979; Reddy, 1990). Damage to deep subcutaneous tissue has been noted on animals when a load is applied to the surface of the skin (see Section 1·3)

The hydrostatic stresses calculated in this chapter can be compared to measurements of the pressure in the tissues of pigs (Le et al,1984; Dodd & Gross, 1991). Dodd & Gross measured pressures of upto 81 mmHg (10.8 KPa) when a loader was applied to the skin surface over the spinous process. Hydrostatic stresses of the same order of magnitude were calculated in the FE analyses at the ischial tuberosity.

The analyses with the rotationally-symmetric FE model calculated a maximum von Mises stress in the soft material around the ischial tuberosity, close to the bone-soft tissue interface and a maximum hydrostatic stress in the soft material under the bony prominence. The stress distributions were similar in magnitude and form to those calculated in Chow's model (1978). It is difficult to make a detailed quantative comparison between the stress values because different load distributions were applied in the two studies, and the geometry of the models was significantly different. Interface shear stresses caused the von Mises stresses to more than double in the system that was analysed by Chow. With the analyses in this chapter, it has been shown that the peak von Mises stresses may increase or decrease depending on the exact configuration of the system.

The implications of the results reported in this chapter for seat design are discussed fully in Section 8·5.

CHAPTER 8 EXPERIMENTAL AND ANALYTICAL RESULTS FROM THE BODY-SEAT INTERFACE

8.1 Background and Scope

Up to this point in the study, a system for producing shaped supporting surfaces for the body has been developed and tested. The effects of seat shape, interface friction and body posture have been investigated with simple finite element models. It appears from these studies that the shape of the seat has a great effect on the stresses within the soft tissues of the body during sitting. In general the deeper the supporting surface and the closer the shape of the seat to the external body shape, the more even the von Mises stress distribution and hence the lower the maxima in the soft tissues.

In this chapter the interface pressures and deformations calculated from the FE analyses in the previous chapter are reported. The correlation between these calculated interface quantities and the stress state within the tissues is examined, to see whether it may be possible to predict the stress state in the soft tissues from outside the body. The tissues under the ischial tuberosity and around the sacrum and coccyx are investigated because of their susceptibility to pressure sores. Interface measurements that could be a useful clinical tool for determining the optimum seat or cushion design for an individual are proposed. The pressure distribution is also reported when the able-bodied subject was sitting on a rigid seat which was the same shape as the suspended buttock. The measured interface pressure distribution is compared with the pressures calculated in the FE analyses. Principles of shaped seating design are discussed and shape designs are suggested for specific seating requirements.

8.2 Interface Pressures and Deformations Calculated from FE Analyses

In each of the analyses described in the last chapter, the interface pressures and deformations when the weight of the body was supported through the seat were calculated. For the models with the ischial tuberosity, it was assumed that half the weight transferred through the buttocks during sitting, was transferred through the seats in the FE analyses (186·9 N). For the analyses with the sacrum, the weight transferred through the seat sections was estimated from interface pressure measurements on a planar seat (0·38 N).

Approximate pressure distributions between the body and the seat surfaces in the FE models were calculated from the position and forces on the nodes at the interface. The normal forces on nodes at the interface were assumed to be associated with half of the surface area of each of the two adjacent elements. In the axi-symmetric analyses, the forces on the central axis were calculated to be zero. The formulation of STIF84 elements was such that the forces through the mid-side nodes were less than those through the corner nodes. Therefore the pressures associated with the nodes at the mid-side and corners of the elements were calculated and averaged in order to obtain smoothly varying distributions. A Stineman interpolation was made between the non-zero pressure results in analyses 1 to 5 (Cricket Graph Macintosh Software, Reference Manual). The data was not extrapolated to the central axis, due to the limited load information in this region. The calculated pressure distributions are shown in Figure 36.

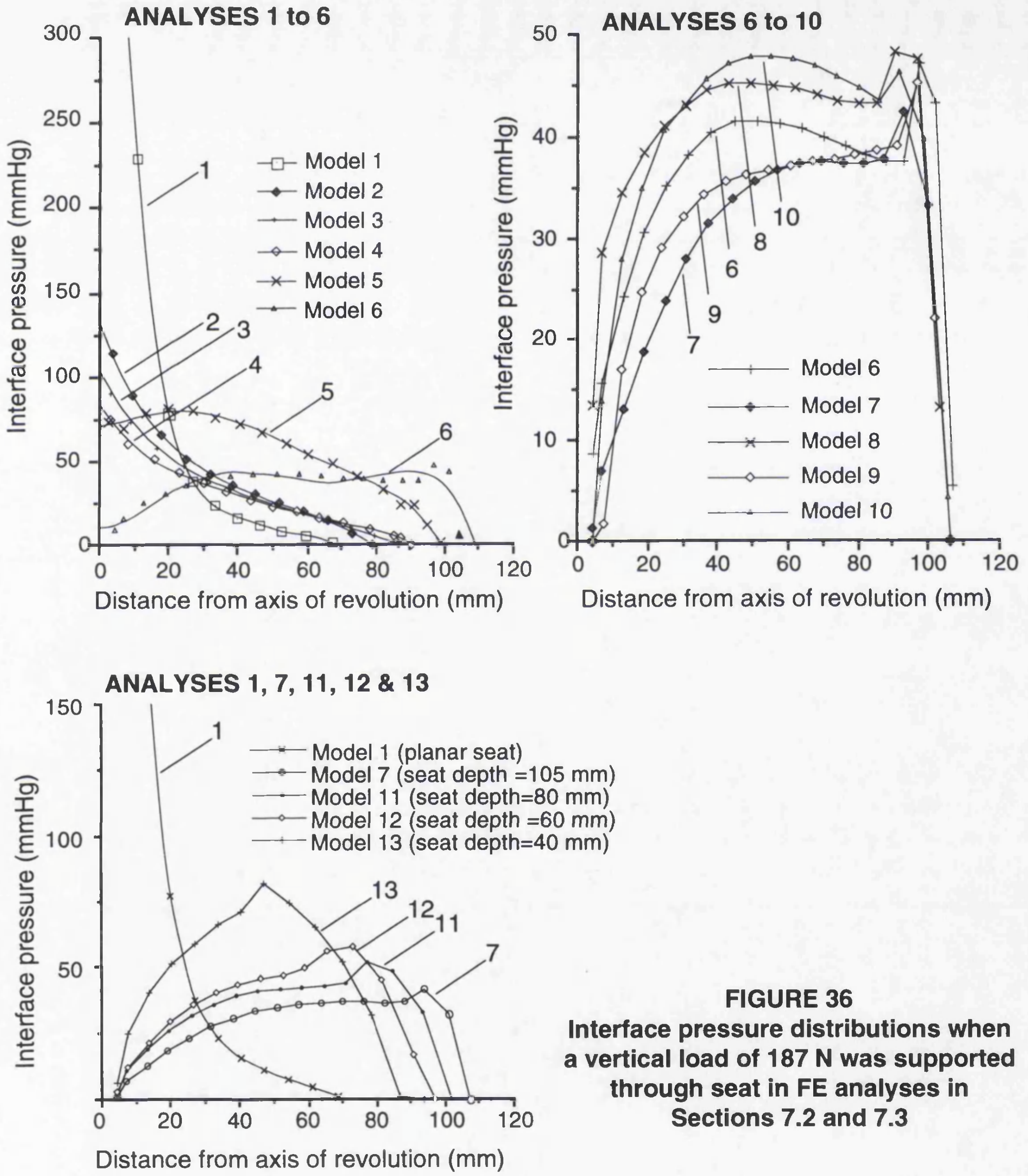

FIGURE 36
Interface pressure distributions when a vertical load of 187 N was supported through seat in FE analyses in Sections 7.2 and 7.3

In analyses 1 to 5 the maximum pressures were under the ischial tuberosity and they then decreased with distance from the axis of revolution. The peak pressure was very much smaller in the analyses with contoured seat shapes, compared to the analysis with a planar seat. In analyses 6 to 10 the pressure distributions were very similar. The interface pressures increased with distance from the central axis. The distributions went from zero on the axis to near-constant values of about 40 mmHg (5·3 KPa) over most of the interface. The pressures further increased by about 10 mmHg before the interface boundary was reached. Thus the ring of peak pressure was around the boundary of the interface. In analyses 6 to 9, the trough in the pressure distribution under the ischial tuberosity was wider, when the seat was locally deepened along the axis of revolution.

Compared to the results with shallow seats, the interface pressure distributions were more evenly distributed over the interface and the peak pressures were lower in the analyses with deeply shaped seats. The maximum pressure values ranged from under 50 mmHg (6·7 KPa) when the seat depth was 105 mm (analysis 7) to over 80 mmHg (10·7 KPa) when the seat depth was 40 mm (analysis 13).

In the plane strain analyses of the central section through the buttock, the maximum interface pressures were between 36 mmHg (analysis B) and 54 mmHg (analysis E). The pressure peak was at or close to the tip of the sacrum in analyses A, C, and F. The interface pressure peak was anterior to the tip of the sacrum in analyses B and D. In analysis E there were two pressure peaks, one close to the sacrum and one located at a more anterior position along the interface. The calculated pressure distributions are shown in Figure 37.

The soft tissue surface deformations from each analysis were compared. The outlines were graphically aligned such that the bony interfaces were superimposed. In general the body surfaces moved inward in the areas where there was contact between the body and the seat, and moved outward in the areas outside the boundary of contact. When contact was locally lost due to a depression in the seat, the soft tissue surface moved either inwards or outwards by a small amount in these regions. The soft tissue surface deformations from analyses 1 to 13 are shown in Appendix 11. The soft tissue surface deformations were largest along the axis of revolution in analyses 1 to 5. They ranged from over 48 mm in analysis 1 to less than 22 mm in analysis 5.

When the seats were shaped similarly to the soft tissue surface (6 to 10), the body deformations were a lot smaller than in analyses 1 to 5. For analysis 6 the maximum displacement of a node at the surface of the body (relative to the bone-soft tissue interface) was 13·5 mm. For analyses 6 to 10, the maximum inward displacement was located lateral to the central axis. There were lower levels of deformation at the tissue surface under the ischial tuberosity, when the depth of the seat along the axis of revolution was increased (analyses 6 to 9). The deformations were smaller and more evenly distributed when the seats were deeply contoured. For example, the maximum surface deformation in the area of contact was only 15 mm in model 7.

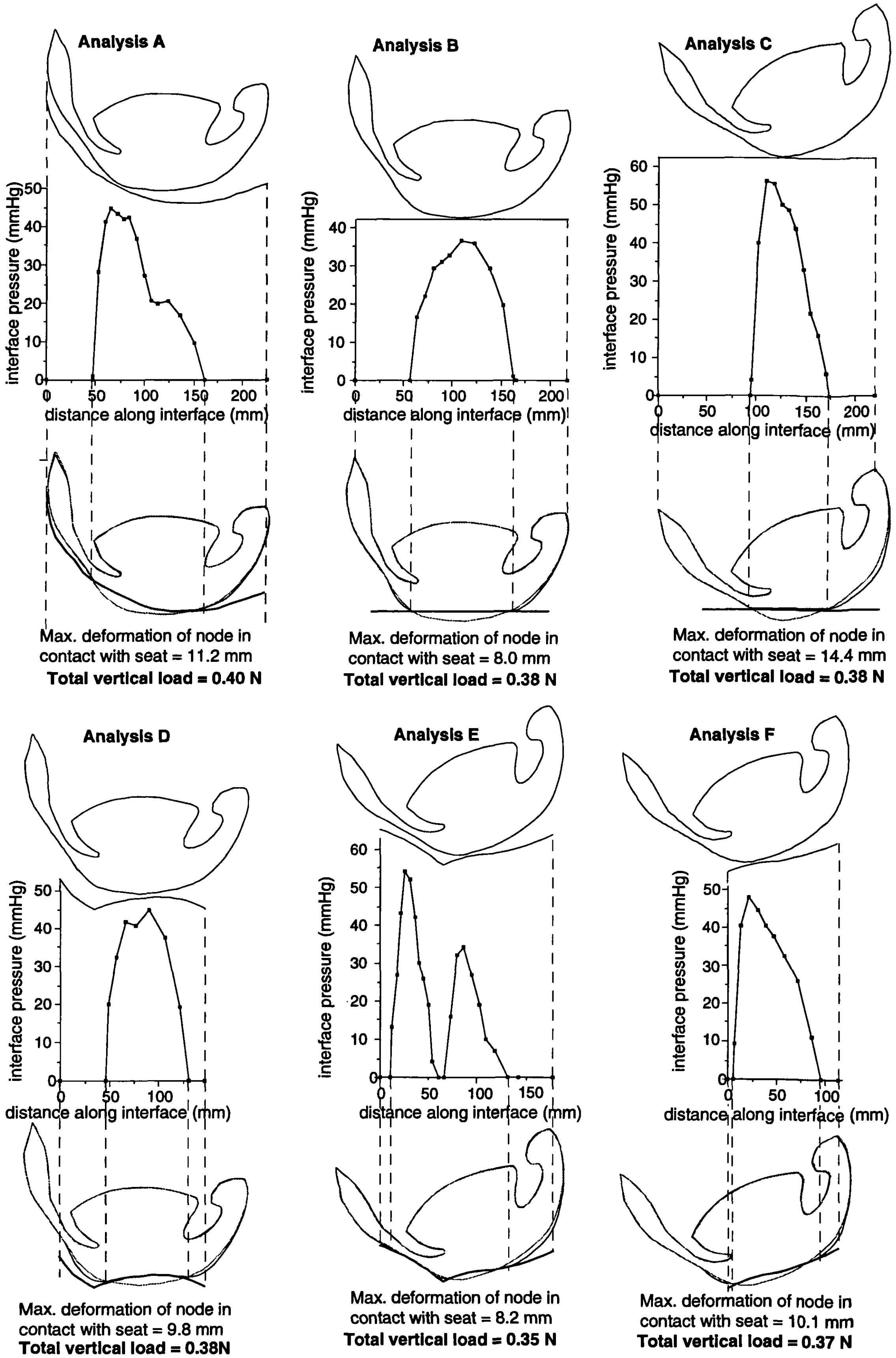

FIGURE 37
Interface pressures and surface deformations on sagittal section through sacrum from FE analyses in Section 7.4

From the analyses of the central section through the buttock, the maximum displacement of nodes in contact with the seat was between 8·0 mm (analysis B) and 14·4 mm (analysis C). For most of the analyses, the maximum displacements were located near the mid-point of the body-seat interface. The soft tissue surface deformations from each of the plane strain analyses are shown in Figure 37.

In the next section, the interface quantities which have been described in this section were related to the stress state in the soft material, to see whether it might be possible to gain information on the stress distribution in the soft tissues from outside the body.

8.3 Correlation in FE Analyses between Interface Data and the Stress State in Soft Tissues

The relationships between the stress state in the soft tissues and quantities which could be measured non-invasively on seated patients were investigated by examining the results from the FE analyses. The relationships were examined between interface pressures, deformations, pressure gradients and the vertical load supported at the interface and the peak von Mises stress in the soft tissue near the bony prominence. Both the ischial tuberosity and the sacrococcygeal region are considered below. The tissues over the dorsal surface of the sacrum are considered in Appendix 12.

The interface pressures and pressure gradients were difficult to calculate accurately from the FE analyses, because of the concentration of loading at the nodes on the interface. To calculate pressure gradients, a polynomial curve was drawn through the pressure values in the region of interest with commercially available software (Cricket Graph®, graphics software for the Macintosh computer). In most cases fifth-order polynomial equations fitted the pressure distributions best and the squares of the correlation coefficients were greater than 0·95. The pressure gradients were estimated from the equations.

Under the Ischial Tuberosity

With the analyses of the soft tissue around the ischial tuberosity (models 1 to 13), the correlation between the von Mises stress maxima in the tissues and interface quantities was investigated when 186.9 N vertical load was transferred through the seats. The peak von Mises stress in the column of material within a 10 mm radius of the axis of revolution was noted. The pressures, pressure gradients, vertical loading and interface deformations were calculated at points along the interface up to a horizontal distance of 25 mm from the axis. The relationships involving vertical load and deformation at the interface are shown in Figure 38 and those involving interface pressures and pressure gradients in Appendix 13.

The peak von Mises stress at the tip of the ischial tuberosity was large in analyses where there was a large vertical deformation under the ischial tuberosity. The relationship between the two quantities was close to exponential. Near linear correlations were found between the peak von Mises stresses and the vertical load supported through areas of the interface directly under the ischial tuberosity, with horizontal diameters between 20 and 50 mm. The peak von Mises stress tended to be large in analyses where the interface pressure and pressure gradient under the ischial tuberosity were large. However the correlation between these quantities was limited. There was most scatter at locations close to the axis of revolution, probably due to limited load information in these regions.

Under the Tip of the Sacrum

With the analyses of sections through the sacrum (models A to F), the correlation between the von Mises stress maxima near the tip of the sacrum and interface quantities was observed when 0.38 N vertical load was transferred through the seats. The interface pressures, pressure gradients, vertical loading and the deformations at points on the interface up to 25 mm horizontally from the tip of the sacrum were examined. The peak von Mises stresses in the soft material tended to be large when the pressure, interface deformation and total vertical load were high at the nearby interface. However the scatter in these relationships was greater than with the ischial tuberosity. There was no significant correlation between the interface pressure gradient and the von Mises stress peaks at the tip of the sacrum. The relationships involving vertical load and deformations at the interface are shown in Figure 38 and those involving interface pressures and pressure gradients in Appendix 13.

Discussion

In the theoretical analyses there was not a simple, accurate method of relating measurements outside the body to the stress distribution in the soft tissue-like material near a bony prominence. The vertical deformation of the interface and the total vertical load supported through an area of the interface under the bony prominence were the most reliable indicators of the stress distribution. For an even stress distribution in the soft tissues the body surface displacements, and loads supported at the interface under the bony prominence should be lower than in other areas of the interface. The approach of calculating the total load supported through an area of the body, rather than using interface pressure measurements directly, agrees with the empirical work of Drummond et al (1985). They showed that the risk of ulceration is high when more than 30 percent of the weight of the body is supported through one ischium, more than 11 percent through the saccrococcygeal area or more than 55 percent through the ischia and saccrococcygeum in combination.

Analyses at Ischial Tuberosity : Models 1 to 13

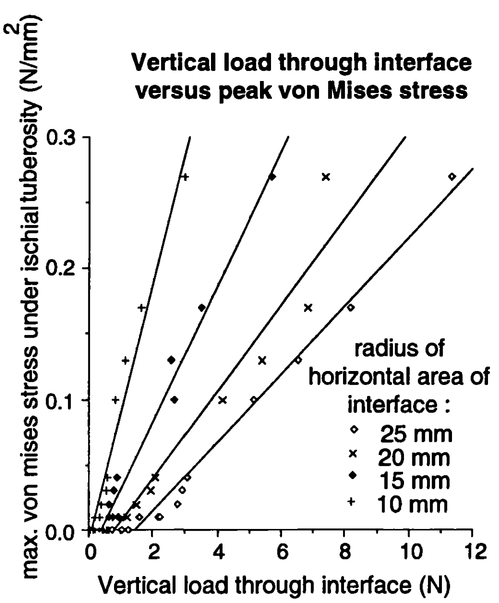

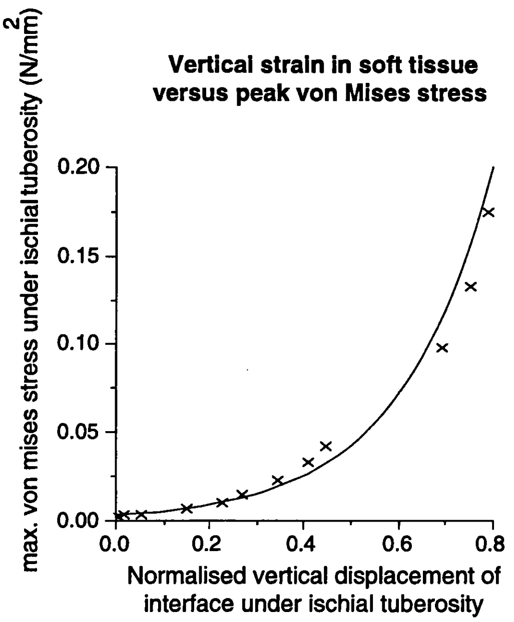

Analyses of Sacral Section : Models A to F

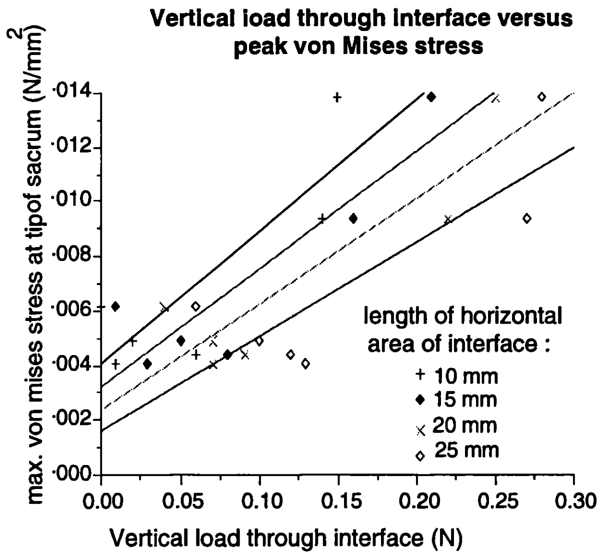

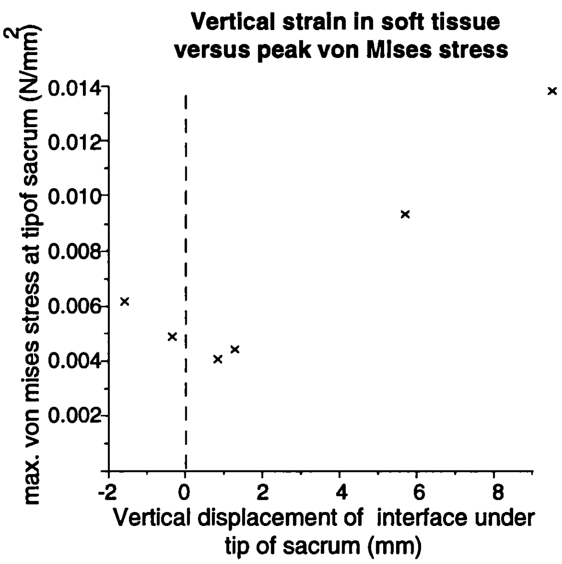

FIGURE 38
Correlation between deformations and vertical load supported through interface, and the peak von Mises stress at the bony prominence

Previously it has been suggested that an even pressure distribution at the interface between a person and a cushion will give the optimum support for pressure sore prevention. The results from this study suggest that for an even stress distribution in the tissues of the buttock, the pressures under the bony prominence should be lower than those in other regions of the body-support interface.

Body surface deformation measurements could also be useful in the design and assessment of cushioning and seating since they may give an indication of the distortional stress state in the adjacent soft tissues. For seating and cushioning design purposes the person could sit on a shaped template seat and the soft tissue thickness over the bony prominences could be measured with ultra-sound, or with small indenters. The thickness of the soft tissues prior to the interaction with the seat would have to be measured at the same anatomical location.

Closer correlations were found with the analyses of the ischial tuberosity compared to the analyses of the sections through the sacrum. The inferior correlation in the sacral model could be a consequence of its more complex geometry or of the smaller loads supported through the seat sections. It may be that some of the scatter in the plots of pressure and pressure gradient was due to the approximate method of estimating the interface pressure distribution. It was not possible to apply pressure loading with ANSYS software, and therefore it was difficult to determine whether this was the case.

8.4 Comparison of Experimental and Calculated Interface Pressures.

The pressure distribution between the body of the subject and a contoured seat was examined and compared with the pressure distributions which were calculated from the theoretical models in Section 8·2. This provided a means of assessing the validity of the results of the modelling. The methodology and equipment used to make the measurements are described in Chapter 2.

The average pressure normal to the surface at each grid point is shown in Figure 39. For clarity approximate contours were drawn around the grid points above pressure levels of 25, 50 75, 100 and 200 mmHg. There was a pressure peak which was over 200 mmHg (26·7 kPa) at the location of the distal sacrum. The interface pressure over the most of the contact area was between 25 and 50 mmHg. There were small areas of the interface under each ischial tuberosity where the pressure was between 50 and 65 mmHg (6·7 - 8·7 kPa). Over the lateral and posterior upper borders of the interface the pressure was less than 25 mmHg (3·3 kPa).

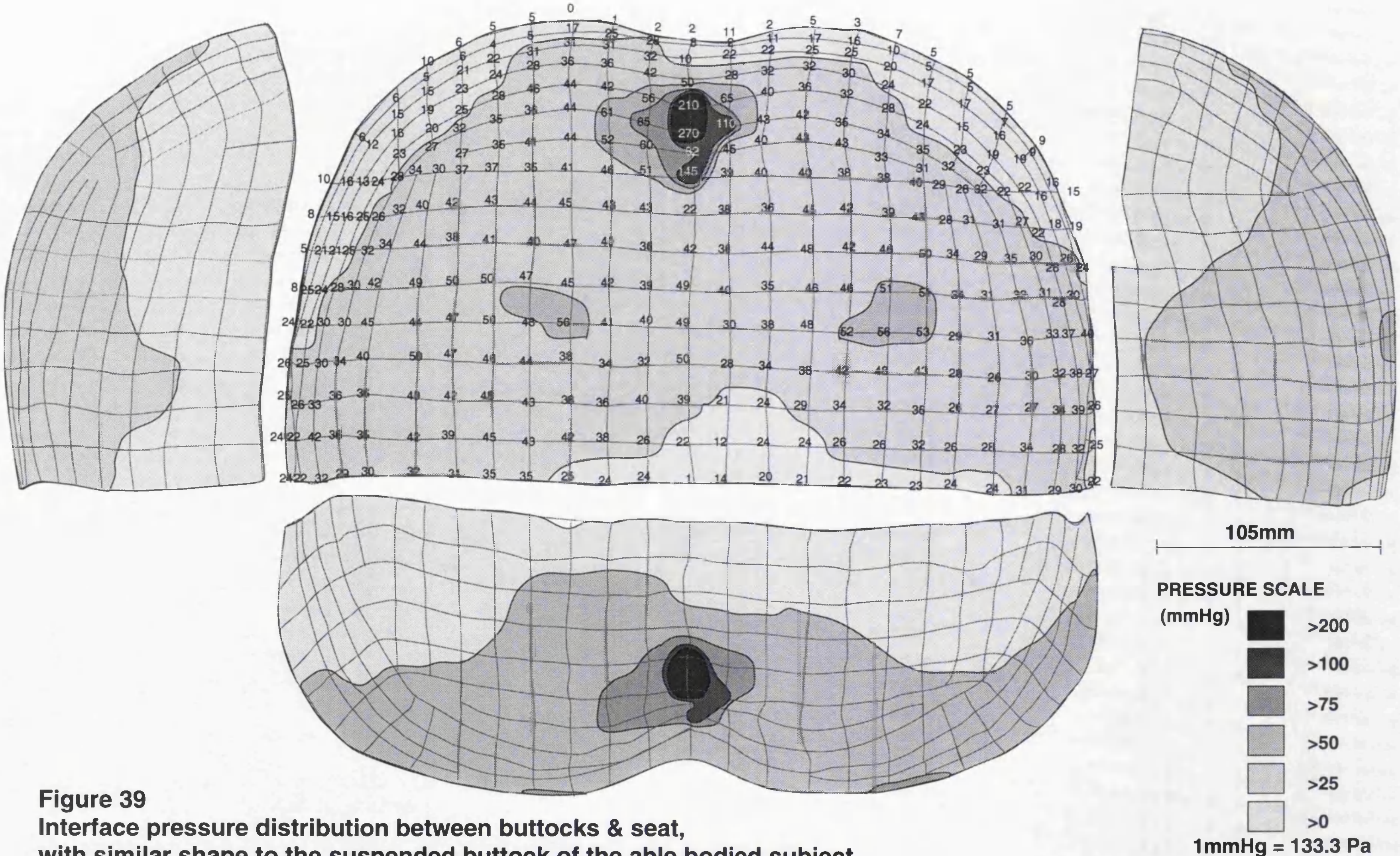

Figure 39
Interface pressure distribution between buttocks & seat, with similar shape to the suspended buttock of the able bodied subject

The measured pressure distribution was compared with the calculated pressure distributions from the FE analyses, where there were similar seat shapes. A pressure distribution was calculated from model 6, which decreased to about 25 mmHg in the area of the interface directly under the ischial tuberosity. The measured pressure distribution was closer in form to those predicted by models 4 and 5, where the seats did not follow the contours of the body so closely.

With model A, where the seat section had a similar shape to the central section through the manufactured seat, little contact was made with the back of the seat, and thus the analysis clearly did not realistically represent the system in which the pressure distribution had been measured. The analysis was repeated with the body initially located further back relative to the seat section so there was greater contact with the back of the seat. A location 20 mm further to the back of the seat was selected, since it was though that this might give a contact region similar to the one that was measured. When 1·8 N was supported through the seat section, the calculated pressure distribution was similar in form and magnitude to the measured one. However the maximum calculated pressure was still lower than the measured one. The calculated pressure distributions are shown in Appendix 14.

The measured pressure distribution with the subject sitting on a planar seat (described in Chapter 5) was compared with the pressure distribution calculated from theoretical model B. The theoretical pressures were very evenly distributed, similarly to with the measurements, however the area in contact with the seat was smaller and thus the calculated pressures were higher.

Various factors could have contributed to the differences between the calculated and measured pressure distributions. The contoured seat did not have exactly the same geometry as the unloaded buttock when the subject was in the sitting position, because the shape of the seat was not exactly the same as the average casting of the suspended buttock and the casting process may have affected the shape of the 'unloaded' buttock. Also the presence of interface shear forces when the measurements were taken could have lead to errors in the readings from the pressure transducers and also could have affected the extent to which the tissues were constrained by the seat and therefore the load distribution at the interface. The curvature of the seat may also have affected the output from the transducers. The simplified material formulation for the soft tissue-like material and the geometry in the theoretical models would both have limited the extent to which the models resembled the real system.

In this section the interface pressure distribution produced by the able-bodied subject sitting on one seat shape was measured and compared with analytical results. From the measurements of interface shape, displacement and pressure and the theoretical analyses, criteria were suggested in the next section, on which basis shaped seating and cushioning could be designed.

8.5 Application of Results to Clinical Seat Design

The empirical and theoretical results from the previous chapters were used to propose design algorithms for shaped seating and cushioning which could be integrated into a CAD/CAM production system. In Chapter 7 the effects of various seat- and body-related factors on the stresses distributed in the tissues were investigated. It was analytically shown that the distortional stress concentration around bony prominences could be reduced by shaping seating similarly to the external geometry of the soft tissue surrounding the bony prominences. The proposals for seat shape designs were derived from the needs of the chair-bound population, the results of the FE analyses, the measurements in Chapters 2 and 3, and other considerations discussed below.

The optimum designs of supporting surface depend on the specific seating requirements of the client (e.g. postural control, pressure sore prevention, reduction in discomfort, ability to move around on the chair) and their physical characteristics (e.g. weight, body shape, soft tissue stiffness, posture, soft tissue thickness). When someone is sitting the weight of the upper body is transferred through the soft tissues which surround the pelvis and femora. Distortional stresses tend to be concentrated around the skeletal bony prominences such as the ischial tuberosities, sacrum and trochanters (see Chapter 7). The body weight and sitting posture determine the total vertical load transferred through the body-seat interface. Postural adjustments may redistribute the body weight between the back rests, arm rests, foot supports and the seat. The position of the pelvis during sitting also influences the distribution of the body weight over the area of the interface. The material properties, geometry, and interactions of the soft tissues also affect the internal stress distributions and state of strain near the body/seat interface.

The action of the seat on the body influences the distribution of stresses within the soft tissues and this depends on the seat's design.

In the ischial region, a supporting surface for pressure sore prevention should be shaped similarly to the suspended buttock. With this type of supporting surface, the gross lateral soft tissue displacements which occur during sitting on a flat surface, can be reduced or prevented. It was shown in Chapter 7 that a supporting surface which was shaped similarly to the contours of the buttock prior to deformation, vastly reduces the distortional stresses and hydrostatic pressure gradients in the soft material around a bony prominence. In the small area directly under the ischial tuberosities, the seat contour can be locally depressed to reduce the strain energy in this location still further (similarly to with FE model 9). A localised depression of only a few millimetres over an area of about 20 mm^2 under the bony prominence, is needed to remove the distortional stress concentration completely. However this increases the total load through the rest of the interface, causing the stresses and deformations over the rest of the interface to increase.

Distortional stress concentrations occur in the soft tissue at the tip and dorsal surface of the sacrum with many seats. The comparatively thin nature of the soft tissue around the sacrum means the stress concentrations are greatly affected by soft tissue compressions of only a few millimeters. To reduce these von Mises stress concentrations in this area with shaped seats, there should be no contact between the seat and the body in the region of the sacrum. This design strategy results in a reduction in interface area available to support the body weight, and so is not without cost. It is difficult to produce effective shaped seating for a person whose pelvis is severely posteriorly rotated during sitting. The region of the body available for load bearing through the seat is dominated by the sacrum. Ideally in this situation, the position of the person's pelvis should be changed by the use of back supports, an alteration in seat orientation, knee straps, etc. However this might not be possible or desirable in all clients and for these people a seat cushion should be specially designed to support the weight of the upper body through the gluteal muscles and proximal thighs. A tendency to slide forward in the seat is often experienced by chair-bound people with a posteriorly rotated pelvis. In some cases it would be possible to stop this occurring by providing a 'shelf' in the seat to support the proximal thighs and also holding the pelvis in position.

The perineum and genitalia are other regions where there may be a special need for reducing the risk of pressure sores. The damp, unhygenic conditions associated with incontinence are thought to be predisposing factors to pressure sores in these regions (Cochrane, 1990). Again the best solution for removing this risk in the region is to remove the load, by moving the seat surface outward away from the body. The loads which would no longer be supported in this area could be supported through the gluteal muscles and the proximal thighs with most people. These regions of the body are well covered in muscle, adipose tissue and skin, and there are few underlying bony prominences which could act as stress raisers and bring about soft tissue damage.

Many chair-bound people are able to shift themselves around in their seat and in this way they are able to periodically reduce or remove the loading on the soft tissues. This is probably an important mechanism which prevents the tissues getting damaged (Reddy, 1990) and should therefore not be prevented by a supporting surface. For a person who is not able to move around in the chair under any circumstances, the cushion design should maximise soft tissue containment. It may be possible to allow the sitter to change position on the seat and still redistribute the body weight away from the bony prominences by shaping the seat. When this is not possible, a balance must be reached between these two seating requirements.

One potential problem with shaped seating is that of a person sitting at an unforseen location on the shaped surface. This could cause stress concentrations in unexpected regions of the body and, for those people with no sensation from the buttocks and thighs, this could be particularly dangerous. This could be prevented with shaped seating, by giving clear instructions to the person on how to check position, contouring the seat so the person tends to slips into the correct position and ensuring that there are no prominent areas on the supporting surface near the bony prominences.

Another vital function of seating is the control of sitting position. A cushion can provide lateral forces to hold the pelvis in a fixed position on the seat. It may also be required to abduct the hips, by providing forces on the medial surface of the distal thigh. Chair-bound people commonly have a non-fixed lateral tilt to their pelvis and a non-fixed spinal scoliosis while sitting. Corrective loading can be applied through the cushion or seat to reduce or remove the pelvic obliquity. The seat should apply additional loads to the lower side of the pelvis to force it into a more symmetrical location (Patterson & Michael, 1991).

However a fixed or nearly-fixed deformity at the hips, pelvis or lower spine is likely to produce locally high loading under the pelvis or thighs (Drummond et al., 1985). For these people a seating intervention to correct posture could produce even higher localised loading. This may lead to an unacceptable risk of pressure sores. Thus a balance between postural correction and weight redistribution has to be reached when designing cushioning for such people. In some cases it may be possible to improve posture by other means (lumbar supports, trunk braces, changing the orientation of the seat) and then to redistribute weight with a cushion once the person is sitting in the best posture.

8.6 Examples of Shaped Seat Surface Designs

Designs for specific clinical requirements can now be developed using the principles described in the sections above. The work in the previous chapters could lead us to suggest that there is a unique optimum seat design for each subject, depending on his or her seating requirements and body characteristics. However shaped seat cushioning is also produced in standard shapes with contours and 'cut outs' over regions vulnerable to pressure sores. Such cushions are probably better than flat foam cushions for the large group of chairbound people who require comfort and postural support from their cushion and who are not at high risk of pressure sores. Inevitably the envelopment of the buttocks and the extent of lateral support provided by standardised cushions are less than that which could be provided by individualised designs. Computer-aided manufacture is still a quick, automated method of producing contoured surfaces for such cushions. To be able to adjust the shape and size of the cushions to fit an individual, computer aided design would be required.

The shape design of 'off-the-shelf' seat cushions requires detailed information of the anthropometry and weight of the chair-bound population. Data is available on the width of the hips, distance from the back of the buttock to the back of the knee and distance apart of the tips of the ischial tuberosities whilst sitting (Diffrient et al., 1974; Chung & Weimar, 1988; Harris & Mayfield, 1983). The information has been tabulated in Appendix 15.

The distance between the back of the seat and the back of the buttocks varies over several centimeters depending on the seating circumstances of an individual. With 'standard' shaped seating a strip could be cut off the back of the standard surfaces to achieve the necessary dimensions. Examples of customised and 'off-the-shelf' designs are described and sketched in Figure 40. Typical dimensions for the surfaces are shown in Appendix 16.

Shaped Supporting Surface to Improve Comfort and to Control Pelvic Position

This supporting surface design would be useful for people who have poor control of the position of their pelvis on the seat or who are uncomfortable during sitting due to excessive loading of the ischial or sacral regions of the buttock. This design would be effective if it were available in a range of standard sizes and shapes. To allow for body motion during sitting, the contours would be quite shallow (for example, 40 mm deep) and 'open'. It would not be idea for people who are at high risk of pressure sores or who have a pronounced postural asymmetry during sitting that could not be reduced via a seating intervention.

Shaped Supporting Surface to Reduce the Risk of Pressure Sores around the Pelvis

This supporting surface design would be useful to someone who has developed a pressure sores over the left buttock, as a result of an oblique pelvis causing weight bearing through the left buttock and who is not able to move around in their seat. It is designed to contain the soft tissues in the gluteal region of the buttock and to minimise the load supported through the left ischium. The pelvic obliquity is neither increased or corrected by the seat. This design would need to be customised to the body characteristics of each client. The surface geometry in Figure 40 is based on the shape of the able-bodied female who was measured in the early chapters of this thesis.

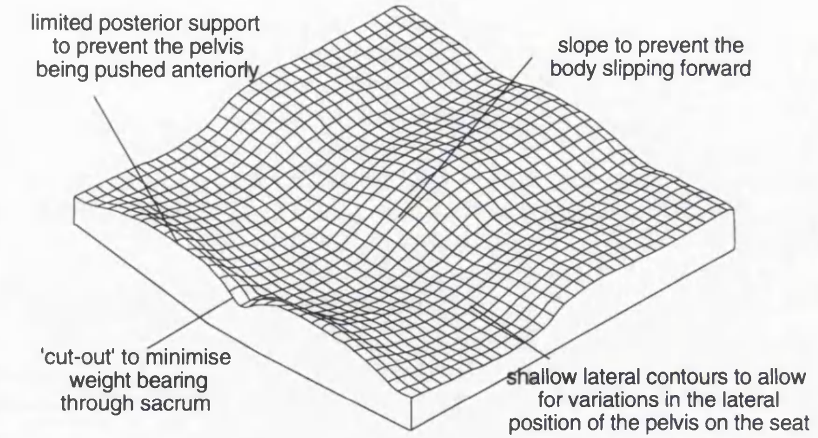

Seat Surface to Prevent Sliding Off the Front of the Seat and a Postero-Inferior Rotation of the Dorsal Surface of the Sacrum

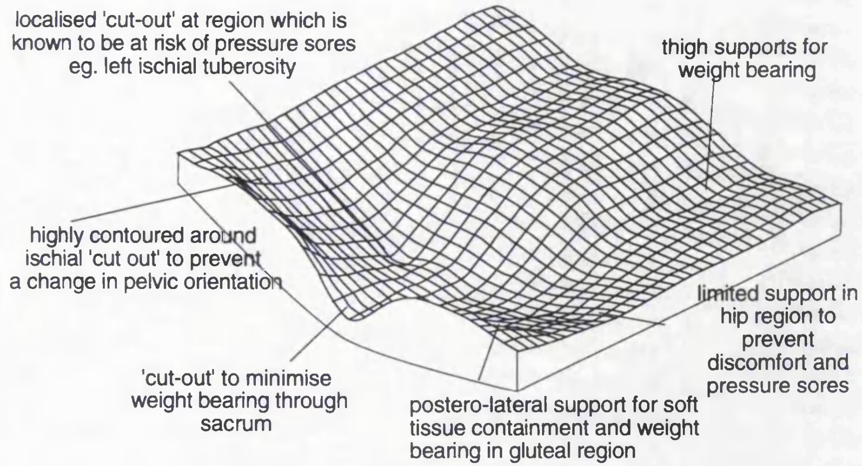

Individualised Seat Surface for Pressure Sore Risk Reduction

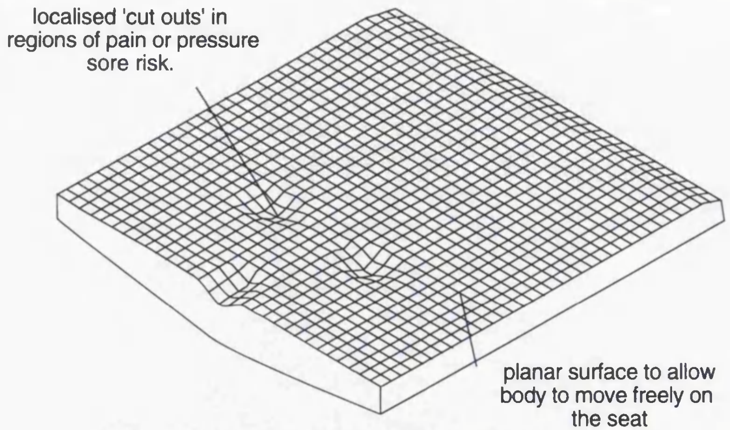

Seat Surface for Localised Reductions in Weight Bearing through the Bony Prominences and to Allow Full Motion of the Body on the Seat

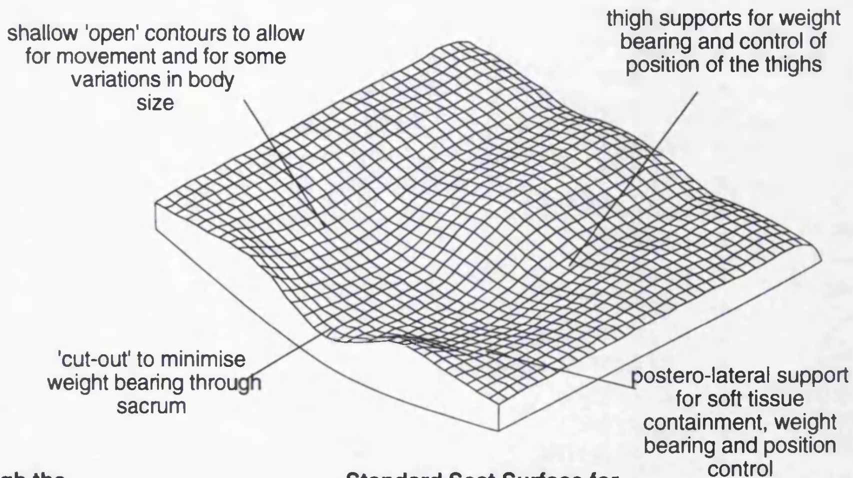

Standard Seat Surface for Comfort and Postural Control

FIGURE 40
Examples of shapes seat surfaces for specific clinical problems

Shaped Supporting Surface to prevent the Body Moving Forward in the Seat and /or an Anterior Pelvic Rotation

This supporting surface design would be useful to people who have a pronounced posterior pelvic tilt which is causing them to slip forward on the seat. It would be used in conjunction with a sacral pad, so that correcting forces would be supplied through the proximal thigh and sacral pad to force the hips into flexion and the pelvis into a position where its dorsal surface has less of a postero-inferior orientation. Also such designs would have to be well tested to ensure the client would not slip forward onto the thigh support.

Shaped Supporting Surface to Allow Full Motion of the Body on the Seat

This design would be useful to someone who needs to and is able to move around in their seat, but is uncomfortable due to load bearing through one or both ischial tuberosities or through the sacrum. It could be designed with 'cut outs' over one or more of the the bony prominences. By keeping the 'cut-outs' shallow and of small area, there is a minimal reduction in contact area and there is unlikely to be a change in pelvic orientation due to the 'cut-outs'. This design would be most effective if it were available in several sizes.

The designs to meet particular clinical needs could be produced as prototypes. It would then be necessary to test them extensively.

CHAPTER 9 DISCUSSION & CONCLUSIONS

In this work a system to produce individually shaped supporting surfaces for chair-bound people was researched into and developed. The system was made versatile by the use of computer-based technology for measuring body shape, and for designing and manufacturing the supporting surfaces. It was shown from the testing of, and clinical experience with the supporting surfaces, that surfaces produced with the system can improve comfort, control posture and redistribute the body weight over the body-support interface. These findings are consistent with the results of studies from the Rehabilitation Engineering Center at the University of Virginia. These have shown superior posture and pressure distributions for groups of people sitting on customised, contoured wheelchair cushioning compared to other cushion designs (Sprigle et al, 1990-B, Sprigle & Chung, 1989).

From the results of the analytical studies, it appears that shaped seating can greatly reduce the distortional stress peaks and the hydrostatic pressure gradients around the skeletal bony prominences. In general when the body-seat interface is similarly shaped to the undeformed body surface, the load is well distributed through the tissues and internal distortions have been minimised. It was also found that for the optimum stress distribution in the tissues, the load supported at the interface under a bony prominence should be lower than in other areas of the interface. The seat design information that was found from these studies could be integrated into the CAD/CAM system for seat production.

There were differences between the interface pressure distributions and soft tissue stiffnesses calculated from the analytical studies and measured on the subject. By developing analytical models with more realistic geometries and soft tissue characteristics, pressures and deformations could probably be calculated which resemble the real system to a greater extent. It was not possible to gain information from the analytical studies on the interactions between tissues such as muscle and skin because a homogeneous soft tissue layer was considered.

The implications of the studies for the design of body contoured seating for the chair-bound population have to be extrapolated from the results, because the model was based on a single able-bodied subject. Many chair-bound people will have a less extensive soft tissue covering and with more viscous, less elastic tissues than the person measured in this study. If the theoretical models had been based on measurements of such individuals, the detailed results would probably have been affected. Sprigle et al noted that people with flaccid tissues produce a deeper, narrower interface shape compared to people with spastic tissues when sitting on planar foam blocks (1990-A).

Shaped seats and cushions are often made from, or lined in, soft materials to accommodate body movements during sitting, vibrations from the ground, and geometric mismatch between the body and the seat. The deformation of the supporting material was not studied in the theoretical and empirical work to simplify the system under examination. The combined effect of material properties and seat surface shape is an important area for further study. Empirical and analytical studies would be necessary to fully examine these combined effects, however the behaviour can be reasoned out in general terms from the effects of the supporting surfaces in the present study. The fundamental factors affecting the performance of a shaped, deformable seat for an individual are the surface shape, material properties, boundary constraints and dimensions of the seating material. A soft seating material would be a disadvantage if the seat had been heavily contoured to provide constraining forces to the tissues around the bony prominences, because the sides of the troughs on the seat surface would spread out laterally when loaded. The seat would have to have very steep initial contours to balance this effect.

If a cushion surface is only slightly contoured, a soft cushioning material would be an advantage because it would be able to spread out of heavily loaded areas, thus reducing the loading of the tissues under the bony prominences. However with soft cushioning materials, in localised areas the cushioning material may not be able to support the weight of the body without becoming over-compressed. Sprigle et al noted that the decrease in thickness of contoured cushioning at the bottom of troughs, leads to a localised reduction in the stiffness of the cushion in these regions (1990-B). The level of load which can be supported through various thicknesses and stiffnesses of shaped cushioning material before excessive compression occurs could be determined in a laboratory-based investigation. One method of utilising soft materials in contoured cushioning might be to make cushions with a firm shell and a soft inner core. This construction would limit the amount by which the interface contours were reduced on loading. However the soft cushioning would not have to be very thin or very soft to avoid 'bottoming'.

One method of clinical assessment for the design of individualised, shaped cushioning would be to have a set of 'test' surfaces, which were instrumented for pressure distribution and interface deformation measurements. The patient would be asked to try a number of these surfaces and the resulting interface load distribution, and soft tissue deformations would be measured on each. The fine adjustments to the designs on the computer could be made, based on the measurements. The 'adjusted' design would then be produced with the computer aided manufacturing techniques discussed in Appendix 1. It would also be possible to manufacture 'off-the-shelf' shaped cushioning for groups of chair-bound people with similar seating needs with computer-aided production techniques. These cushions however could not provide the intimate envelopment of the buttock, given by individually shaped supports.

The performance of anatomically shaped designs could be tested out further with measurements of interface properties and posture. The success of a design depends on the seating needs of the person who will use it, therefore careful subject selection would be required for similar designs to be tested in the same study. The efficacy of shaped cushioning in controlling and correcting sitting posture in chair-bound people could be demonstrated. It might be possible to provide corrective forces through the seat when a deformity is not fixed.

The posture of the seated subjects could be assessed by measuring the shape of the trunk with a body shape scanner such as ISIS (Oxford Metrics, UK), or by measuring the position of markers on the bony prominences with a device such as the 3Space Isotrak (Polhemus Navigation Systems, USA). Sprigle and Schuch have suggested that interface contour measurements are useful for the evaluation of posture (1993). The more the deformity is fixed or where there is a high risk of pressure sores under the main regions of loading, it would not be possible to correct the deformity through the seat to the same extent.

From the studies reported in this thesis the following have been concluded:

1. It is possible to develop a system to produce supporting surfaces for the body where the system is operable by a therapist and technician, the measurement equipment is portable, and the design and manufacturing process is of less than two hour duration.
2. Seat surfaces that are anatomically contoured have been shown to improve comfort, and redistribute vertical loading to areas of the body-seat interface which are less susceptible to pressure sores.
3. Concentrations of distortional stress develop in the soft tissues around the bony prominences of the pelvis when the body is loaded against a supporting surface. The more the soft tissues around the body are displacement constrained by the supporting surface, the lower the distortional stress concentration in the soft tissues.
4. Good indicators of the stress distribution around the bony prominences are the deformation of the body surface and the vertical load supported at the nearby body-seat interface. For the optimum stress distribution in the tissues the load supported at the interface under the bony prominences should be lower than in other areas of the interface and the interface shape should be similar to the shape of the unloaded buttock.
5. The location and distribution of the hydrostatic and distortional loading in the soft tissue is highly influenced by the posture of the seated person. When the pelvis is posteriorly rotated, a lot of load is transferred through the sacrum, and there is a very high concentration of distortional stress in the soft tissues in this region.
6. When the body moves about on a seat surface and there is a high friction coefficient at the body-seat interface, the soft tissues are constrained by the interface forces and additional distortional stress develops in the soft tissues. If the body remained stationary on a shaped supporting surface, interface friction can reduce the distortional loading by preventing the soft tissues flowing away from the bony prominences.

The scope for further study of the issues covered in this thesis is extensive, as described earlier in Chapter 9.

REFERENCES

Alexander H. & Cook T., Variation with Age in the Mechanical Properties of Human Skin in Vivo, in *Bed Sore Biomechanics,* Proc. of a Seminar on Tissue Viability and Clinical Applications, Kenedi R.M., Cowden J.M. & Scales J.T., Eds., Macmillan Press, London, 1976,109.

Allman R.M., Laprade C.A., Noel L.B., Walker J.M., Moorer C.A., Dear M.R. & Smith C.R., Pressure sores amongst hospitalized patients, *Annals of Internal Medicine*, vol. 105, 337, 1986.

Armstrong C.G., Bahrani A.S., Gardner D.L., Changes in the deformational behaviour of human hip cartilage with age, *Trans.of the ASME J. of Biomechanical Engineering*, vol. 102, Aug, 214,1980.

Bader D.L., The recovery characteristics of soft tissue following repeated loading, *Journal of Rehabilitation Research and Development*, vol. 27, no. 2, 141, 1990.

Bader D.L. & Bowker P., Mechanical characteristics of skin & underlying tissue in vivo, *Biomaterials*. vol. 4, Oct, 305,1983.

Bader D.L. & Gant C. A., Changes in transcutaneous oxygen tension as a result of prolonged pressure at the sacrum, *Clinical Phys. Physiolo. Measurement*, 9, 33, 1988.

Bao H.P., Automated Orthopaedic Shoe Last Production, Proc. RESNA 12th Annual Conference, New Orleans, Louisiana, 1989,151.

Barbenel J.C., Evans J.H., & Finlay J.B., Stress-strain-time relations for soft connective tissues, in *Perspectives in Biomedical Engineering*, Proc. of a Symposium at the Univ. of Strathclyde, Glasgow, Kenedi R.M., Ed., MacMillan Press ltd, London & Basinstoke, 1972, 165.

Bardsley G.I., The Dundee seating programme, *Physiotherapy*, vol. 70, no. 2, 59, 1984.

Barton A. & Barton M., *The Management and Prevention of Pressure Sores*, Faber & Faber, London, 1981,26.

Bennett L., Kavner D., Lee B.K., Trainor F.A. & Lewis J.M., Skin blood flow in seated geriatric patients, *Arch Phys Med Rehabilitation, vol.* 62, 392, 1981.

Bennett L., Kavner D., Lee B.K. & Trainor F.A., Shear vs pressure as causative factors in skin blood flow occlusion, *Arch Phys Med Rehabilitation, vol.* 60, 309, 1979.

Brienza D.M., Chung, K.C. & Inigo R.M., Design of a Computer Aided Manufacturing System for Custom Contoured Wheelchair Cushions, Proc. International Conference of the Association for the Advancement of Rehabilitation Technology - ICAART 88, Montreal, Canada, 1988, 312.

British Standard Methods of Test for Flexible Cellular Materials, BS 4443 Part 2 Method 7, Indentation Hardness Tests. British Standards Institute, 1988.

Cadadai R.S., & Reddy N.P., Stress distribution in a physical buttock model : Effect of simulated bone geometry, *J. Biomechanics*, vol. 25, no. 12, 1403, 1992.

Chow W.W. & Odell E.I., Deformations and stresses in soft body tissues of a sitting person, *J. of Biomechanical Engineering*, Vol.100, May, 79, 1978.

Chung K.C. & Weimar W., Anthropometric Studies for the Physically Disabled Population - Volume II Spinal Cord Injury, report UVA-REC 102-89, Rehabilitation Engineering Centre, University of Virginia,1989.

Clark M., Rowland L.B., Wood H.A. & Crow R.A., Measurement of the soft tissue thickness over the sacrum of elderly hospital patients using B-mode ultrasound, *J. Biomed. Eng.*, vol. 11, May, 200, 1989.

Cochrane G., The severely disabled, in *Pressure Sores - Clinical Practice and Scientific Approach*. Bader, D.L., Ed., Macmillan Press, London & Basingstoke, 1990, 81.

Cousins S.L., Ackerley k., & Jones K.N., A Body Support System for the Disabled, Annual Report, Bioengineering Centre, Roehampton, UK, 1982, 75.

Cricket Graph Presentation Graphics for Science and Business, Reference Manual, Cricket Software, PA, USA, Ch. 9.

Daniel R.K., Wheatley D. & Priest D., Pressure sores and paraplegia : An experimental model, *Annals of Plastic Surgery*, vol. 15, no. 1, 41,1985.

Dewar M.E., & Reynolds D.P., The UCL System for Computer Aided Socket Design - 1. Principles, Annual Report, Bioengineering Centre, Dept of Mechanical Engineering, University College London, 315, 1986.

Diffrient N., Tilley A.R., Bardagjy J.C., *Humanscale 1/2/3,* A Portfolio of Information: 1. Sizes of People 2. Seating Considerations 3. Requirements for the Handicapped and Elderly, the M.I.T. Press, Massachusetts,1974.

Dinsdale S.M., Decubitus ulcers: role of pressure and friction in causation, *Arch. Phys. Med. & Rehabil.* , vol. 55, 147, 1974.

Dodd K.T. & Gross D.R., Three-dimensional tissue deformation in subcutaneous tissues overlying bony prominences may help to explain external load transfer to the interstitium, *J. Biomechanics*, vol. 24, no. 1, 11, 1991.

Drummond D., Breed A.L. & Narechania R., Relationship of spine deformity and pelvic obliquity on sitting pressure distribution and decubitus ulceration, *Journal of Pediatrics Orthopaedics*, vol. 5, no. 4, 396, 1985.

Duck F.A., *Physical Properties of Tissue, A Comprehensive Reference Book.*, Academic Press, London, 1990, 151.

Ek A.-C., Gustavsson G. & Lewis D.H., Skin blood flow in relation to external pressure and temperature in the supine position on a standard hospital mattress, *Scand J Rehab Med* 19, 121, 1987.

Fenwick D., Wheelchairs and their Users, Report of a Survey carried out on behalf of the Department of Health and Social Security by the Social Survey Division of Office of Population Census and Surveys, London, 1977.

Frisbie J.H., Wound healing in acute spinal cord injury: effects of anticoagulation, *Arch. Phys. Med. & Rehabil.* , vol. 67, 311, 1986.

Fung Y.C., Stress-strain-history relations of soft tissue in simple elongation, in *Biomechanics : Its Foundations and Objectives*, Fung, Y.C., Perrone, N. & Anliker, M. Eds., Prentice Hall, New Jersey, 1972, 181.

Fung Y.C., *Biomechanics : Mechanical Properties of Living Tissues*, Springer, New York, 1981.

Garber S.L., Krouskop T.A., & Carter R.E., A system for clinically evalution wheelchair pressure relief cushions, *The American Journal of Occupational Therapy*, vol. 32, no. 9, 565, 1978.

Gargano R., A System to Rapidly Manufacture Custom Contoured Foam Seating, Proc. RESNA 9th Annual Conference, Minneapolis, Minnesota, 1986, 375.

Harris C. & Mayfield W., Seating for Elderly and Disabled People, Report no. 2, Anthropometric Survey, Institute of Consumer Ergonomics, University of Loughborough, Leicester, April 1983.

Hayes W.C., Keer L.M., Herrmann G. & Mockros L.F., A mathematic analysis for indentation tests of articular cartilage, *J. Biomechanics*, vol. 5, 541, 1972.

Hefzy M.S., Jackson W.T., Saddemi S.R., Hsieh Y.-F., Effects of tibial rotations on patellar tracking and patello-femoral contact areas, *J. Biomed. Eng.*, vol. 14, July, 329, 1992.

Hindle R.J. & Pearcy M.J., Rotational mobility of human back in forward flexion, *J. Biomed. Eng.*, vol. 11, May, 219, 1989.

Houston V.L., Considerations in Optical Digitization of Lower Limb Segments for Prosthetics CAD/CAM, Proc. RESNA 12th Annual Conference, New Orleans, Louisiana 1989, 153.

Hutchison J.M.S., Imaging by nuclear magnetic resonance, in *Medical Images: Formation, Perception and Measurement.* Proc. 7th Gray Conference, University of Leeds, Hay G.A., Ed., Inst. of Physics & John Wiley & Sons,13-15 Apr. 1976, 135.

IMSL Math/Library User's Manual Volume 2. Problem-Solving Software Systems, Fortran Subroutines for Mathematical Applications, Version 1.1. , Texas, USA, Aug, 516, 1989.

Jordan M.M. & Barbenel J.C., Pressure sore prevalence in *Pressure Sores.* Barbenel, J.C., Forbes C.D. & Lowe G.D.O. Eds., Macmillan Press, London & Basingstoke, 1983, 59.

Kadaba M.P., Ferguson-Pell M.W., Palmieri V.R. & Cochran G.Van B., A technique for mapping the contour of buttock-cushion interface using ultrasound, *Arch. Phys. Med. & Rehabil.* 65, 467, 1984.

Kao B.G. & Razgunas L., On the Determination of Strain Energy Functions of Rubbers, Paper 860816, Proc. 6th International Conference on Vehicle Structural Mechanics, Detroit, Michigan, April 22-24 1986, 145.

Keane F.X., The function of the rump in relation to sitting and the Keane reciprocating wheelchair seat, *Paraplegia*, vol. 16, no. 4, 390, 1979.

Keane F.X., The minimum physiological mobility required for man supported on a soft surface, *Paraplegia*, vol. 16, 383, (Proc. Annual Scientific Meeting of International Medical Society of Paraplegia, Stoke Mandeville, July, 1978),1979.

Keegan J.J., Alterations of the lumbar curve related to posture and seating, *The Journal of Bone and Joint Surgery*, vol. 35-A, no. 3, 589 , 1953.

Kirk J.E., & Kvorning S.A., Quantitative measurements of the elastic properties of the skin and subcutaneous tissue in young and old individuals, *J. Gerontol.*, vol. 4, 273, 1949.

Kirk J.E. & Chieffi M., Variation with age in elasticity of skin & subcutaneous tissue in human individuals, *J. Gerontol.* , 17 , 373, 1962.

Kosiak M., Etiology and pathology of ischemic ulcers, *Arch. Phys. Med. & Rehabiliation*, vol. 40, 62, 1959.

Krouskop T.A., Reddy N.P., Spencer W.A., & Secor J.W., Mechanisms of decubitus ulcer formation - An hypothesis, *Medical Hypotheses*, vol. 4, no. 1, 37, 1978.

Krouskop T.A., A synthesis of the factors that contribute to pressure sore formation, *Medical Hypotheses*, vol.11, 255, 1983.

Krouskop T.A., Doughtery D.R. & Vinson F.S., A pulsed doppler ultrasonic system for making noninvasive measurements of the mechanical properties of soft tissue, *Journal of Rehabil. R. and D.*, vol. 24, no. 2, 1, 1987.

Kwan M.K., Lai W.M. & Mow Van C., A finite deformation theory for cartilage and other soft hydrated connective tissues- I. equilibrium results, *J. Biomechanics*, vol. 23, no. 2, 145, 1990.

Landis E.M, Micro-injection studies of capillary blood pressure in human skin, *Heart*,15,209,1930.

Lanir Y., Dikstein S., Hartzshtark A. & Manny V., In-vivo indentation of human skin, *Trans. ASME J. of Biomechanical Engineering*, vol. 112, 63, 1990.

Lanir Y., A structural theory for the homogeneous biaxial stress-strain relastionships in flat collagenous tissues, *J. Biomechanics*, vol. 12, 423, 1979.

Lanir Y., Constitutive equations for fibrous connective tissues, *J. Biomechancs*, vol. 16, no. 1,1,1983.

Lamid S. & El Ghatit A.Z., Smoking, spasticity and pressure sores in spinal cord injured patients, *American Journal of Physical Medicine*, vol. 62, no. 6, 300, 1983.

Le K.M., Madsen B.L., Barth P.W., Ksander G.A., Angell J.B. & Vistnes L.M., An in-depth look at pressure sores using monolithic silicon pressure sensors, *Plastic & Reconstructive Surgery,* vol. 74, no. 6, 745, 1984.

Lee M.C., LeWinter M.M., Freeman G., Shabetai R. & Fung Y.C., Biaxial mechanical properties of the pericardium in normal and volume overload dogs, *Am. J. Physiol.*, vol. 249, H222-H230, 1985.

Linney A.D., Grindrod S.R., Arridge S.R., Moss J.P., Three-dimensional visualisation of computerised tomography and laser scan data for the simulation of maxillo-facial surgery, *Med Inf (Lond)*, Apr- Jun 1989, 14(2), 109.

Lowthian P.T., Some Hazards of Patient Support Systems and Their Mitigation, M.Phil. thesis, University of Surrey, Guildford, 1983.

Malinauskas M., Krouskop T.A., Barry P.A., Noninvasive measurement of the stiffness of tissue in the above-knee amputation limb, *Journal of Rehabil. R. and D.*, vol. 26, no. 3, 45, 1989.

Manschot J.F.M. & Brakkee A.J.M., The measurement and modelling of the mechanical properties of human skin in vivo - 1. the measurement, *J. Biomechanics*, vol. 19, no. 7, 511, 1986.

Markenscoff X. & Yannas I.V., On the stress-strain relation for skin, *J Biomechanics*, vol. 12, 127, 1979.

Michael, S.M. & Walker, P.S., Clinical trial of body-contoured wheelchair cushioning, *Clinical Rehabilitation, vol.* 4, 229, 1990.

Michael S.M. & Walker, P.S., Advances in wheelchair cushioning, *Critical Reviews in Physical and Rehabilitation Medicine*, vol. 3, no. 1, 1, 1991.

Moss J.P., Linney A.D., Grindrod S.R., Arridge S.R. and Clifton J.S., Three-dimensional measurement of the face and skull using computerised tomography and laser scanning techniques. *Eur. J. Orthod.* , 9(4), 247,1987 .

Mow V.C., & Lai W.M., Recent development in synovial joint biomechanics, SIAM Rev., vol. 22, 275, 1980.

Nelham R.L., Principles and practice in the manufacture of seating for the handicapped, *Physiotherapy*, vol. 70, No.2, 54 , Feb. 1984

Nelham R.L., The manufacture of moulded supportive seating for the handicapped, *J. Biomedical Engineering*, 379, Oct., 1975.

Noble P.C., Goode B., Krouskop, T.A. & Crisp B., The influence of environmental aging on the loadbearing properties of polyurethane foams. *J. Rehabilitation Research & Development,* vol. 21, no. 2, 31, 1984.

Nola G.T. & Vistnes L.M., Differential response of skin and muscle in experimental production of pressure sores, *Plastic and Reconstructive Surgery*, vol. 66, no. 5, 728, 1980.

Oden J.T., *Finite Elements of Nonlinear Continua*, McGraw-Hill,1972, 325.

Parsons J.R. & Black J., The viscoelastic shear behaviour of normal rabbit articular cartilage, *J Biomechanics*, vol. 10, 21, 1977.

Patterson K. & Michael S.M., Correcting the sitting posture of a person with a hind-quarter amputation, *Australian Journal of Occupational Therapy*. vol. 38, no. 1, 1991.

Payne P.A., Application of ultrasound in dermatology, *Bioengineering and the Skin*, vol. 1, 293, 1985.

Pinchcofsky G.D. & Kaminski M.V., Correlation of pressure sores and nutritional status, *J. Am. Geriatric Soc.*, vol. 34, no. 6, 435, 1986.

Reddy N.P., Cochran G. Van B. & Krouskop T.A., Interstitial fluid flow as a factor in decubitus ulcer formation, *J. Biomechanics*, vol. 14, no. 12, 879, 1981.

Reddy N.P., Patel H., Cochran G. Van B. & Brunski J.B. , Model experiments to study the stress distribution in a seated buttock, *J. Biomechanics*, vol. 15, no. 7, 493, 1982.

Reddy N.P., Effects of mechanical stress on lymph and interstitial fluid flows, in *Pressure Sores - Clinical Practice and Scientific Approach.* Bader, D.L., Ed., Macmillan Press, London & Basingstoke, 1990,203.

Reddy N.P. & Kesavan S.K., A technique for determination of stress fields in the contact loading of highly deformable polymeric materials, *Polymer Engineering and Science*, vol. 27, no. 13, 979, 1987.

Reswick J.B. & Rogers J., Experience at Rancho los Amigos Hospital with devices and techniques to prevent pressure sores in *Bed Sore Biomechanics,* Proc. of a Seminar on Tissue Viability and Clinical Applications, Kenedi R.M., Cowden J.M. & Scales J.T., Eds., Macmillan Press, London, 1976, 301.

Reynolds D., Shape Design and Interface Load Analysis for Below-Knee Prosthetic Sockets, Ph.D. thesis, University of London, 1988.

Rivlin R.S., Forty years of non-linear continuum mechanics, in *Advances in Rheology, vol. 1 (Theory)*, Proc. 9th International Congress on Rheology, Mena B., Garcia-Rejon A., & Rangel-Nataile C., Eds., October 8-13, 1984, Universidad Nacional Autonoma de Mexico, Ciudad Universitaria 04510, Acapulco, Mexico, 1.

Sahay K.B., Mehrotra R., Sachdeva U. & Banerji A.K., Elastomechanical characterization of brain tissues, *J. Biomechanics., vol.* 25, no. 3, 319, 1992.

Seiler W.O., Allen S. & Stahelin H.B., Influence of the 30^0 laterally inclined position and the 'Super-Soft' 3-piece mattress on skin oxygen tension on areas of maximum pressure - implications for pressure sore prevention, *Gerontol.*, *vol.* 32,158, 1986.

Seiler W.O. & Stahelin H.B., Skin oxygen tension as a function of imposed skin pressure: implication for decubitus ulcer formation, *J. Am. Geriatrics Soc., vol.* 27, no. 7, 289, 1979.

Seiler W.O. & Stahelin H.B., Decubitus ulcer prevention: a new method using transcutaneous oxygen tension measurement, *J. Am. Geriatrics Soc., vol.* 31, no. 12, 786, 1983.

Seiler W.O. & Stahelin H.B., Recent findings on decubitus ulcer pathology: Implications for care, *Geriatrics*, *vol.* 41, no. 1, 47, 1986.

Seymour R.J. & Warren E.L., Wheelchair cushion effect on pressure and skin temperature, *Arch Phys Med. Rehabilitation*, vol. 66, 229, 1985.

Shaw B.H. & Snowdon C., The Mechanics of Mattresses, Annual Report of Department of Health & Social Security Biomechanical Research and Development Unit, Roehampton, London,1979, 123.

Shoemaker P.A., Schneider D., Lee M.C. & Fung Y.C., A constitutive model for two-dimensional soft tissues and its application to experimental data, *J. Biomechanics*, vol. 19, no. 9, 695, 1986.

Silverman M., Commercial options for positioning the client with muscular dystrophy, *Clinical Prosthetics and Orthotics*, vol. 10, no. 4, 159, 1986.

Spilker R.L., Donzelli P.S. & Mow V.C., A transversely isotropic biphasic finite element model of the meniscus, *J. Biomechanics*. vol. 25, no. 9., 1027, 1992.

Sprigle S.H., Chung K.C., & Faisant T., Clinical Evaluation of Custom Contoured Cushions on Spinal Cord Injured Subjects, Proc. of the International Conference of the Association for the Advancement of Rehabilitation Technology - ICAART 88, Montreal, Canada, 1988, 264.

Sprigle S.H., Chung K.C. & Brubaker C.E., Factors affecting seat contour characteristics, *Journal of Rehabilitation Research and Development*. vol. 27, no. 2, 127, 1990 - **A**.

Sprigle S.H., Chung K.C. & Brubaker C.E., Reduction in sitting pressure with custom contoured cushions, *J. Rehabilitation Research & Development*. vol. 27, no. 2, 135, 1990 - **B**.

Sprigle S.H. & Chung, K.C., Development and Analysis of Custom Contoured Wheelchair Cushions, report UVA-REC 101-89, Rehabilitation Engineering Centre, University of Virginia,1989.

Sprigle S.H. & Schuch J.Z., Using seat contour measurements during seating evaluations of individuals with S.C.I., Assist. Technology, vol. 5, no. 1, 24, 1993.

Statutory Instruments, No.1324, Consumer Protection, The furniture & furnishings (fire) (safety) regulations, 1988.

Supplement to Structural Nonlinearities Seminar Notes , Reference Manual (DN_S201) , Ansys® Revision 4.3, Swanson Analysis Systems, Inc., Houston, USA. 1990.

Theoretical Reference Manual, Ansys® Revision 4.3, Swanson Analysis Systems Inc., USA, 1990.

Thiyagarajan C. & Silver J.R., Aetiology of pressure sores in patients with spinal cord injury, *B.M.J.*, vol. 289, 1487, 1984.

Todd B.A., Chung K.C. & Thacker J.C., Material Properties of Soft Tissue in Compression, Proc. RESNA 12th Annual Conference, New Orleans, Louisiana, 1989, 73.

Todd B.A., Thacker J.C. & Chung K.C. , Finite Element Model of the Human Buttocks, Proc. RESNA 13th Annual Conference, Washington, DC, 1990, 417.

Tong P. & Fung Y.C., The stress-strain relationship for the skin, *J. Biomechanics*, vol. 9, 649, 1976.

Tregear R.T., *Physical Functions of the Skin*, Academic Press, London & New York, 1966,73.

Treloar L.R.G., *The Physics of Rubber Elasticity*, Claredon Press, Oxford, 1975.

Turner-Smith A.R., Harris J.D., Houghton G.R., & Jefferson J.R., A television/computer three-dimensional surface shape measurement system, *J. Biomechanics*. Vol.21, no. 6., 497, 1988.

Turner-Smith A.R., A method of analysis of back shape in scoliosis, *J. Biomechanics*. Vol.21, no. 6., 515, 1988.

User Reference Manual, Ansys® Revision 4.4, Swanson Analysis Systems, Inc., USA, 1990.

Veronda D.R. & Westmann R.A., Mechanical characterization of skin - finite deformations. *J. Biomechanics*. vol. 3.,111, 1970.

Welter R.J. & Zysman S., Three Dimensional Machining of Custom Contoured Polyethylene Foam Cushions, Proc. RESNA 10th Annual Conference, San Jose, California, 1987, 576.

Wood P. & Badley E., The epidemiology of disablement, in *Rehabilitation of the Physically Disabled Adult*, Goodwill C.J. & Chamberlain M.A., Eds., Croom Helm Ltd, London, 1988, 6.

Yamada H., *Strength of Bioiogical Materials*, Evans F.G., Ed., Williams & Wilkins Company, Baltimore, USA, 1973, 19.

Ziegert J.C. & Lewis J.L., In-vivo mechanical properties of soft tissue covering bony prominences, *Trans. ASME J. of Biomechanical Engineering*, vol. 100, 194, 1978.

Zienkiewicz O.C. & Taylor R.L., *The Finite Element Method*, 4th Edition, McGraw-Hill Book Company, London, 1989.

LIST OF APPENDICES

Page No.

APPENDIX 1 DEVELOPMENT & TESTING OF A CAD/CAM SEATING SYSTEM

SECTION A Development of System

In this Appendix, the development of a computerised system to produce individually-shaped supports for the body is described. The performance criteria are :

The system should be operable by a therapist and technician.

The measurement equipment should be portable, so that the procedure can be performed in a hospital ward or a client's home.

The design and manufacturing process should be of less than 2 hours duration, so that low cost support systems can readily be available to the client.

For a relatively soft cushioning material the manufactured surface should be accurate to within 4 mm of the required surface at all points, since localised errors of this height are unlikely to affect the overall support characteristics. For a relatively rigid supporting surface, greater accuracy may be necessary.

The procedure should be applicable to the production of individually-shaped back supports as well as seat cushions.

An on-site facility to produce body-shaped supports such as wheelchair seating and cushioning was required to provide a service for clients from the Royal National Orthopaedic Hospital. The client group was mainly orthopaedic patients who required cushioned supporting surfaces in order to reduce discomfort and control posture.

Shape Measurement.

A method of seat production was developed through an evaluation of the previous methods, creation of possible procedures and testing of concepts and mock-ups. Some of the tests which were important in the development are described in the following sections together with the procedures which would be normally used for providing a service to clients. Shape measurement was performed by the vacuum consolidation procedure whose principles have been described by Nelham (1975). This allowed the body to maintain the sitting position during measurement and allowed immediate shape modifications to be made. The measuring bag consisted of polystyrene beads, surrounded by a 30 micron thick layer of extensible polyurethane sheet (Platilon, Plate Bonn G.m.b.H., Bonn, Germany).

The effects of various external factors on the interface pressure distribution were explored with measurements on two able bodied individuals. Pressure distribution measurements were made with shaped surfaces under the bags and also after the shape of the bag surface had been modified post-consolidation. The effects on pressure distribution of horizontal and sloped rigid, planar seat surfaces and surfaces which were slightly concave under the ischium were examined. It was found that the interface pressure distributions were highly dependent on the surface under the bag, the number and initial distribution of the beads inside the bag and the posture of the subject. Ten pressure maps were measured with one able-bodied subject repeatedly sitting on the bag, with a flat surface under it. The bag extended at least 70 mm beyond the body contact area both laterally and posteriorly and about half the volume of the bag was filled with beads. The subject sat in a predetermined repeatable sitting position (see Chapter 2). Interface pressure measurements were taken after the subject had been seated for four minutes and the bag had been consolidated. No shape rectifications were attempted prior to the measurement.

The Texas Interface Pressure Evaluator was used during the initial testing and for subsequent clinical work to monitor the whole of the body-seat interface without the subject having to be repositioned between pressure measurements. The Evaluator consists of a pad containing a twelve by twelve array of interconnected cells at 29 mm intervals. A printed circuit on the inside of the pad gave contact switches in each cell. The cells measured the average pressure over an area of 22 mm in diameter. Because of the extent of the device major alterations to the load distribution across the interface could be expected, so inevitably the device could only be used to estimate and compare interface pressures. Maximum errors of less than 5 percent and a resolution of ± 2 mmHg (0.3 kPa) have been reported for this device (Garber et al, 1978).

The pressure maps for repeated sitting are shown in Figure 1A. The distributions were similar but not identical. The maxima were located under, or slightly proximal to, the ischial tuberosities and ranged from 69 mmHg to 81 mmHg (9.2 to 10.8 kPa). The approximate area of the interface between the body and the bag ranged from 94 to 106 cm^2. The correlation between pressure readings in the same columns and rows was calculated to quantify the reproducibility of the readings over repeated sittings. The pressure maps were assumed to be optimally aligned. A fifth-order polynomial was fitted to the data, using commercial software and the coefficient of correlation for each row and column was calculated to quantify the reproducibility of the readings over repeated sittings. The method did not simultaneously take account of the pressure readings from the surrounding transducers which were not in the column or row under consideration. The calculated correlation factors were generally greater than 0·8 for the columns and greater than 0·5 for the rows (see Section B), where a correlation factor of 0 is for random distributions and 1 is for identical ones. The difference between the distributions can be partly accounted for by a large transducer spacing resulting in peak pressures being unrecorded in the regions between the transducers. In addition it is likely that small variations in the posture of the subject, and in the distribution of beads in the bag prior to and during consolidation also had an effect on the load distribution across the interface (and also the interface shape).

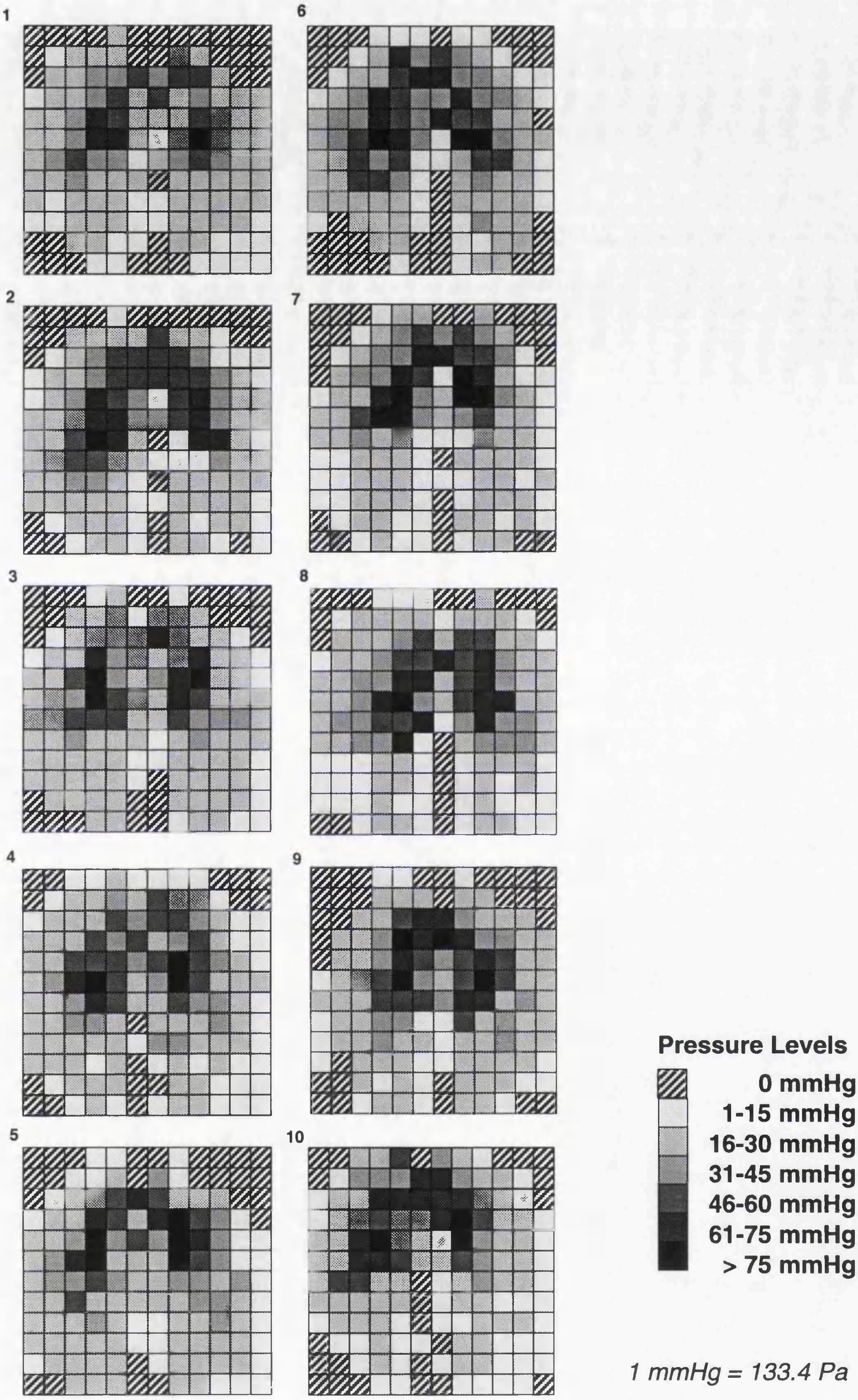

FIGURE 1A
Pressure distributions during repeated sittings on bead-filled bag (same subject, same posture, same seat, same bag)

When the surface was moved outward radially locally under the ischial tuberosities and sacrum the local pressure decreased and when it was moved inward under the gluteal muscles and the proximal thighs, it increased. A concave surface to the rigid seat under the bag increased the loading on the lateral parts of the interface and decreased the high loading under the ischia and along the central axis of the area of contact. The pressures were particularly sensitive to surface modification over the bony prominences.

A procedure for clinical shape measurement was established from the exploratory activities which are described above. The measurements were usually performed on the chair in which the client intended to use the cushion. The bag was roughly shaped prior to the subject sitting. The interface pressure mat was then positioned on the bag surface. After the air had been partly sucked out of the bag, the client was removed and the bag surface was rectified by manipulation or by inserting wedge-shaped blocks under the bag. The client was re-seated and the pressure distribution remeasured. It usually took several alterations before a shape was produced which was acceptable to the client and other individuals involved in his or her care on the basis of subjective comfort, pressure distribution and the client's position and ability to move about in the shape.

Once the client had been removed, the bag orientation and the shape of the surface in contact with the body, were measured with the 3 dimensional position measuring device (Polhemus Navigation Systems, 3 Space ISOtrak®). The device is described in Section 2.2 of Chapter 2. During measurment of the bag surface shape, a grid of light from a photographic enlarger was projected onto the bag, as an aid to digitisation.

Data Processing and Manufacture

A smooth bivariate interpolated grid was calculated from the cushion surface position data. A routine called Surf from the IMSL library was used. The Fortran subroutines in this commercially available library, can be incorporated into a user-written software.

Investigations were initially made to see whether Surf could generate the required contours and to determine the effects of the interval between measurement points on the accuracy of the generated surface. A curved 3 dimensional 'test surface' was generated, based on an extremely curved seat profile (see Figure 1b). The height of the surface z varied along the x-axis but was independent of y. The variation in z with x could be fully described by a fifth-order polynomial equation. Thus all the points on the surface were known. Sets of points were calculated along the surface at 5, 10, 15, 20, 25, 30, 35, 40 & 45 mm intervals along x and at y=0 and y=15 mm. These data sets were assumed to have been measured. The routine Surf was used to generate points at 15 mm intervals along the x-axis and at y=0 and y=15 mm from each of the data sets. The generated points were compared with the 'measured' surface (see Figure 1b). When the 'measurement' interval was less than 15 mm, the generated points lay on the original surface. When the interval between measurement points was 25 mm, the accuracy over the whole of the

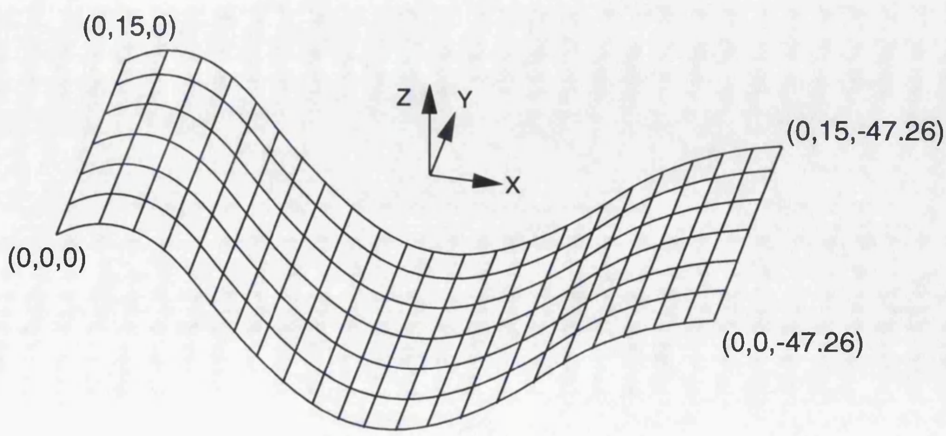

Original surface described by equation :

$$z = 2.4733e\text{-}4 + 0.61525x - 4.4441e\text{-}2x^2 + 5.0051e\text{-}4x^3 - 2.1089e\text{-}6x^4 + 3.0641e\text{-}9x^5$$

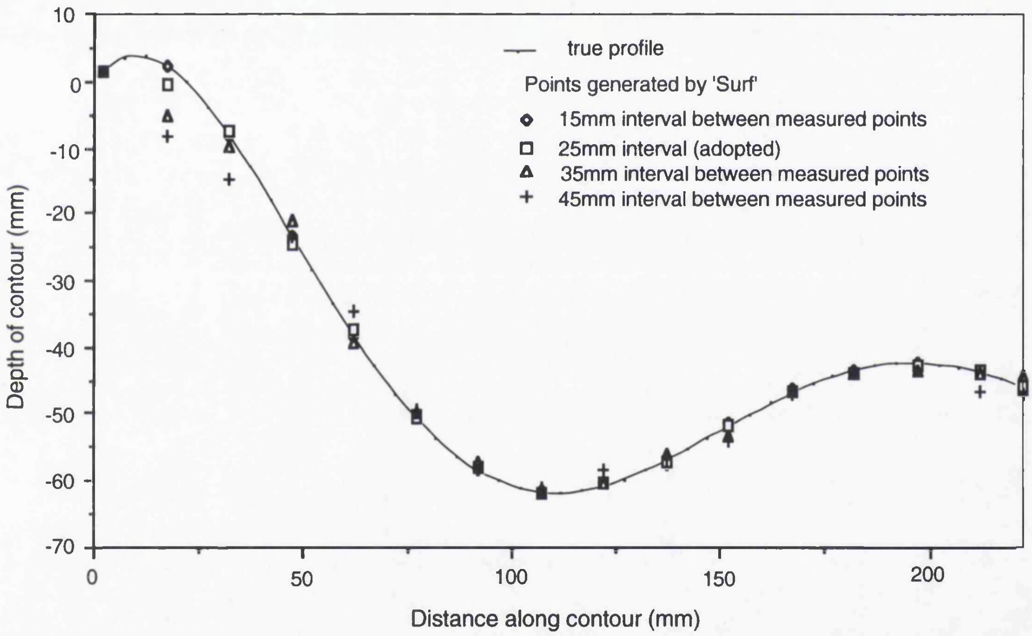

Smoothed profiles generated by 'Surf' from the true profile, for various intervals between 'measured' points

FIGURE 1B

Testing of smoothing algorithm : Surfaces generated by 'Surf' smoothing subroutine from a representative 'measured' surface

surface remained better than 2 mm. This was considered to be a sufficiently accurate degree of precision and a 25 mm interval was therefore used between measurement points during subsequent surface production.

The measured data points were transferred to a MicroVAX II computer. A program was written which incorporated Surf to create the machining grid. When the program is run the user is prompted for the dimensions of the required cushion and the height of keypoints on the lateral and back edges of the cushion relative to the measured surface.

Another Fortran program was written by the author to create the machining program from the machining grid. The machining program contained the toolpath, spindle speed and feed rate commands. The commands were written in a language which was specially developed by the company who made the CNC machine (Heidenhain programming language). The tool path algorithm moved the tool along one row and then back along the adjacent row, following a linear path between machining points. The machining program was exported from the MicroVAX computer to the local memory of a 3-axis milling machine with a computer numerical controller via an RS232 interface.

Blocks of high resilience polyurethane foam were set on the machining table by lateral compressions of 8 mm. The post release increases in the size of the final surface were compensated for by a corresponding reduction in the interval between machining points in the grid generated by the smoothing routine. The change in height of the cushion post release was neglected because of the low Poisson's ratio of polyurethane foams. It was found that a spindle speed of over 3,000 r.p.m. was required to cut the foam adequately. Lower speeds caused the softer and reconstituted foams to rip or pull away from the tool during cutting. A feed rate of 14.5 mm/second was found to be the maximum which could safely be used.

The data for the pressure readings is presented in Section B. The selection of machining grid, tool path and tool path radius was based on the production analysis described in Section C. The initial testing of the system is described in Section D of this appendix.

SECTION 1B
Pressure Readings in the Same Columns and Rows
(measured with the same subject, same posture, same seat, same bag)

Intra Column Correlations

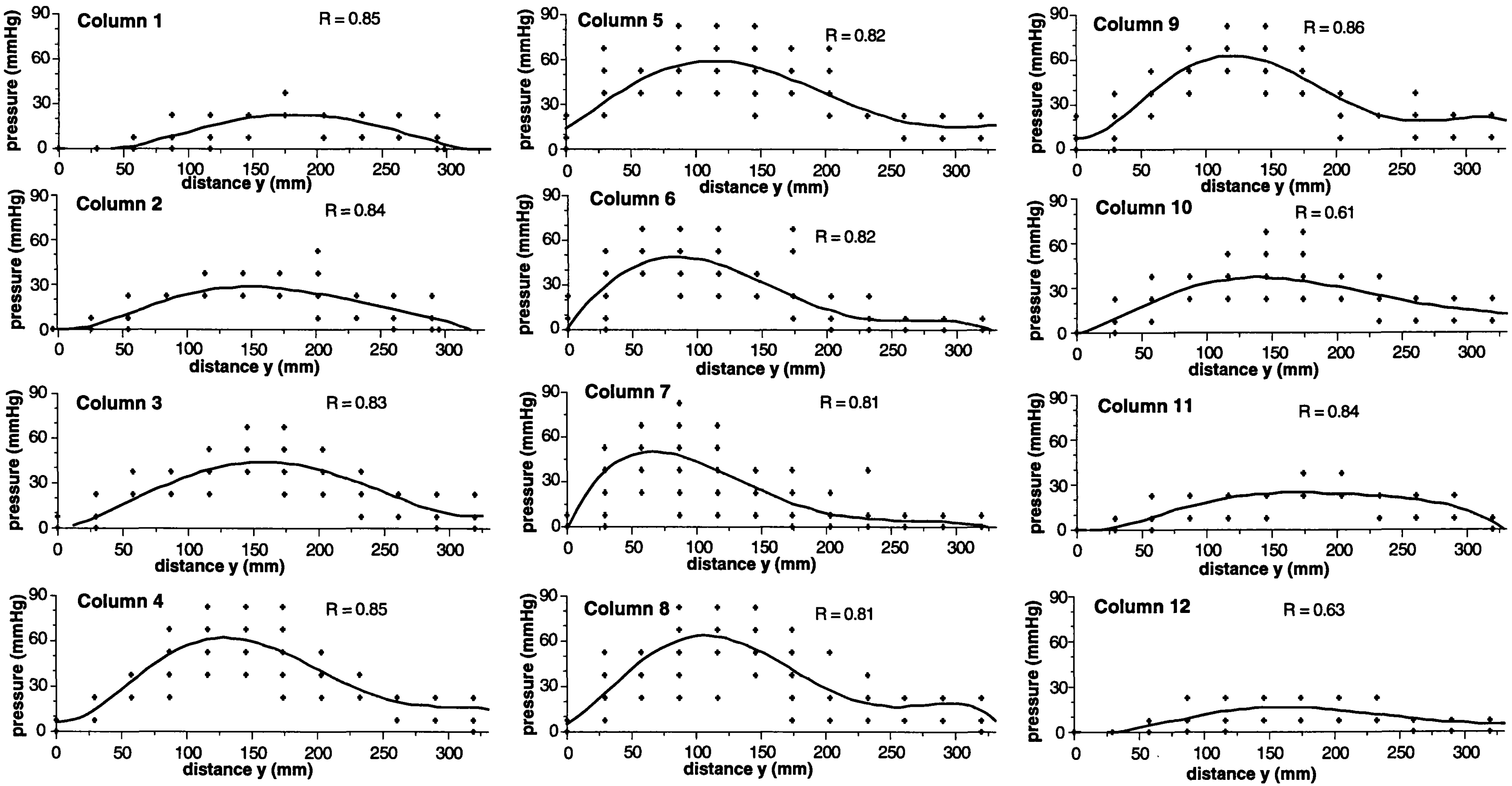

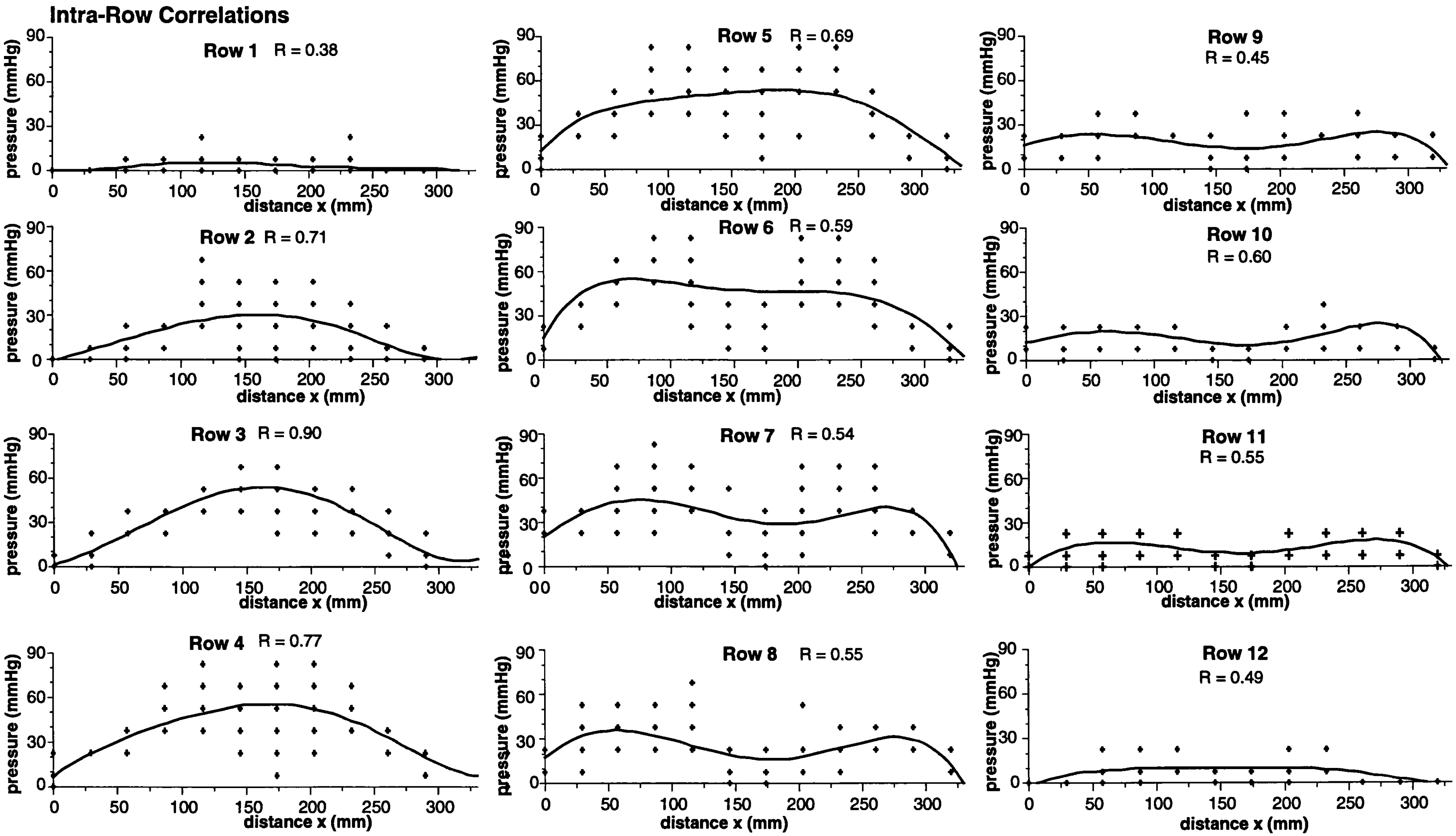
Intra-Row Correlations
Row 1 R = 0.38
Row 2 R = 0.71
Row 3 R = 0.90
Row 4 R = 0.77
Row 5 R = 0.69
Row 6 R = 0.59
Row 7 R = 0.54
Row 8 R = 0.55
Row 9 R = 0.45
Row 10 R = 0.60
Row 11 R = 0.55
Row 12 R = 0.49
pressure (mmHg)
distance x (mm)
0
30
60
90
0
50
100
150
200
250
300

SECTION C - Production Analysis

The toolpath algorithm, point spacing and tool radius were selected from considerations of the sources of error in the final surface. The toolpath was selected so the tool passed along a row between adjacent maching points and returned in the opposite direction along the next row.

Relationship between toolpath and machining errors

The theoretical error from cutting a machining point with the tip of the tool, when the surface is at a slope from horizontal can be calculated. This is estimated below for a planar surface at orientation ø when point P is cut by a tool of radius r.

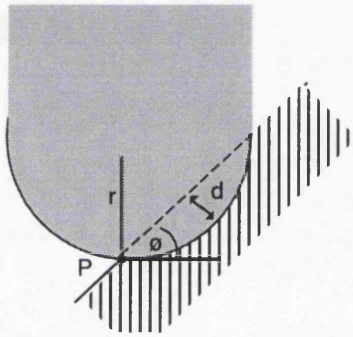

d= maximum error from surface orientation; r = tool radius; ø = local surface slope

The theoretical error is as follows :

$$d_{\text{ø}} = r\,(1-\cos\text{ø}) \qquad \ldots\ldots\ldots\ldots\ldots\ldots\ldots \quad \mathbf{1.1}$$

The local slope of the surface was not expected to be greater than 35^{o}. If the greatest tool radius was limited to 20 mm , the maximum error caused at this slope was 3·6 mm. This error was below that in the original specification, for a soft supporting material. Also the tissue under the bony prominences is likely to be supported at the bottom of troughs where the slope of the supporting surface is low. For these reasons a more complex tool path algorithm was not used.

Relationship between in-row point spacing and machining errors

An expression for the error from a linear interpolation between machining points in a row can be formed in terms of the local surface radius and the in-row point spacing.

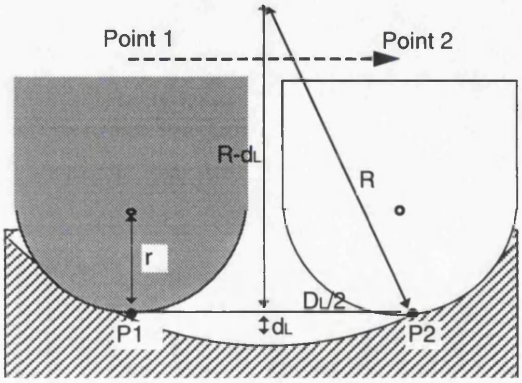

Where
P1, P2 are machining points;
d_L =maximum error;
r=radius of tool;
R=local radius of surface;
D_L=distance between adjacent points

$$D_L^2 - 8\,Rd_L + 4d_L^2 = 0$$

$$D_L = 2\,d_L^{0.5}(2R\text{-}d_L)^{0.5} \qquad \text{...1.2}$$

The largest acceptable point spacing along a row was estimated from equation 1·2. By deciding d_L=1 mm and assuming R=60 mm, the value for the spacing of points along a row was calculated to be 22 mm. This along-row point spacing was used for production.

Relationship between inter-row point spacing and machining errors

An expression for the error from the finite spacing between rows can be derived in terms of the spacing between rows and tool radius.

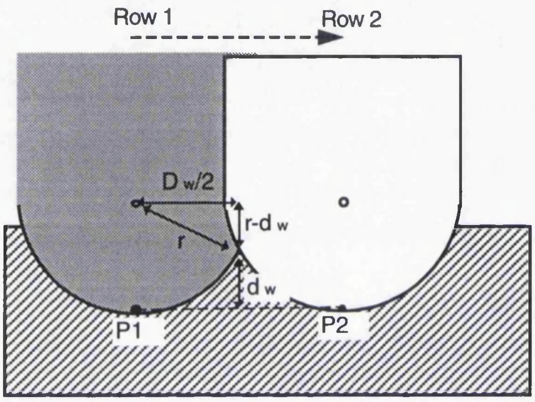

Assuming $D_W \leq 2r$

$$4d_W^2 - 8r\,d_W + D_W^2 = 0$$

$$D_W = 2\,d_W^{0.5}(2r\text{-}d_W)^{0.5} \qquad \text{..1.3}$$

The largest acceptable distance apart of the rows was estimated from equation 1·3. By deciding d_W was 2 mm and assuming r =15 mm, the value for the spacing of points along a row was calculated to be 15 mm. This between-row point spacing was used for production.

Relationship between Cutting Time and Machining Errors

A balance between machining time and the accuracy of the finished surface had to be found. An approximate parametric expression was derived from basic principles which related the time to cut a surface to the tool radius, surface machining errors, the smallest local surface radius, the feed rate, the dimensions of the surface and the average time for the tool to cut each point.

From observations of machining it was apparent that the table slowed down and speeded up again when each machining point was cut. The time to cut each point was estimated from measurements of the time to cut a row of points and a knowledge of the table feed rate.

Assuming

Time for the tool to change direction at the end of each row is negligible.

The tool travels between points at a constant velocity.

It takes a uniform time to cut each point c

where

Minimum local radius of surface (mm)	$=R$
Tool radius (mm)	$=r$
Time to cut surface (sec)	$=T$
Feedrate (mm/sec)	$=f$
Length of surface (mm)	$=L$
Width of surface (mm)	$=W$
Height of ridge between rows (mm)	$=dw$
Error from linear interpolation along a row (mm)	$=d_L$
Tool time to slow down and speed up at each machining point (sec)	$=c$
Number of rows of machining points	$=N_W$
Number of points in each row	$=N_L$
Distance between points	$=D_L$
Distance between rows	$=D_W$

$$T = c\ N_W\ N_L + \frac{LN_W}{f} \qquad \text{.......... 1.4}$$

$$N_L\text{-}1 = \frac{L}{D_L} \quad \text{and} \quad N_W\text{-}1 = \frac{W}{D_W} \qquad \text{.......... 1.5a ,1.5b}$$

Substituting 1.5a and 1.5b into 1.4 the following expression is formed.

$$T=\left(c\left(\frac{W}{D_W}+1\right)\left(\frac{L}{D_L}+1\right)\right)+\left(\frac{L}{f}\left(\frac{W}{D_W}+1\right)\right)$$

This can be simplified

$$T=\left(\frac{W}{D_W}+1\right)\left(\frac{cL}{D_L}+c+\frac{L}{f}\right) \qquad \text{.......... 1.6}$$

By substituting 1.2 and 1.3 into 1.6, the following expression can be derived :

$$T=\left(\frac{W}{2d_W^{0.5}(2r-d_W)^{0.5}}+1\right)\left(\frac{cL}{2d_L^{0.5}(2R-d_L)^{0.5}}+c+\frac{L}{f}\right) \qquad \text{.......... 1.7}$$

Figure 1C shows the relationship between the greatest machining error over the surface and the cutting time, when values for the other variables in the equation are assumed. The relationship suggested that the cutting times and surface tolerances in the original performance specification (see Section A) could be simultaneously achieved.

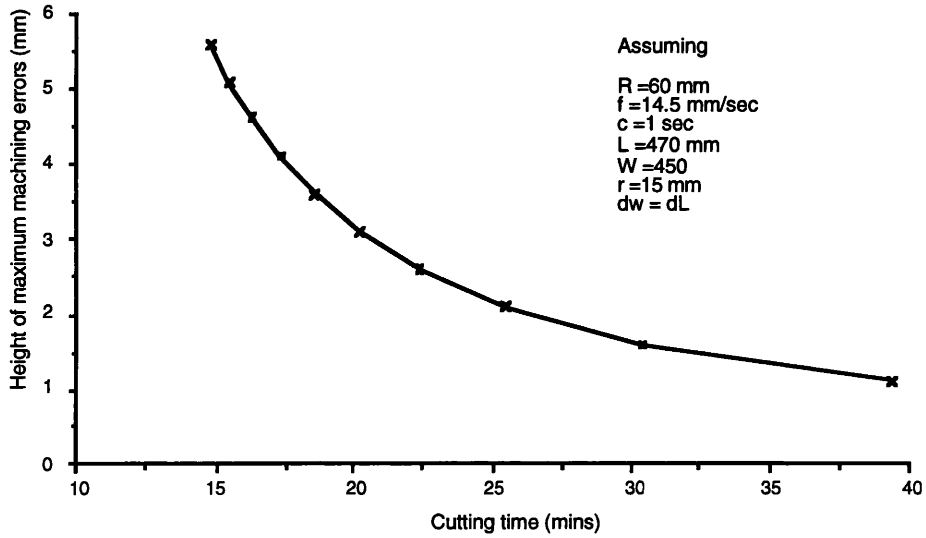

FIGURE 1C

Relationship between surface tolerance and cutting time

Equation 1.7 was also used to estimate the minimum tool radius which would give a machining time of less than 25 minutes. Assuming R=60 mm ; T=1500 sec ; f=14.5 mm/sec ; c=1 sec. ; L=470 mm; W=450 mm ; d=4 mm , the tool radius was found to be 14.7 mm. In fact a tool which produced an acceptable cut was selected from availability (Otto Bock, plastic machining rasp). With a hemispherical tip and a spike length of 0.3 mm the effective radius of the tool was 15 mm.

SECTION D Discussion and Initial Testing of the System

A small-scale pilot trial of individually body-shaped wheelchair cushioning was performed. The range of seating needs which exist within the disabled population and the existence of factors such as motivation and environment make the assessment of comfort on seating and cushioning systems a difficult task. Nonetheless a trial was considered essential at this stage, to establish whether the continued development of the designs and production system was required. The main aim of the trial was to see whether individually body-contoured wheelchair seat cushions were more comfortable than flat ones of equivalent design during long term sitting. The trial also gave the opportunity to test out the production system on potential users. The trial is reported in detail in the publication which is reproduced in the following pages (Michael & Walker, 1990).

Clinical Rehabilitation 1990; **4**: 229–234

Equipment assessment

Clinical trial of body-contoured wheelchair cushioning

SM Michael and **PS Walker** Department of Biomedical Engineering, Institute of Orthopaedics, University College, London

The preliminary trial of a body-contoured wheelchair cushioning system is described. Ten wheelchair users were tested on individually contoured and on flat cushions. A subjective assessment method was used to compare the cushions. The contoured cushions produced higher median comfort rating than the flat ones. The differences in comfort were found to be significant at the 10% level both over the buttocks and overall.

Introduction

This study aimed to show whether body-contoured cushions were more comfortable than the equivalent unshaped ones. It was part of a project to develop a system to produce customized, shaped foam wheelchair cushioning, and was intended to give an initial assessment of the cushioning. Custom contoured wheelchair cushions are thought to reduce the loads through the bony prominences and improve sitting posture.[1]

A comfortable seat allows the sitter to perform activities without being distracted by adverse sensations from his/her body parts. These sensations could be due to muscle fatigue, interface temperature and humidity, or excess weightbearing on certain body areas.[2,3] Comfort has been assessed by quantative techniques such as electromyography, body movements and task performance measures. A subjective comfort evaluation method, based on those of Shackel[4] and Harms,[5] was considered most appropriate for this preliminary trial.

Specialist wheelchair seat cushions are available to people who are at risk of pressure sores, or who have a poor posture or discomfort during sitting. These cushions may contain materials such as air, water or gels. A gel is intended to flow away from loadbearing areas and produce even support over the seat interface.

Address for correspondence: Shona Michael, Research Assistant, Department of Biomedical Engineering, Institute of Orthopaedics, Royal National Orthopaedic Hospital, Brockley Hill, Stanmore, Middlesex HA7 4LP, UK.

Some patients find that these cushions are too heavy or that the movement of the gel during sitting leads to sensations of instability. For one cushion, consisting of rows of interconnecting rubber balloons on a flat base, air flows between the sacs to support the patient evenly over the whole seat interface. There may however be a problem with maintaining the correct inflation in the cushion. There are also alternating pressure cushions where the pressure in separate chambers cycles between preset values. These cushions require regular maintenance. Cushions made of polymeric foams tend to be less expensive than other specialist cushions. These have been designed with cut-outs over the areas which are at high risk of pressure sores and wedges at the front to improve the sitting position. The position and size of the cut-out areas may not be ideal for some potential users.

The null hypothesis was that there is no difference between subjective comfort levels on contoured and flat cushions of equivalent size and design.

Method and materials

Individually shaped cushions and equivalent unshaped cushions were produced and compared for ten disabled subjects.

Cushion design

Examples of the flat and shaped cushions are shown in Figures 1a and 1b. They were made of high-resilience fire-retardant foam. The reconstituted foam base (density 96kg/m^3) was chamfered to fit the sling seat of the wheelchair. The contoured upper layer had a density of 75kg/m^3 and an indentation hardness[6] of about 270N. The control cushions were made of the same materials and had the same dimensions and design, apart from a flat surface. The cushions were sized for each subject. Maximum depths ranged from 75 to 125mm.

Production system

The production system for the cushions is still under development and will be fully reported in

Figure 1a Body-contoured cushion: custom-made for subject number seven

Figure 1b Cushion with flat surface: used as a control for subject number seven

a later paper. A brief description is as follows.

The subject sat in the required posture in his/her wheelchair on a bag filled with polystyrene beads. The air was evacuated from the bag so that an impression was formed of the bottom and thighs. A negative plaster cast of the bag surface was taken and used as the basis for the shape of the body-contoured cushion.

A three-dimensional digitiser (Polhemus Navigation Systems, 3 Space ISOTrak®)[7] was used to measure the shape of the surface. Points on the casting surface were measured from a user-defined co-ordinate system. The shape information was processed on a MicroVAX II computer. The data were mathematically smoothed out and then sent to a computer numerically controlled milling machine (Matchmaker Machines Ltd, 700 HG) where the cushion was manufactured.

Subject selection

The following criteria were used to select the subjects. They should:

1) Use a nonspecialist wheelchair with a sling seat and back rest.
2) Normally spend at least eight hours per day in a wheelchair.
3) Have poor control of sitting posture in the pelvic, thigh and trunk areas.
4) Be at risk of pressure sores, scoring less than 14 on the Norton scale.[8]
5) Be at high risk of (or have) skeletal deformities of the hips, pelvis or spine.
6) Be aged between 18 and 60.
7) Understand simple questions about the seating, and recognize and reliably communicate the differences between the cushions.
8) Be under the supervision of healthcare staff at a residential institution.
9) Have sensation over the lower body.
10) Have a medical condition not changing over the period of the trial.

Criteria (one to five) selected a sample which could potentially benefit from use of the cushion. More limiting criteria were not desirable for this initial assessment. The other criteria selected a sample group which could safely perform the trial and give reliable feedback on the cushions (Table 1).

Procedure

The assessment procedure was as follows:

1) Overall comfort ratings and body area comfort ratings were taken at intervals over eight-hour periods. The body areas under investigation were the right and left buttock, right and left thigh, lower back, upper back and neck. Five subjects started the trial on each type of cushion. During testing, the subjects continued with normal activities. The test was stopped if a subject ever felt severely uncomfortable. The shaped and unshaped cushions were tested on consecutive days. Ratings were taken 15 minutes after the test began, after four hours and at the end of the assessment period.
2) At the end of (1), the subjects were asked to use the shaped cushion for seven days. However, if a subject or the trial supervisor was not satisfied with the cushion the trial was terminated and the design was immediately assessed with the cushion features checklist.

A single-blind trial minimized the effects of subject bias. The subjects were told both cushions had been specially made for them and they should compare the two cushions. To balance the effects of the order in which the cushions were assessed, five subjects were selected at random to start on the shaped cushion. The others started on the unshaped one. It was impractical to use a supervisor who was unaware of which cushion was being tested.

The cushions were tested with a cover made of an elasticated polyurethane film (Speciality Polymers and Chemicals Ltd, Platilon®) to prevent soiling. A heavy cover was considered an unnecessary variable for this initial trial.

The long-term sitting test extended over the period the subjects spent each day in a

Table 1 Background details on test subjects

Subject no.	Diagnosis	Weight (kg)	Height (cm)	Age	Sex	Pressure sores	Sitting posture
1	MS	55	160	40	F	N	Pelvis tilted backward. Poor control of thighs, pelvis, trunk.
2	CVA	58	157	50	M	N	Paralysed left side. Sits with legs crossed. Laterally tilted pelvis.
3	MS	67	163	59	F	N	Pelvis tilted backward. Kyphotic spine. Poor control of thighs, pelvis, trunk.
4	MS	73	157	60	F	N	Fixed right hip. Right femur shorter than left.
5	HI	67	175	19	M	N	Contractures of hips. Rotated pelvis, windswept hips.
6	CP	44	147	23	F	N	Laterally tilted pelvis and functional scoliosis.
7	FA	67	163	40	F	N	Poor control of thigh, pelvis and trunk position. Functional scoliosis.
8	BG	27	122	38	F	Y	Pelvis tilted sideways and backwards. Fixed scoliosis and kyphosis.
9	CP	52	163	41	F	N	Functional kyphosis, pelvis tilted backwards. Tends to slide forward in chair.
10	HI	55	180	51	M	Y	Pelvis tilted sideways, backwards and rotated. Fixed scoliosis and kyphosis. Tends to slide forward in chair.

MS = Multiple sclerosis
BG = Deterioration of the basal ganglia
HI = Head injury
FA = Friedreich's ataxia
CVA = Cerebral vascular accident
CP = Cerebral palsy

wheelchair. This timescale was chosen to allow the subjects to experience a range of activities and mental and physical states during the day. A longer timescale was considered unnecessary since the subjects were thought to experience a similar degree of discomfort at the end of each day sitting.

Questionnaire

The questionnaire was filled in by the trial supervisor in collaboration with the test subject. This allowed the supervisor to note down any relevant verbal comments, and observe the subject's position in the wheelchair.

The comfort ratings were intended to identify the body areas, causing comfort or discomfort. The checklist asked about the subject's position in space, posture and stability, and also ease of transfer from the chair. The subjects were asked whether they intended to continue using the contoured cushion and how it compared with their original one.

Statistical approach

The forced response questionnaire produced comfort ratings on an ordinal scale as follows:

Very comfortable	5
Fairly comfortable	4
Indifferent	3
Fairly uncomfortable	2
Very uncomfortable	1

The analysis was made with the Wilcoxon signed rank statistical test. It compared the median comfort ratings on the two cushions, and was suitable for matched pairs of ordinal data.[9]

Results

Body area comfort rating test

One subject insisted on covering both cushions in a pillowcase during the trial. The other subjects completed the trial with the Platilon® cover on their cushions.

For all the subjects the difference in the comfort ratings either stayed the same or became more pronounced as the trial progressed. The median comfort ratings for the two cushions at the end of the trials were calculated (Table 2).

For all the body areas and overall, the median ratings were higher for the body-contoured cushion. In cases where the trial was not completed due to discomfort on the flat cushion, the last matched pair of data was used in the subsequent analysis.

Table 2 Median comfort ratings over body areas and overall

Area	Shaped cushion	Unshaped cushion
Overall	4	2–3
Right buttock	4	2
Left buttock	4	2
Right thigh	4	3
Left thigh	4	3
Lower back	4	3
Upper back	4	3
Neck	4	3–4

Table 3 shows the results of the statistical analysis. The difference in the rating overall and over the buttocks is unlikely to be due to sampling variations. The result suggests that over certain areas the shaped cushioning is significantly more comfortable than the unshaped.

Table 3 Significance of the difference in median comfort ratings

Area	Difference between ratings on shaped and unshaped cushions
Overall	Significant ($p<10\%$)
Right buttock	Significant ($p<10\%$)
Left buttock	Significant ($p<10\%$)
Right thigh	Not significant @ 10% level
Left thigh	Not significant @ 10% level
Lower back	Not significant @ 10% level
Upper back	Not significant @ 10% level
Neck	Not significant @ 10% level

Cushion features checklist

Two subjects filled in the checklist immediately after the comfort rating trials. The others continued with the contoured cushion for a seven-day period before completing the checklist.

Eight subjects preferred the contoured cushion to their original one and continued using it after the trial had ended. They had previously used either gel or foam cushions. None of the subjects felt they were positioned at the wrong height or tilted excessively in the medial or coronal planes. Eight subjects felt fairly or very stable on the contoured cushions. No one found them unstable. One subject had to be lifted slightly higher when she was put into her chair to clear the pommel at the front of the cushion. The other subjects noticed no difference in their transfers.

Discussion

Wheelchair users who had potentially severe seating problems, but who could safely perform the trial and give reliable feedback, were selected for the trial. It is felt that contoured cushioning may be suitable for a wider group of wheelchair users who do not meet these trial criteria.

The cushion features checklist did not find any widespread problems with the use of contoured cushioning. Both the subjects who found the flat cushion more comfortable tended to slide forward in the seat during the day and could not lift themselves back into a more upright position. They slipped out of the shaping and continued sitting in a poor position on the cushion. This suggests that the cushion may be unsuitable for patients who tend to slide out of their seats during the day.

It was felt that the difference between the comfort ratings on the two cushions was very important. In spite of the small sample, the flat cushion was significantly more comfortable ($p<10\%$) over the buttocks and overall. The results of the trial have provided the initiative for further development and evaluation of the system.

Acknowledgements

This work has been financially supported by the Development Trust for the Young Disabled and the Institute of Orthopaedics. The authors wish to thank the Advisory Committee (Dr K Andrews, Dr N Mustapha, Dr L Marks and Mrs P Pope) who guided this work, and also the test subjects from the Royal Hospital and Home, Putney and the John Grooms Home for the Disabled, Edgware.

References

1 Sprigle S, Chung KC, Faisant T. Clinical evaluation and custom contoured cushions on spinal cord injured subjects. In: *Proceedings of the International Conference of the Association for the Advancement of Rehabilitation Technology, ICAART 1988*. Montreal: RESNA Press, 1988: 264–65.

2 Branton P. Behaviour, body mechanics and discomfort. In: Grandjean E ed, *Sitting Posture*. London: Taylor & Francis, 1969: 202–13.

3 Brattgard SO, Carlsoo S, Serverinsoon K. Temperature and humidity in the sitting area. In: RM Kenedi, Cowden JM, Scales JT eds, *Bedsore biomechanics*. London and Basingstoke: Macmillan, 1976: 185–88.

4 Shackel B, Chidsey KD, Shipley P. The assessment of chair comfort. In: Grandjean E ed, *Sitting posture*. London: Taylor & Francis, 1969: 154–92.

5 Harms M. An investigation into the effects of wheelchair seating design on posture, pressure distribution and comfort (Thesis). Loughborough: Loughborough University, 1987: 100–12.

6 British Standards Institution. BS 4443: Part 2: Procedure A. *British standard methods of test for flexible cellular materials*. London: British Standards Institution, 1972.

7 Schrager RJ, Madson MJ, Walker PS. A magneto-mechanical 3-D surface contouring system to be used for generating soft tissue anthropomorphic data. In: *Proceedings of the 10th Annual Conference of the Association for the Advancement of Rehabilitation Technology, RESNA 1987*. Washington: RESNA Press, 1987: 267–68.

8 Norton D, McLaren R, Exton-Smith AN. *An investigation of geriatric nursing problems in hospital*. Edinburgh: Churchill Livingstone, 1975.

9 Siegel S, Castellan NJ. *Nonparametric statistics for the behavioural sciences*, second edition. New York: McGraw-Hill, 1989.

Appendix 2 Calibration of Equipment & Development of Experimental Methodology

Section A - 3Space ISOTrak Calibration

Apparatus - Prismatic Joint Driven by Lead Screw

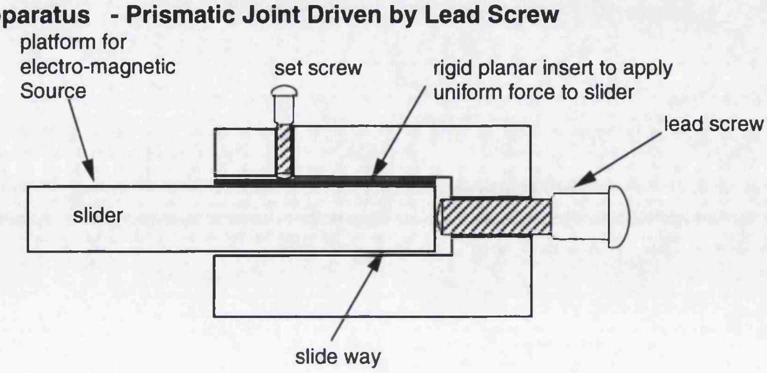

Incremental Displacements along X,Y & Z axes

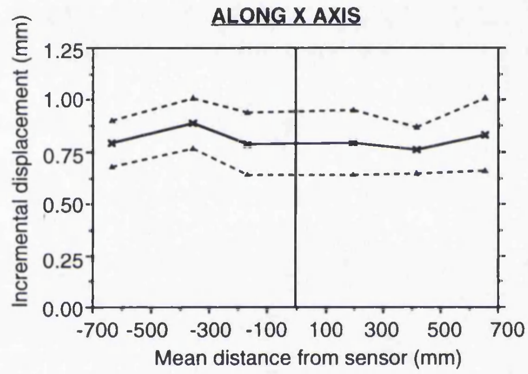

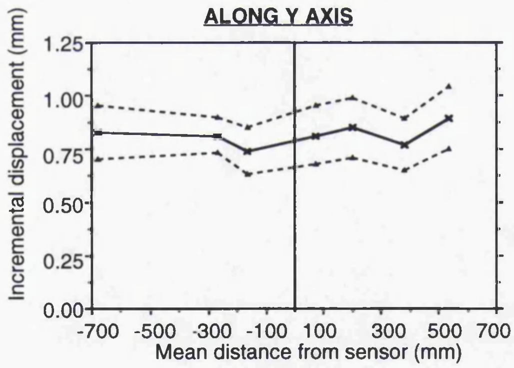

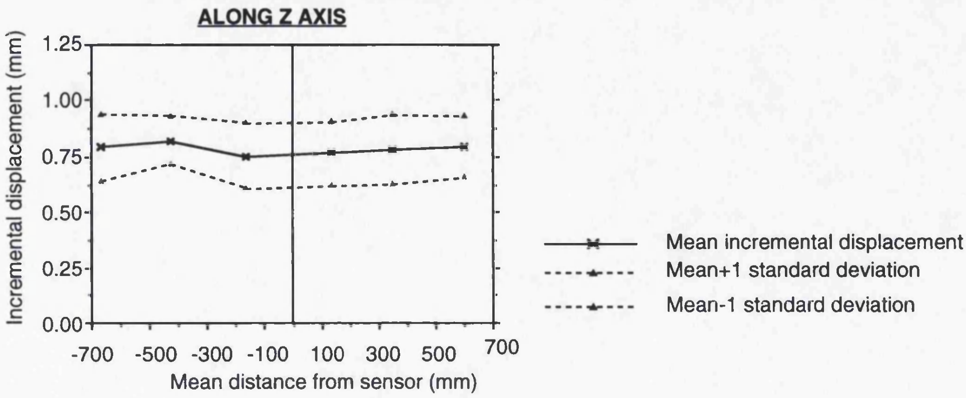

SECTION B - Pressure Transducer Calibration

The pressure measurement system was composed of 12 transducers and a control and display unit. The transducers were calibrated under loading conditions which were similar those at the interface where they were to be used.

A rubber bag, 165 mm in diameter, was inserted between a pair of parallel perspex plates, fixed at a distance apart of 4 mm. Each transducer was placed separately between the centre of the rubber bag and one of the plates. The rubber bag was inflated with air from a compressed air cylinder. The bag was connected via a branch in the tubing to a mercury-filled manometer. The reading on the pressure monitor display unit and the mercury manometer were compared at each level of inflation of the air bag.

The resulting calibration curves and data are shown below.

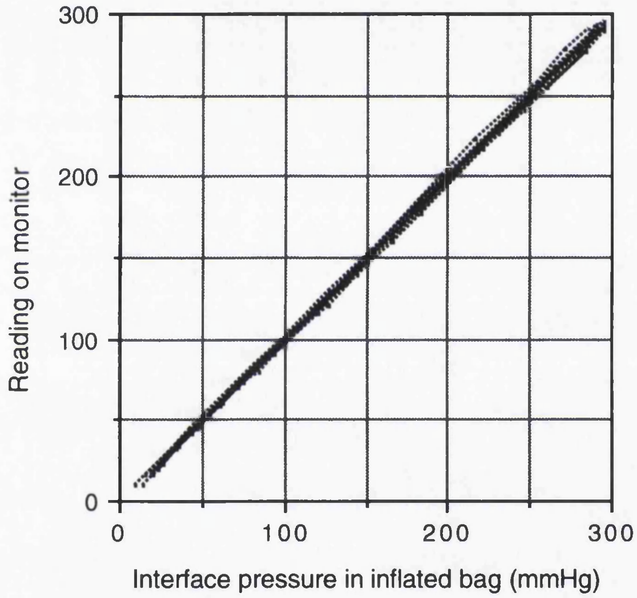

Transducer	1	2	3	4	5	6	8	9	10	11	12
Maximum non linearity (mmHg)	1	0.5	2.5	1.5	4	0.5	1	1	2.5	1.5	3
Maximum In accuracy (mmHg)	2	4	7	3	6	1	2	2	7	5	6

The small differences between the manometer readings and the readings from the monitor could be due to creasing of the transducers or bag or a non-uniform pressure distribution over the rubber bag surface.

SECTION C - Digitised Sections for Graphical Reconstruction of Pelvis

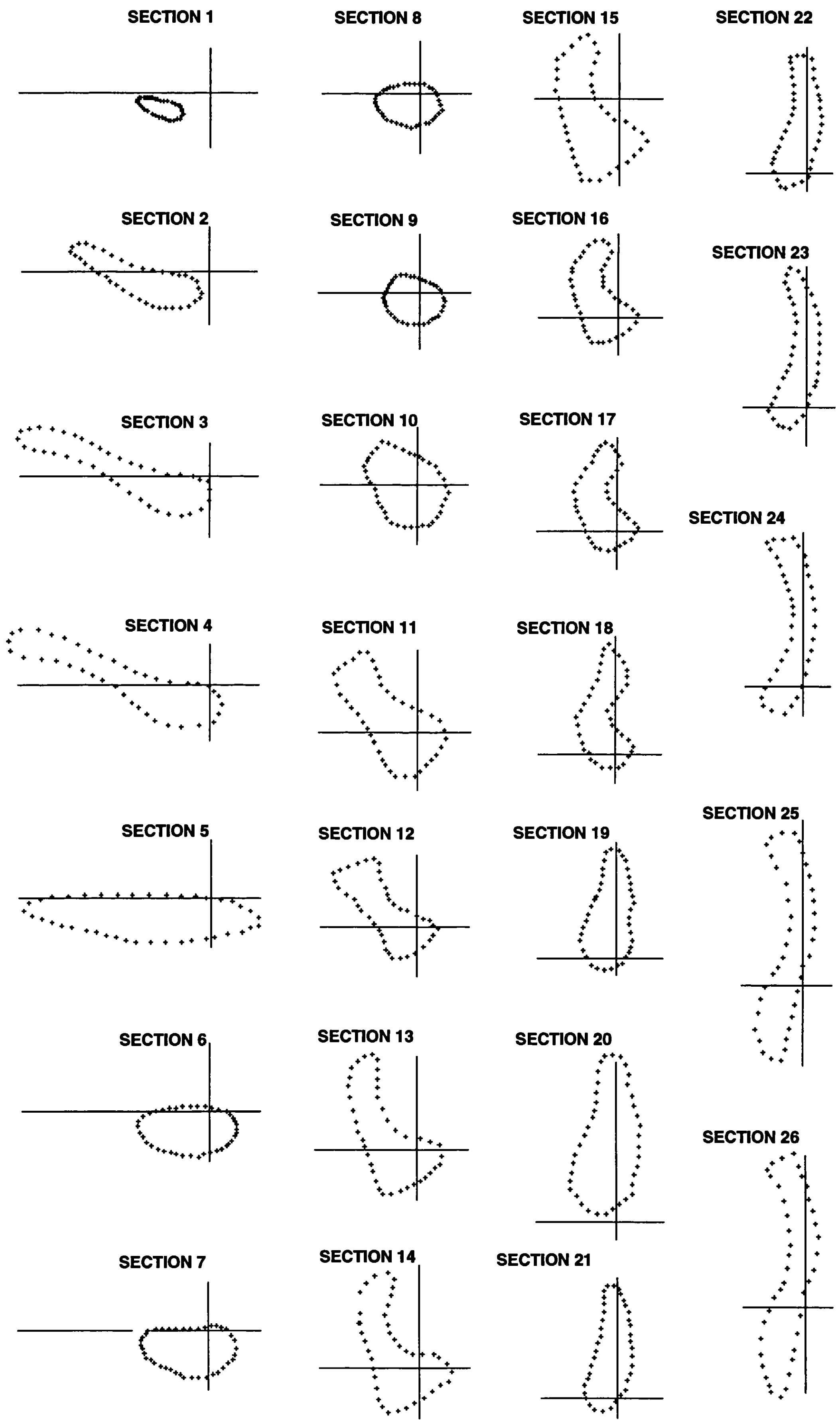

SECTION D - Outline of Contact - Pilot Trial

The pilot study was to establish the method for the main trial. There were practical difficulties with measuring the outline of the body from under a transparent seat. Thus in the pilot trial, another method was devised to measure the outline of a body. A water-filled thin rubber balloon was used to simulate the contact of the body with the seat. The measured outlines from the new method (method 2) were compared with the outlines measured by observations under a glass seat (method 1).

The 15 mm thick glass plate was positioned horizontally, such that it could be viewed from above and below. The new measurement method which was established in the pilot trial and used in the main trial is fully described in Section 3.2. The balloon was carefully laid on the surface, so that it did not roll. The outline of contact was measured with the 3Space ISOtrak on the underside of the glass (method 1). The balloon was carefully removed and the outline measured on the surface of the glass with the 3Space IsotraK (method 2). Ten outlines of contact area were measured by each method.

A notch in the outlines was used to align the outline data from sequential tests by co-ordinate transformation. The spherical co-ordinates of the outlines were then calculated. The variation in the radial dimensions was calculated in all of the thirty-six 10^{o} sectors . The above analysis was repeated for the outlines as measured from below, and the variation in the radial dimensions for the two measurement techniques was compared using the Independent T Test. The Null Hypothesis was that there was no difference between the standard deviation in the radial dimension, for the outlines measured from above and below the glass plate. The transformed outlines are shown in the following figure.

RANGE Ø	Standard deviation in R from method 2 (mm)	Standard deviation in R from method 1 (mm)
Mean value	0.25	0.23
Standard deviation	0.07	0.06
Sample size	36	36

There was no difference between the variation in the radial dimensions for the two measurement methods at the 10% level of significance (t=0.002).

PILOT TRIAL - TRANSFORMED OUTLINES

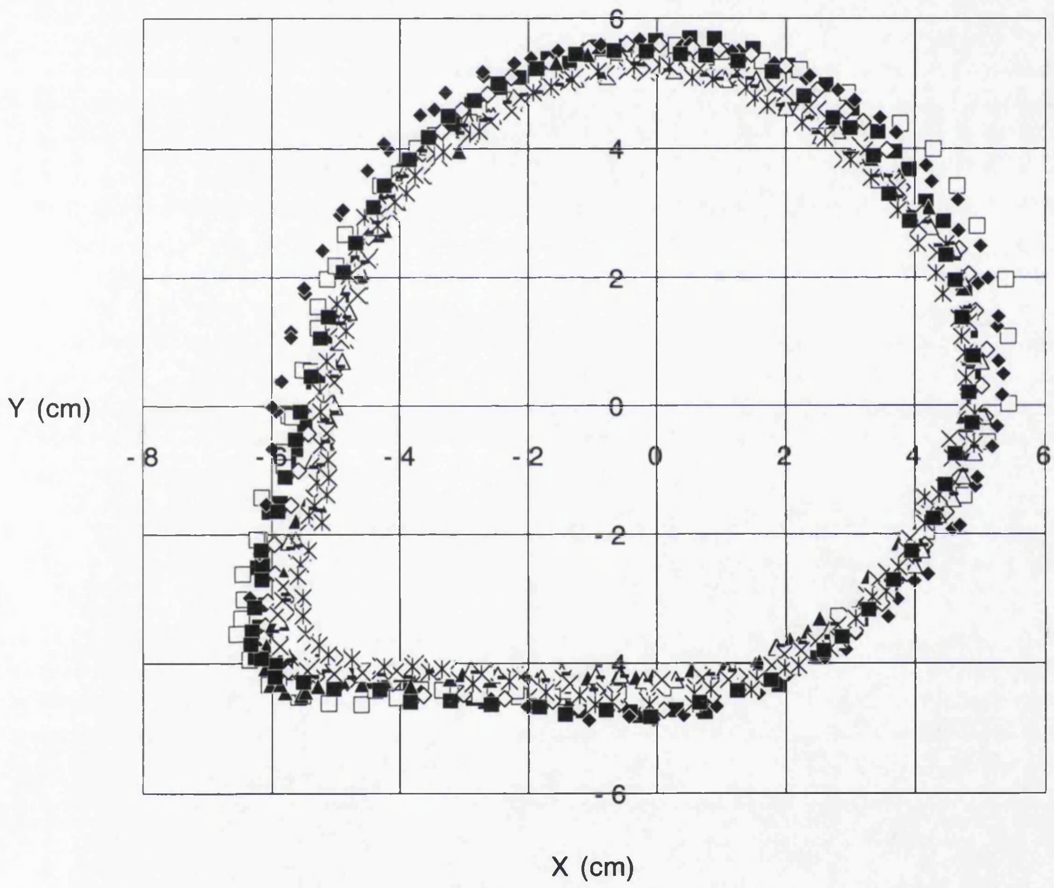

SECTION E
Buttock Tissue Stiffness Testing Device - Calibration

The mass has been plotted which, when applied to loading pan, caused a motion of the loaded seat plate.

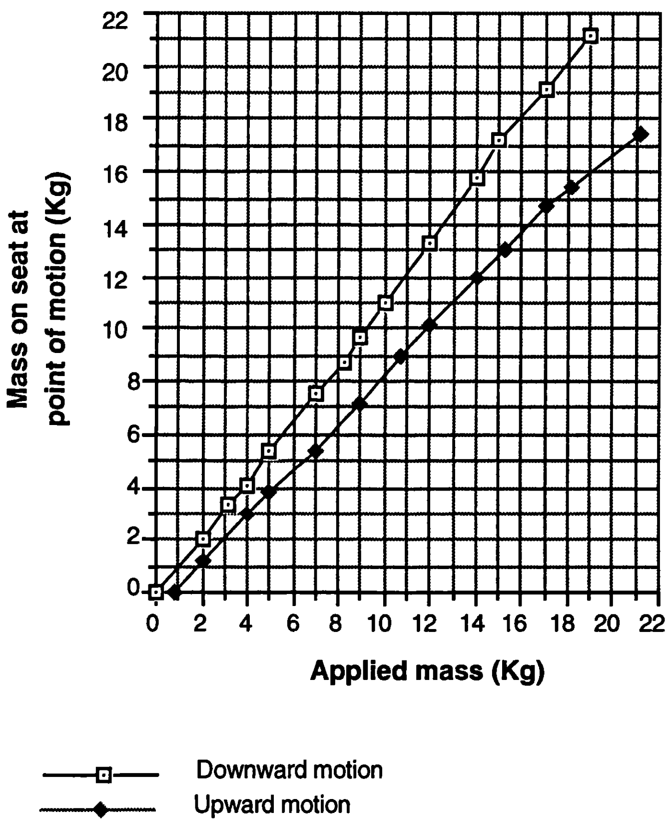

Linear curve fit:

$y = -0.33463 + 1.1402x \quad R^2 = 0.999$

$y = -0.56620 + 0.87878x \quad R^2 = 0.998$

SECTION F

Comparison between Average Casting of Suspended Buttock and Manufactured Seat Shape

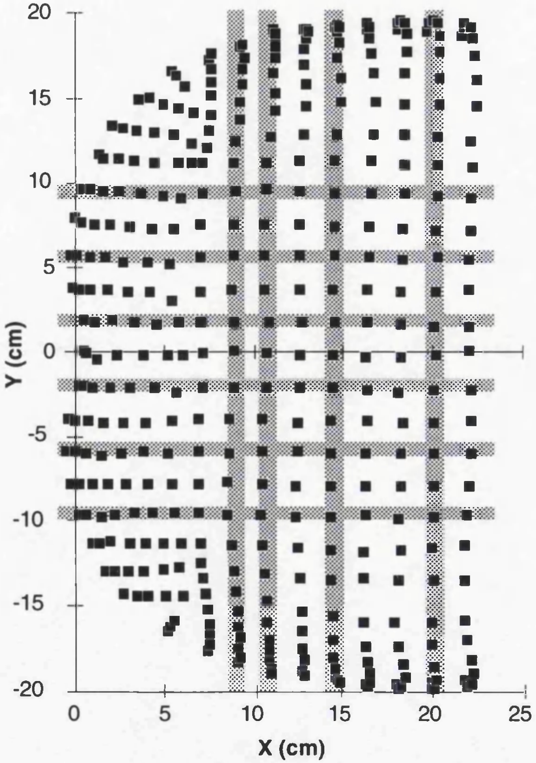

Plan view to show position of horizontal and transverse sections

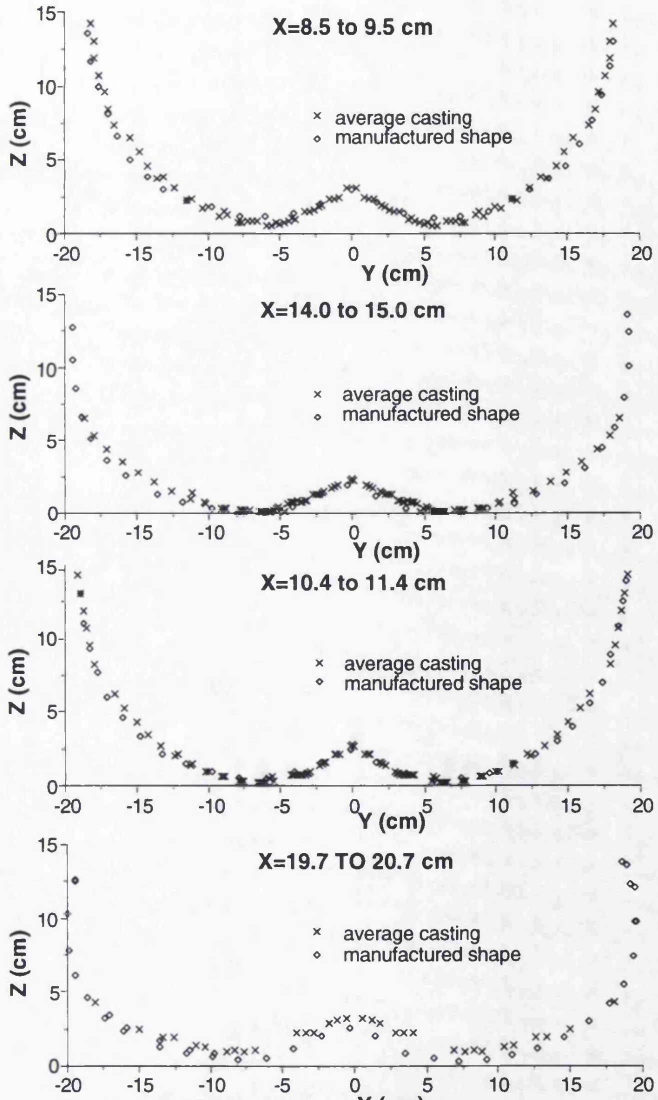

Transverse Sections

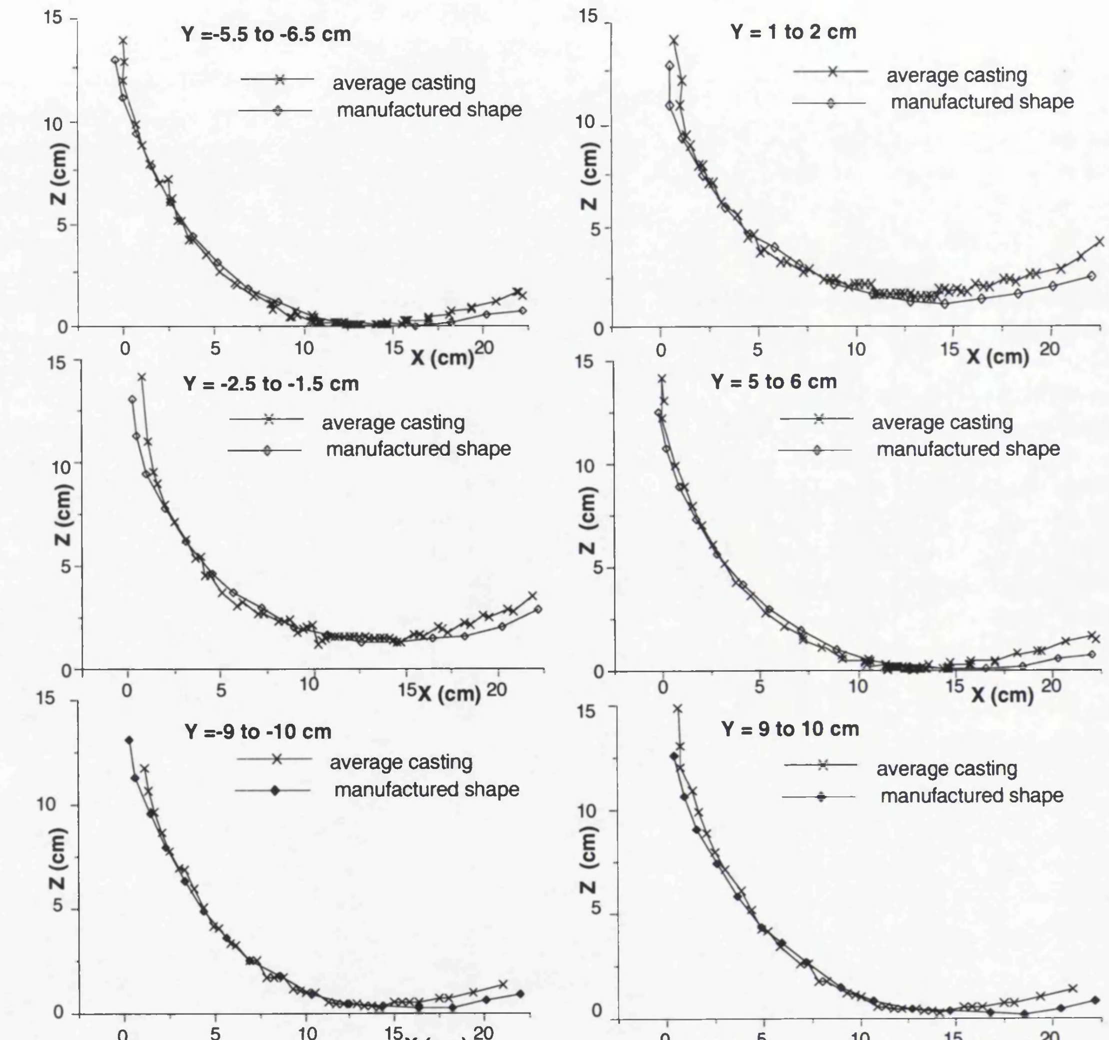

Longitudinal Sections

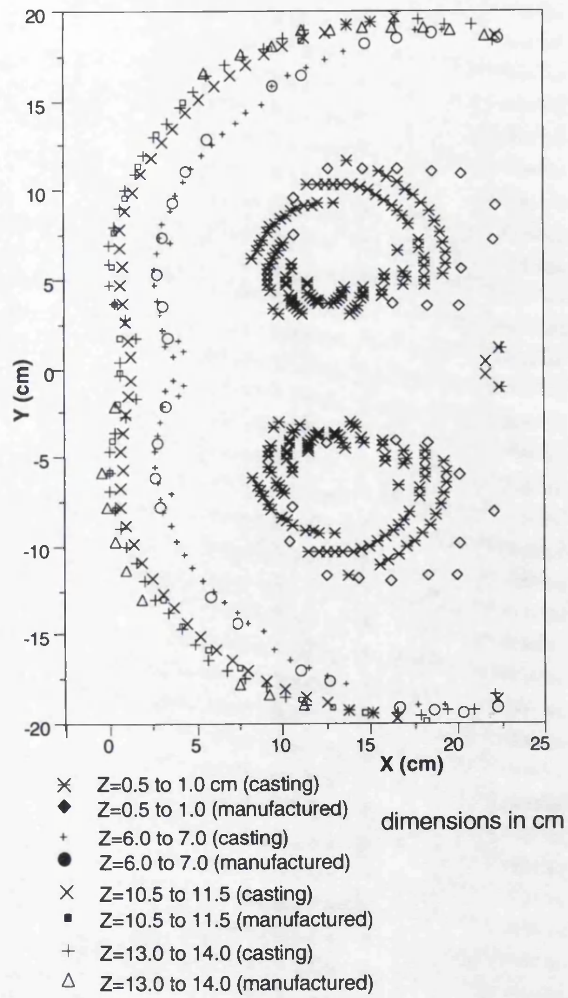

Horizontal Sections

APPENDIX 3 - Deformation, Strain & Stress Relationships

Deformation and Strain Tensors

The motion of a particle in a body which is subject to a deformation can be expressed by equations of the form

$$x_i = x_i\,(X_1, X_2, X_3, t) \qquad \text{...3.1}$$

Where x_i is the present location of the particle which occupied X_1,X_2,X_3 at time t=0.

The material **deformation gradient,** F_{ij} is the tensor $\frac{\partial x_i}{\partial X_j}$ formed on the partial differentiation of equation (3.1) with respect to Xj.

The displacement vector for a particle is

$$u_i = x_i - X_i \qquad \text{.. 3.2}$$

The material **displacement gradient,** J_{ij} is the tensor $\frac{\partial u_i}{\partial X_j}$ formed on the partial differentiation of equation (3.2) with respect to Xj.

$$J_{ij} = \frac{\partial u_i}{\partial X_j} = \frac{\partial x_i}{\partial X_j} - \delta_{ij} \qquad \text{.. 3.3}$$

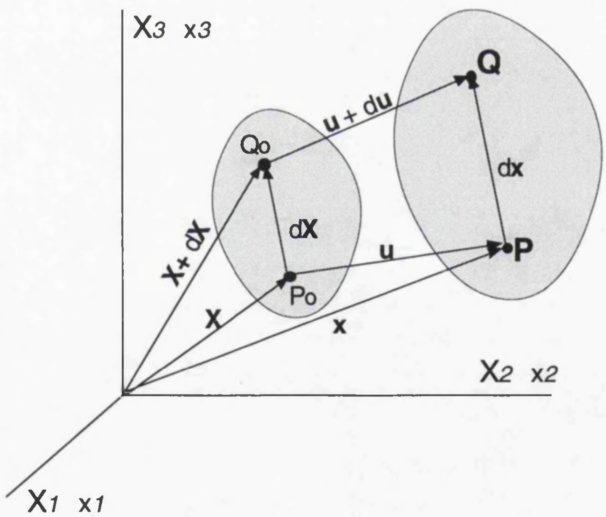

The particles which occupy points P_0 and Q_0 before deformation move to points P and Q in the deformed configuration. Initial and final configurations referred to superposed rectangular Cartesian co-ordinate axes X_1,X_2X_3 and x_1,x_2,x_3.

The square of the differential element of length between P_0 and Q_0 is

$$(dX)^2 = dX_i\, dX_i = \delta_{ij} dX_i\, dX_j \qquad \text{.. 3.4}$$

The square of the differential element of length between P and Q is

$$(dx)^2 = dx_i\, dx_i = \delta_{ij} dx_i\, dx_j \qquad \text{.......... } 3.5$$

From equation (3.1) the distance differential here is

$$dx_i = \frac{\partial x_i}{\partial X_j} dX_j$$

so $(dx)^2$ in equation (3.5) may be written as follows:

$$(dx)^2 = \frac{\partial x_k}{\partial X_i}\frac{\partial x_k}{\partial X_j} dX_i dX_j = G_{ij}\, dX_i dX_j \qquad \text{.......... } 3.6$$

G_{ij} is known as **Green's deformation tensor.**

The principal invariants of Green's deformation tensor are then :

$$\begin{aligned} I_1 &= \text{trace } G_{ij} \\ I_2 &= (G_{ii}\, G_{jj} - G_{ij}\, G_{ji})/2 \\ I_3 &= \text{determinant } G_{ij} \end{aligned} \qquad \text{.......... } 3.7a,b,c$$

The quantity $(dx)^2 - (dX)^2$ is a measure of deformation in a body. If it equals zero, the motion is referred to as a rigid body rotation. If this is not equal to zero at any point the body is in a state of strain at that point. Using equations (3.4) and (3.6)

$$dx^2 - dX^2 = \left(\frac{\partial x_k}{\partial X_i}\frac{\partial x_k}{\partial X_j} - \delta_{ij}\right) dX_i dX_j = 2\, L_{ij} dX_i dX_j \qquad \text{.......... } 3.8$$

Where the **Lagrangian finite strain tensor**

$$L_{ij} = \frac{1}{2}\left(\frac{\partial x_k}{\partial X_i}\frac{\partial x_k}{\partial X_j} - \delta_{ij}\right). \qquad \text{.......... } 3.9$$

An especially useful form of the Lagrangian finite strain tensor is that in which these tensors appear as functions of the displacement gradients. If $\frac{\partial x_i}{\partial X_j}$ from equation (3.3) is substituted into equation (3.9), the following strain - displacement relationship can be formed :

$$L_{ij} = \frac{1}{2}\left(\frac{\partial u_i}{\partial X_j} + \frac{\partial u_j}{\partial X_i} + \frac{\partial u_k}{\partial X_i}\frac{\partial u_k}{\partial X_j}\right) \qquad \text{.......... } 3.10$$

Stress Tensors

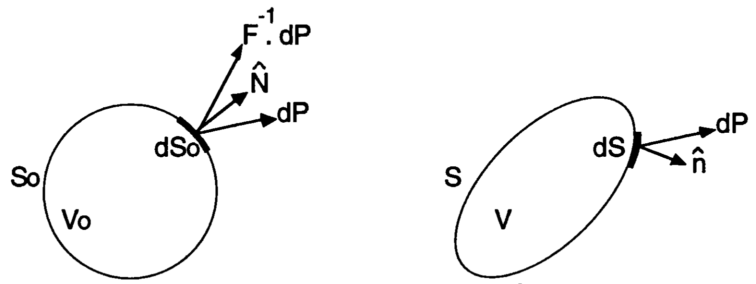

Force and area terms in stress definitions

The Cauchy or **true** stress tensor **T** can be expressed as the actual force on a deformed area per unit of deformed area.

$$\hat{\mathbf{n}} \cdot \mathbf{T} = \frac{d\mathbf{P}}{dS}$$

$\hat{\mathbf{n}}$ unit vector perpendicular to dS ; **dP** resultant force vector ; dS elemental area

The **engineering** stress tensor (first Piola-Kirchoff stress tensor) $\mathbf{S}^0$ can be expressed as the actual force on a deformed area per unit of undeformed area.

$$\hat{\mathbf{N}} \cdot \mathbf{S}^o = \frac{d\mathbf{P}}{dS_o}$$

$\hat{\mathbf{N}}$ unit vector perpendicular to dS_o

The **second Piola-Kirchoff** stress tensor **S** can be expressed as the dot product of $\mathbf{F}^{-1}$ into the actual force on a deformed area per unit of undeformed area.

$$\hat{\mathbf{N}} \cdot \mathbf{S} = \frac{\mathbf{F}^{-1} \cdot d\mathbf{P}}{dS_o}$$

Thus the Cauchy stress can be expressed in terms of the second Piola- Kirchoff stress.

$$\mathbf{T} = \frac{\rho}{\rho_o} \mathbf{F} \cdot \mathbf{S} \cdot \mathbf{F}^T = \frac{1}{I_3^{0.5}} \mathbf{F} \cdot \mathbf{S} \cdot \mathbf{F}^T$$

S Cauchy stress tensor ; ρ, ρ_o mass densities in initial and deformed configurations

I_3 Third Invariant of Green's deformation strain tensor ; **F** deformation gradients

APPENDIX 4 - Finite Element Method

The reader is referred to comprehensive texts such as Zienkiewicz (1989) for a complete explanation of the finite element method. In this appendix the aspects of the finite element method which are of particular relevance to the studies in this thesis are reported.

Principles of the Finite Element Method

The finite element method is an approximation technique that can be used to solve the differential equations which are produced by stress analysis in complex structures. The method is based on minimising the total potential energy of the system in terms of a prescribed displacement field.

Initially the structure is spatially divided into discrete elements connected together at nodal points. The nodal points are situated at the element boundaries. A set of functions is chosen to uniquely define the displacements within each element in terms of the nodal displacements. Therefore the state of strain within the elements is known. It is possible to define the stress state in the elements in terms of these strains, the initial strain within the element and the constitutive properties of the material. The equations governing the behaviour of the elements are then formulated and assembled into the governing equation for the whole structure.

The displacement at any point within a finite element e is approximated to a column vector **u**.

$$\mathbf{u} = \mathbf{N}\mathbf{a}^{e} \qquad \ldots\ldots\ldots\ldots\ldots \; 4.1$$

where **N** are functions of position (shape functions) and $\mathbf{a}^e$ are nodal displacements for a particular element. The shape functions are often taken as linear functions of position.

With displacements known at all points within an element the strains at any point can then be determined. These result in relationships that can be written as

$$\varepsilon = \mathbf{S}\mathbf{u} \qquad \text{where } \mathbf{S} \text{ is a suitable linear operator} \qquad \ldots\ldots\ldots\ldots\ldots \; 4.2$$

Using equation (4.1) the above equation can be approximated as

$$\varepsilon = \mathbf{B}\mathbf{a} \qquad \text{with } \mathbf{B}=\mathbf{S}\mathbf{N} \qquad \ldots\ldots\ldots\ldots\ldots \; 4.3$$

For the plane stress case, the relevant strains are those occurring in the plane and are defined in terms of the displacements by well-known relations. Equation (4.3) becomes :

$$\left\{ \begin{matrix} \varepsilon_x \\ \varepsilon_y \\ \gamma_{xy} \end{matrix} \right\} = \left\{ \begin{matrix} \dfrac{\partial u}{\partial x} \\ \dfrac{\partial v}{\partial y} \\ \dfrac{\partial u}{\partial y} + \dfrac{\partial v}{\partial x} \end{matrix} \right\} = \begin{bmatrix} \dfrac{\partial}{\partial x} & 0 \\ 0 & \dfrac{\partial}{\partial y} \\ \dfrac{\partial}{\partial y} & \dfrac{\partial}{\partial x} \end{bmatrix} \left\{ \begin{matrix} u \\ v \end{matrix} \right\} \qquad \ldots\ldots\ldots\ldots\ldots \; 4.4$$

With the shape functions **N** already determined the matrix **B** will easily be obtained.

The material within the element boundaries may be subject to initial strains ε_0 from temperature changes, etc. The stresses will be caused by the difference between the initial and actual strains. In addition the material may be subject to a set of initial residual stresses σ_0. When there is linear elastic behaviour the following stress-strain relationship applies:

$$\sigma = \mathbf{D}\,(\varepsilon-\varepsilon_0) + \sigma_0 \qquad \text{4.5}$$

Where: σ = stress vector ; $\mathbf{D}$ =elasticity matrix

For the plane stress case, the stresses occur in the plane and are $\{\sigma_x\ \sigma_y\ \tau_{xy}\}$. For a homogeneous isotropic material the elasticity matrix **[D]** may be obtained from the stress-strain relationships :

$$\sigma_x = \frac{E}{1-\upsilon^2}\left(\varepsilon_x+\upsilon\varepsilon_y\right) \qquad \sigma_y = \frac{E}{1-\upsilon^2}\left(\varepsilon_y+\upsilon\varepsilon_x\right) \qquad \tau_x = \frac{E}{2(1-\upsilon)}\,\gamma_{xy} \qquad \text{4.6}$$

Where E =Youngs modulus. υ=Poisson's ratio. Thus the elasticity matrix is as follows:

$$\mathbf{D} = \frac{E}{1-\upsilon^2}\begin{bmatrix} 1 & \upsilon & 0 \\ \upsilon & 1 & 0 \\ 0 & 0 & (1-\upsilon)/2 \end{bmatrix} \qquad \text{4.7}$$

When an isotropic material is in an axisymmetric stress state, 3 dimensional stress state or in a state of plane strain, each term in the elasticity matrix includes a $(1-2\upsilon)$ denominator. This leads to the results of FE analyses of nearly incompressible materials being extremely sensitive to the exact value of Poisson's ratio.

To obtain finite element equations for an element the external and internal work done by various forces and stresses are equated under applied virtual displacements $\delta\mathbf{a}^e$. Assuming there are no surface loads:

$$\underbrace{\delta\mathbf{a}^{eT}\mathbf{q}^e}_{\text{work done by nodal forces } \mathbf{q}} = \underbrace{\int_V \delta\mathbf{a}^{eT}\mathbf{B}^T\sigma\, d(vol)}_{\text{work by stresses } \sigma} - \underbrace{\int_V \delta\mathbf{a}^{eT}\mathbf{N}^T\mathbf{b}\, d(vol)}_{\text{work by distributed forces } \mathbf{b}} \qquad \text{4.8}$$

Substituting the constitutive relationship (4.5) into equation (4.8) results in a system of algebraic equations :

$$\mathbf{q}^e = \mathbf{K}^e\,\mathbf{a}^e + \mathbf{f}^e \qquad \text{4.9}$$

where

$$\mathbf{K}^e = \int_V \mathbf{B}^T\mathbf{D}\,\mathbf{B}\, d(vol) \qquad \text{4.10a}$$

and

$$\mathbf{f}^e = -\int_V \mathbf{N}^T\mathbf{b}\, d(vol) - \int_V \mathbf{B}^T\mathbf{D}\,\varepsilon_0\, d(vol) + \int_V \mathbf{B}^T\sigma_0\, d(vol) \qquad \text{4.10b}$$

The terms in (4.10b) represent the forces due to body forces, initial strains and initial stresses.

The element equations are assembled into the finite element equation for the structure by considering the conditions for equilibrium at the nodes. The external applied nodal forces **r** must equal the sum of the component forces from the elements meeting at the nodes, $\mathbf{q}^e$. This system matrix equation can be represented as :

$$\mathbf{K}\,\mathbf{a} = \mathbf{r} - \mathbf{f} \qquad \text{.......... 4.11}$$

Where **a** = Displacements of each node in system

$\mathbf{K}_{ij}$ = System stiffness matrix $=\Sigma_{e=1,N}\,\mathbf{K}_{ij}^e$

$\mathbf{r}_i$ = External nodal forces loading structure $=\Sigma_{e=1,N}\,\mathbf{q}_i^e$

$\mathbf{f}_i$ = Forces due to initial strains ε_0 and distributed loads $\mathbf{b} =\Sigma_{e=1,N}\,\mathbf{f}_i^e$

Once the system stiffness matrix has been determined, the inverse matrix can be calculated using computer techniques. The matrix **a** is then evaluated, which yields the displacement of each node within the system. Finally the strains and stresses are evaluated using equations (4.3) and (4.5) for each element.

Nonlinear Analyses and Iterative Solution Methods

A structure is called nonlinear when the system stiffness matrix varies with displacement. The structure cannot be represented directly by a set of linear equations. Methods involving successive linear approximations can be used to solve such problems. The Newton Raphson technique is one such approximation method. The technique is also discussed in the Supplement to Structural Nonlinearities Seminar Notes and the Theoretical Reference Manual (Ansys, 1990). The stiffness matrix is updated at each iteration, and when the displacement solutions from successive iterations are sufficiently close, the analysis is said to have converged. The computational stages employed in the analysis procedure are as follows:

For the first iteration, the stiffness of each element $\mathbf{K}_i^e$ is calculated.

$$\mathbf{K}_i^e = \int_V \mathbf{B}_i^T\,\mathbf{D}_i\,\mathbf{B}_i\,d(VOL) \qquad \text{.......... 4.12}$$

$\mathbf{D}_i$ =Tangent stress-strain matrix

$\mathbf{B}_i$ =Tangent strain-displacement matrix

The total tangent stiffness matrix $\mathbf{K}_i$ is the sum of the element tangent stiffnesses

$$\mathbf{K}_i =\Sigma_{m=1,N}\,\mathbf{K}_i^e \qquad \text{.......... 4.13}$$

The nodal increment displacement vector is then calculated from

$$\mathbf{K}_i \Delta\mathbf{U} = \mathbf{R} - \mathbf{F}_i \qquad \text{..........} 4.14$$

$\Delta\mathbf{U}$ Nodal increment displacement vector

$\mathbf{R}$ Total applied load for iteration i

$\mathbf{F}_i$ restoring force corresponding to element stress at iteration i

The nodal displacements U_{i+1} for the next iteration can be estimated:

$$\Delta\mathbf{U} = \mathbf{U}_{i+1} - \mathbf{U}_i \qquad \text{..........} 4.15$$

$\mathbf{U}_{i+1}$ New displacement vector

$\mathbf{U}_i$ Displacement vector at iteration i (U_i =0 for iteration 1)

The stresses and strains are then calculated.

$$\Delta\sigma = \mathbf{D}_i \Delta\varepsilon. \qquad \text{..........} 4.16$$
$$\sigma_{i+1} = \sigma_i + \Delta\sigma$$

$$\Delta\varepsilon = \mathbf{B}_i \Delta\mathbf{U} \qquad \text{..........} 4.17$$
$$\varepsilon_{i+1} = \varepsilon_i + \Delta\varepsilon$$

Convergence is checked by comparing the displacement increment ΔU with a preset criterion. If $\Delta\mathbf{U}$ is greater than the criterion, the solution has not converged and the process is repeated until convergence is reached. For iterations after the first, the element restoring forces are computed from the elemental stresses and strain displacement matrix.

$$\mathbf{F}_i^e = \int_V \mathbf{B}^T \sigma_i d(VOL). \qquad \text{..........} 4.18$$

The element restoring forces are assembled into the total restoring force

$$\mathbf{F}_i = \Sigma_{m=1,N} \mathbf{F}_i^e \qquad \text{..........} 4.19$$

The Newton Raphson solution method is depicted graphically below for a one degree of freedom model.

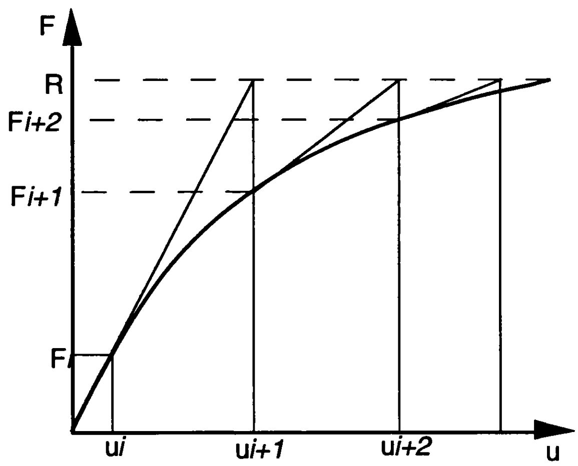

Newton Raphson Solution Method

Finite Element Method for Hyperelastic Materials

A hyperelastic material is defined and discussed in chapters 4 and 6 of this thesis. Some of the discussion is reproduced here because of its importance in the formulation of the finite element equation for hyperelastic materials. A nonlinear equation solving technique, such as the Newton-Raphson is required to take account of the nonlinear nature of this element. An in depth discussion of the finite element method for hyperelastic materials can be found in the Structural Nonlinearities Seminar Notes (Ansys, 1990).

For a hyperelastic material the strain energy density function is a scalar function of one of the strain or deformation tensors, whose derivation with respect to a strain component determines the corresponding stress component (see Appendix 3 for the definitions and relationships between the deformation, strain and stress tensors).

$$S_{ij} = \frac{\partial W}{\partial E_{ij}} \equiv 2\frac{\partial W}{\partial C_{ij}} \qquad \text{4.20}$$

S_{ij} = Component of 2 nd Piola-Kirchoff stress tensor
E_{ij} = Component of Lagrangian finite strain tensor
W = Strain energy density function per unit undeformed volume
C_{ij} = Component of Green's deformation tensor

The invariants of Green's deformation tensor are shown in equations 3.7 a,b,c (Appendix 3).

Using the chain rule on equation (4·20) the following expression for the stress components can be formed:

$$S_{ij} = 2 \left(\frac{\partial W}{\partial I_1}\cdot\frac{\partial I_1}{\partial C_{ij}} + \frac{\partial W}{\partial I_2}\cdot\frac{\partial I_2}{\partial C_{ij}} + \frac{\partial W}{\partial I_3}\cdot\frac{\partial I_3}{\partial C_{ij}}\right) \qquad \text{4·21}$$

The derivatives of the strain invariants with respect to Green's deformation tensor can be calculated from the expressions for the strain invariants (Appendix 3). The derivative of the strain energy density function with respect to the strain invariants can be calculated from equation (4·22).

Some nearly incompressible hyperelastic can be described by the following constitutive equation (Mooney-Rivlin equation):

$$W = A(I_1-3) + B(I_2-3) + C(1/I_3^2-1) + D(I_3-1) \qquad \text{4.22}$$

A, B, C and D are constants. C and D can be expressed in terms of A, B and Poisson's ratio. I_i are the strain invariants.

During the finite element solution with a hyperelastic material the true stresses are calculated from the Second Piola -Kirchoff stress components. The true stresses take into account the change in shape of the elements during the deformation. These stresses are calculated in the elements from equation (4·21). The strain energy density equation for the material and the components of Green's deformation tensor must be known.

During the solution the Lagrangian finite strain tensor is calculated (Appendix 3, equation 3·9), so there is no limit to the magnitude of the strains in the system.

The following is a summary of the derivation of the finite element equation for such materials. The incremental principle of virtual work is used in the derivation. Internal and external work and their increments are expressed in an equilibrium statement for an element.

$$\underset{\text{internal virtual work}}{\delta U} + \underset{\text{increment of internal virtual work}}{\dot{\delta U}} = \underset{\text{external virtual work}}{\delta V} + \underset{\text{increment of external virtual work}}{\dot{\delta V}} \qquad 4{\cdot}23$$

The internal virtual work is expressed as the integral over the volume of the current strain energy density function W . The external virtual work is the work of the surface pressures over the current surface and the work of the nodal point loads.

$$\underset{\text{total internal work}}{\int_{vol} (\delta W + \dot{\delta W})\, d(vol)} = \underset{\text{work of surface loads}}{\sum_{surface} \int_{s} (P + \dot{P})\hat{n}_i\, \delta u_i\, dS} + \underset{\text{work of point loads}}{\sum_{nodes} (F_i^{(n)} + \dot{F}_i^{(n)})\, \delta\Delta_i^{(n)}} \qquad 4{\cdot}24$$

Where:

vol	=	current element volume
W	=	strain energy density function per unit current volume
P	=	scalar pressure magnitude from previous iteration
$\dot{P}$	=	increment of P for current iteration
$\hat{n}_i$	=	components of the unit normal of the current deformed surface
$F_i^{(n)}$	=	currently applied nodal force in the i^{th} direction at node n
$\dot{F}_i^{(n)}$	=	increment in $F_i^{(n)}$ for current iteration
δu_i	=	displacement field variation of the i^{th} coordinate
S	=	current deformed surface area of element
$\delta\Delta_i^{(n)}$	=	variation in nodal displacement in the i^{th} direction at node n

The element stiffness and load correction matrices can be derived from the total internal work term in the basic equilibrium relationship (4.24). Expressions for the variation W and an increment of the variation of W can be formed in terms of the deformation gradients, and the derivatives of the strain energy density function with respect to deformation.

$$\delta W = \frac{\partial W}{\partial C_{ij}}\delta C_{ij} \qquad \delta\dot{W} = \frac{\partial^2 W}{\partial C_{ij}\,\partial C_{kl}}\delta C_{ij}.\ \dot{C}_{kl} + \frac{\partial W}{\partial C_{ij}}\,\delta\dot{C}_{ij}$$ .... 4.25 a,b

$$\delta C_{ij} = \delta f_{ki}\,f_{kj} + f_{ki}\,\delta f_{kj} \qquad \delta\dot{C}_{ij} = \delta\dot{f}_{ki}\,f_{kj} + f_{ki}\,\delta\dot{f}_{kj} \qquad \dot{C}_{ij} = \dot{f}_{ki}\,f_{kj} + f_{ki}\,\dot{f}_{kj}$$ .... 4.26 a,b,c

Where f_{ki} = deformation gradients, as defined in Appendix 3.

Equations (4.25) can be substituted into equation (4·24). The element equilibrium equation is thus expressed in terms of the external loads and internal strains:

$$2\int_{vol}\left(\frac{\partial W}{\partial C_{ij}} f_{ki}\,\delta u_{kj} + \frac{\partial W}{\partial C_{ij}} f_{ki}\,\delta u_{kj} + 2\frac{\partial^2 W}{\partial C_{ij}\,\partial C_{kl}} f_{mi}\,\delta f_{nj}\,f_{mk}\,f_{nl}\right) d(vol)$$

$$= \sum_{surface}\int_{so}(P + \dot{P})\det(f)\,f^{-1}_{ij}\,\hat{N}_j\,\delta u_i\,dS_o + \sum_{nodes}(F_i^{(n)} + \dot{F}_i^{(n)})\,\delta\Delta_i^{(n)}$$

.... 4.27

$\hat{N}_j$ = Component of the normal to the original undeformed surface

δu_j = variation of the j-coordinate displacement field

S_o = undeformed surface over which $P + \dot{P}$ acts.

$\frac{\partial^2 W}{\partial C_{ij}\,\partial C_{kl}}$ = incremental moduli (4th order tensor)

The equation (4·27) then becomes (4.28) - in matrix form :

$$\mathbf{K}_e(u)\,\dot{\mathbf{u}} = \mathbf{F}^{pr} + \dot{\mathbf{F}}^{pr} + \mathbf{F}^{nd} + \dot{\mathbf{F}}^{nd} - \mathbf{R}(u)$$ 4.28

$\mathbf{K}_e(u)$ = current element stiffness matrix

$\mathbf{R}(u)$ = current nodal load correction vector

$\dot{\mathbf{u}}$ = unknown nodal displacement increments

$\mathbf{u}$ =current total nodal displacements from last iteration

$\mathbf{F}^{pr} + \dot{\mathbf{F}}^{pr}$ = current total applied pressure

= pressure magnitude from previous iteration + pressure increment

$\mathbf{F}^{nd} + \dot{\mathbf{F}}^{nd}$ = current total applied nodal point loads

= directly applied nodal forces from the previous iteration + force increments

The unknown quantity is $\dot{\mathbf{u}}$, while the stiffness matrix and the load correction array are functions of the current value of displacement **u**, through the deformation gradient **f** and the derivatives of the strain energy density.

APPENDIX 5 - Finite Elements Used in the FE Analyses

An in depth description of the characteristics of the elements can be found in the Ansys User Reference Manuals (1990).

2-D 1-NODE GAP ELEMENT (STIF 26)

This element represents surfaces which may maintain or break physical contact and may slide relative to one another. The element has 2 degrees of freedom at each node : translation in the nodal x and y directions. Either a straight or a curved rigid region can be defined with each element. Multiple elements may be used to define a complex surface.

The force-deflection relationship for this element is based upon the normal direction. In the tangential direction no forces act upon a node. At the start of the first iteration the node location determines the initial stiffness. If the gap is open no stiffness is associated with the element for this iteration. If the gap is closed the stiffness K is used for the gap resistance. During the solution, when the normal force Fn is negative, the gap remains in contact and responds as a linear spring. As the normal force becomes positive, contact is broken and no force is transmitted. The force-deflection relationship is illustrated below. The element is non liear and therefore requires an iterative solution.

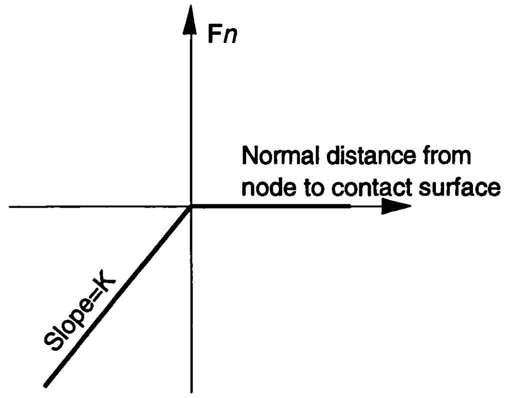

Force Deflection Relationship

This element does not have a shape function, nor integration points.

ELEMENT MATRICES

When node I is inside the contact surface, the element stiffness matrix in the contact surface coordinate system is :

$$K_I = \begin{bmatrix} 0 & 0 \\ 0 & k \end{bmatrix} \qquad \text{.......................................5.1}$$

Where K = stiffness (input quantity)

The Newton-Raphson load vector is:

$$F_I^{nr} = \left\{ \begin{matrix} 0 \\ F_n \end{matrix} \right\} \quad \text{.......................................5.2}$$

Where F_n =force normal to contact surface (from the previous iteration)

When node I is outside the contact surface, the stiffness matrix and load vector are both null matrices

2-D INTERFACE ELEMENT (STIF 12)

The element represents surfaces which may maintain or break physical contact and may slide relative to one another. The element can support only compression in the direction normal to the surface and shear in the tangential direction. The element has 2 degrees of freedom at each node : translation in the nodal x and y directions.

This element does not have a shape function, nor integration points.

ELEMENT MATRICES

The element may be closed and not sliding, closed and sliding or open. These options are discussed below:

Closed and not sliding. This condition occurs if

$$\upsilon |F_n| > |F_s| \quad \text{.......................................5·3}$$

Where υ = coefficient of friction

F_n = normal force across gap (from previous iteration)

F_s = sliding force parallel to gap (from previous iteration)

The normal force is :

$$F_n = K_n (u_{n,j} - u_{n,I} - \Delta) \quad \text{.......................................5·4}$$

Where K_n = normal stiffness

$u_{n,j}$ =displacement of node I in normal direction

$u_{n,j}$ =displacement of node J in normal direction

Δ = interference =-distance between the nodes

The sliding force is :

$$F_s = K_s (u_{s,j} - u_{s,I} - u_o) \quad \text{.......................................5·5}$$

Where K_s = normal stiffness

$u_{s,j}$ =displacement of node I in sliding direction

$u_{s,j}$ =displacement of node J in sliding direction

u_o = distance that nodes I and J have slid with respect to one another.

The element stiffness matrix in element coordinates is :

$$K_I = \begin{bmatrix} k_s & 0 & -k_s & 0 \\ 0 & k_n & 0 & -k_n \\ -k_s & 0 & k_s & 0 \\ 0 & -k_n & 0 & k_n \end{bmatrix} \qquad \text{.......................................5·6}$$

The Newton-Raphson load vector in element coordinates is :

$$F_I^{nr} = \begin{Bmatrix} F_s \\ F_n \\ -F_s \\ F_n \end{Bmatrix} \qquad \text{.......................................5·7}$$

Closed and sliding. This condition occurs if

$$\upsilon \, |F_n| < |F_s| \qquad \text{.......................................5·8}$$

The element stiffness matrix in element coordinates is :

$$K_I = \begin{bmatrix} 0 & 0 & 0 & 0 \\ 0 & k_n & 0 & -k_n \\ 0 & 0 & 0 & 0 \\ 0 & -k_n & 0 & k_n \end{bmatrix} \qquad \text{.......................................5·9}$$

and the Newton-Raphson load vector is the same as in 5·7.

Open. There is no stiffness matrix or load vector.

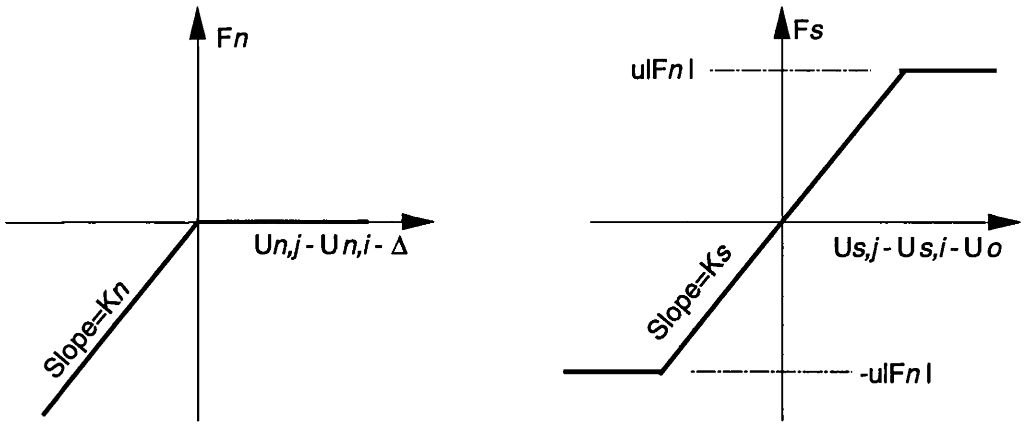

Force Deflection Relationships

The element is nonlinear and so an iterative solution is required. Also because energy is lost in sliding, loads are applied in stages.

2-D ISPARAMETRIC HYPERELASTIC SOLID (STIF 84)

This element has two basic configurations: four noded and 8 noded quadrilateral forms. Three and six noded triangular degenerate forms are also available. When the element is defined with midside nodes, there is a quadratic representation of the geometry and displacement functions. The element can be used either as a plane strain element or an axisymmetric ring element.

The element's nonlinear nature requires an iterative solution. Also problems are very sensitve to the rate of load application and so loads are usually applied in several load increments.

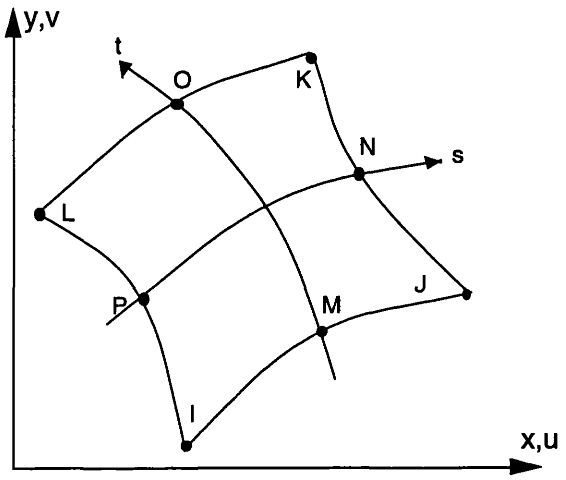

$$U=N_1U_1 + N_2U_2 + \dots\dots\dots N_8U_8$$

$$V=N_1V_1 + N_2V_2 + \dots\dots\dots N_8V_8$$

The shape function is defined as follows:

$N_1=1/4\ (1-s)\ (1-t)\ (-s-t-1)$ $\qquad$ $N_5=1/2\ (1-s^2)\ (1-t)$

$N_2=1/4\ (1+s)\ (1-t)\ (s-t-1)$ $\qquad$ $N_6=1/2\ (1-t^2)\ (1+s)$

$N_3=1/4\ (1+s)\ (1+t)\ (s+t-1)$ $\qquad$ $N_7=1/2(1-s^2)\ (1+t)$

$N_4=1/4\ (1-s)\ (1+t)\ (-s+t-1)$ $\qquad$ $N_8=1/2\ (1-t^2)\ (1-s)$

APPENDIX 6

Normalised Vertical Stiffness Data From FE Analyses in Chapter 5

ANALYSIS 1		ANALYSIS 2		ANALYSIS 3		ANALYSIS 4		ANALYSIS 5		ANALYSIS 6		ANALYSIS 7		MEASURED DATA	
Def.n %	Force %	Def.n %	Force %	Def.n %	Force %	Def.n %	Force %	Def.n %	Force %	Def.n %	Force %	Def.n %	Force %	Def.n %	FORCE
0	0.00	0	0.00	0	0.00	0	0.00	0	0.00	1.46	0.02	1.46	0.02	0	0
4	0.00	4	0.00	4	0.00	4	0.22	4	0.22	7.46	0.27	7.46	0.27	24	0
9	1.37	9	0.98	9	0.00	9	0.90	9	0.91	17.46	1.33	17.46	1.33	36	2
14	2.74	14	2.94	14	2.12	14	1.93	14	1.94	27.46	3.52	27.46	3.52	43	6
19	5.48	19	3.92	19	3.70	19	3.32	19	3.35	37.46	7.41	37.46	7.41	53	10
24	6.85	24	6.86	24	5.82	24	5.07	24	4.22	47.46	13.77	47.46	13.77	62	22
29	9.59	29	8.82	29	8.47	29	7.30	29	7.34	57.46	23.78	57.46	23.78	70	28
34	13.70	34	12.75	34	11.11	34	9.97	34	10.02	67.46	39.16	67.46	39.16	76	40
39	17.81	39	15.69	39	14.81	39	13.28	39	13.35	73.46	52.35	73.46	52.35	79	52
44	21.92	44	20.59	44	19.05	44	17.19	44	17.28	75.46	57.61	75.46	57.61	82	58
49	27.40	49	25.49	49	23.81	49	21.91	49	22.02	78.46	66.57	78.46	66.57	84	70
54	34.25	54	31.37	54	28.04	54	27.46	54	27.59	81.46	77.14	81.46	77.14	85	88
59	41.10	59	38.24	59	36.51	59	34.03	59	34.18	83.46	85.32	83.46	85.32	86	100
64	49.32	64	46.08	64	44.44	64	41.88	64	42.06	85.46	94.69	85.46	94.69		
69	57.53	69	55.88	69	53.44	69	51.05	69	51.25	86.46	100.00	86.46	100		
74	69.86	74	65.69	74	67.20	74	61.99	74	62.18	88.46	112.17	88.46	112.2		
80	80.82	80	80.39	80	79.89	80	75.09	80	75.29	89.46	119.27	89.46	119.3		
84	91.78	84	92.16	84	92.06	84	90.83	84	90.93						
85	94.52	85	95.10	85	95.24	85	94.77	85	94.85						
86.2	100.0	86.2	100.0	86.2	100.0	86.0	100.0	86.0	100.0						

APPENDIX 7
Sections through Tip of Ischial Tuberosity Showing Pelvis and Buttock Surface

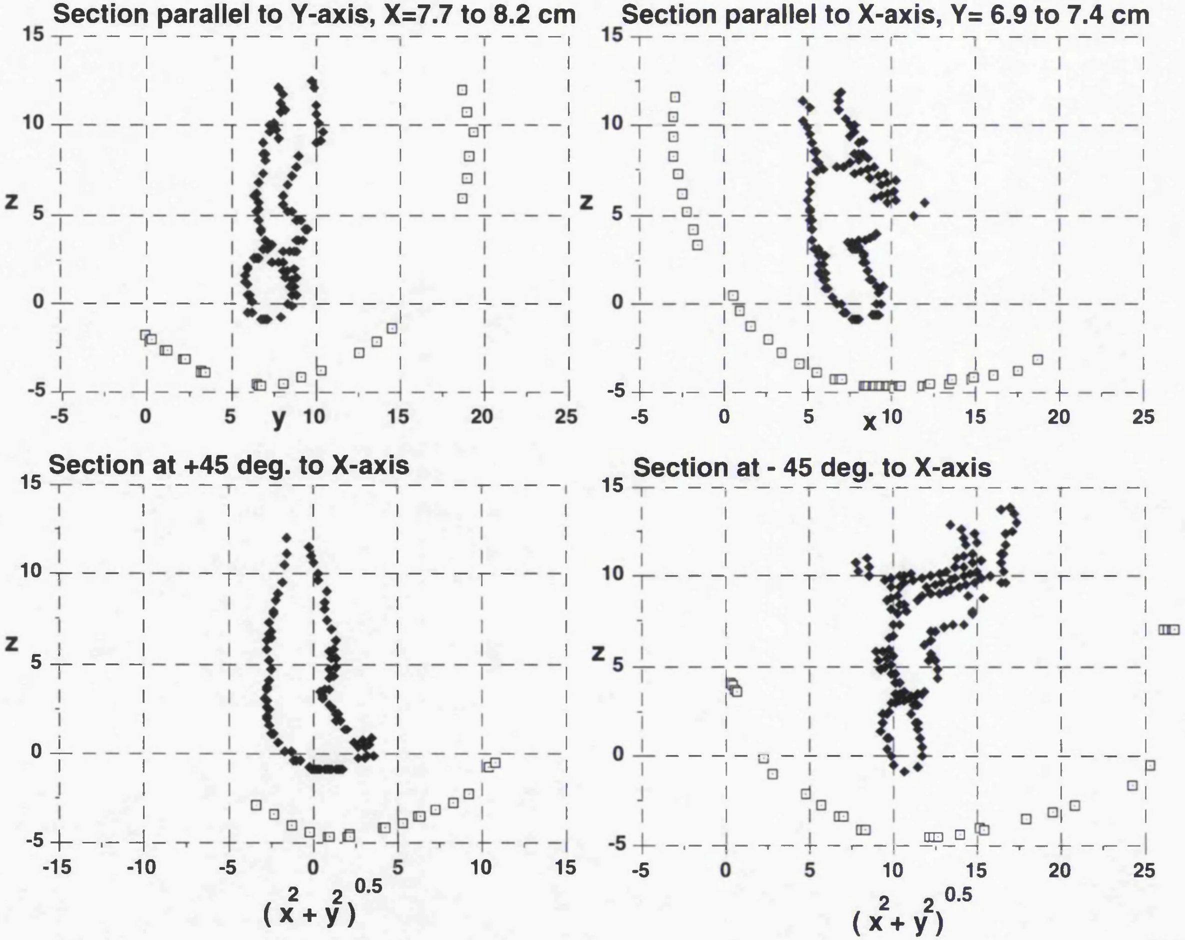

Dimensions in cm.

APPENDIX 8 - Geometry of FE Models in Chapters 7 and 8

Rotationally Symmetric Models of Soft Material around Seat (7.2, 7.3 and 8)

Model 1: Planar surface, modelled with one linear element.

Model 2: Spherical surface (R=300 mm), modelled with 1 arc-shaped element.

Model 3: Spherical surface (R=200 mm), modelled with 1 arc-shaped element.

Model 4: Spherical surface (R=150 mm), modelled with 1 arc-shaped element.

Model 5: Surface of revolution formed by rotating 1 arc-shaped element (R=300 mm) about the axis. The centre of curvature of the arc was not on the axis of revolution.

Model 6: Complex surface of revolution similar in shape to the external surface of the soft tissue layer. The surface was formed with 3 elements (1 planar, 2 arc-shaped with radii of 125 and 20 mm). The contour depth was 102 mm. The centre of curvature of the arcs was not on the axis of revolution.

Model 7: Complex surface of revolution formed with 3 elements (1 planar, 2 arc-shaped with radii of 150 and 40 mm). The contour depth was 105 mm (there was about 5 mm between the seat and soft tissue along axis of revolution when initial contact between the body and the seat was made). The centre of curvature of the arcs was not on the axis of revoiution.

Model 8: Complex surface of revolution formed with 3 elements (1 planar, 2 arc-shaped with radii of 150 and 40 mm). The contour depth was 115 mm (there was about 14 mm between the seat and the soft tissue along axis of revolution when initial contact between the body and the seat was made). The centre of curvature of the arcs was not on the axis of revolution.

Model 9: Complex surface of revolution formed with 3 elements (1 planar, 2 arc-shaped with radii of 120 and 20 mm). The contour depth was 120 mm (there was about 21 mm between the seat and soft tissue at axis of revoiution when initial contact between the body and the seat was made). The centre of curvature of the arcs was not on the axis of revolution.

Model 10: Complex surface of revolution formed with 3 elements (1 planar, 2 arc-shaped with radii of 190 and 40 mm). The contour depth was 115 mm (there was about 15 mm between the seat and soft tissue along axis of revolution when initial contact between the body and the seat was made). The surface less 'steep' than that of model 8, otherwise similar. The centre of curvature of the the arcs was not on the axis of revolution.

Model 11: Complex surface of revolution formed with 3 elements (1 planar, 2 arc-shaped with radii of 140 & 80 mm). The contour depth was 80 mm (there was about 15 mm between the seat and soft tissue along axis of revolution when initial contact between in body and the seat was made). The centre of curvature of the arcs was not on the axis of revolution.

Model 12: Complex surface of revolution formed with 3 elements (1 planar, 2 arc-shaped with radii of 150 & 80 mm). The contour depth was 60 mm (there was about 15 mm between the seat and soft tissue along axis of revolution when initial contact between in body and the seat was made). The centre of curvature of the the arcs was not on the axis of revolution.

Model 13: Complex surface of revolution formed with 3 elements (1 planar, 2 arc-shaped with radii of 100 & 110 mm). The contour depth was 40 mm (there was about 15 mm between the seat and soft tissue along axis of revolution when initial contact between in body and the seat was made). The centre of curvature of the arcs was not on the axis of revolution.

Plane Strain models of Central Section through Buttock (7.4 7.5 and 8)

Model A: A complex seat surface formed with 4 arc-shaped elements (radii of 75,300,160, 400). A seat was produced with the same central profile and the interface pressure distribution was measured with the subject sitting on this seat. A comparison between the manufactured and modelled shapes and pressure distribution is shown in Appendix 19.

Model B: A planar seat surface formed with 1 straight line element. Friction coefficients of 0.0, 0.1, 0.4 and 0.8.

Model C: A planar seat surface formed with 1 straight line element. The pelvis was rotated posteriorly by 25 deg. compared to model B.

Model D: A complex surface formed with 3 arc-shaped elements (radii of 80, 200 and 100 mm). The seat was shaped so that there was little contact between the tissue surface around the sacrum and supporting surface.

Model E: Complex surface formed with 3 arc-shaped elements (Radii of 200, 120 and 200 mm). The seat shape was the similar to model D. The pelvis was rotated posteriorly by 25 deg. compared to in model B.

Model F: Complex surface formed with 3 arc-shaped elements (Radii of 200, 140 and 300 mm). The seat was similar to in model E, however there was not contact between the seat and the surface of the tissues in the region of the sacrum. The pelvis was rotated posteriorly by 25 deg. compared to in model B.

APPENDIX 9

Estimate of Vertical Load Through Central Section of Buttock-Seat Interface from Interface Pressure Measurements on Two Seat Surfaces

1. Planar Seat

Assumptions

i. Section is 1 mm thick and the pressure does not vary across this section.

ii. The boundary of contact between the body and the seat is at x =0 and x = 150 mm.

iii. The total vertical load can be estimated from sample pressure measurements at 20 mm position intervals with the pressure transducers described in Chapter 2. The interface was divided up into elemental areas each of which was assumed to be at a uniform pressure.

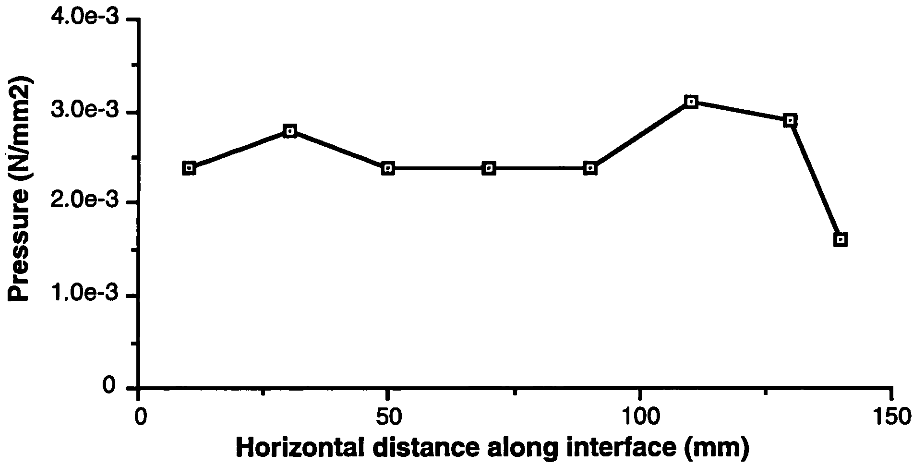

Pressure (mmHg)	Pressure (N/mm^2)	X (mm)	Area (mm^2)	Load (N)
18	2.4e-3	10	15	0.036
21	2.8e-3	30	20	0.056
18	2.4e-3	50	20	0.048
18	2.4e-3	70	20	0.048
18	2.4e-3	90	20	0.048
23	3.1e-3	110	20	0.061
22	2.9e-3	130	20	0.059
12	1.6e-3	140	15	0.024

The total vertical load was estimated by adding the loads through each elemental area

Total vertical load= 0.38 N

2. Concave Seat

Assumptions

i. Section is 1 mm thick and the pressure does not vary across this section.

ii. The boundary of contact is at x =77.9 and x = 303.8 mm.

iii. The total vertical load can be estimated from sample pressure measurements at the position intervals described below, with the pressure transducers described in Chapter 2. The interface was divided up into elemental areas each of which was assumed to be at a uniform pressure.

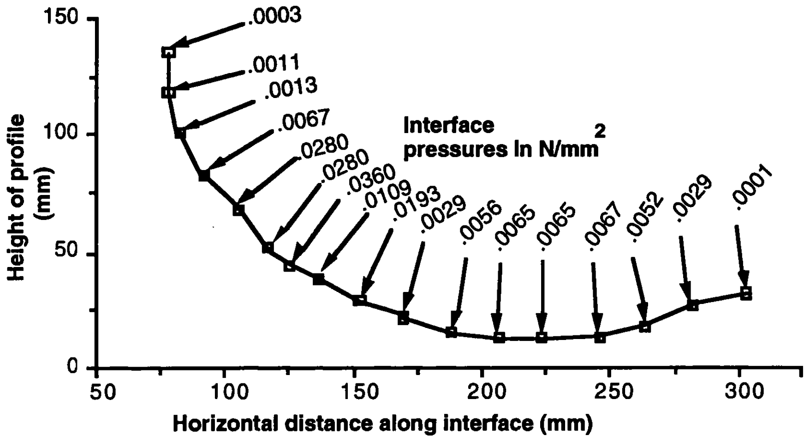

Pressure (mmHg)	Pressure (N/mm^2)	X (mm)	Y (mm)	Surface area (mm^2)	Load nornal to surface (N)	Orientation of surface(deg.)	Vertical load (N)
2	2.7e-4	77.949	134.75	8.43	0.002	179.4	0.000
8	1.07e-3	77.78	117.9	8.57	0.009	15.1	0.002
10	1.33e-3	82.254	101.35	26.92	0.036	15.0	0.009
50	6.67e-3	91.869	82.74	19.87	0.136	35.1	0.076
210	2.80e-2	105.11	68.84	20.23	0.566	38.8	0.355
270	3.60e-2	117.22	51.21	15.98	0.575	39.48	0.366
82	1.093e-2	125.43	44.17	11.39	0.125	55.83	0.103
145	1.933e-2	136.07	38.42	15.54	0.301	61.49	0.264
22	2.93e-3	152.75	29.33	18.86	0.055	63.53	0.050
42	5.6e-3	169.84	21.62	19.20	0.108	67.87	0.100
49	6.53e-3	188.32	14.88	19.10	0.125	76.71	0.121
49	6.53e-3	207.01	12.84	17.81	0.116	86.46	0.116
50	6.67e-3	223.87	12.68	19.37	0.129	90.46	0.129
39	5.2e-3	245.74	13.53	20.11	0.105	97.15	0.104
22	2.93e-3	263.72	18.08	19.34	0.057	108.34	0.054
1	1.3e-4	282.33	26.06	21.17	0.003	108.48	0.003

The total vertical load was estimated by adding the loads through each elemental area

Total vertical load = 1.85 N

APPENDIX 10
Comparison of Results of FE Analyses With and Without Interface Friction for Soft Tissue Around Ischial Tuberosity Loaded Against a Planar Seat Surface

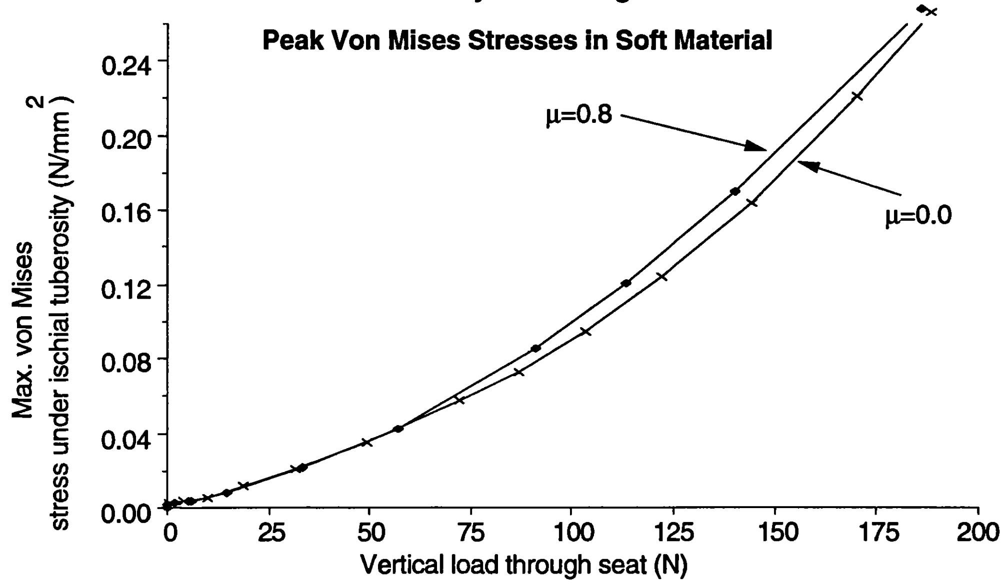

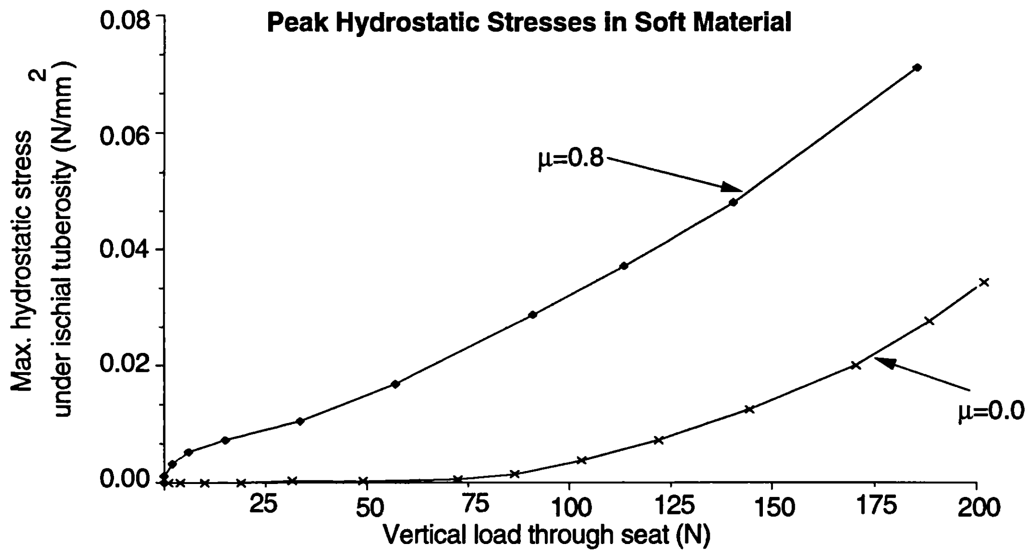

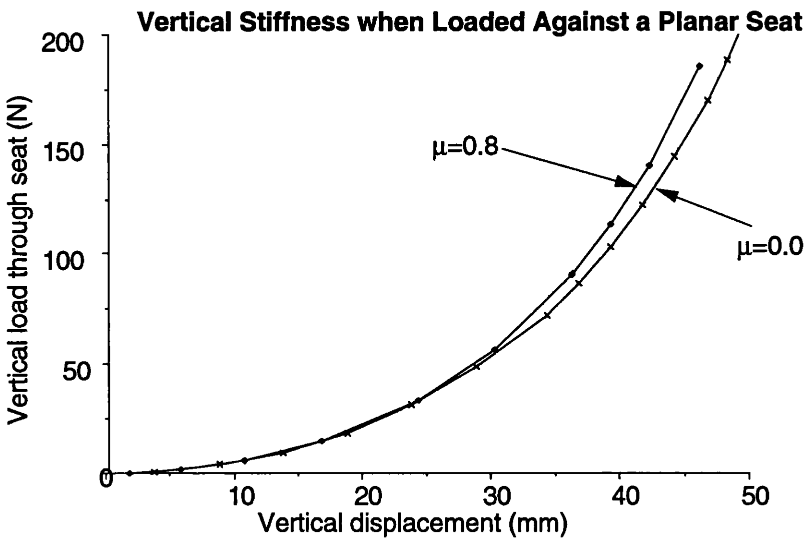

APPENDIX 11
Deformations of Buttock Surface When a Vertical Load of About 187 N is Supported Through the Seat in the FE Analyses in Sections 7.2 and 7.3

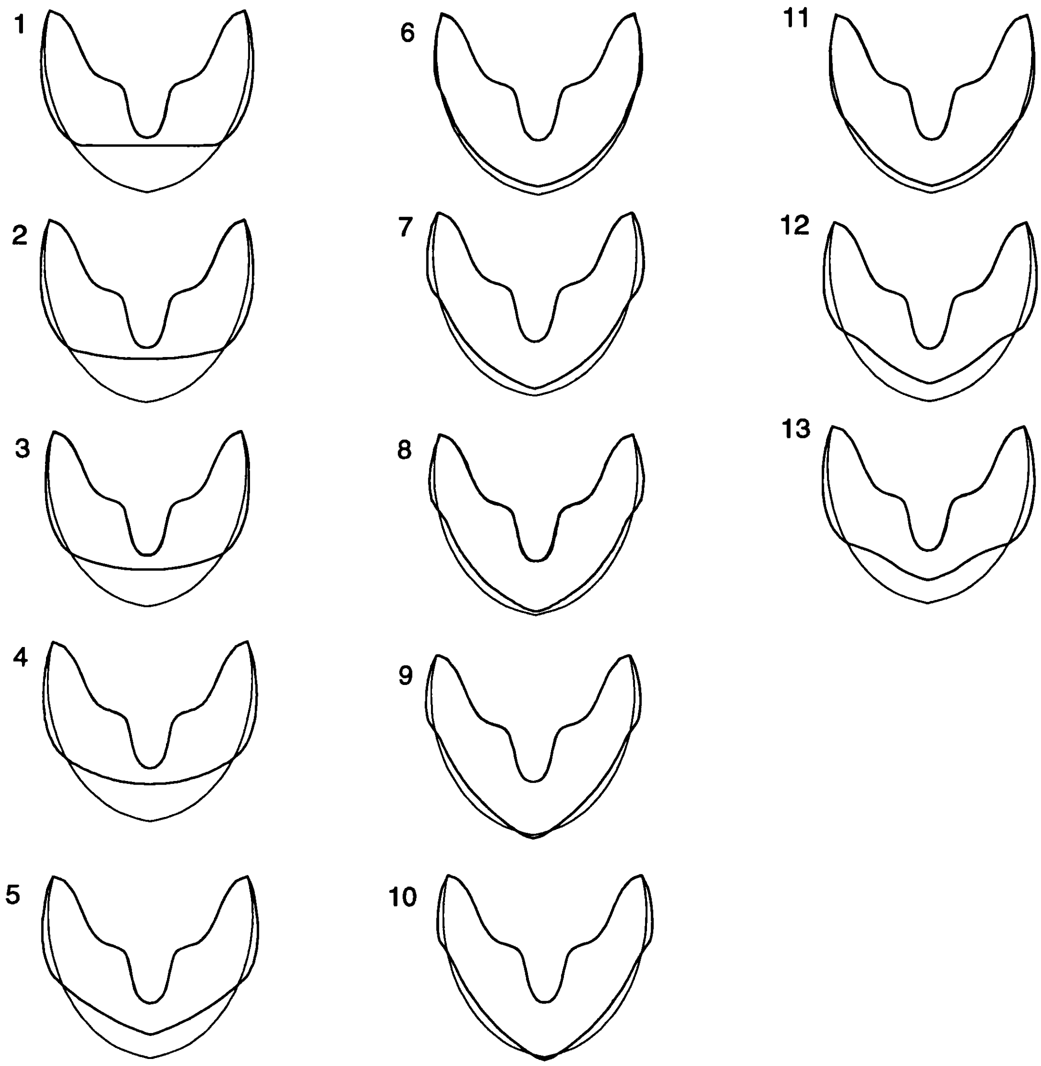

APPENDIX 12

Correlation between Interface Measurements and the Stress State in the Tissues Over the Dorsal Surface of the Sacrum

For models A and E the relationships between the stresses in the soft tissues over the dorsal surface of the sacrum, and the interface quantities were examined at various positions along the interface. The analyses were selected because they both involved substantial loading of the tissues in this region of the body. The inter-relationships between these quantities are plotted on the following pages for seat design E at a location 29 mm proximal to the tip of the sacrum, where the layer of soft tisse over the sacrum was about 8 mm thick, and also for seat design A, at a location closer to the tip of the sacrum where the tissue over the sacrum was 26 mm deep.

The distortional stresses in the models were usually largest close to the interface with the sacrum. As the compressive strain in the soft tissue layer increased, the distortional stresses in the soft tissues increased. The stresses increased at a much more rapid rate when the compressive strain was large. The interface pressures also increased as the distortional stresses in the tissue layer increased. For the same magnitude of interface pressure the distortional stresses were larger at the location closer to the tip of the sacrum (Analysis A). The distortional stress peaks also increased with increasing interface pressure gradient, however the correlation between these quantities was low.

The results are discussed in Chapter 8, together with results from other analyses.

SEAT DESIGN E: Relationship between Interface Pressure, Pressure Gradient, Vertical Deformation and the von Mises Stresses in the Soft Tissue Over Dorsal Surface of Sacrum

Calculated at a location where the total depth of soft tissue over the dorsal surface of the sacrum is 7.6 mm

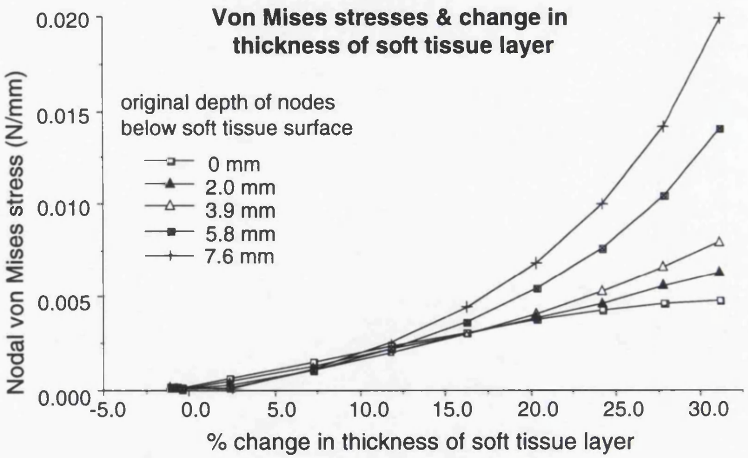

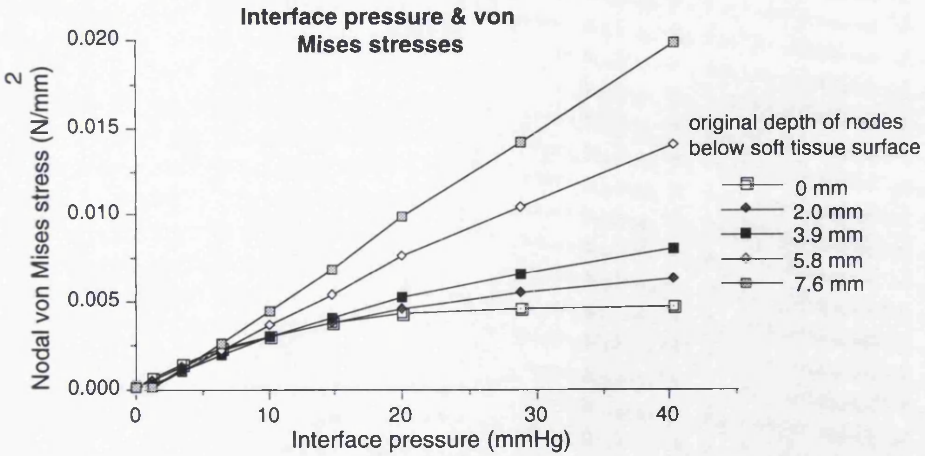

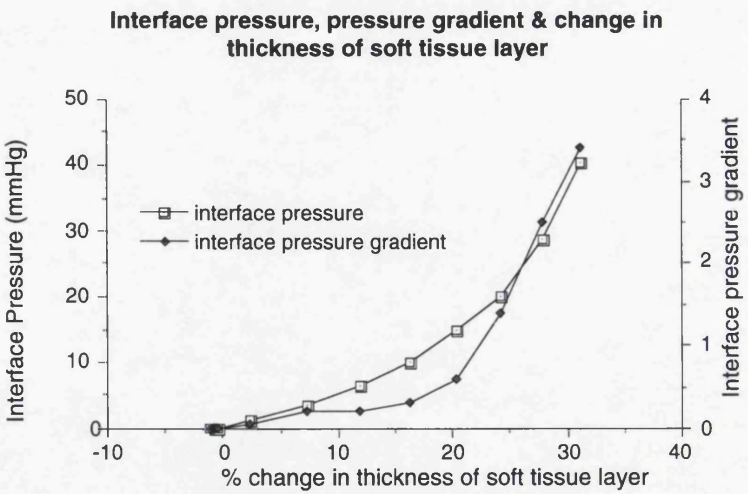

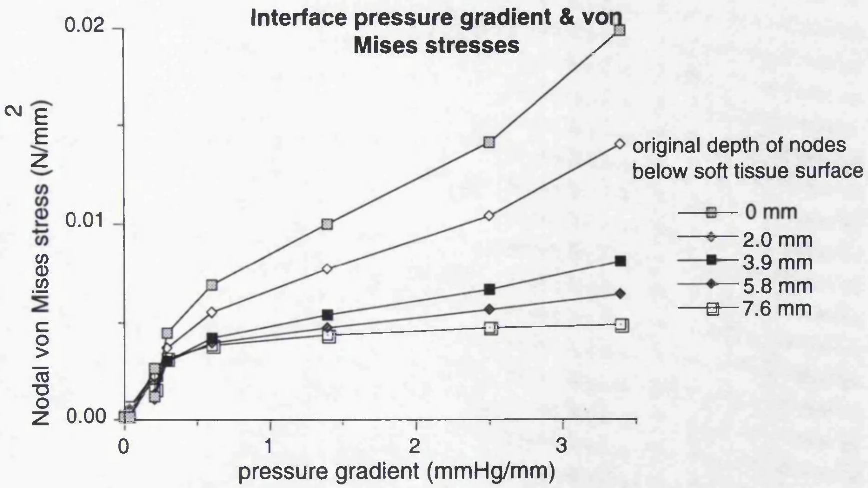

Seat Design A Relation Between Interface Pressure, Pressure Gradient, Vertical Deformation and the von Mises Stresses in the Soft Tissue Over Dorsal Surface of Sacrum

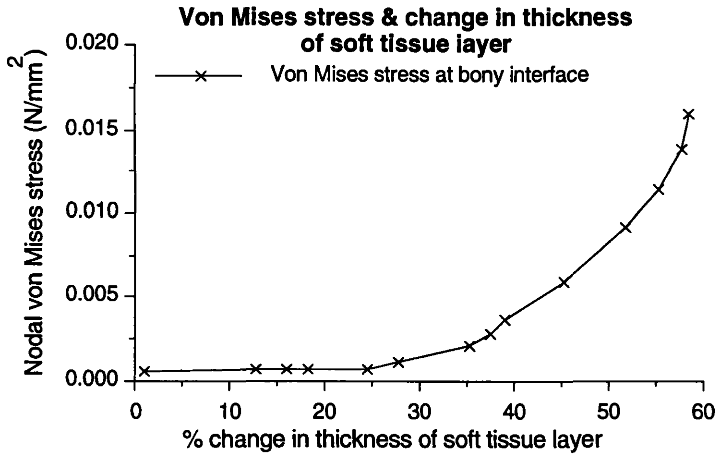

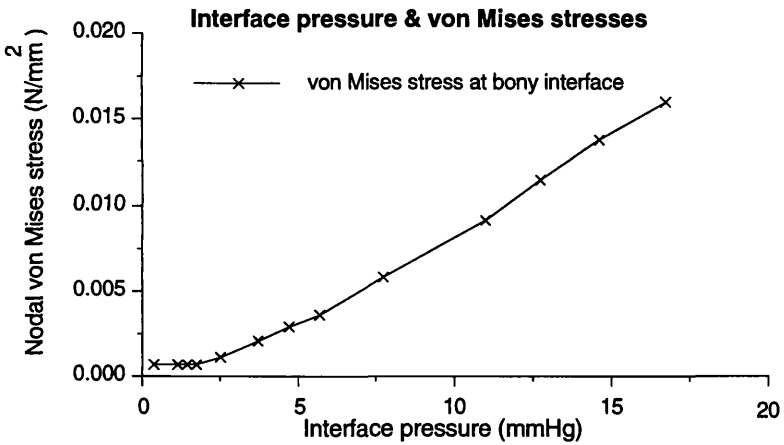

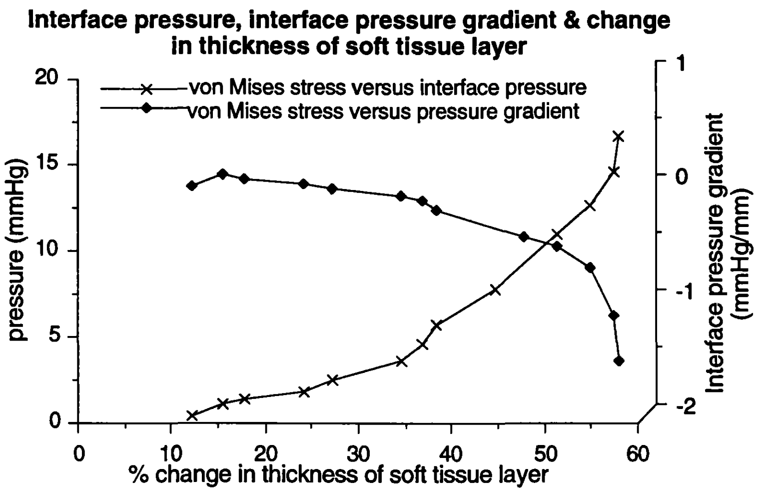

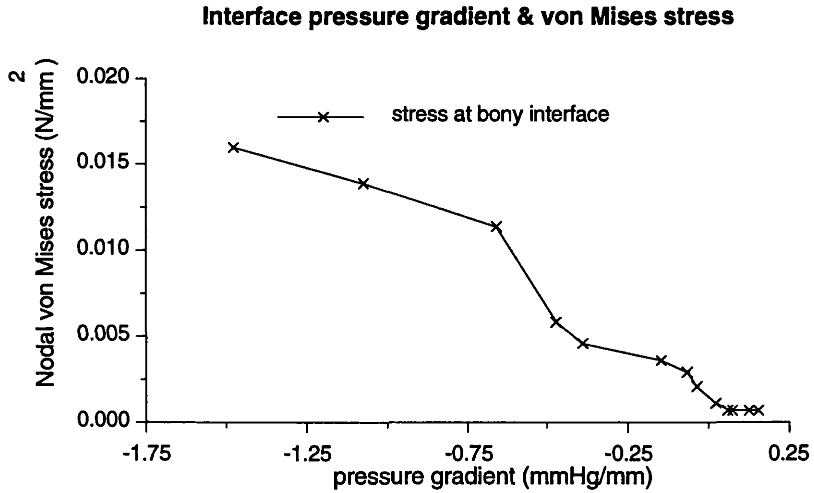

APPENDIX 13- Relationship Between Interface Pressure, Pressure Gradient and the Peak von Mises Stress in the Adjacent Soft Material

Analyses at Ischial Tuberosity (Models 1 to 13)

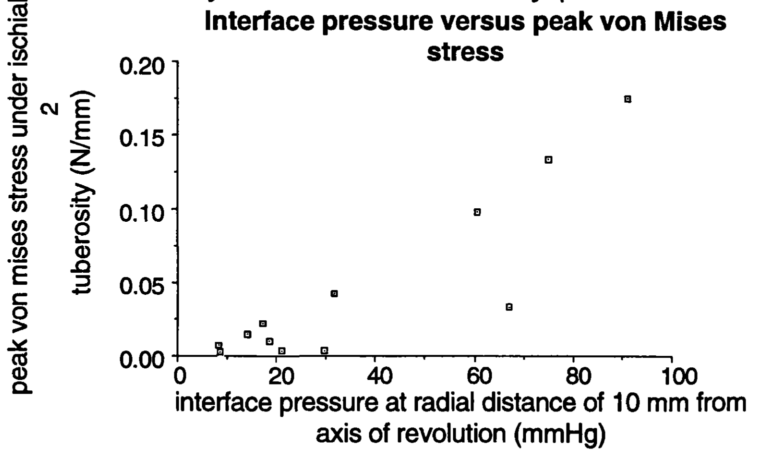

Analyses of Sacral Section (Models A to F)

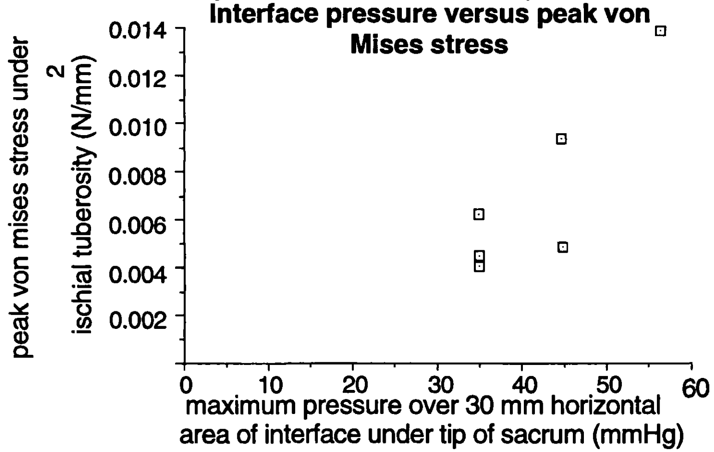

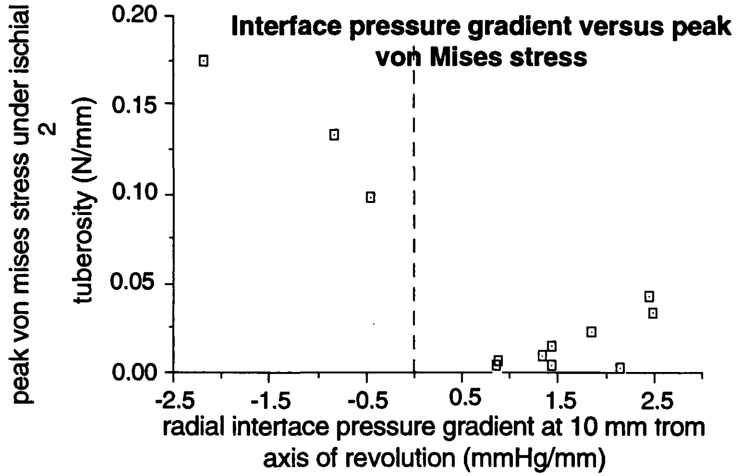

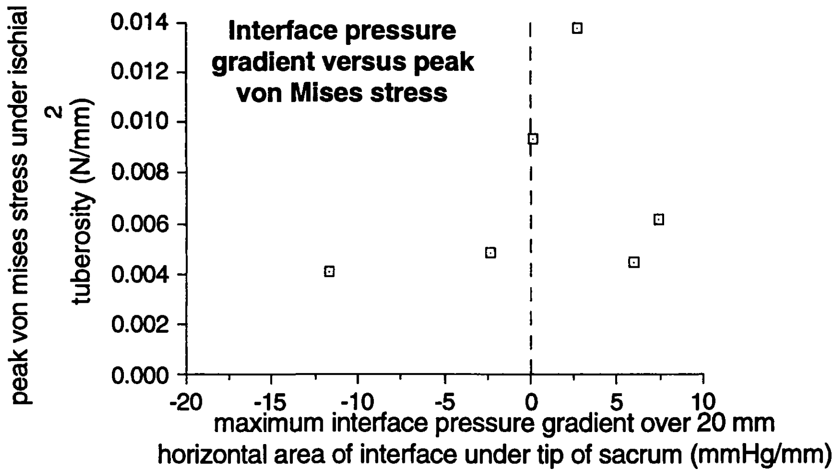

APPENDIX 14

Interface Pressure Calculated from FE Analysis A when 1.8 N was Supported through the Seat Section

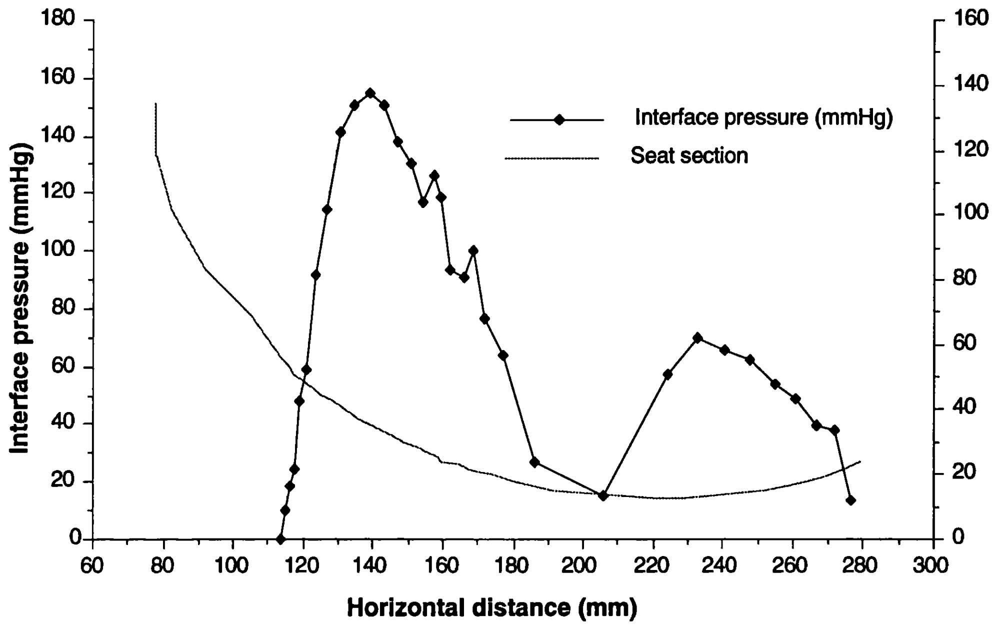

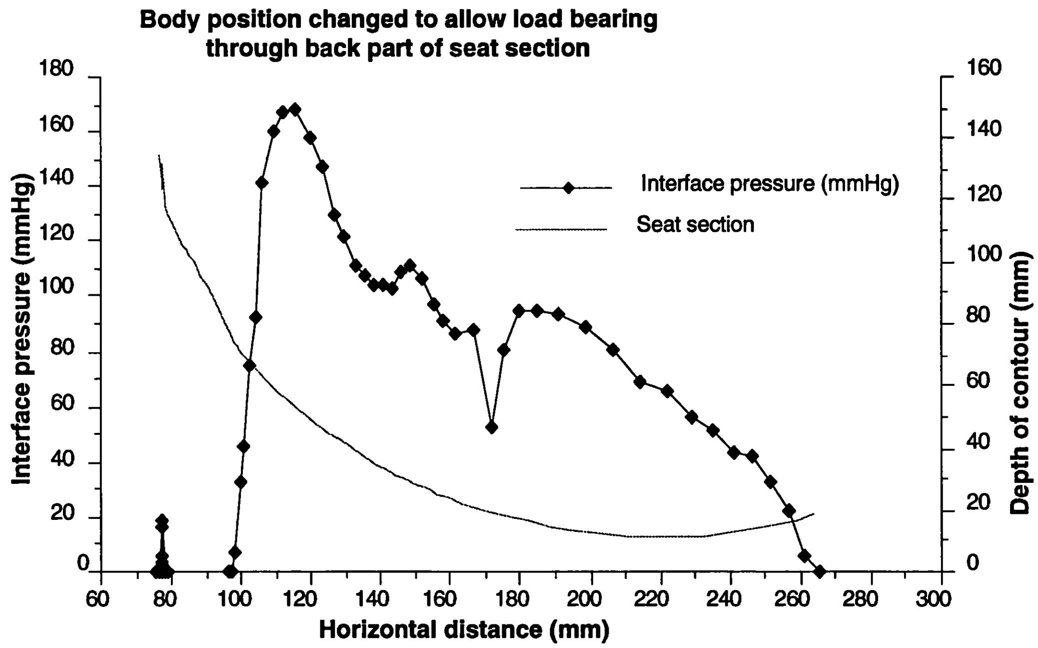

APPENDIX 15 - Anthropometric Data for the Design of Shaped Supporting Surfaces in Standard Sizes

1. Sitting Hip Width

Mean Value (mm)	Standard deviation (mm)	No in Sample	Population Characteristics	Reference
406	46	235	Disabled female	1
395	44	511	Elderly female	1
399	46	267	Disabled male	1
411	44	247	Elderly male	1
407	51	16	Paraplegic male	2
398	41	9	Quadraplegic male	2
396	28	6	Quadraplegic female	2
371	41	-	US adult females	3
353	25	-	US adult males	3

2. Horizontal Distance Between Back of Seat and Back of Knee

Mean Value (mm)	Standard deviation (mm)	No in Sample	Population Characteristics	Reference
490	24	235	Disabled female	1
497	26	511	Elderly female	1
514	24	267	Disabled male	1
525	26	247	Elderly male	1
523	4	16	Paraplegic male	2
529	4	9	Quadraplegic male	2
505	3	6	Quadraplegic female	2

3. Distance Between Back of Seat and Back of Buttocks

Mean Value (mm)	Standard deviation (mm)	No In Sample	Population Characteristics	Reference
23	20	511	elderly female	1
15	21	235	disabled female	1
38	20	247	elderly male	1
33	21	267	disabled male	1

4. Horizontal Distance Between Back of Knee and Back of Buttock

Mean Value (mm)	Standard deviation (mm)	No in Sample	Population Characteristics	Reference
475	39	235	Disabled female	1
473	32	511	Elderly female	1
481	39	267	Disabled male	1
486	32	247	Elderly male	1
480	-	-	US adult males	3
436 *	-	-	US adult females	3

5. Distance Between Ischial Tuberosities

Mean vaiue (mm)	Popuiation characteristics	Reference
132	US adults (military & civilian sources)	3

6. Body Weight

Mean Value (Kg)	Standard deviation (Kg)	No in Sample	Population Characteristics	Reference
73.9	2.6	-	Elderly female	2
63.5	4.7	-	Elderly male	2

1. Harris & Mayfield, 1983
2. Chung & Weimar,1989
3. Diffrient et al., 1974.

* It is not known why this is so much shorter than the other mean values.

APPENDIX 16- Designs of Shaped Supporting Surfaces for Special Seating Needs

A

Surface to Prevent the Body Moving Forward on the Seat and / or a Pelvic Rotation in the A-P Plane

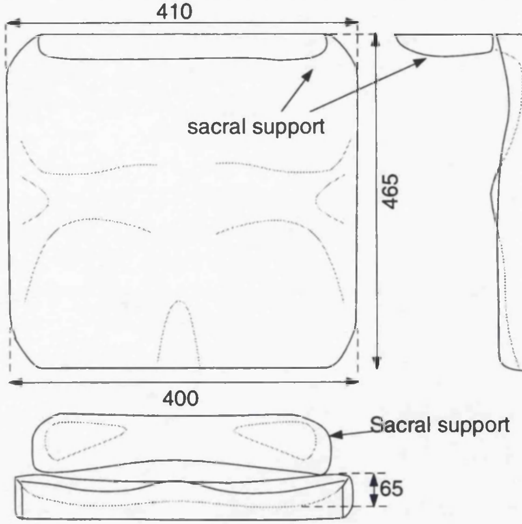

B

Surface to Improve Comfort and to Control Pelvic Position

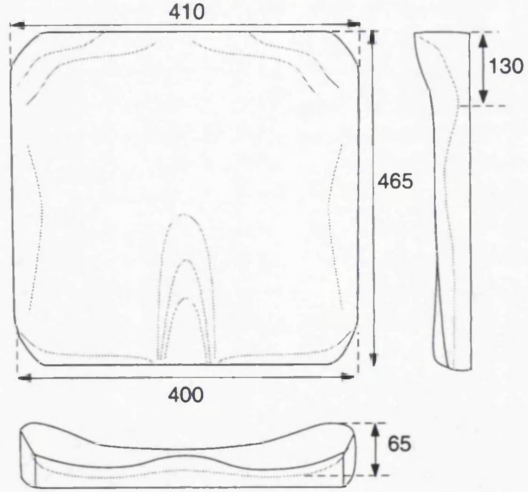

C

Surface to Reduce the Risk of Pressure Sores around the Pelvis

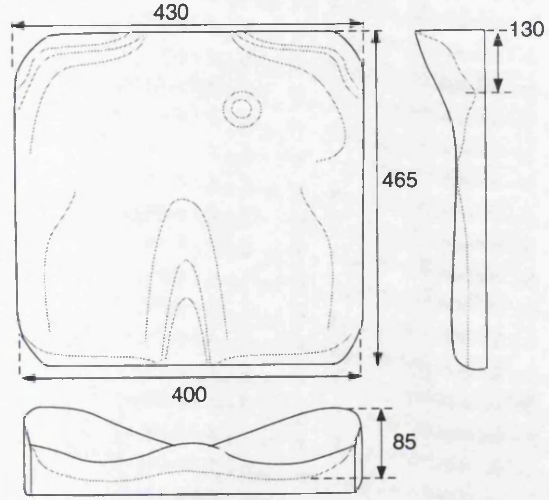

D

Surface to Allow Full Motion of the Body on the Seat

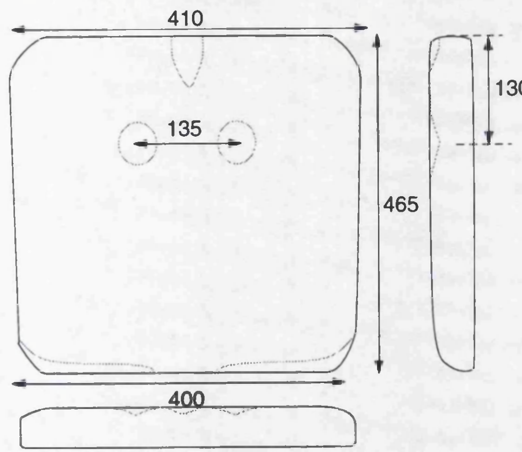

Designs A, B and D are based on the average dimensions of a disabled female.

Design C is based on the dimensions of the able-bodied subject measured earlier in this thesis.